INVESTIGATION OF ELECTRIC ARC INTERACTION WITH AERODYNAMIC AND MAGNETIC FIELDS

DISSERTATION

Presented in Partial Fulfillment of the Requirements for the Degree Doctor of Philosophy in the Graduate School of The Ohio State University

By

Ward Charles Roman, B. M. E., M. Sc.

******

The Ohio State University
1966

Approved by

Adviser
Department of Mechanical Engineering

ACKNOWLEDGMENT

The author wishes to express his appreciation to Professor Lit S. Han for the advice and guidance given throughout this research.

I must especially thank Mr. Erich E. Soehngen, Director of the Thermomechanics Research Laboratory, without whose interest in electric arc technology this investigation of a most challenging subject would not have been possible. His understanding, support, and patience was invaluable in contributing to the successful completion of the work.

Acknowledgment is given to Mr. Ralph Lyons for his most effective work in the construction and assembly of the test apparatus and dependable assistance in conducting the tests. As much gratitude is due to visiting research associate, Dr. Thomas Myers, for experimental assistance and counsel.

This research is the result of a support effort of many people within the Aerospace Research Laboratories. In particular; Supply personnel within the Thermomechanics Research Laboratory, and Aerospace Research Laboratories' library and Machine Shop personnel. Photographers from the Aeronautical Systems Division technical photo group also deserve due recognition. Above all, a very special expression of gratitude is due to the Aerospace Research Laboratories and the AFSC of the USAF, for making it possible for the author to attend The Ohio State University and to complete this research effort.

Finally, a note of thanks to Mrs. Olga Hensler for her expeditious job of typing this dissertation.

VITA

June 16, 1936	Born - Baldwin, Long Island, New York
1958	Bachelor Mechanical Engineering, Rensselaer Polytechnic Institute, Troy, New York
1958-1959 . .	(2/Lt.) Project Engineer - Air Defense Systems Project Office, Wright-Patterson Air Force Base, Dayton, Ohio
1959-1961 . .	(1/Lt.) Project Engineer - Satellite Re-entry System - Dyna-Soar Space Project - Wright-Patterson Air Force Base, Dayton, Ohio
1961-1962 . .	(1/Lt.) Project Engineer - Booster and Propulsion Division - Dyna-Soar Space Project, Wright-Patterson Air Force Base, Dayton, Ohio
1962-1963 . .	Task Scientist - Thermomechanics Research Laboratory, Wright-Patterson Air Force Base, Dayton, Ohio
1963-1964 . .	Resident Graduate Student - Department of Mechanical Engineering, The Ohio State University, Columbus, Ohio
1964-present	Research Scientist - Thermomechanics Research Laboratory - Aerospace Research Laboratories, Wright-Patterson Air Force Base, Dayton, Ohio

PUBLICATIONS

Aeronautical Systems Division, Dyna-Soar Technical Notes (4) Classified, 1960-1961

"Investigation of the Behavior of Magnetically Driven Plasma Arcs." Aeronautical Research Laboratory Technical Report, ARL 63-207, 1962

"The Behavior of Magnetically Driven Electric Arcs." Office of Aerospace Research Review, Vol. I, No. 17, 1962

"Observations on Magnetically Driven Electric Arcs." ARL Technical Report 63-151, Proceedings of the First ARL Plasma Arc Symposium, 1963

"The Motion of Electric Arcs in Transverse Magnetic Fields." The Fourth Symposium on the Engineering Aspects of Magnetohydrodynamics, University of California, Berkeley, 1963

"Observations on the Forward and Retrograde Motion of Electric Arcs in Transverse Magnetic Fields." Sixth International Conference on Ionization Phenomena in Gases, Paris, France, 1963

"The Mysterious Phenomena of Retrograde Motion." Office of Aerospace Research Review, Vol. II, No. 18, 1963

TABLE OF CONTENTS

Page

FIGURES

FIGURE | PAGE

FIGURE		PAGE

TABLES

SYMBOLS

SYMBOL	
A	Area
B	Magnetic Induction
C_D	Drag Coefficient
cm	Centimeter
cps	Cycles Per Second
C_p	Specific Heat at Constant Pressure
D	Significant Dimension, Arc Diameter
E	Electrical Field Strength
f	Frequency
F	Force
g	Acceleration of Gravity
h	Average Value of Heat Transfer Coefficient
h^*	Enthalpy
I	Arc Current
J	Current Density
k or $\mathscr{k}$	Thermal Conductivity
k^*	Boltzmann Constant
L	Arc Length
mm	Millimeter

SYMBOL

mm Hg	Millimeter Mercury
M	Mach Number
$\dot{m}$	Mass Flow Rate
N_{Nu}	Nusselt Number hD/k
N_{Re}	Reynolds Number $\rho DV/\mu$
P	Pressure
%	Percent
Q	Heat Transfer
rms	Root-Mean-Square
R	Gas Constant
sec	Second
T	Temperature
V	Velocity
V_o	Voltage
W	Power Density

GREEK LETTERS

σ	Electrical Conductivity
μ	Dynamic Viscosity
ν	Kinematic Viscosity
ρ	Gas Density
ω	Cyclotron Frequency
τ	Collision Time

SYMBOL

Θ	Temperature Difference
∇	$(i \frac{\partial}{\partial x} + j \frac{\partial}{\partial y} + k \frac{\partial}{\partial z})$

SUBSCRIPTS

e	Electron
f	Film Value
i	Positive Ion
n	Neutral
∞	Free Stream Conditions

I. INTRODUCTION AND BACKGROUND

Throughout the last 60 years electric arc phenomena have become widely known, but still not well understood. Most of the very early work in electric arc discharges, commencing in 1803, was concerned with the corona or glow discharge regime. This regime was restricted to low current and low pressure. Stemming from this came studies of the mysterious phenomena of "retrograde motion" i. e., motion in a direction opposite to that predicted by the Lorentz equation. At the turn of the 20th century, systematic studies were just beginning on investigating the electrical properties of the electric arc discharge.

At first glance, the seemingly novel technique of employing a high current electric arc as a gas heater or plasma generator appears as a relatively new development. Surprisingly however, the energy exchange processes in electric arc discharges have been utilized since 1904. At that time the first arc heater of high power level was used in the chemical industry for producing nitric oxides by dissociating air at very high temperatures (1). Simultaneous with the chemical industries' use of the electric arc discharge was the switchgear industry's interest in extremely high current switches. The primary application was the design of circuit breakers whereby an arc is rapidly extinguished by moving it with respect to the electrodes (2).

An electric arc may be considered as an electric heating element of nearly unlimited temperature range. Through interaction with gas flows and magnetic fields, the arc discharge not only converts electrical energy into thermal energy; it also produces plasma jets of high kinetic energy. The latter are generated by self-magnetic field interaction. The electric arc energy exchange processes are difficult to explain or predict theoretically, consequently a major portion of the research efforts has been experimental. The fact that the number of parameters upon which these energy exchange processes depend is extremely large leads to a very complex problem. The solution is made even more difficult by the lack of accurate, well documented experimental techniques whereby specified parameters are measured. Although more than 60 years of research in plasma physics have greatly advanced knowledge of the electric arc discharge, understanding of the basic energy exchange and conversion processes between electric arcs, gas flows, electrodes, and external magnetic fields is not sufficient to permit the design of arc heating devices compatible with the requirements of modern aerospace technology. The design of these devices is still based on empirical techniques rather than on fundamental scientific knowledge. This involves time-consuming costly trial and error procedures and is more an "art" than a science.

Specifically, it is not possible to extrapolate the research results obtained from low power experiments to the multi-megawatt arc heating devices. Several of these devices are being planned and built for future space flight requirements by governmental agencies e.g., the 50 megawatt electro-gas-dynamic facility at Wright-Patterson Air Force Base, Ohio. The U. S. Air Force and NASA, in their desire to test aerospace vehicles under realistic thermal conditions, at large scale and long test duration, projected their specifications on arc heater performance regarding power, enthalpy, duration, and pressure level far beyond the current state-of-the-art. Cooperative work has been started in industry for the development of arc heating devices of up to 300 megawatts of power at pressure levels exceeding 200 atmospheres (3).

According to a recent Air Force survey (4), during the last five years, more than 50 million dollars have been spent by the United States Government Agencies for the development and utilization of electric arc devices for aerospace applications. Most of the efforts are concerned with the utilization of arc heaters for material testing (e.g., the electric arc thermal plasma jet) and re-entry simulation. The simulation of realistic thermal conditions, in order to facilitate studying plasma sheath effects, wakes, and boundary layer interactions, uses the hypervelocity tunnel arc heater. These applications fall mainly into the aerodynamic and heat transfer areas.

Considerable efforts are also being devoted to the development of electric arc devices for space propulsion. Some examples are the magnetic-propulsion-device (MPD) engines, thermal arc thrustors, and pulsed plasma thrustors. Another area receiving much attention within the last few years is the power generation field. To this group belong such devices as the Faraday and Hall magnetofluiddynamic generators. Closely related to these generators but with different objectives are the magnetofluiddynamic accelerators currently under investigation. The above areas represent the majority of the effort. The applications remaining fall into the categories of: infrared high-intensity light sources, radiation heat sources for solar radiation simulation, high temperature research specimen work, plasmagun flame spraying of materials, and combustion flame augmentation.

A relatively small effort appears to be concerned with basic research. This is due, in part, to the fact that the development of the present electric arc technology for aerospace application has mainly been generated by the need of the sponsoring governmental agencies to obtain usable physical facilities in the minimum possible time. In some cases, applied research is conducted as exploratory development, usually as a first stage toward development of a finished product.

The preceding discussion illustrates that fundamental and basic research in the problem areas of electric arc interactions with aerodynamic and magnetic fields is very necessary. In order to improve this overall situation, an integrated electric arc technology research program was established by the U. S. Air Force Office of Aerospace Research, Washington, D. C. The objective was to obtain and distribute vital information on the fundamental energy exchange processes which dominate the performance of devices employing the electric arc discharge. One of the specific goals under this Air Force program was to assess the ultimate performance capability (i. e., power, temperature, duration, and pressure) of the various basic arc -- gas flow -- magnetic field interaction configurations. This was to be accomplished through analyses of the underlying energy exchange processes. As a part of the first phase of this program, an analysis was made of the simplest possible interaction model: an electric arc column in a co-axial gas flow. In this model the amount of energy transferred from the arc column to the gas to be heated was limited by its equilibrium temperature distribution. The temperature of the arc column and the temperature of the cooled outer walls of the confining cylinder determined the boundary conditions. For this reason, the final mean temperature of the gas to be heated was considerably lower than the temperature of the arc column. Even with this imposed limitation, the axial flow geometry has been very popular for the plasma generators and arc heaters presently being developed for the Air Force and NASA. The following reasons may be cited: the arc behaved in a more stable manner if gas flowed close to the arc boundary in the axial direction; by injecting the gas with a slight vortex flow additional stability of the arc column was gained; the arc in axial flow is rotationally symmetric and, therefore, was more amenable to theoretical and experimental analyses. The theoretical performance limits, more specifically the maximum possible enthalpy at a given pressure, have been determined for this simple co-axial flow model (5). It was found experimentally that the actual performance limits of such devices in the higher pressure regime were approximately an order of magnitude lower than those predicted. The primary reason was electrode failure under the high rates of heat transfer involved. In numerous studies presently being conducted within the Air Force and industry, magnetic fields are being employed to drive the arc-electrode attachment points (so-called arc spots or roots) at a high speed over the electrode surface in an effort to circumvent this serious electrode problem (6). This spreads the very high heat load over a much larger surface area. In these devices an interaction takes place between the electric arc column and mutually orthogonal aerodynamic and external magnetic fields. Therefore, the arc column moves, normal to its axis, into the gas to be heated. This is designated the "cross-flow" interaction model of the electric arc column. Unlike the co-axial model, the unsymmetrical cross-flow model so far has no generally accepted theory.

The cross-flow model, coupled with the external or self-magnetic field interaction which takes place in many of the large high-pressure magnetofluiddynamic accelerators and power generators, has become of increasing interest to the aerospace technology. This is because the most efficient way in which a continuously flowing cold gas stream can be heated to extremely high temperature by an electric arc is to drive the gas stream directly through the arc column. This type of flow may be more nearly achieved in a cross-flow configuration than in one utilizing axial flow. In this way the largest amount of energy can be withdrawn from the arc and transferred directly to the gas flow without having the additional wall losses associated with the axial flow method. Both methods, however, have inherent electrode losses present. Unfortunately, great difficulty is encountered in trying to force a cold gas stream directly through the discharge column, particularly at pressures $\geq$ 0.5 atmospheres. Another problem is the instability which may occur as a result of the mutually acting external fields. The cross-flow situation is further complicated by the present emphasis of aerospace electric arc technology toward extremely high power, pressure, and current levels. This in turn generates new problems in electrode phenomena, electrode surface cooling, insulation techniques, arc stability and external field interaction phenomena. Work is presently being done by the Air Force in conceiving novel designs in hopes of reducing some of these problems (3).

Another area requiring more basic research is that of high temperature transport properties of electric arc plasma. The lack of data on these thermo-physical properties and the large disagreement (as great as 50% difference) between the several reported sources questions the validity of the interpretation and assessment of the experiments already performed and reported.

Numerous experiments have been performed by the switchgear industry on extremely high current electric arcs moving between rail electrodes (8). The application is the development of extremely high current switches for arc extinguishment employing the blowout induced by magnetic and/or cross-flow interactions.

The author, in fulfilling the thesis requirements for the Master of Science degree in Mechanical Engineering at The Ohio State University, has investigated high current electric arcs driven along rail electrodes by an external transverse magnetic field. Only empirical gross data could be obtained. Theoretical work was unsuccessful because of the lack of a suitable mathematical model representing the actual physical interaction mechanism between the electric arc and gas flow relative to the arc. Figure 1 is a sequence of high-speed photographs, taken by the author, of a high current atmospheric pressure electric arc magnetically driven along parallel rail electrodes by an external transverse magnetic field. The electrodes were water-cooled copper. The arc was initiated at one end of the rail

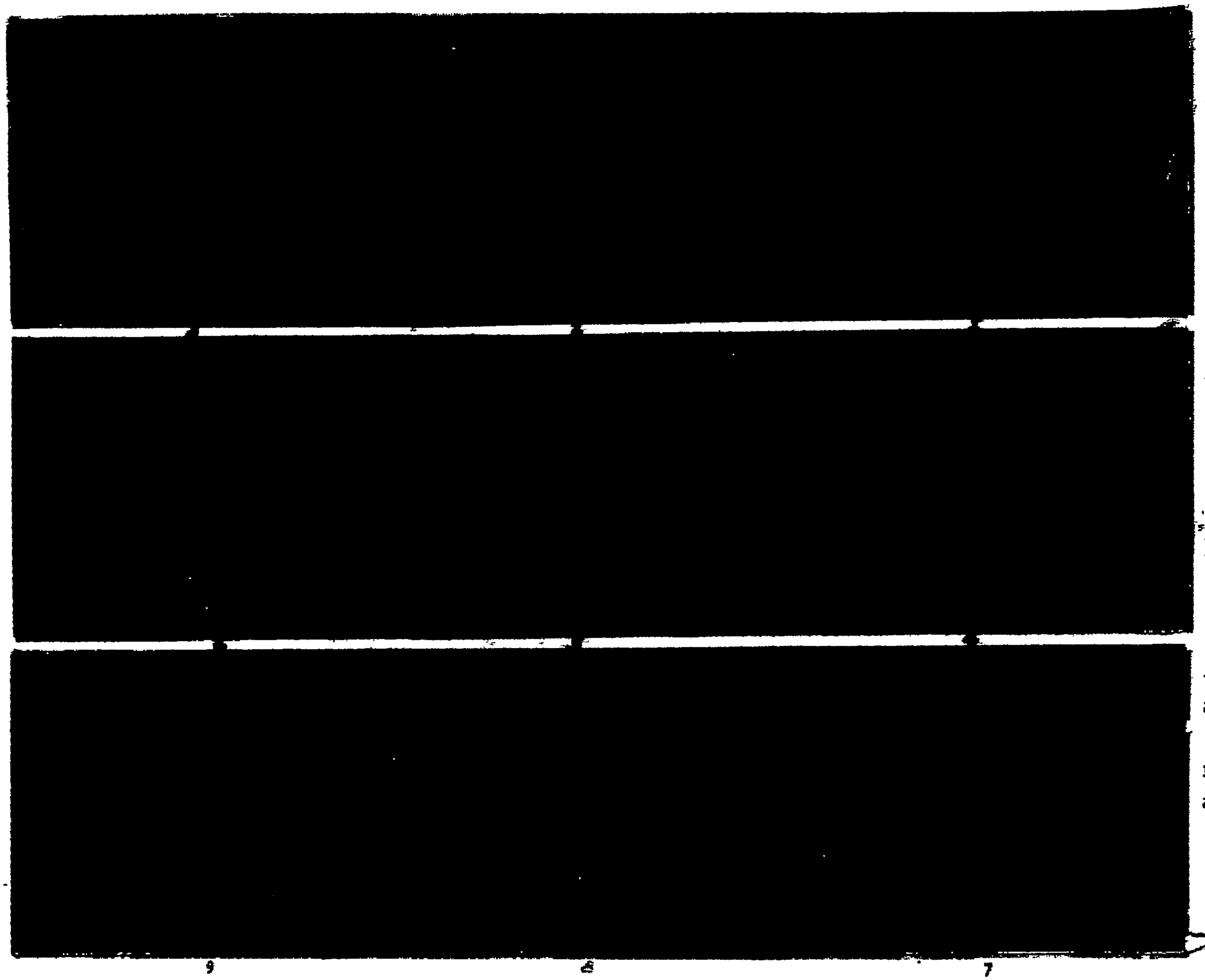

arc travel
direction
right to left
top to bottom

I = 240 amps
B = 600 gauss
gap - 0.6"
$\overline{v}$ = 143 ft/sec

cathode - top
electrode

Dynafax
camera speed
26,000 frames/sec

4.2 μ sec exposure
across frame

note multiple cathode
and anode spots

FIGURE 1 D.C. ARC MAGNETICALLY DRIVEN ALONG RAIL ELECTRODES

electrodes by exploding a tungsten wire. The small white spots seen in the individual photographs were the result of the exploding starter wire. These photographs clearly showed the very drastic shape change which takes place in the order of microseconds. Detailed evaluations of the cathode and anode spot behavior indicated an irregular jumping pattern with random sticking. This example of the cross-flow moving arc indicates the extreme difficulty involved in trying to analyze moving arcs due to the unknown influence of the moving electrode spot effects. Although the rail type and circular annular gap rotating arc devices are of more pertinent interest from the immediate applications standpoint, detailed diagnostics can only be done on relatively stationary arc columns.

Attempts have been made to treat the cross-flow arc as a solid "drag body" moving through a stationary cold gas (9). Others tended toward considering the arc as a moving state i.e., a "temperature hill" progressing through a stationary cold gas (10). Other experimental studies of arc movement due to an external transverse magnetic field have shown the importance of the processes occurring in the cathode-fall region. Recent experiments with moving arcs at high currents ($\geq$ 400 amps) and high pressure ($\geq$ 1 atm.) indicated that processes occurring in the positive column became increasingly important, if not totally dominant (11). Three regimes have been observed, the first where the cathode fall conditions predominate, then the regime where transition occurs, and finally the positive column dominated regime. Results of some of the more recent experiments (12) in the latter regime indicated reasonably good agreement with theoretical predictions of the arc column in a transverse magnetic field. However, numerous simplifying assumptions had to be made concerning phenomena whose effects may be more significant than had been assumed. Examples are the radiation losses, electrode surface effect, cathode jet effect, anode jet effect, self-magnetic field effect and the arc configuration effect. These phenomena and associated effects are difficult to isolate and measure experimentally, due primarily to the required physical apparatus which does not lend itself readily to access for diagnostic work.

It is still not known whether cold gas moves through a moving electric arc discharge column, only around it, or a combination of the two. Experiments so far have failed to shed light on the problem due to the difficulties in measuring transient thermal phenomena in a fast moving heat source.

The preceding discussion led the author to believe that by holding the arc column fixed in space instead of moving the entire column and electrode spots, many of the unknown electrode effects may be eliminated. In addition, no research effort is presently known which deals with a detailed experimental investigation of the fundamental energy exchange mechanism of a cross-flow arc under the influence of an external magnetic field. In the effort directed toward solution of this important problem, experimentation must, of necessity, be in the foreground, since no adequate analytical model has been set forth from which a concerted theoretical effort might proceed. In the search for explanations of this cross-flow interaction and also to provide an experimental base upon which to build a sound analytical model, the author investigated this area with the following objective: To gain information on the basic interaction and energy exchange processes of electric arcs in transverse aerodynamic and magnetic fields through detailed measurements of the flux of energy from the arc to the environment under various transverse gas flow and external transverse magnetic field conditions.

The research effort was broken down into three basic phases.

A. Review of the Fundamentals of the Arc Discharge, Magnetic Field Effects, and Aerodynamic Cross-flow Interaction.

Because of the complexity and wide range of possible interactions and arc parameters, a brief review of the nature and characteristics of the high current arc discharge together with magnetic field and flow field interaction effects was included.

B. An Extensive Literature Survey and Critical Review of Cross-flow Arc Phenomena Both With and Without External Magnetic Fields.

To complete an up-to-date critical survey of all the available literature is a sizeable task, but by excluding some related areas and breaking the survey down into defined subheadings, a reasonable result was obtained. The related areas excluded are those falling into the low pressure arc discharge regime (e.g., retrograde motion investigations) and into the electric arc rail or circular annular gap accelerator and switchgear category. Over 75 papers are in existence in this first area alone. Since the author had the privilege of conducting some research investigations in this area, a comprehensive chronological reference list is included in Appendix F for completeness. The area of rail or circular annular gap accelerators and switchgear investigations also provides close to 100 papers. The investigations in this area which have direct bearing on the immediate study are included. Because of their relevance to the overall problem, a complete chronological list is included in Appendix F.

In addition to the literature survey a brief historical development section which chronologically reviews the investigations to date was included. The literature survey, based on a systematic examination of over 34 American, British, German, and Russian papers, was broken down into the following subheadings:

Theoretical	Experimental
a) Cross-flow only	a) Cross-flow only
b) Transverse external magnetic field only	b) Transverse external magnetic field only

c) Combined a) and b)

c) Combined a) and b)
1) non-preionized flow
2) preionized flow

C. Detailed Experimental Investigation of the Basic Interaction Phenomena and Energy Exchange Processes of a High Current Electric Arc Under the Influence of External Mutually Orthogonal Aerodynamic and Magnetic Fields.

The essence of the experimental work under Phase C was the determination of the local energy balance throughout the system under various energy input and flow conditions. This involved the measurement of the local distribution of the gas enthalpy and velocity throughout the flow field in the wake and near to the arc boundary. A miniaturized calorimetric type enthalpy and stagnation pressure probe was used for the measurements. A portion of the investigation included micron particle flow visualization studies and photographic observation of the arc column size and shape. Measurement of the position of the arc column wake boundary region and a determination of the relative heat flux and turbulence level downstream of the arc column and across the wake boundary comprised another portion. A miniaturized water-cooled heat flux sensor was used to measure the local heat flux and rms per cent power fluctuation in the downstream region of the arc. Also included was an overall power distribution analysis to determine power losses relative to the ohmic power input. These measurements, which could not be made in a fast moving arc, were facilitated by holding the arc column stationary with respect to the diagnostic instruments to be applied. The arc column was more or less "locked" in place so that the transverse gas stream could be directed against the arc column. A specially designed external magnetic field provided the balancing force necessary to hold the arc column against the aerodynamic drag forces induced by the transverse blowing. Such an arc will be designated a "balanced arc" because there must be a balance between the aerodynamic force due to the cross-flow and the magnetic force due to the interaction of the arc current and the magnetic field.

II. FUNDAMENTALS OF THE ARC DISCHARGE

Introduction

In order to conduct electricity through gases, a means of electrical conductivity between a set of electrodes in direct contact with the gas is required. Some mechanism must be provided for the generation of a supply of charged particles in this conduction region. Then there is a certain percentage of free electrons and positive gas ions which are free to move under the impetus of an applied electric field. The electrical conduction in gases is similar to that in solids except that the ions in solids are relatively immobile. Therefore, a transition must occur from a solid conductor, where the current flow is carried totally by the electrons, to a gaseous conductor in which both electrons and positive ions carry the current flow.

During an arc discharge there is a spontaneous increase in the number of free electrons and positive ions contained within the gas volume. This gas column exists between the two electrodes, it creates an approximately constant electrostatic field within the column that accelerates the free electrons and positive ions, between their respective collisions, within the column. The total movement of charges is, therefore, composed of the sum of the free electrons moving toward the anode and the positive ions moving toward the cathode. These accelerated electrons and positive ions upon colliding with neutral gas atoms and molecules combined with mutual collisions continually dissipate the energy obtained from the electric field. These collisions are so frequent and numerous that the larger percentage of average particle energy consists of random thermal kinetic energy, and causes an increase in the thermal energy of the plasma. The total motion of the charged particles can, therefore, be thought of as a combination of positive ion and electron drift toward the respective electrodes superimposed upon the random thermal motion. This increase in thermal energy and corresponding temperature rise causes an increase in ionization. Figure 2 (17) depicts a typical relationship between the number density of the various particles and the absolute temperature for a nitrogen plasma. Initially, when the accelerated electrons and positive ions collide with the molecules the number density of the molecules decreases while that of the electrons, positive ions, and neutral atoms increases. When the temperature increases to the point where the rate of decrease in molecule density is quite large (8,000 °K) the source of atoms is greatly reduced. The number density curve for atoms then starts to decrease while that for positive ions, and electrons continues to rapidly increase. As the temperature reaches still higher values, in the ideal case the atom density curve would decay to zero and the positive ion and electron curves would increase directly proportional to the temperature.

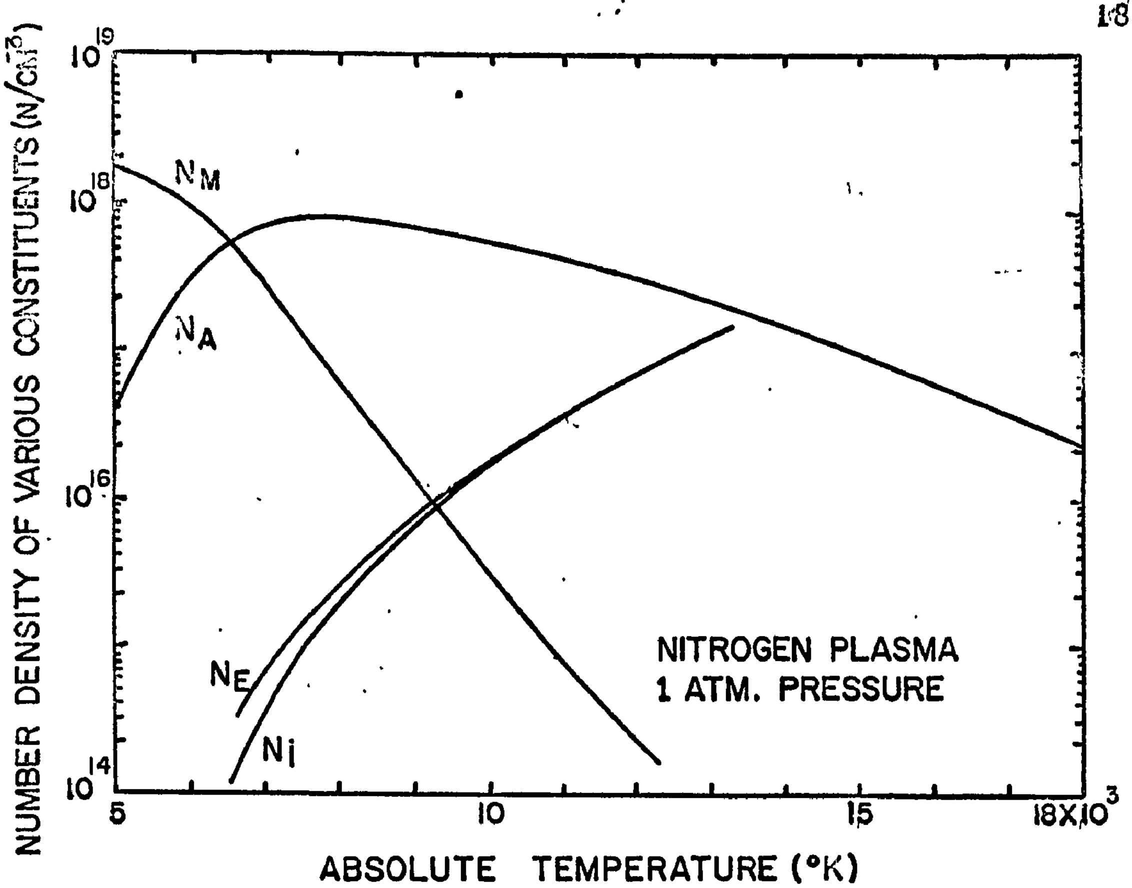

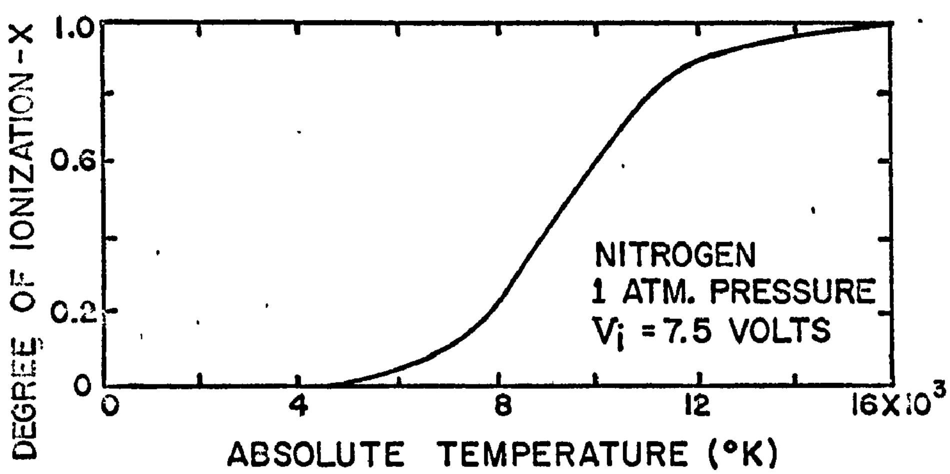

RELATIONSHIPS BETWEEN NUMBER DENSITY OF VARIOUS PARTICLES, DEGREE OF IONIZATION, AND THE ABSOLUTE TEMPERATURE FOR A NITROGEN PLASMA.

FIGURE 2

This would indicate a state of complete ionization. At even higher absolute temperatures, more complex occurrences, such as double and triple ionization may take place.

On the basis of thermodynamic reasoning, Saha (13) analyzed thermal ionization by assuming the ionization process to be completely reversible. Complete thermal equilibrium was also assumed i.e., temperature electron = temperature positive ion = temperature atom, and the number of ions lost by recombination were equal to those formed through thermal ionization. No account was made for the time required to establish equilibrium or the mechanism of ionization. Saha obtained the following relationship: when n is the original concentration of atoms in the gas, $n = n_n + n_i$, and the fraction of ionized atoms is $x = n_i/n = n_e/n$.

$$\frac{x^2}{1 - x^2}\ P = 3.16\,(10)^{-7}\ T^{2.5} \exp\left(\frac{-eV_i}{k^* T}\right) \qquad (1)$$

where x = degree of thermal ionization

P = total pressure in atmospheres

T = gas temperature in °K

eV_i = ionization energy of the gas atoms in ergs

k^* = Boltzmanns constant.

This relationship can also be expressed in another form as follows:

$$\log_{10}\left(\frac{x^2}{1 - x^2}\ P\right) = \frac{-5050V_i}{T} + 2.5\log_{10} T - 6.5 \quad (2)$$

Figure 2 illustrates this latter relationship between the degree of ionization and the absolute gas temperature for nitrogen. It is important to realize that numerous assumptions e. g., thermal equilibrium, no turbulence, and a homogeneous gas were made in arriving at these ideal relationships and, therefore, actual conditions may deviate from this idealized concept.

The thermal motion of the electrons, positive ions, and neutral particles is determined by their many collisions. Only when the electrons and positive ions gain sufficient kinetic energy between collisions can they ionize a neutral gas particle when a collision occurs. The thermal energy of the plasma will increase until the heat losses become equal to the energy input and then a steady state condition is reached. The gas volume within this discharge has then attained the state of a quasi-neutral plasma i. e., containing equal numbers of charged particles of both signs. It may also contain some neutral particles. If the kinetic energy of the electrons, positive ions, and neutral particles is the same, they are in a state of thermal equilibrium.

Previous investigations have shown that the following factors establish the conditions for a discharge:

a) density of the gas (mean free path of the electrons),

b) separation distance between the electrodes,

c) mean speed of the free particles between collisions,

d) the electrical potential between the electrodes.

Direct current gas discharges of a steady-state nature are categorized into either glow discharges or arc discharges. The glow discharge is characterized by high terminal voltage, low current density, and low gas pressure. The arc discharge generally operates at low terminal voltage, relatively high current densities, and relatively high pressures. There are several other types of electric discharges, however, only the electric arc discharge is of pertinence in this study and will be discussed here.

Basic Energy Exchange Phenomena

Since the underlying physical principles of the electric arc discharge are independent of its application, the basic energy exchange phenomena and fundamentals of the electric arc will be briefly reviewed. The electric arc may be defined as a gaseous discharge capable of passing large electric currents at relatively low voltage. Figure 3 depicts a typical direct current electric arc discharge between two electrodes. Ohmic heat is produced by means of the electrical current flowing from the cathode to the anode

	cathode	anode	positive column
voltage gradient (V/cm)	$\leq 10^6$	$\leq 10^3$	5-250
current density amps/cm^2	10^2-10^6	10^3-10^5	10^1-10^4
surface heat flux kw/cm^2	1-10^3	1-10^4	10^{-1}-10^2
heat content kw/cm^3	10^{12}-10^{14}	10^3-10^8	5-10^4

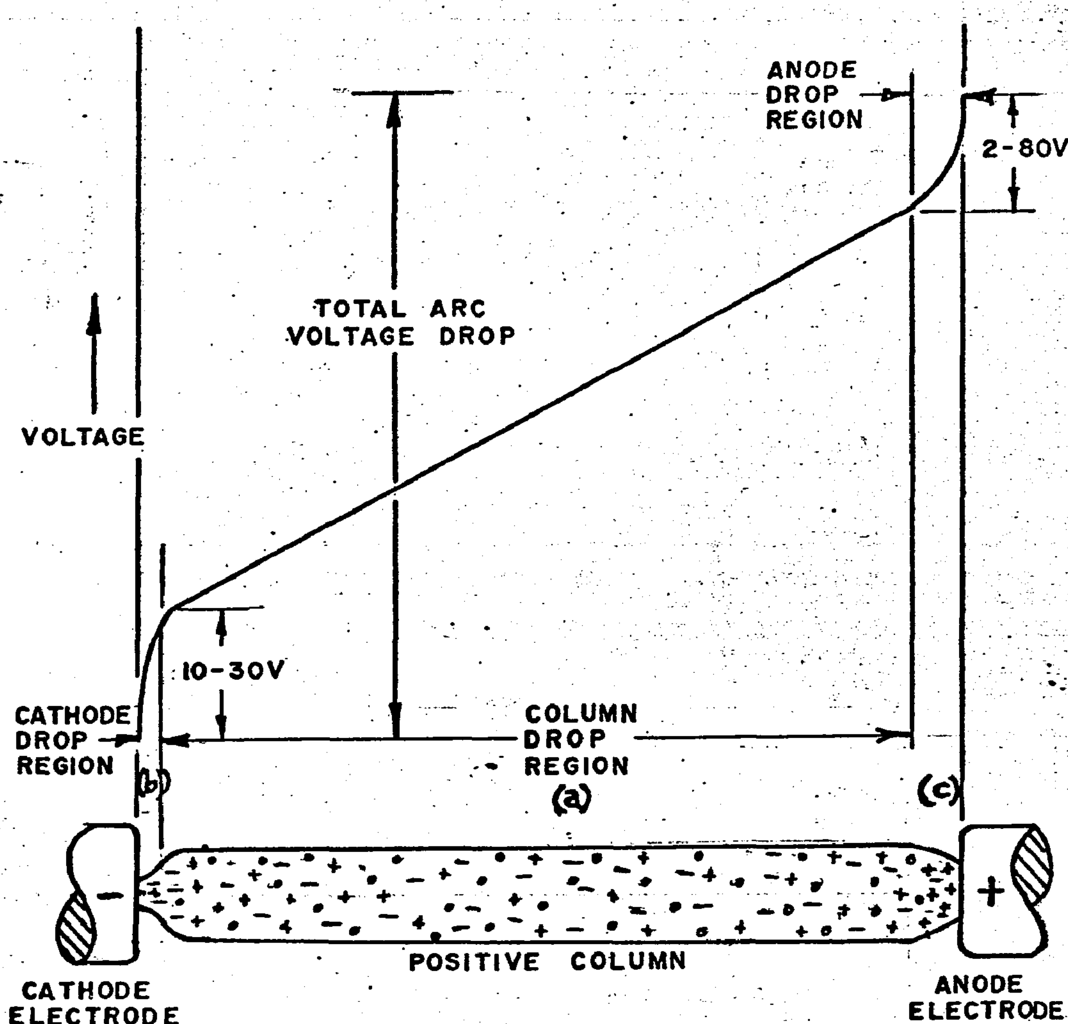

CHARACTERISTIC REGIONS AND ENERGY DISTRIBUTION OF THE D.C. ARC DISCHARGE

FIGURE 3

through an electrically conducting gas, the arc plasma. One may distinguish the three distinct regions of the electric arc discharge.

Region a) The positive column or main part of the arc.

In this region the voltage gradient and arc diameter remain relatively constant.

Region b) The cathode drop region. An extremely thin region in the order of less than or equal to several mean free path lengths.

Region c) The anode drop region. Similar to Region b) but adjacent to the anode.

The drop regions are characterized by very high voltage gradients accompanied by a contraction of the arc diameter. The voltage distribution over the arc length is shown in the upper right portion of Figure 3. Another distinguishing characteristic of the drop regions is the thermal boundary conditions at the electrode-gas interface. The anode and cathode drop regions represent transition boundary regions between extremely hot gaseous plasma and relatively cool solid electrodes. This causes an increased thermal gradient through the drop region and, hence, an increase in the voltage gradient. In the normal free burning arc, the voltage gradient is high in the region of the electrodes and decreases to much lower magnitudes as one proceeds away from the electrodes. The table in Figure 3 indicates the ranges of the voltage gradient, current density, surface heat flux, and heat content which have been measured under certain conditions in the three regions of the arc (2).

The electric arc is by no means a simple heating element, but rather an extremely complex one. This is mainly due to its non-uniformity over its length and cross-section, but also its ability to change very rapidly its thermal and electrical characteristics with the mode and degree of heat removal. At this point the arc-paradox may be mentioned. In conventional electrical solid state heating elements the peak temperature normally decreases when heat is removed from the surface. However, in the electric arc discharge, the arc peak temperature may and usually does increase when heat is removed from its surface. It has been experimentally verified by numerous authors (15, 16) that upon removing heat from the arc boundary, the conductive cross-section decreases accompanied by a shift in the isotherms toward the arc's axis. For a constant power input per unit column length an increase in the current density is required. This is accompanied by an increase in the maximum temperature along the arc's axis.

The over-all energy transport phenomena are determined by the energy exchange processes between electrons, positive ions, and atoms in the three regions of the arc. Briefly, in a very simplified manner, they can be explained as follows: at the cathode, electrons are emitted from the surface by a complex, still not completely understood process. Many investigators (14) have put forth electrode emission theories; however, no single theory is generally accepted. In fact, the cathode mechanism is still considered an open problem in arc physics. For example, the controlling mechanism of electron emission at the cathode, for copper electrodes (non-refractory), is postulated to be a combination of thermionic and field emission (17). It is beyond the scope of this investigation to include all the details of these very complex electrode mechanisms.

When the emitted electrons enter the cathode fall region, they are electrostatically accelerated to very high velocities due to the high voltage gradient. Upon entering the positive column, the velocity of the electrons is considerably reduced by collisions with neutral particles and positive ions of the gas in the column. This process generates ohmic heat, which the column dissipates to its environment by the various transport processes. In the anode fall space, the electrons are again accelerated to high velocities by the strong electric field existing in the anode drop region. By means of high-speed collisions with neutral gas atoms in this region, ionization occurs. This process produces the positive ions necessary for maintaining electrical neutrality in the positive column. It is worthwhile to note that the energy dissipation at the anode is usually much greater than at the cathode even though the current density may be less. This is because a large amount of thermal energy corresponding to the work function is removed from the cathode surface by electron evaporation during the emission process. At the anode, this equivalent energy appears as heat of condensation (17). Therefore, the electrons which bombard the anode surface give rise to a large heat increase both from the heat of condensation and the kinetic energy of the impinging particles.

A similar process occurs with the positive ions which are produced in the anode fall space, but because of their charge move in the opposite direction. Because of the considerably higher mass of the positive ions relative to the electrons, they drift at rather low velocities through the positive column under the influence of the negative potential of the cathode. Acceleration of the positive ions in the cathode fall and subsequent bombardment on the cathode electrode surface heats the cathode to high temperatures. In the positive column, approximately 95% of the total current is transported by the drift of the free electrons. This is due to their lighter mass and much greater mobility.

External Field Effects

Because the mechanism of arc discharges is so complex, and available information on the various physical processes and phenomena is not self-consistent, it becomes extremely difficult to predict the effects of the superposition of external fields (aerodynamic and/or magnetic) on the arc discharge. Changes in both the basic collision phenomena and the temperature, velocity, and current density distributions within the discharge proper can be expected due to the interaction with the external fields. For example, certain properties such as the electrical conductivity may become tensors. In the present investigation, only those phenomena occurring in the high pressure regime will be discussed i.e., ≥ 1 atmosphere.

When a uniform external magnetic field is applied transverse to the current flow in an electric arc discharge, a vector force is exerted on the arc column. The magnitude and direction of this force is related by $\overline{F}_{\text{unit length}} = \overline{I} \times \overline{B}$ ($\overline{I}$ is the current and $\overline{B}$ is the magnetic flux density.) For a steady state situation, this magnetic force will have to be balanced by an equal and opposite force. In the present investigation this opposing force was provided by the external transverse blowing. The interaction effect of the columns' self-magnetic field with the externally imposed transverse magnetic field must also be considered. This is thought to be the primary cause of the distorted shapes and instabilities observed in the high-speed pictures taken of a moving arc column. A kink-type instability has also been reported (18). Thiene (19) postulated that when an external magnetic field is applied perpendicular to an electric arc column, a circulatory convection (double-vortex) occurs within the column due to the magnetic body force on the arc plasma. For a parallel rail electrode type apparatus, (or circular annular ring electrode type), a sufficiently strong external transverse magnetic field may cause the arc discharge to travel at very high speeds. Speeds up to 12,000 ft/sec have been reported (20). If the discharge is magnetically driven along parallel rail electrodes, a drag effect is present because of the momentum transfer from the positive ions to the large number of neutral gas atoms and also from the induced aerodynamic drag aspects. The arc, therefore, moves through a cold gas. This gas does not reach temperatures sufficient for thermal equilibrium.

When a uniform external gas flow is applied transverse to the current flow in an electric arc discharge, a vector force is exerted on the arc column. For a steady state condition, this aerodynamic force will again have to be balanced. This balancing mechanism has been partially explained on the basis of an energy balance. However, no generally accepted theory exists. The explanation depends strongly on the arc columns' perviousness to external transverse flow, and this is still an open problem in plasma physics.

For the combined interaction of both transverse, external aerodynamic and magnetic fields, the previously discussed effects now become superimposed. For the steady-state balanced mode, some simplification may result, in particular when the arc column curvature is eliminated as was done in the present experiment. Because the two opposing forces are simultaneously present and the arc is in the balanced mode, the relationship $BI = (1/2)\rho\, C_D V^2 D$ defines the force balance.

Property Variations with Temperature

The temperature distribution within the column is determined by the balance between the generated and the dissipated energy. Under steady-state conditions, the thermal energy generated by ohmic heating within the column must be dissipated to the environment by the various transport processes e.g., thermal conduction, convection, diffusion, and radiation. These processes constitute an extremely complex energy exchange system which can be solved analytically only for the very simple cases. A further complication is that the dominating gas properties are strong functions of the temperature which itself varies across the arc column diameter.

The gas in the positive column of an electric arc is never in true thermodynamic equilibrium i.e., the electron temperature must always slightly exceed the gas temperature (16). Exact determination of the equilibrium state of the electric arc plasma can only be obtained through diagnostic measurements. These measurements may provide the gas and electron temperatures or values of the column voltage gradient and other variables from which these temperatures can be obtained. Figure 4 illustrates some of the difficulties by the examples of two property variations of a nitrogen arc, free-burning in an atmospheric quiescent environment (23). Figure 5 illustrates the same two property variations for the case of an argon arc (24).

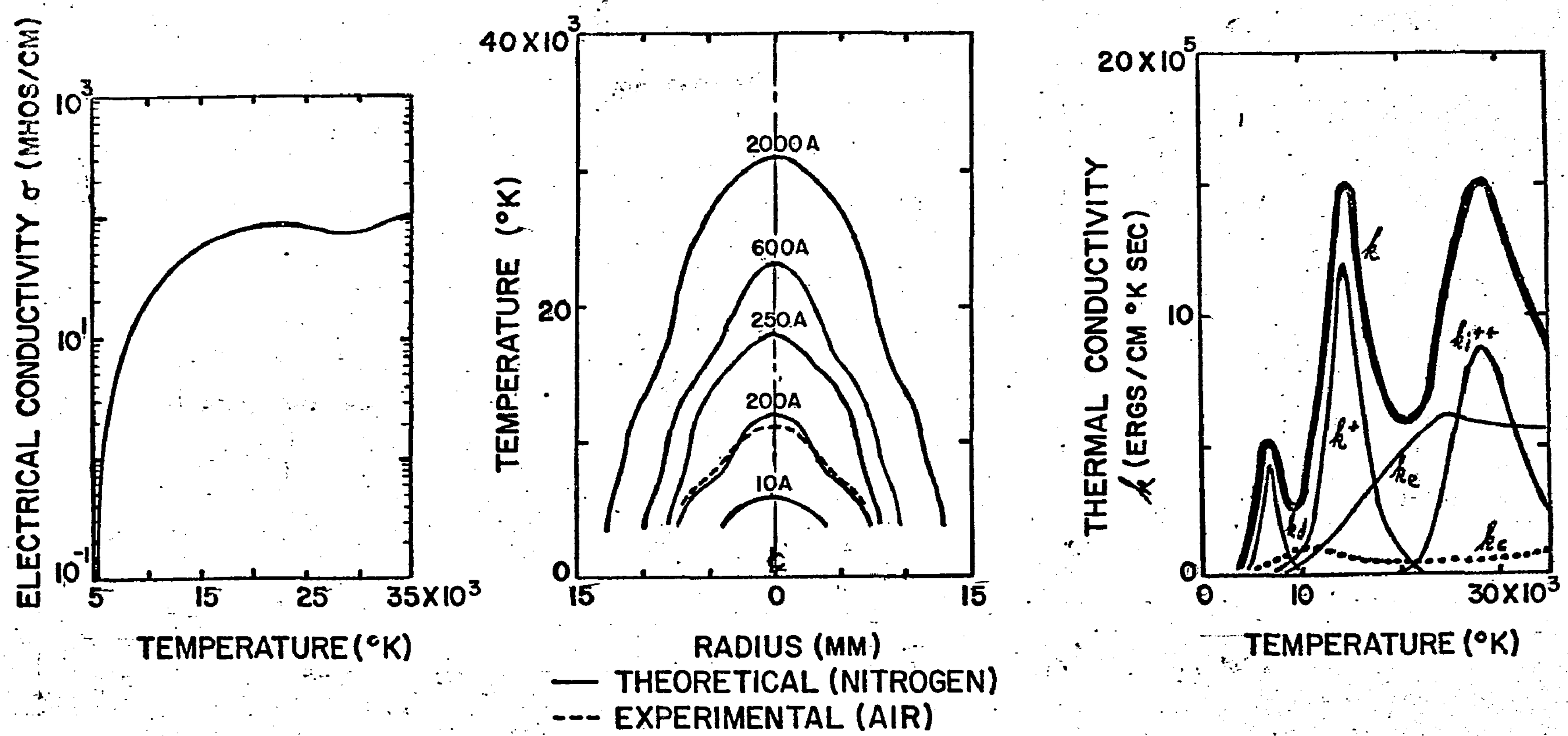

PROPERTY VARIATIONS OF A NITROGEN ARC, FREE BURNING IN AN ATMOSPHERIC QUIESCENT ENVIRONMENT

FIGURE 4

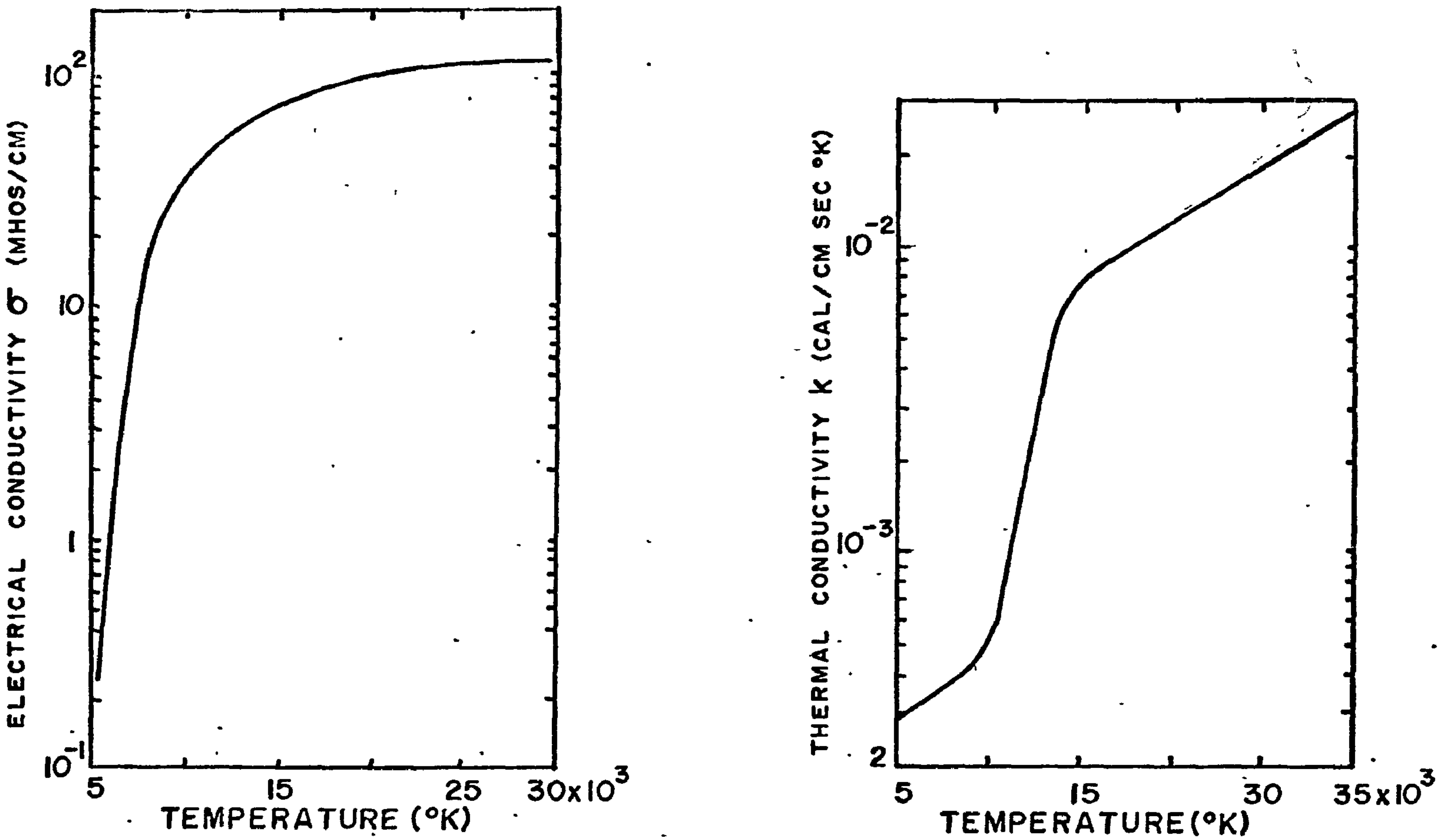

PROPERTY VARIATIONS OF AN ARGON ARC - FREE BURNING
IN AN ATMOSPHERIC QUIESCENT ENVIRONMENT

FIGURE 5

In Figure 4 the diagram on the far right shows the variation of thermal conductivity k of nitrogen with temperature. The heavy solid line represents the overall conductivity, while the remaining lines indicate the contributions of the various constituents of the gas e.g., k_e is the classical conductivity due to the drift motions of the electrons, k_d is the conductivity due to the diffusion of molecules and associated atoms, and k_i^{+} and k_i^{++} are the conductivities due to the diffusion of electrons and singly ionized atoms and of the electrons and doubly ionized atoms,respectively. The dotted line would indicate the thermal conductivity if nitrogen remained a simple molecular gas over the entire temperature range (i.e., the conductivity due to the microscopic motions of atoms and ions). However, because of the effects of dissociation, and single, double, or multiple ionization, the nitrogen plasma actually consists of a mixture of various gases. The peaks of the k versus temperature curve indicate the completion of each dissociation or ionization process with its associated energy absorption. The electrical conductivity σ versus temperature, shown at the far left of Figure 4, does not vary so drastically, and approaches uniformly its maximum value of approximately 100 mhos/cm. The reason for the reduced slope of the electrical conductivity with temperature above approximately 10,000 °K is mainly due to the influence of the large collision cross-section of the positive ions (and subsequent reduction in the mean free path of the electrons).

In Figure 5 the thermal conductivity k and electrical conductivity σ for an argon arc free-burning in an atmospheric quiescent environment is shown. By comparison with nitrogen (diatomic) the main distinguishing difference is the absence of dissociation.

The energy balance equation of the arc column

$$\sigma E^2 + \nabla \cdot (k \nabla T) - \rho \left(\frac{\partial h}{\partial T}\right)_P V \cdot \nabla T + \left[1 - \rho \left(\frac{\partial h}{\partial P}\right)_T\right] V \cdot \nabla P - R = 0 \quad (3)$$

designated the Heller-Elenbaas equation, expresses the balance between the generated joule heat and the heat dissipated by various means. By neglecting pressure changes, this equation reduces to

$$\sigma E^2 + \nabla \cdot (k \nabla T) - \rho C_P V \cdot \nabla T - R = 0 \quad (4)$$

The first term is the generated joule heat, the remaining terms are the heat conduction, heat convection, and radiation, respectively. The equation in this form is extremely complicated for mathematical solutions, therefore, numerous simplifying assumptions must be applied in order to solve it by analytic integration. Many investigators have assumed that the generated heat is dissipated only by radial conduction to the arc environment; therefore, the equation becomes

$$\sigma E^2 + \nabla \cdot (k \nabla T) = 0 \quad (5)$$

Further, if cylindrical symmetry is assumed, the equation may be written as

$$\sigma E^2 + \frac{1}{r} \frac{d}{dr} \left(rk \frac{dT}{dr}\right) = 0 \quad (6)$$

The gas properties, σ and k, must be known as functions of the temperature for solving the Heller-Elenbaas energy equation. The considerable mathematical difficulties in finding analytical solutions become more apparent when the radial temperature distributions are taken into consideration. A typical set of these radial temperature profiles for a nitrogen arc are shown in the middle of Figure 4. They span a current range from 10 to 2000 amperes.

For this simple form of the energy equation (Eq. 6), the radial temperature distribution and the temperature gradient along the positive column are functions of the heat dissipation. Therefore, increasing the radial heat transfer will result in increased peak temperatures and higher voltage requirements (i. e., higher power consumption/unit arc length). Therefore, any mechanism which improves the heat transfer from the arc to its boundaries will result in higher power density of the arc and higher peak temperatures for any given current input. This occurs if an arc column is confined and constricted within cooled cylinder walls or is acted upon by axial forced convection, axial vortex flow, or transverse forced convection. The wall constricted, axial forced convection, or axial vortex method of confinement (or any combination of the three) is currently being utilized in many of today's electric arc devices.

The theoretical treatment of the arc column confined and stabilized in a forced convection flow field is considerably more difficult than that of the free-burning case or the arc within cooled solid cylindrical walls.

By referring again to Figure 3 and the tabulation of arc data, one notes the considerable range of voltage gradients and energy densities which have been experimentally reported for the arc column. The lower limits correspond to arcs in the free-burning case; the upper limits were obtained under transient conditions for arc columns in a very high velocity parallel gas flow field (2).

Electrical Characteristics

Another important aspect to consider is that the electric arc, besides being an electrical gaseous heating element, is also a current carrying conductor with a definite voltage-current characteristic. The electric arc in steady-state operation is recognized by the familiar non-linear voltage versus current characteristic curve. A typical curve is shown in Figure 6. This curve is applicable to constant ambient conditions which may extend over a reasonably wide range. An immediate consequence of the negative characteristic curve is that a steady-state arc requires a stabilizing series resistance for operation in a constant electro-motive-force circuit.

Typically, the external characteristic circuit curve (see also Appendix B, Figure 63) will intersect the arc characteristic curve at two points, shown as (1) and (2) in Figure 6. Steady-state arc conditions can exist only at the intersection point (2), which is a stable equilibrium point. At point (2) a sudden perturbation in the current will give rise to a voltage unbalance tending to restore

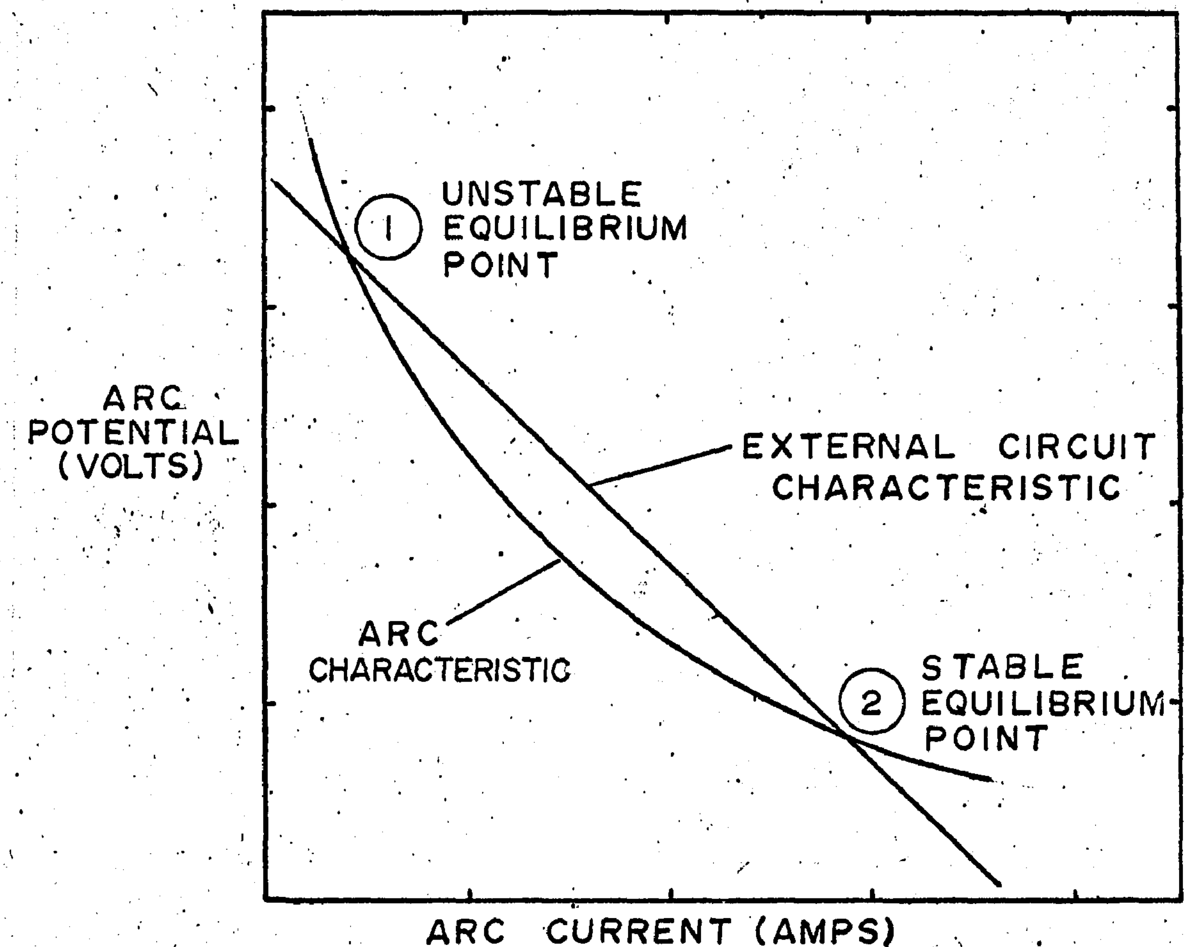

TYPICAL VOLTAGE - CURRENT STATIC
CHARACTERISTIC CURVE OF ARC
AND EXTERNAL CIRCUIT

FIGURE 6

equilibrium. The arc circuit stability is very much dependent upon the static characteristic behavior which in turn depends strongly upon the energy transfer from the arc column (affected by such factors as: convective velocity, ambient temperature, ambient pressure, external magnetic fields, electrode jet effects, column confinement effects, and motion of the arc relative to the surroundings). Thus, the thermal and electrical characteristics of electric arcs are directly dependent on one another, both being strong functions of the mechanism of energy transfer to the surroundings.

Self-Magnetic Field Effects

Since the arc is a current-carrying conductor it will generate magnetic fields, and will be subject to the effects of external magnetic fields. As a straight cylindrical conductor, the arc generates a "self-magnetic" field whose field lines are concentric circles around the arc column center line. Two conductors carrying current in the same direction will attract each other. Thus, if the arc column is considered simply as a collection of parallel current filaments, the attraction forces between these individual filaments will result in a radial-compression of the arc column. This is known as the "pinch-effect" and becomes appreciable at current levels of $\geq$ 1000 amperes (26). At these high levels of current, a radial pressure distribution is produced within the column proportional to the product of the current and the current density.

$$P_{(radial)} = \frac{I \cdot j}{c^2} \left(1 - \frac{r^2}{r_a^2}\right) \qquad P_{(axial)} = \frac{I^2}{Ac^2} \qquad (7)$$

where P = pressure

I = arc current

j = arc current density

A = arc cross-sectional area

r = arc radius

c = constant = 3×10^8 m/sec

The reader is referred to Maecker (26) for a detailed discussion and derivation of these jet effects. From these equations it can be seen that at a given current, the generated pressure depends on current density, therefore, at a region of constriction (e.g., electrode spot region) the internal pressure will increase accordingly. The pressure is highest where the current density is highest and, therefore, as one proceeds away from a constriction the current density falls and correspondingly the magnetic pressure. This difference of internal pressure at various arc diameters may result in an axial flow of plasma in a direction away from the constriction and toward the larger diameter. This is schematically shown in Figure 7. The ionized gas particles moving away from the constricted region sweep along neutral gas particles which are radially entrained inward from the surroundings. They become ionized, are magnetically transported toward the arc column center, and then accelerated in the

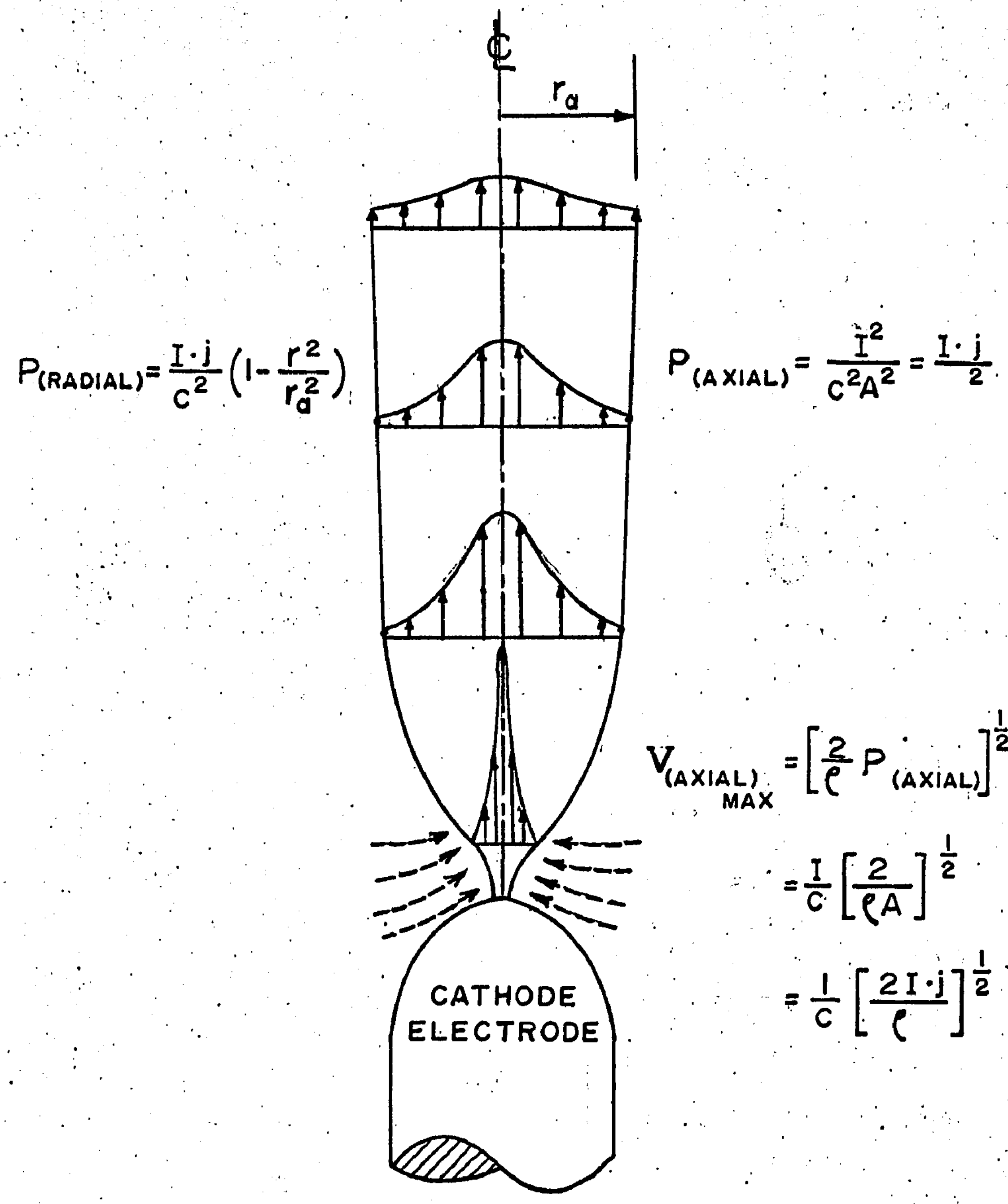

SCHEMATIC OF MAECKER JET RESULTING FROM SELF-MAGNETIC FIELD "PUMPING" EFFECT

FIGURE 7

axial direction as shown in Figure 7. The constriction region thus acts as a pump receiving its input power from the self-magnetic field. This shows up as a continual plasma jet along the arc column. The maximum velocities obtainable were found to be related by

$$V_{(axial)_{max}} = \left[\frac{2}{\rho} P_{axial}\right]^{1/2} = \frac{I}{C}\left[\frac{2}{\rho A}\right]^{1/2} \quad (8)$$

Velocities as high as 30,500 ft/sec have been obtained in extremely high current arcs (26). If the electrode surface melts, some of the metal vapor is entrained by the incoming neutral gas particles and magnetically pumped along the arc axis. This metal vapor contaminates the arc column and can greatly affect the voltage gradient, especially in the vicinity of the jet. This jet effect occurs at both the cathode and anode electrodes. These jets definitely affect the voltage gradient (cause it to rise), since more of the column is occupied by the self-magnetically generated axial gas flow which requires a greater voltage for the same current input. The strength of the jet depends on many factors. A predominant one is the arc column length. For a long column, frictional shear effects of the surrounding ambient environment rapidly decay the strength of the jet. Another predominant factor is the geometry and material of the electrode from where the jet originates. The temperature of the electrode, because of its direct effect on the local current density, also affects the magnitude of the jet. Several other factors must be taken into consideration.

1) Arc current level,

2) mutual impingement of jets from both the cathode and the anode,

3) electrode mechanism (thermionic or field emission or a combination of the two),

4) the electrode chamber configuration and associated presence of secondary flow fields. Since each of these effects are present to a certain degree in all electric arc devices, their elimination is impossible and assessment of their relative magnitude is extremely difficult.

The aspects of tensor conductivity need not be considered in the present investigation, since the magnitude of the externally applied magnetic field and transverse aerodynamic flow velocities are far too low for any appreciable effects to be noted.

III. HISTORICAL DEVELOPMENT OF STATIONARY ARC LITERATURE

Over the past 17 years many valuable and interesting investigations have been conducted related to the interaction of an electric arc with transverse aerodynamic and/or magnetic fields. The first related cross-flow investigation was done in Leipzig, Germany, and reported in 1949 in the classic article by Weizel and Rompe (28). This theoretical investigation, however, was directed primarily at the effects of free convection on a free-burning horizontal electric arc. The possibility of balancing a convective velocity on an arc with a magnetic field in order to cause it to remain a straight body was mentioned.

Little if any work was reported during the next five years until a report was published in 1954 by Smith and Early (29). This was an experimental investigation to determine the feasibility of heating an air stream in a wind tunnel by means of an electric arc. This was the first reported experimental study where an external magnetic field was used to oppose the aerodynamic forces of a supersonic flow on the arc column. An unusual characteristic slant angle of the column, with respect to the electrodes, was observed.

In 1957, Rother (30), in Germany, applied the energy equation to a horizontal electric arc subject to an upward convection to gain information on arc curvature and temperature distribution. This was the first paper to question the validity of the work of Weizel and Rompe.

In 1959 Thiene (31) published an extensive experimental and theoretical study of the flexure of an electric arc under forced convection. An analogy was made between the convected arc and the distributed load on a structural beam. An energy balance provided arc curvature, temperature distribution, a so-called flexural rigidity, and blowout criteria. This investigation set the pattern both theoretically and experimentally for much of the work that followed.

A Russian article by Serdyuk (32) concerned with a welding arc in a transverse magnetic field appeared in 1960. This was comprised of both an experimental and an analytical portion. A force balance was applied to a deflected arc column,and this was used to calculate the stability limit of the arc and the magnitude of the bowing due to the external magnetic field.

In 1961 some preliminary work was done by Chen (33) on a theory for an arc positive column subjected to a transverse gas flow. The column was assumed to behave as a solid cylinder and by applying the steady-state energy equation, it was shown that the arc may be stable or unstable depending on the perturbation introduced. At this same time, Sherman and Yos (34) conducted an analysis of scaling laws for electric arcs subject to forced convection. Numerous assumptions were made and the analysis was tested experimentally. The results indicated the importance of certain parameters in the forced convection arc.

From 1961 until the latter part of 1963 little was reported until Lord (35) in England published a theoretical investigation of some magnetofluiddynamic problems involving electric arcs. A portion of this report included a magnetically balanced arc in cross-flow. A solid body analogy was made and by applying conservation equations, Ampere's law, and Ohm's law, the arc characteristics were obtained in non-dimensional form.

Toward the end of 1963 two Russian scientists, Alferov and Bushmin (36), conducted an experimental investigation of an arc discharge across the exit of a convergent-divergent nozzle at both subsonic and supersonic flows. The results included photographs of the form of the discharge as well as current and voltage characteristics.

By 1964 keen interest had been aroused and focused on the electric arc interacting with both aerodynamic and magnetic fields. This was primarily motivated by the immediate aerospace applications as discussed previously in Section I. The first reported research in 1964 was that of Kalachev (37) in Russia. His investigation was an extension of the work of Alferov and Bushmin with the same apparatus being used. This was again mainly a photographic study of a pulsed arc discharge.

Fay (38) published a short note as a comment on the previously reported work of Thiene.

Bond (39) published a series of papers concerning the magnetic stabilization of an electric arc in supersonic flow. These were primarily experimental observations of the arc column configuration. One interesting observation was that the arc had a characteristic slant angle between the electrodes with the anode root always upstream of the cathode root. Unfortunately, the explanations given for this slant were quite speculative, and no final conclusions could be reached.

An investigation was started by Hogan (40), and later continued by Malliaris (41) on an experimental and analytical study of the fundamental interaction and energy exchange process between electric arc discharges and cross-flow fields of preionized gases both with and without the presence of external transverse magnetic fields. The objective was to examine the phenomena taking place in the $\overline{J} \times \overline{B}$ region and obtain information on the appearance and behavior of the discharge under varying conditions.

Baranov and Vasileva (42) of the USSR published a report on an electric arc struck across a high velocity cross-flow of argon. They suggested application to a non-equilibrium magnetohydrodynamic generator. Velocity, shape of the luminous region, and other arc characteristics were experimentally measured by high-speed photography.

Lord (43) of England published a paper concerning the effects of a radiative heat sink on arc voltage-current characteristics of a cross-flow arc stabilized by an external magnetic field. The characteristics were expressed in a non-dimensional form which showed the importance of different parameters. Numerical examples, based on some published magnetically-driven arc rail-type experiments showed the heat loss from the arc bore little resemblance to that due to forced convection from a solid cylinder.

Anderson (44) reported an analytical and experimental study on the Hall effect and electron drift velocities in the plasma of a positive column under the influence of an external transverse magnetic field. The arc column was confined within a cylindrical tube in which probes were used to measure the Hall voltage and column gradient.

Following Anderson was a purely theoretical investigation by Ecker and Kanne (45), in Germany, of a cylindrical plasma conductor in a transverse magnetic field. This investigation was limited to small magnetic fields which allowed linear perturbation theory to be applied to the two cases of a collision dominated and collision free plasma.

By the start of 1965 there appeared to be on an average of almost one publication every few months treating the cross-flow arc problem both with or without external magnetic fields. The first of these was Broadbent (46) in England, who published a technical report on a theoretical exploration of the flow about an electric arc transverse to an air stream using potential flow methods. The conservation equations were applied to the arc which was treated as a source and a heat sink was assumed in the flow downstream. This model, however, gave unrealistic temperature distributions.

Paralleling this work, Lord and Broadbent (47) in England, published a report on an electric arc across an air stream. The paper discussed an electric arc in a transverse subsonic air stream held stationary by an external transverse magnetic field. Non-dimensionalized arc characteristics were obtained and the theory was compared with experimental annular gap traveling arc data of Adams (48), also of England. The conclusion was that the solid cylinder analogy is not very satisfactory.

Olsen (49) published a report concerning a series representation method for inverting externally measured asymmetrical spectral intensity distributions to true radial distribution of the emission coefficients for optically thin sources. The method was successfully applied to both analytical and experimental data. The experimental portion dealt with the interaction of a preionized transverse gas flow with an electric arc.

Broadbent (50) published another report concerning electric arcs in cross-flow. The experimental portion was a rail accelerator setup, but the analysis of heat transfer aspects and comparison with the solid cylinder analogy links the results closely to the cross-flow category. Useful similarity laws were also derived.

Noeske (51) presented analytical work on the behavior of an arc in cross-flow. The porosity of an arc in cross-flow was examined as a function of temperature and properties of the gas. Temperature fields were compared with solid heated cylinders and horizontal free-burning arcs with natural convection. Analytical expressions and a stability criterion were developed which related the geometrical, electrical, and thermodynamical parameters of the arc current-sheet model.

Myers (52) published a paper concerning an investigation of a magnetically balanced electric arc in a transverse argon gas flow. This was an experimental study of an electric arc in crossed convective and magnetic fields. The arc was found to behave similar to that of a solid cylindrical drag body. The application to non-equilibrium conductivity was also discussed.

Kookekov (53), in Russia, published a paper treating the mechanism of heat transfer in transverse blown arcs. The motion of an electric arc with transverse blowing and a perpendicular magnetic field was studied. Experimental data were obtained on the arc velocity and characteristics. A theoretical analysis was also included using conservation of energy, Ohm's law, and the minimum principle.

The results indicated that by excluding radiation and heat conductivity, the energy transfer is primarily by means of turbulence i.e., there is turbulence within the transverse blown arc.

Schrade (54) presented a paper on arc pumping and the motion of electric arcs in a transverse magnetic field. This was a theoretical study concerned with calculating the transverse forces which act on an arbitrarily curved current-carrying conductor in a transverse magnetic field. The arc motion was concluded to depend on the external magnetic field, the self-magnetic field, and the curvature of the discharge axis.

To complete chronologically the historical development of the investigations up to 1966, three other studies, which are currently being conducted, shall be included. Benenson (55) is investigating the effects of low velocity forced convection upon the steady-state characteristics of electric arcs. He is primarily interested in the arc shape, curvature, voltage gradient, and temperature distribution (asymmetrical) within the arc. An experimental technique is being employed to determine the arc shape and local integrated intensity of the arc radiation. Following this phase will be an analytical determination of the asymmetrical temperature distribution within the arc column using information gained from the experimental phase.

Fischer (56), in Germany, is investigating interactions of an electric arc with transverse magnetic and gas flow fields. This is an analytical study of the arc discharge cross-section, temperature distribution and mass flow distribution, which occurs in transverse external fields. Work to date has been on a confined arc in a transverse magnetic field and an arc under transverse convection. Preliminary calculations have provided temperature distributions and flow fields.

Han (57) is investigating the convective heat transfer and arc curvature in cross flow. This is an analytical study directed between the two asymptotic cases of a solid cylinder (no penetration) and a completely porous cylinder (full penetration). The first portion of the study deals with establishing the asymptotic size of the vertical arc core based on a heat dissipation viewpoint. The convective heat transfer correlations are solved using a numerical integral method. One portion of the study is concerned with establishing the radiation loss from the arc column. Another portion considers an approximate analysis of the asymptotic column growth for turbulent flow.

General Summary of Stationary Arc Phenomena

Experimental Studies

The number of experimental studies which have been made on the stationary arc is too few to allow definite conclusions to be reached, but only trends to be indicated. The investigations of the stationary arc in supersonic flow have generated more questions than they have answered. For instance, why does the arc assume a characteristic slant and why does it show the strong preference for the boundary layer of a supersonic tunnel? Little progress has been made toward understanding the nature of the stationary arc's interaction with the supersonic flow. No localized property measurements have been made in the arc or in the gas stream near the stationary arc region.

Similarly, the stationary arc in subsonic flow has been the subject of only a few investigations. However, relatively more trends can be indicated than for the supersonic case. The studies to date have spanned a large range in velocity and magnetic field strength and all indicate that the velocity is approximately proportional to $\sqrt{B}$. Thus, the analogy of the conducting cylinder with aerodynamic drag appears to be the best model for the stationary arc at present.

All of the stationary arc studies in subsonic flow have been of a preliminary nature, and no measurements have yet been made at the boundary between the arc and flow to show the energy exchange mechanisms or inside the arc to determine its internal structure. Reason compels one to expect the stationary arc interactions in these regions to differ significantly from the conducting cylinder analogy. Considerable work is also needed at different pressure ranges and with different gases.

Theoretical Studies

As a consequence of reviewing each of the directly pertinent investigations in detail, some general features and effects of the cross-flow phenomena (both with or without external transverse magnetic fields) which any generally acceptable complete theory should explain for the high pressure case are listed below. In some parameter ranges, several of these effects may be neglected. (It should be re-emphasized that the cross-flow arc interaction phenomena, both with or without external transverse magnetic fields, which have been reported in the literature were determined with a variety of electrode and external field configurations and also under vastly different parameter ranges. Therefore, any correlation between the many different investigations is extremely difficult.)

Cross-flow only

1) Arc curvature (including blow-out criteria),

2) arc cross-sectional shape,

3) electrode material effect,

4) electrode shape and arrangement effect,

5) electrode jet effects (with corresponding induced axial gradients),

6) free-convection effect,

7) drag effects,

8) heat transfer effects,

9) temperature distribution,

10) property variations as a function of temperature,

11) effect of enclosing the arc with channels of different geometry.

Cross-flow with external transverse magnetic field

In addition to those effects listed under cross-flow only, the following are present:

1) External magnetic field interaction,

2) self-magnetic field interaction, and

3) the electrode field interaction effect.

The theory, in addition to describing the above effects, should then clarify some of the following areas:

1) Pervious versus solid body model (or a combination of the two),

2) occurrence of internal double-vortex (including shear effects at boundary),

3) laminar or turbulent flow (both within and surrounding arc column), and

4) mechanism of heat transfer inside the arc, through the boundary, and to the external flow.

IV. DESCRIPTION OF EXPERIMENTAL APPARATUS

The cross-flow arc test facility was designed by the author and fabricated by personnel within the Aerospace Research Laboratories. An exception was the iron-core electromagnet. The specifications were prepared by the author, but it was more economical to purchase the basic magnet from a commercial source.

Since it is felt that the detailed design of the apparatus is pertinent to the results of this investigation, it will be included. The description of the experimental apparatus was divided into three parts:

A. Primary Components.

B. Instrumentation and Support Equipment.

C. Diagnostic Equipment.

A schematic drawing of the overall experimental apparatus arrangement is shown in Figure 8. A photograph of this arrangement is shown in Figure 9.

A. The primary components consisted of the following sub-systems:

1. Electrode Assembly and Starter.
2. Magnet.
3. Blowing Nozzle Assembly.

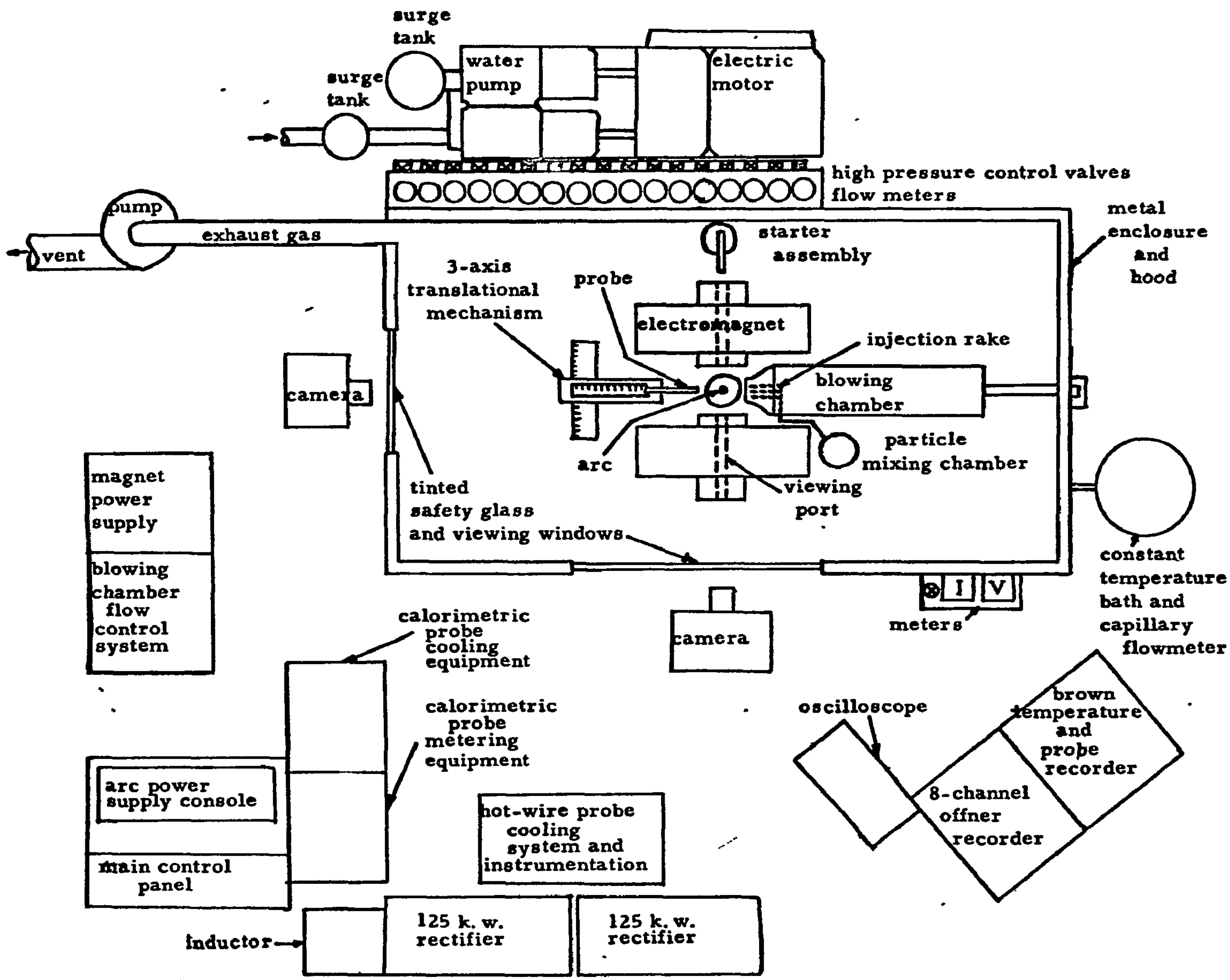

FIGURE 8 ARRANGEMENT OF EXPERIMENTAL APPARATUS

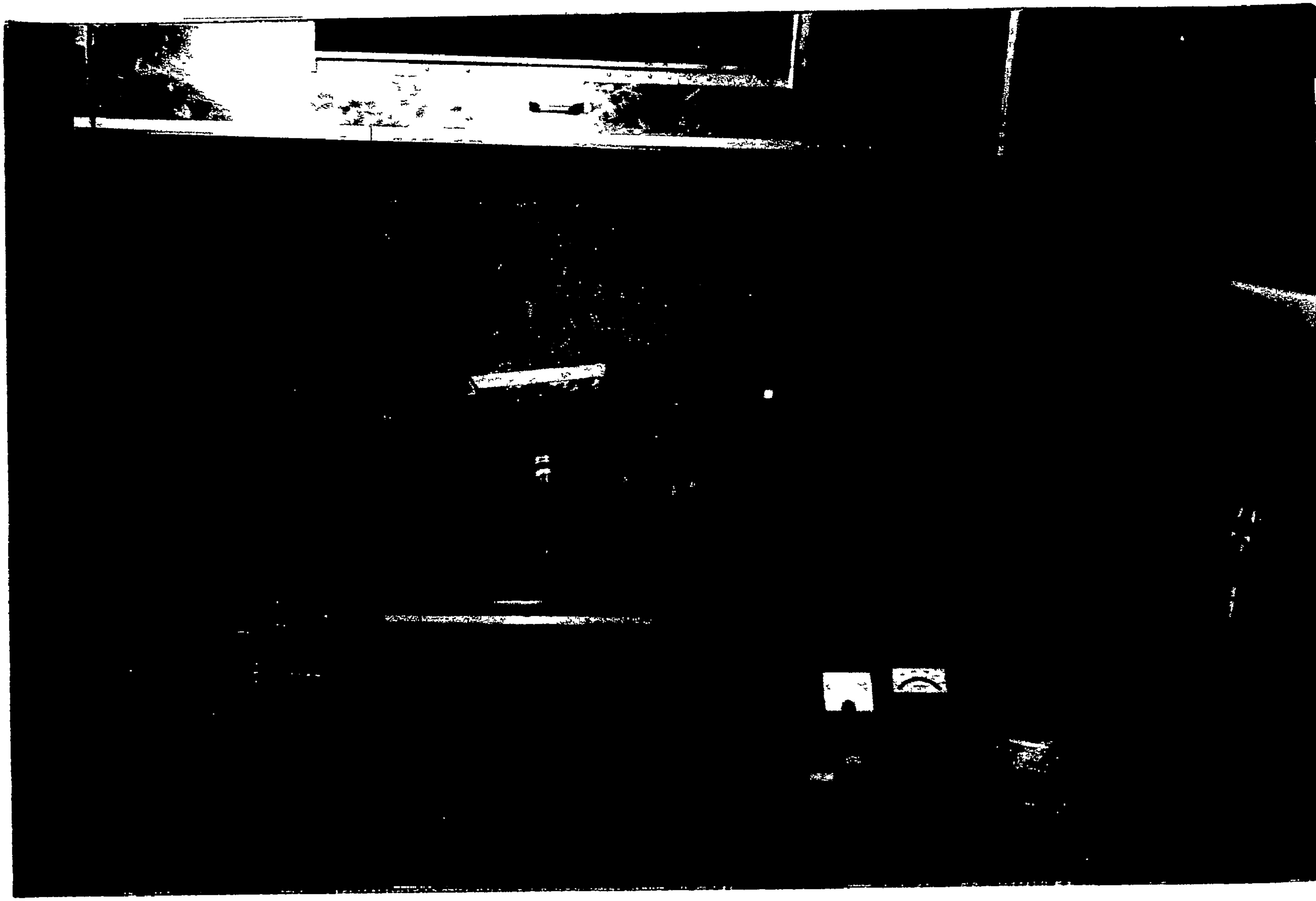

FIGURE 9. PHOTOGRAPH OF EXPERIMENTAL APPARATUS

Each of these subsystems will now be discussed in some detail.

1. Electrode Assembly and Starter.

Figure 10 is a full-scale drawing showing the electrode assembly. The cathode was the lower electrode in all tests. The cathode was a 1/4-inch diameter, two per cent thoriated tungsten cylinder with a hemispherical tip. This 1/2-inch long tungsten slug was recessed and silver soldered into a water-cooled copper base mount. (See Appendix D, Figure 65.) Surrounding the cathode was a gas injector made of brass with four equally spaced, 0.013-inch diameter, injection ports bored through it. (See Appendix D, Figures 66 and 67.) This injector provided a small quantity (approximately 1 lb/hr) of non-oxidizing argon gas necessary to prevent rapid oxidation of the tungsten cathode. The injector disc was insulated from adjoining parts with boron nitride spacers. The cathode gas injection flow system is shown schematically in Figure 11. The gas flow from the high pressure supply was controlled by a pressure regulator and a check valve. Closing the check valve permitted changing the gas bottles at the high pressure manifold without losing pressure and gas in the low pressure reservoir. The low pressure reservoir, used to ensure a large, constant pressure gas supply, was a stainless steel tank of three cubic feet capacity. The reservoir was kept at a pressure of 30 psig and monitored by an attached pressure gage. The reservoir was tested to 75 psig, and a safety valve

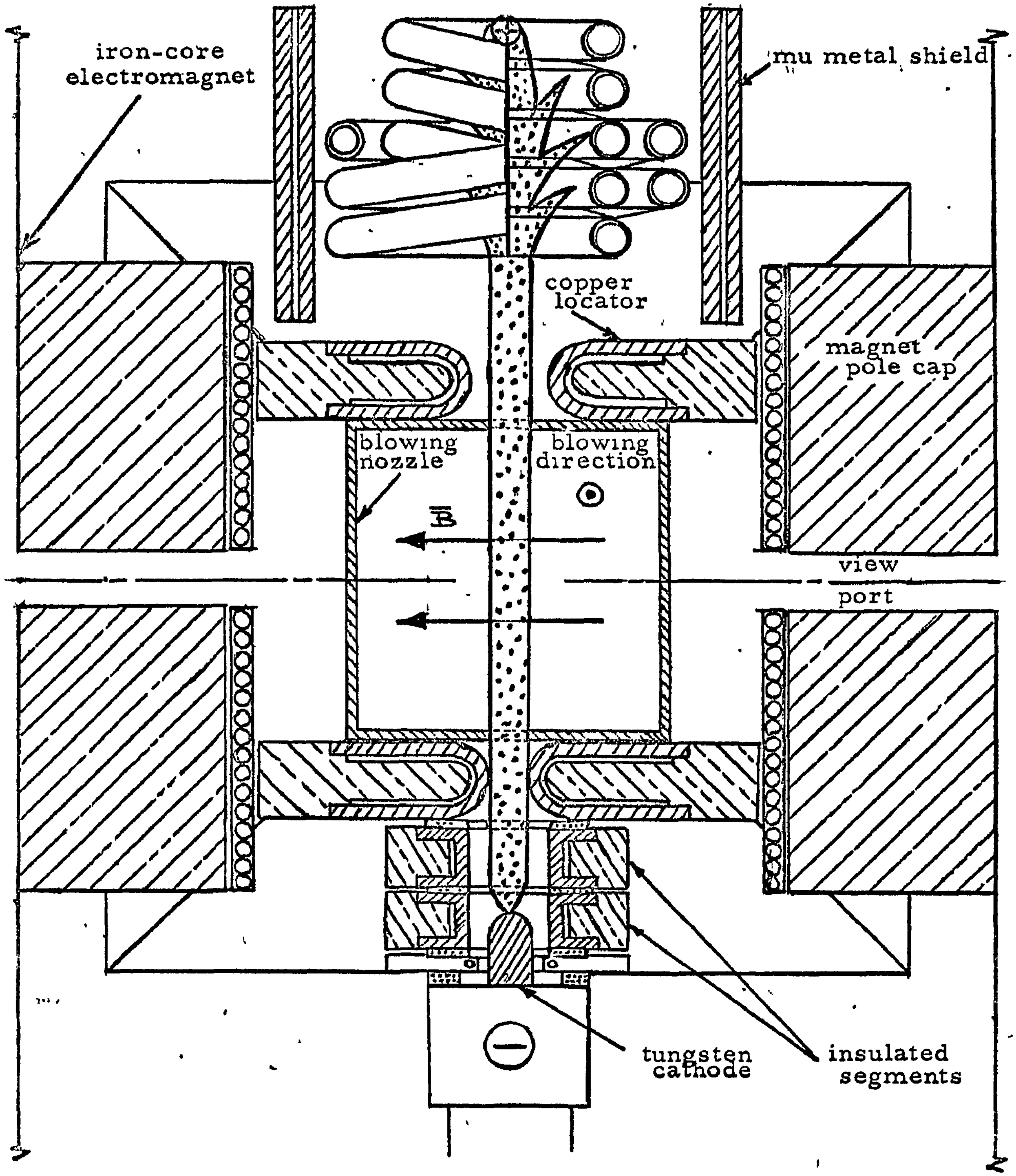

UPSTREAM VIEW OF CROSS-FLOW ARC TEST SECTION
FIGURE 10

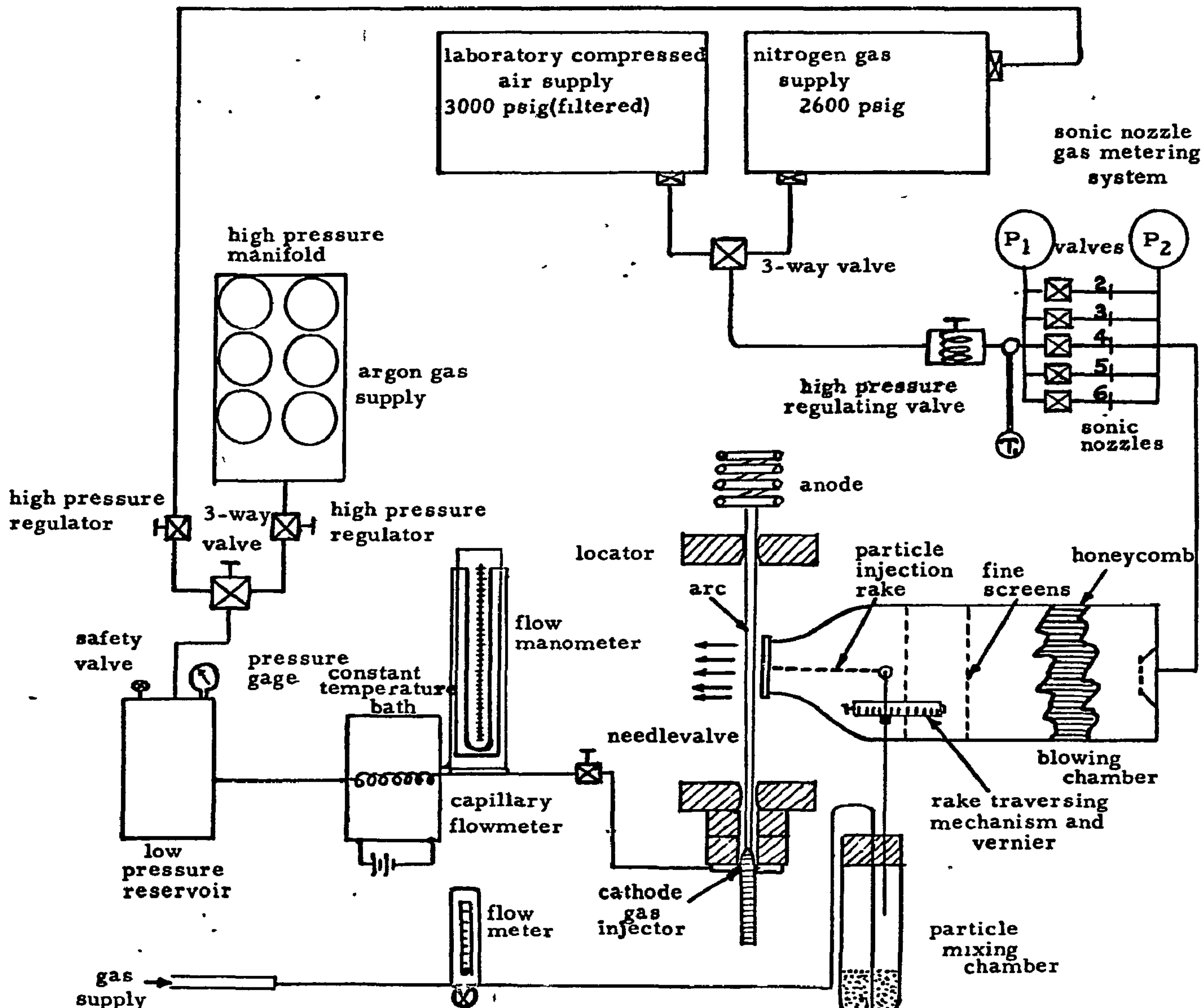

FIGURE 11 SCHEMATIC DIAGRAM OF GAS FLOW SYSTEMS AND PARTICLE INJECTION SYSTEM

was installed to blow at 60 psig. From the reservoir the gas flowed to a coiled capillary flowmeter, which was kept in a constant temperature bath. The pressure drop through the coil was measured with a U-tube water manometer. A calibration curve for argon mass flow through the coil as a function of the U-tube manometer pressure differential reading is included in Appendix B, Figure 55. The constant temperature bath consisted of a heavy galvanized can. The temperature of the bath, set at 78 °F, was maintained by an automatically controlled temperature regulator. The mass flow to the cathode injector was controlled by a Hoke needle valve.

Stacked directly above the gas injector were two water-cooled calorimeter segments. (See Appendix D, Figure 68.) These were made of copper with a 3/8-inch diameter centered hole. They remained at a floating potential, being electrically insulated from each other and adjacent segments by discs of boron nitride surrounded by a silicon rubber seal. Above the upper calorimeter segment was a water-cooled copper locator. (See Appendix D, Figure 69.) Its purpose was three-fold; it provided a transition section between the gas within the cathode chamber and the external environment, helped in locating the arc with respect to a reference centerline, and served as a potential probe for measuring the voltage. (The voltage gradient between the locators was also measured with a separate water-cooled probe.) The convergent-divergent shaped hole through the locator minimized the erosion of the upper and lower edges directly exposed to the arc. The hole diameter of 1/4 inch was chosen to reduce pinching or restricting the effective arc column diameter. The entire cathode assembly was clamped together and sealed as shown in Figure 10. Positioned two inches above the first locator was a second locator identical to the first with the exception that it had a 1/2-inch diameter hole. This again served the purpose of providing a centerline frame of reference through which the arc column could pass on its path to the anode. The reason for the increased hole diameter in the upper locator is discussed in Appendix E. The final design of the copper, water-cooled locators was governed by several factors:

a. The most effective cooling of the inner hole region occurred when the high-speed water flows meridianally over the inner passages.

b. The arc tended to attach itself to any silver solder in its vicinity; therefore, the use of silver solder needed in locator fabrication was minimized.

c. The locator must be as well cooled on the bottom face exposed to the test section as it is in the hole region. This was because a misadjustment of the aerodynamic or magnetic forces could momentarily drive the arc column away from the center position and might lead to locator burnout.

The anode assembly used was arrived at after many optimization studies of alternate anode designs (see Appendix E for discussion.) It was composed of a specially wound helical coil of 1/4 inch o.d. copper tubing (Figure 10). By winding the coil such that the arc interaction with the magnetic field of the coil drove the anode spot circumferentially and at the same time upward around the helical path provided a simple and most effective anode. By magnetically driving the anode spot at high speeds over the anode surface, the very high heat load of the anode spot region was spread over a significantly larger path so that the high pressure cooling water flowing through the anode could effectively remove the heat and prevent local melting. This anode performed satisfactorily at currents up to 600 amperes. The average lifetime of an anode was 45 minutes. A high-speed photograph of the anode spots is included in Appendix E (Figure 70). To provide both an aerodynamic and magnetic shield around the anode coil, a cylindrical water-cooled mu metal shield was fabricated. Due to the influence of the external transverse magnetic field, this protection was necessary or anode burnout resulted at the highest range of testing. The distortion effect of the mu metal shield on the external magnetic field in the test section region was less than three per cent.

The arc was initiated by employing a secondary carbon-tipped rod anode which made contact with the cathode tip,and was then rapidly withdrawn upward through the coiled anode. In this way the arc was drawn upward until it reached the level of the anode. It then transferred from the secondary starting anode to the primary coiled anode as the starting anode continued upward and was rapidly moved away. The starter actuator was a spring-loaded retraction device released by a solenoid and synchronized to follow the main arc power initiation. This method proved to be extremely reliable and eliminated the contamination, which would be given off by an exploding wire starting technique.

2. Magnet

The iron-core electromagnet was designed to provide the necessary external magnetic field anticipated to balance the aerodynamic forces on the arc column. Due to the physical accessibility required for the diagnostic probes and blowing nozzle, the open yoke magnet design was selected. Figure 12 shows the magnet and mounting assembly (also see Appendix D, Figure 64). The optimum field intensities and homogeneity required, commensurate with the accessibility needed within the test section were obtained with a 4-inch air gap and 4-inch diameter cylindrical pole caps. This gap allowed blowing nozzle access and sufficient clearance downstream of the test section for the traversing probes. A 3/8-inch diameter view hole was drilled through the magnet pole pieces and caps to permit viewing of the arc column when it was in the balanced vertical position. Appropriate shims were added to compensate for the bore-hole effect on the magnetic field uniformity. Low-impedance magnet coils were selected which matched the d. c. power supply available. In order to

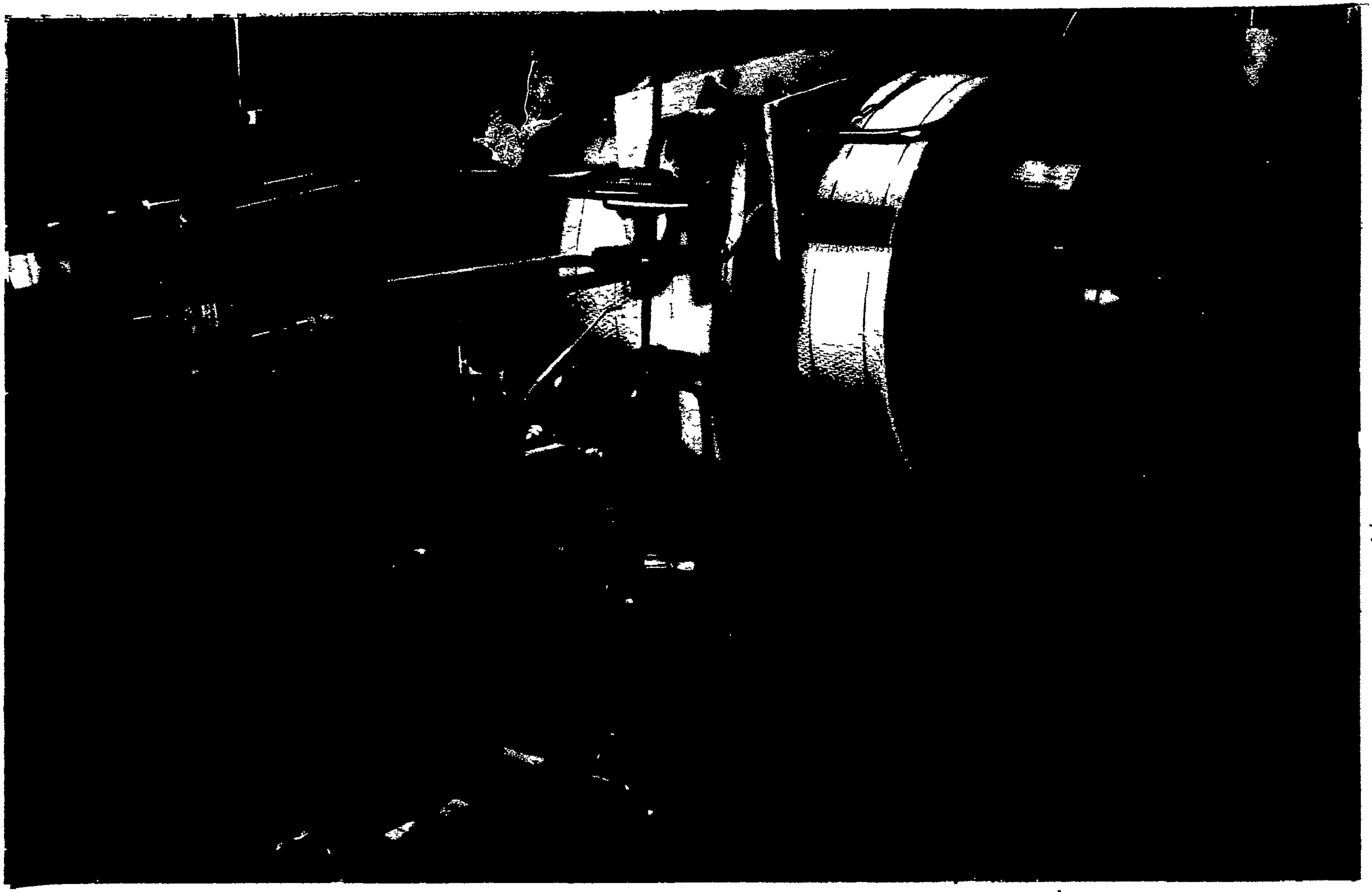

FIGURE 12. ELECTRODE ASSEMBLY, ELECTROMAGNET AND PROBE TRAVERSING MECHANISM

provide a magnetic ramp for the arc to be driven against as it was blown downstream, specially shaped iron pole-caps were fabricated which afforded a slight monotonically increasing magnetic field in the downstream direction (approximately five per cent per inch). In this way the arc could be positioned at any desired location in the test section, specifically at the centerline of the transverse view hole.

The field intensity within the test section was calibrated with a gaussmeter as a function of input power supply current level. A Hall element Bell gaussmeter Model 110 with adjustable ranges between 1 to 30,000 gauss was used with a transverse probe. The calibration curve is included in Appendix B (Figure 59). A built-in calibration unit was used, and this provided an accuracy of ± two per cent of full-scale reading. A special vernier mount and probe holder were constructed to allow accurate flux plotting. Plots of the field intensity and homogeniety are included in Appendix B (Figures 57, 58). Before each test the magnet was nulled by reversing the field.

A traversing slide was built upon which the entire 500 pound magnet assembly could be indexed into place. This provided accessibility in replacing components, allowed preliminary investigations on the arc column to be done without the magnet in place, and protected the magnet from the high heat loads during shake-down tests. The slide also enabled the entire electrode assembly to be visually checked for misalignment, damage, or water leaks before actual testing commenced. Figure 13 shows the magnet assembly indexed to the test position.

Sufficient insulation was applied to protect all exposed surfaces of the epoxy coated magnet coils from the high temperature arc column. A coating of Fiberfrax (asbestos-ceramic material) insulation, 1/4-inch thick, covered the major portion of the exposed area. The two most critically exposed areas were the pole caps themselves and the region immediately adjacent to the anode. Special water-cooled copper heat shields were fabricated to protect both these critical areas. A thin layer (1/16-inch thick) of Saureisen high temperature and high electrical resistance paste and Carborundum QF-150 asbestos-ceramic cement applied to the surface of these areas adequately provided additional heat and electrical insulation. The insulated magnet pole faces were located 1-5/8 inches either side of the balanced arc centerline. The cooling water to the magnet coils and the heat shields was sufficient to remove the heat generated. Thermocouples were located at critical areas to monitor the cooling water temperature. These temperatures were registered automatically on a recorder and in the event of excessive temperature, the experiment was shut down and the source of trouble eliminated.

3. Blowing Nozzle System

A schematic diagram of the blowing nozzle system is shown in Figure 11. It consisted basically of the subsonic blowing nozzle assembly, the gas metering and regulating system, and the high

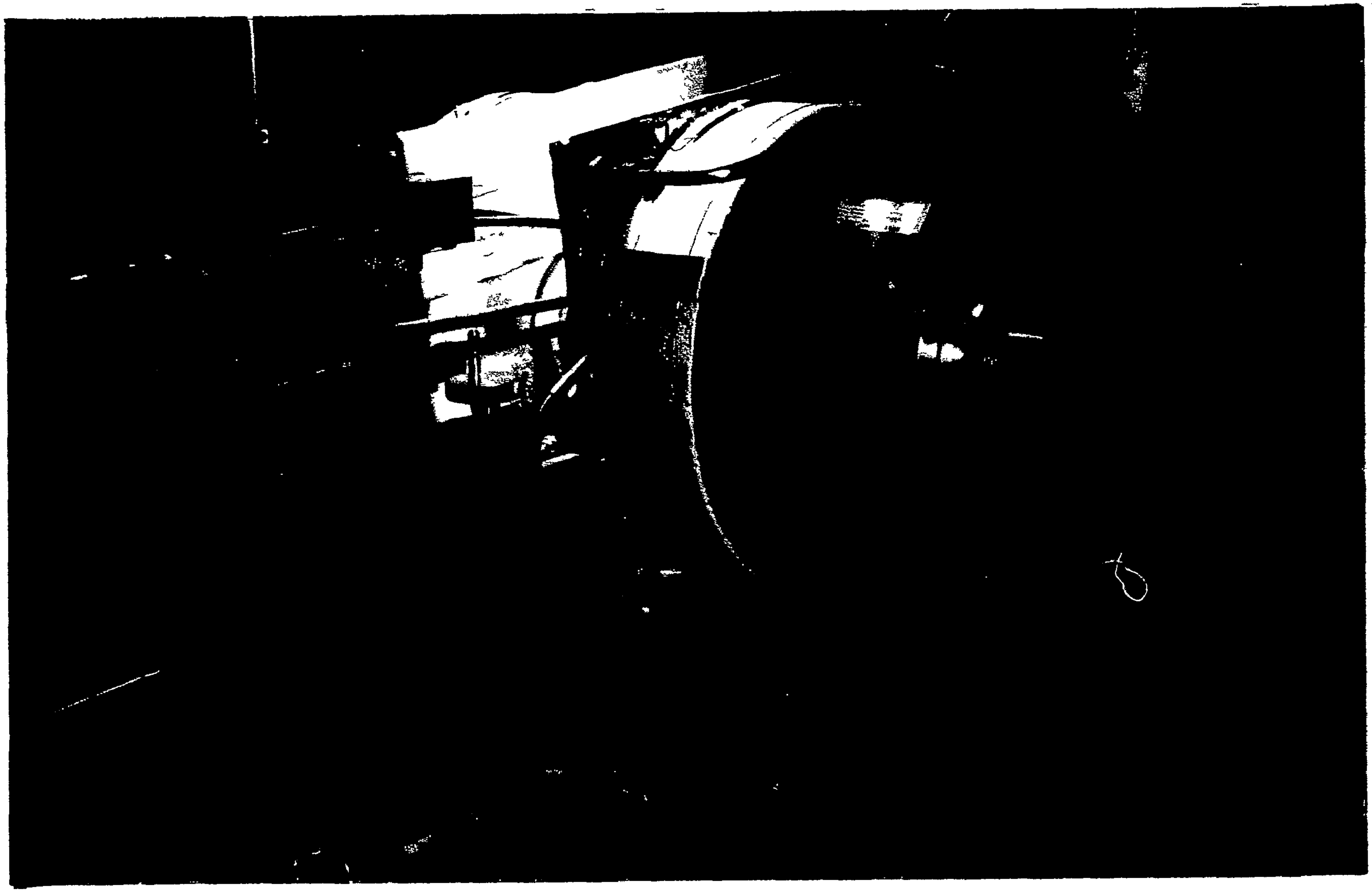

FIGURE 13 ELECTROMAGNET INDEXED INTO TEST POSITION

pressure gas supply system. The blowing nozzle assembly was fabricated from 1/16-inch brass plate. The convergent nozzle design was adapted and scaled down from an existing subsonic nozzle which was experimentally determined to have a flat and uniform velocity profile. It was 24 inches in overall length and had a square cross-section of 25 square inches. The nozzle exit area was two inches square. A baffle plate was positioned slightly downstream of the gas inlet. A series of honeycomb (3/16 inch pore diameter) and fine grid screens were placed at intervals along the tunnel portion from the inlet section to near the nozzle end to straighten the flow and reduce turbulence. Care was taken in the fabrication and positioning of all honeycomb and screens since it was desired to have as flat, uniform and non-turbulent a velocity profile as possible at the test section station where the arc column would exist. The velocity profiles at the test section station and blowing nozzle exit plane were measured both by a pitot-static probe and a hot-wire anemometer. Plots of the velocity profiles at both stations are shown in Appendix B (Figures 60, 61). A water-cooled nozzle shroud surrounded the nozzle exit because of the near proximity of the nozzle exit to the arc column. The remainder of the exposed nozzle assembly was coated with a thin layer of QF-150 cement. The blowing nozzle assembly was aligned perpendicular to the magnet axis and the arc centerline and rigidly mounted to the electromagnet.

Electrical insulation was provided so that the entire assembly was at a floating potential. The rigid mounting of the blowing nozzle assembly to the electromagnet allowed the nozzle to be indexed into test position simultaneously with the electromagnet. Figure 13 shows the test apparatus as it was positioned during a test on the balanced arc. When indexed into the test position, the blowing nozzle was 1-1/2 inches upstream of the arc centerline.

A sonic nozzle gas metering system was used in conjunction with the high pressure compressed gas supply to afford accurate metering of the gas flow. The upper right portion of Figure 11 depicts the basic assembly, and Figure 14 is a photograph of the sonic nozzle system. A series of 5 sonic nozzles, of increasing throat size from 0.024 inches to 0.102 inches, were arranged in a parallel connection. Each was provided with an individual shut-off valve. Stagnation pressure and temperature recorders were located upstream of the nozzle assemblies. A pressure gage was also located downstream of the nozzle to insure choked conditions at the throat. A main pressure regulating and relief valve was situated upstream of the nozzles to reduce the pressure head in the high pressure supply to the range desired for test operation. The high pressure gas supply was obtained from the laboratory filtered, compressed air supply system. The main supply pressure was maintained at approximately 3000 psi. The calibration plots for the sonic nozzle

FIGURE 14 SONIC NOZZLE SYSTEM

system and the test section velocity as a function of the stagnation pressure and temperature are included in Appendix B (Figures 56, 62).

B. The instrumentation and support equipment consisted of the following subsystems:

1. Arc Power Supplies,

2. Auxiliary Power Supplies, Ventilation System, and Shielding,

3. Cooling Water Supply System,

4. Recording Equipment,

5. Cameras.

1. Arc Power Supplies

The d. c. arc power was supplied by two A. O. Smith three-phase transformer-type power supplies employing a three-phase silicon bridge. The power supplies were connected in parallel. The current control was provided by the use of moving-coil type high reactance transformers with the coil coupling controlled by a gear motor drive. The units were operated by a remote start-stop and raise-lower push button control. Current output was selected by the raise-lower control which operated the gear motor drive of the moving primary coils. The output rating per rectifier unit for continuous operation was 500 amperes at 250 volts, equivalent to 125 kw. Open circuit voltage was 500 volts. A characteristic curve for this rectifier is included in Appendix B, Figure 63. An inherent property of a moving coil transformer type rectifier is the relatively high power ripple level. In an effort to reduce this, a large water-cooled coil of 3/8-inch o.d. copper tubing was wound. This served as an inductor when placed in series with the power supplies. The total resistance of the inductor was 0.2 ohms and the inductance was 12 millihenries. The power ripple was reduced from 12 per cent to approximately five per cent by this inductor.

2. Auxiliary Power Supplies, Ventilation System and Shielding

The electromagnet coils were energized by a d.c. Varicell of 0.5 kw output. The current regulation was controlled by a manual crank selector.

The electromagnet positioning linear actuator was powered by a 0.3 kw Labpack d.c. rectifier. The current regulation from 0 to 10 amperes was set manually by a selector knob. A schematic diagram of primary and auxiliary power supply systems is shown in Figure 15.

A vacuum duct ventilation system was used to remove all gas emitted in the housing during arc operation. The system was rated at 900 cfm.

Due to the amount of strong ultraviolet radiation given off by the arc, sufficient safety shielding was positioned both at the downstream and side view positions of the apparatus to allow visual observation of the arc column at all times.

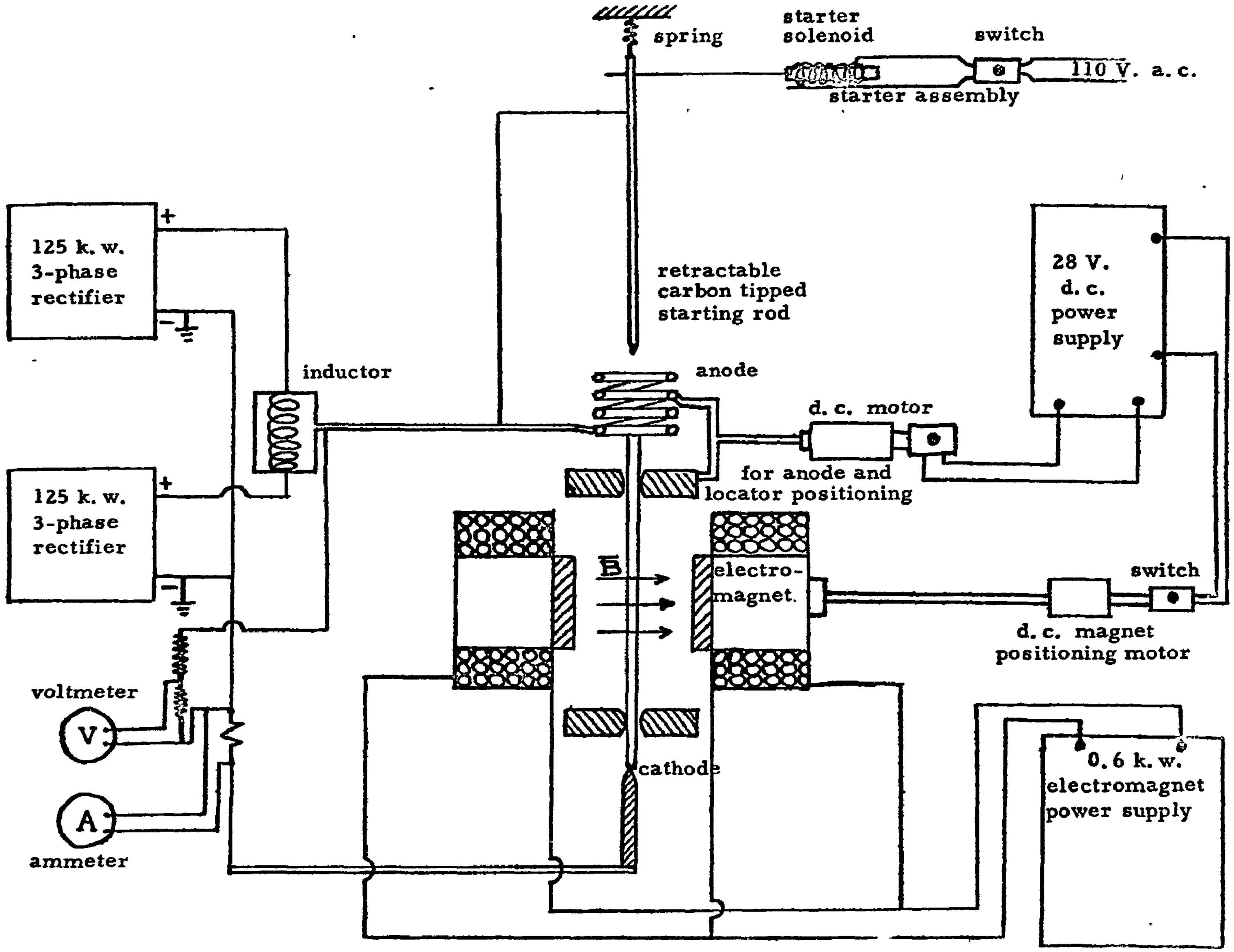

FIGURE 15 SCHEMATIC DIAGRAM OF PRIMARY AND AUXILIARY POWER SUPPLY SYSTEMS

3. Cooling Water Supply System

The cooling water was obtained from the building supply at 75 psig. Because of the large quantities of water used in the experiment, a separate 4-inch line was tapped into the water main. A schematic diagram of the cooling supply system is shown in Figure 16.

A two piston positive displacement Worthington water pump, rated at 68 gpm and 530 psig, was connected between two surge tanks. One surge tank was located on the inlet line and the other on the pump outlet line. The pressure surge inherently present in all positive displacement pumps was undesirable from the standpoint of cooling critical elements. The employment of both surge tanks reduced the pressure surge to a tolerable level. The water pump was driven by a three-phase 25 horsepower electric motor. A by-pass line was used to regulate the pressure head at the exit line. The exit line fed into a long high pressure water manifold. Sixteen high pressure control valves were spaced at intervals along the manifold. High pressure hose was used to route each line to the particular element to be cooled. The low pressure return lines were connected to individual Fisher and Porter flowmeters, each capable of monitoring flow from 0 to 6 gpm. The water lines which supplied the electromagnet first passed the water through an aqua-pure cartridge filter to remove any foreign matter which might clog or contaminate the system.

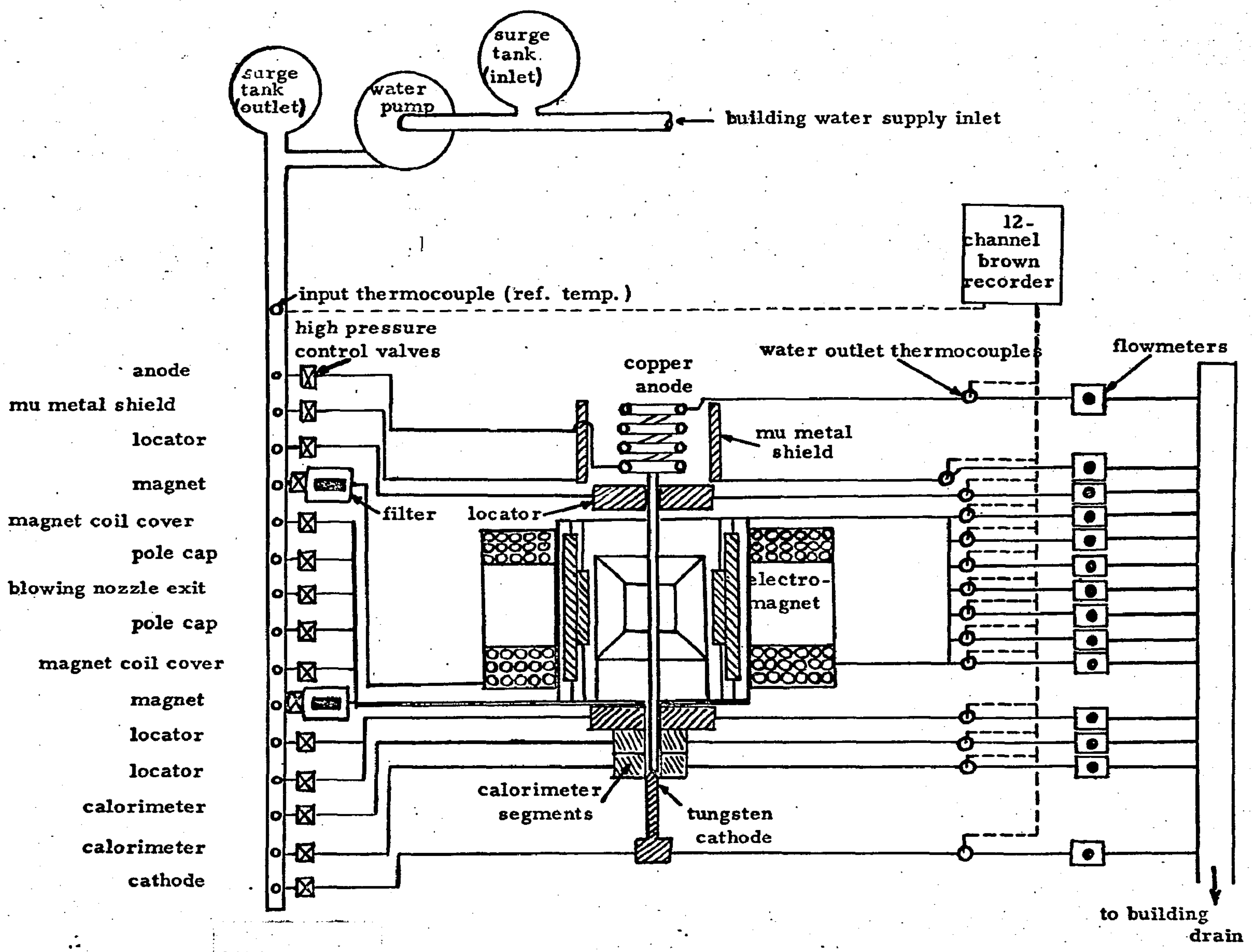

FIGURE 16 SCHEMATIC DIAGRAM OF COOLANT SYSTEM

4. Recording Equipment

The recording equipment is shown in Figure 17. A 12-channel Brown-Honeywell continuous stepping recorder was used to monitor water outlet temperatures. The temperatures were measured by calibrated copper-constantan thermocouples. For a reference, one channel recorded the inlet water temperature. A schematic diagram of the various channels and typical operating values is shown in Figure 18. The temperature differences together with the known mass flow rates read on the flowmeters allowed a heat transfer calculation to be made of the total heat conducted from the arc to the water at each element.

An 8-channel Dynograph individual strip readout recorder was used to monitor arc electrical characteristics, input current to the electromagnet, and stagnation pressure upstream of the sonic nozzle system. The two remaining channels were used in connection with the calorimetric probe.

A Tektronix oscilloscope was used in conjunction with the wake turbulence frequency measurements and the potential probe measurements.

5. Cameras

With proper filtering it was possible to visually study the appearance and behavior of the arc column. However, in order to systematically record the arc column motion and shape, high-speed

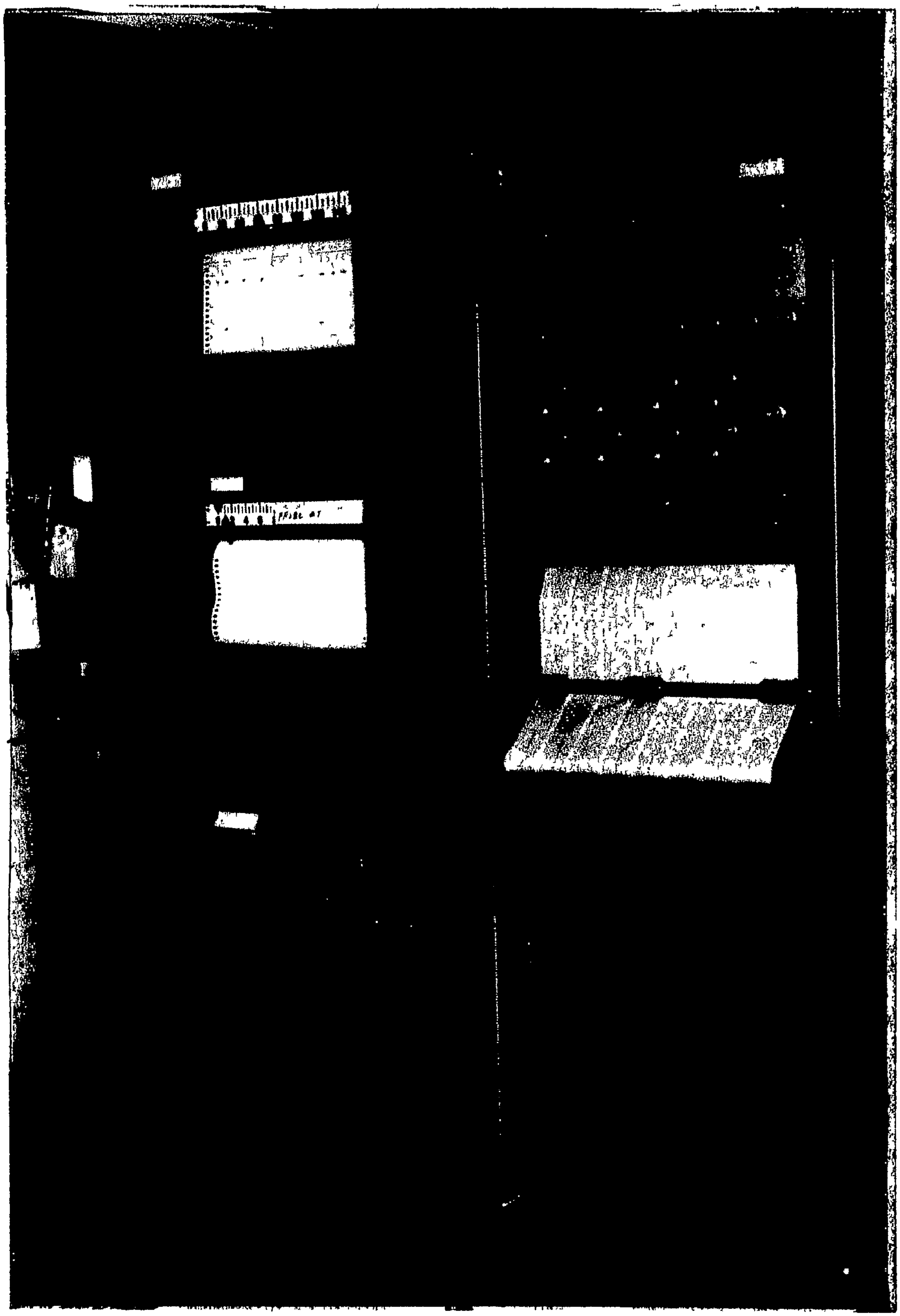

FIGURE 17 ELECTRONIC RECORDING EQUIPMENT

Offner 8-channel recorder

	typical operating values
1 total arc voltage	1 190 volts
2 voltage cathode to top locator	2 80 volts
3 voltage cathode to bottom locator	3 25 volts
4 total arc current	4 300 amps
5 current input to magnet	5 1.5 amps
6 grey-rad inlet orifice thermocouple	
7 grey-rad cooled gas sample thermocouple	
8 pressure transducer from sonic nozzle system	

12-channel Brown-Honeywell stepping recorder

	typical operating valves (°F)
1 reference water inlet temperature	1 48
2 temperature cathode outlet	2 50
3 temperature bottom calorimeter outlet	3 58
4 temperature top calorimeter outlet	4 54
5 temperature bottom locator outlet	5 55
6 temperature top locator outlet	6 59
7 temperature anode outlet	7 72
8 temperature magnet coils outlet	8 52
9 temperature front pole cap outlet	9 51
10 temperature rear pole cap outlet	10 52
11 temperature magnet coil rear face outlet	11 120
12 temperature magnet coil front face outlet	12 125

Thermosystems heat-flux probe readout console

1 heat flux to probe
2 cooling flow rate
3 coolant Δt

Brown-Honeywell recorder Grey-Rad probe readout

1 Δt_c coolant temperature rise
2 Δp impact pressure transducer

FIGURE 18 SCHEMATIC DIAGRAM OF RECORDING AND PROBE DIAGNOSTIC INSTRUMENTATION and press cameras were employed. In this way details of the arc column could then be studied and compared by viewing the slowmotion films and still pictures.

The following types of cameras were used.

a. 16 mm Wollensak Fastax framing camera,

b. Beckman-Whitley Dynafax rotating drum camera,

c. Linhof press camera.

The 16 mm Wollensak Fastax framing camera was of the continuous moving film type with a rotating prism positioned between the lens and the sprocket. A 100-foot roll of film was fed through the camera in 0.6 seconds. The sprocket accelerated to the maximum speed of 7000 frames/sec after the first 55 feet of film. The Fastax camera was equipped with an externally activated timer which provided 1000 cycles/sec timing marks on the edge of the film. The Fastax camera was used to produce slow motion color films of the rotational motion of the anode spots, cathode spot size and shape, simultaneous views of the arc column in the balanced mode, the arc column behavior without external fields applied, and flow visualization by particle injection. Neutral density filters, Ansco color film type 231-D/50 and an f/22 setting provided the best results.

The Dynafax rotating drum camera exposed 224 frames of 35 mm film in 8.62 milliseconds, corresponding to a film speed of 26,000 frames/sec. The film was transported on a rotating drum

(7,000 rpm), and an octagonal rotating mirror (97,500 rpm) was used for shuttering. The Dynafax camera was used to produce a slow motion color film of the rotational motion of the anode spots. Neutral density filters Anscochrome, color film and an f/16 setting provided the best results.

The Linhof press camera was a four by five inch type rated at 1:8/90 employing a super-Angulon lens. A polaroid camera attachment on the back allowed either graphic four by five inch plates or an eight exposure roll of polaroid 10-second developing, 3000 speed, type 47 film to be used. The Linhof camera was used for the simultaneous orthogonal viewing of the arc column size and portions of the flow visualization study. Neutral density filtering was used and the majority of the pictures were taken at f/8, 1/250 sec.

Figure 19 shows the physical arrangement of the arc, lenses, mirrors, and camera for the simultaneous orthogonal viewing. Figure 20 is a schematic of the mirror arrangement and camera used in photographing the flow visualization by particle injection. Neutral density filtering was used together with camera settings of f/8 and 1/500 sec.

C. Diagnostic Equipment

The diagnostic systems consisted of the following primary subsystems.

1. Flow Visualization by Particle Injection,

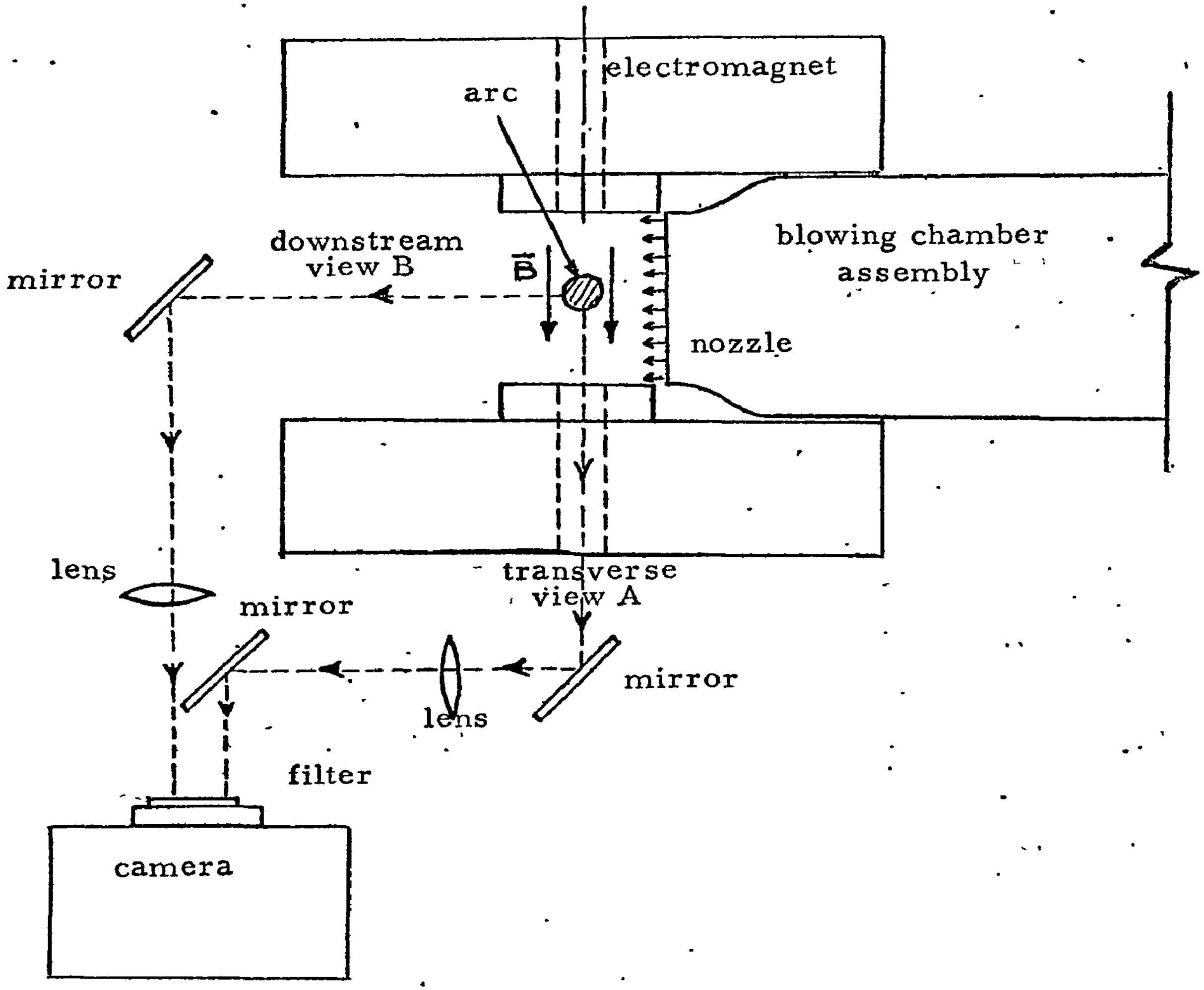

SCHEMATIC PLAN VIEW OF 2-DIMENSIONAL ARC COLUMN
PHOTOGRAPHIC SET-UP
FIGURE 19

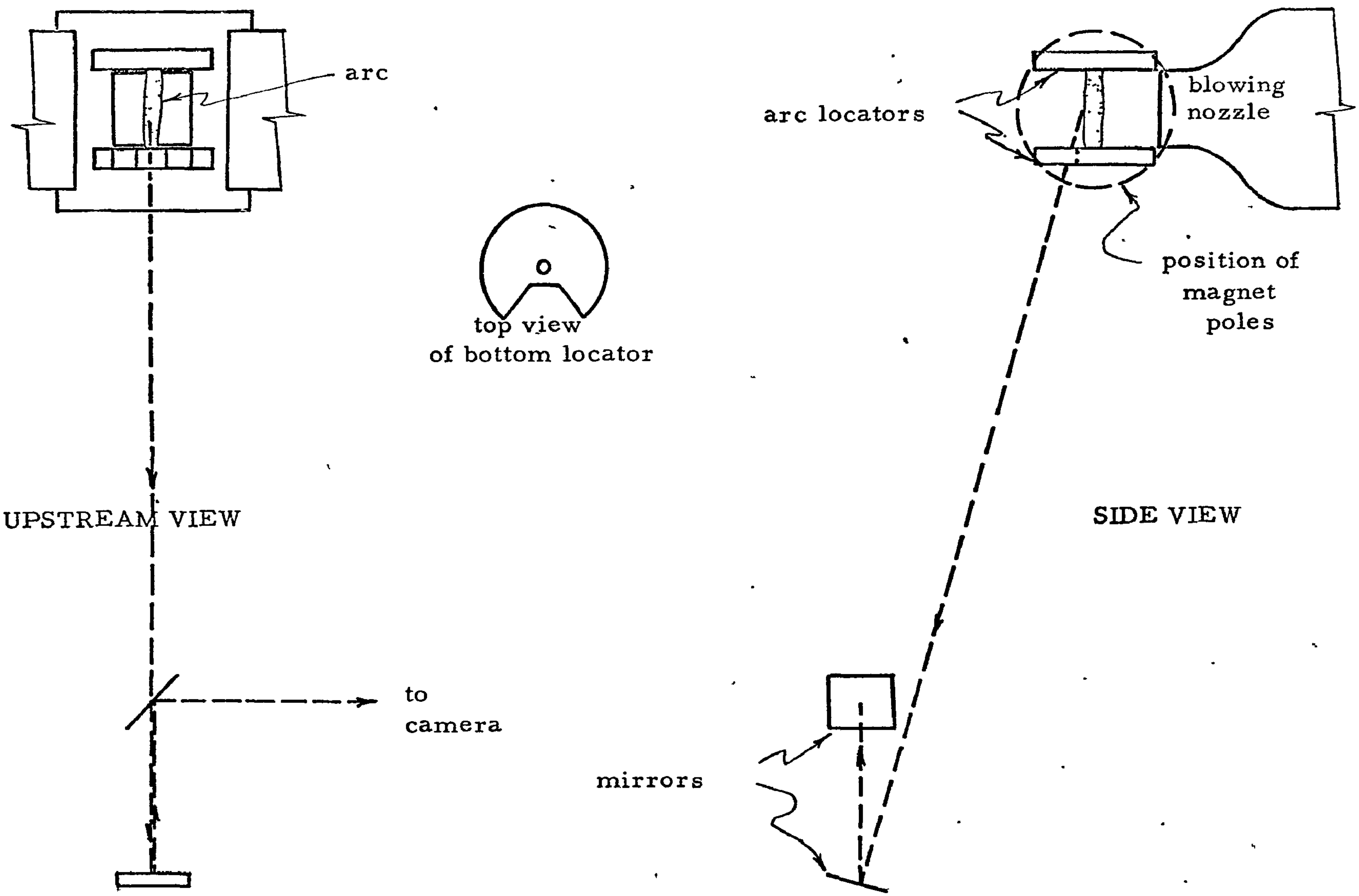

FIGURE 20 SCHEMATIC OF SET-UP USED FOR FLOW VISUALIZATION PHOTOGRAPHS

2. Calorimetric Probe,

3. Cooled Heat Flux Probe,

1. Flow Visualization by Particle Injection

The small particle pressurized injection system for the flow visualization studies is shown schematically in Figure 11. It was originally intended to use a variety of particles, such as boron nitride, lithium hydride, carbon, aluminum, and aluminum oxide; however, it was discovered that it was extremely difficult to obtain particles of these materials within the size range required from a commercial source. Therefore, the particles used throughout the majority of the flow visualization portion of the study were aluminum particles. The small, spherical, aluminum particles of 2 to 20 microns diameter were contained in a cylindrical glass mixing chamber. The chamber was sealed with the exception of two small stainless steel tubes entering at the top. One tube acted as the pressurizing inlet line. It tapered at the tip to a convergent nozzle and extended into the particle supply. By inserting the nozzle of the inlet tube deep into the particle pile, good agitation was achieved. This line was fed by an upstream gas supply system through a pressure regulator and flow meter. The outlet line was positioned with its end at approximately the mid-height of the mixing chamber. The end was plugged and a small exit port was located on the periphery near the plugged end. The exit port on the side of the exit tube allowed particles of approximately the same size to be carried out the exit line and continue on to the blowing nozzle injection tube. The right angle bend of the injection tube also served to filter out some of the larger particles which may have entered into the tube. The injection tube was mounted on a mechanism which allowed it to be traversed in the horizontal plane. A vernier scale was attached for a reference position indication. The particles entered the blowing chamber through a stainless tube inserted through one side wall of the chamber slightly upstream of the start of the converging section. A tee in the line allowed a 1/16 inch o.d. stainless steel injection tube to extend at 90° from the inlet tube and lie on a central plane parallel to the flow streamlines of the nozzle exit. The exit plane of the injection tube tip was 1/8 inch upstream of the nozzle exit plane. The other portion of the tee extended through the back face vertical wall of the chamber and was provided with a bleed valve to further assist in controlling the particle injection rate. One of the problems usually encountered with small particle injectors is a means for keeping the particles from bunching. Various vibration techniques, sifting through fine filters, and other approaches have been used with some degree of success. The reason for using this system was that the pressurization allowed the particles to be injected parallel with a streamline at approximately the same velocity as the flow. This provided a meaningful flow visualization of the streamline path as it approached and was deflected around the arc column.

2. Calorimetric Probe

The basic disadvantage of any probe utilized to measure local gas characteristics is its disturbance on the medium being measured. As a result of the recently achieved miniaturization of many commercially available probes, the error introduced can be greatly minimized. The significant dimension of the arc column varied from 0.34 to 0.45 inches, while the probe o.d. was 0.063 inches. A minimum of disturbance was therefore achieved. The comparatively simple operating principle and associated apparatus, together with its small size, make the miniaturized calorimetric probe an especially suitable device for the measurement of local gas enthalpy and velocity. This was particularly significant in the present investigation due to the imposed accessibility limitation.

The Greyrad Corporation miniaturized calorimetric probe which was used is shown schematically in Figure 21. This probe system was used with a "tare" measurement technique i.e., the probe was first operated with the gas sample flowing, and then operated with the gas sample shut off. This tare measurement technique eliminated the error due to radiation heating of the probe and also that due to heat transfer to or from the outer portion of the jacket. By measuring the coolant water flow rate and temperature rise together with gas sample flow rate and cooled gas temperature at the probe exit and applying

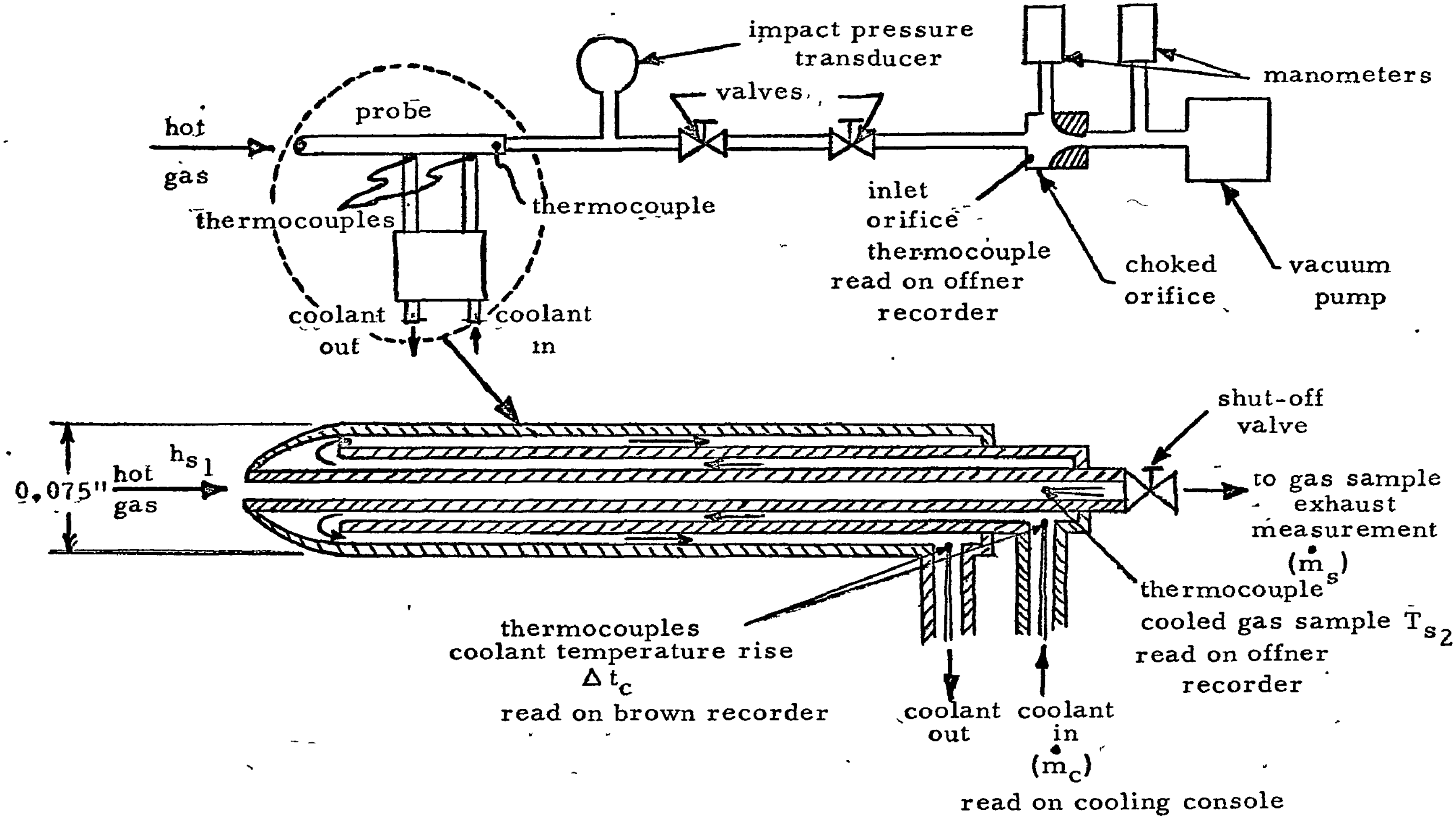

DIAGRAM OF INSTRUMENTATION USED WITH TARE-MEASUREMENT CALORIMETRIC PROBE TO MEASURE VELOCITY AND ENTHALPY

FIGURE 21

the "tare" measurement, the stagnation enthalpy of the unknown gas sample was calculated from a heat balance relation. The resulting stagnation enthalpy was given by

$$h_s = \frac{(\dot{m}_c C_c \Delta T_c)_f - (\dot{m}_c C_c \Delta T_c)_n}{(\dot{m}_s)_f} + (C_{p_s} T_s)_f$$

where subscript f signifies tare measurement with sample flow and n signifies tare measurement with no gas sample flow. Two disadvantages are inherently present in this type of tare measurement probe; however, neither were particularly critical for the cross-flow arc investigation. The first is the requirement for intermittent probe operation which necessitates a steady-state environment of sufficient time duration (approximately 20 seconds) to permit the "flow" and "no-flow" data point to be obtained. Since the arc average run time was 45 minutes, this requirement did not prove to be a problem. The second is the criteria for the selection of a sufficiently small gas sample rate of flow so that duplication of flow conditions near the probe tip are satisfied during the "tare" measurement. This condition was satisfied by taking the "tare" measurement for a particular data point and then repeating the "tare" measurement at a few slightly greater gas sample flow rates. A point was reached where a large error was noted in the gas stagnation enthalpy calculation indicating that the sample flow rate had increased to the point where the tip-flow duplication criteria was no longer valid. It was, however, desirable to use the greatest error-free gas sample rate in order to obtain maximum probe sensitivity.

A three-axis translational scanning device was constructed to allow accurate positionment of the probe in the test region. Figures 12 and 22 show probes mounted on the translational scanning device. Three types of probes were used. Figure 23 shows two of these types. The third was identical to the larger 1/8" o.d. 90°-bend probe shown, except a straight section replaced the 90°-bend.

Figure 24 shows the probe coolant supply and gas sample flow-rate system. The thermocouple readouts were monitored on electronic recorders. A calibration curve for the probe used for the blowing velocity measurements is included in Appendix B, Figure 56.

3. Cooled Heat Flux Probe

The availability of a Thermo-Systems Incorporated miniaturized, internally water-cooled heat flux probe allowed measurements to be taken of the local heat flux, rms per cent power fluctuation and turbulence frequency downstream of the arc. The changes in heat flux which the sensor will measure depend on temperature, velocity, pressure and gas composition. The optimum application for a sensor such as this would be in a high temperature flow where either the velocity or the temperature (together with pressure and gas composition) is known to remain essentially constant. In an environment where pressure, composition, and temperature are essentially constant, an exposed sensor gives a direct

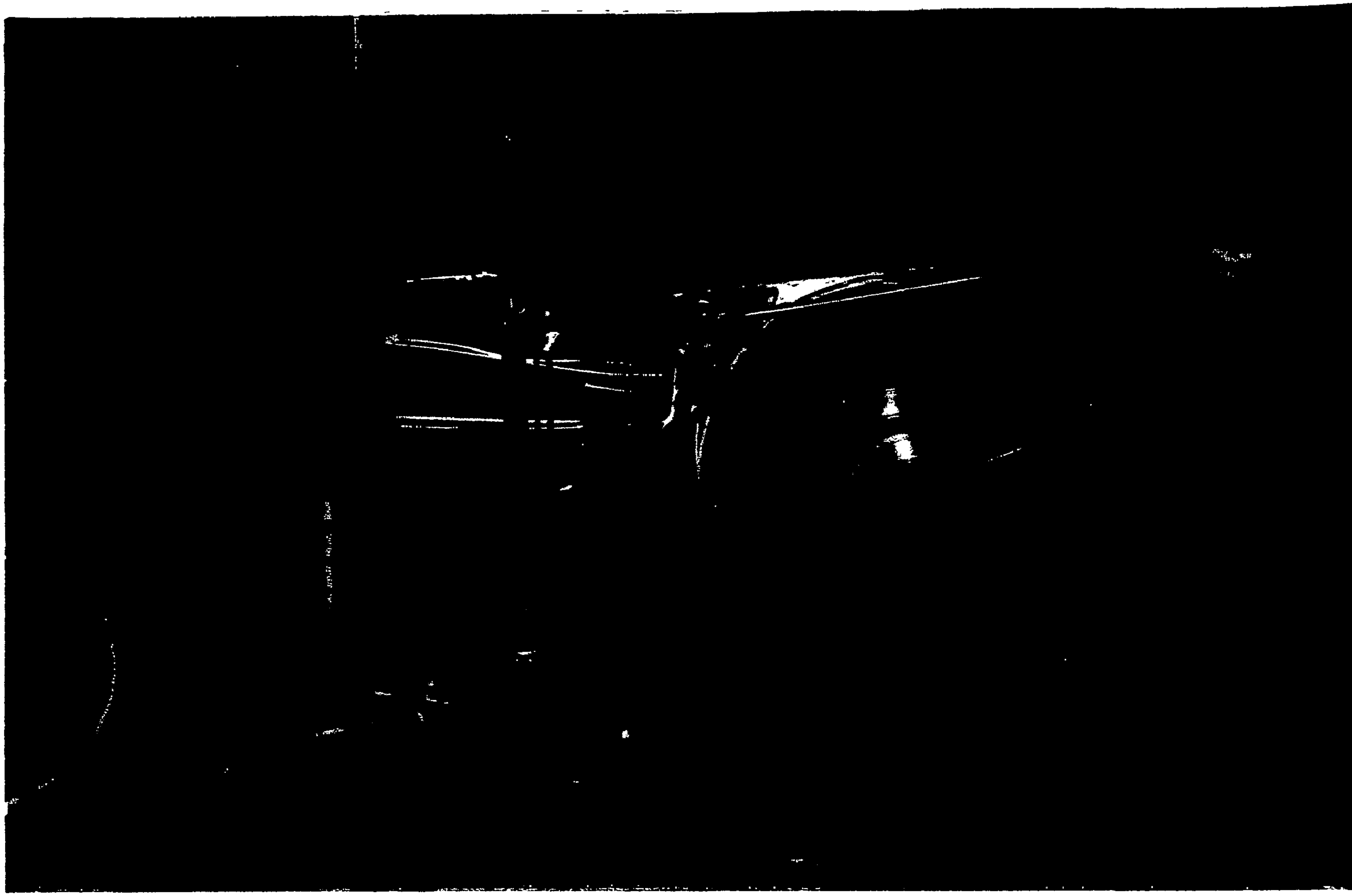

FIGURE 22 90° BEND CALORIMETRIC PROBE MOUNTED ON TRANSLATIONAL SCANNING DEVICE

FIGURE 23 1/16" O.D. and 1/8" O.D. 90° BEND CALORIMETRIC PROBES

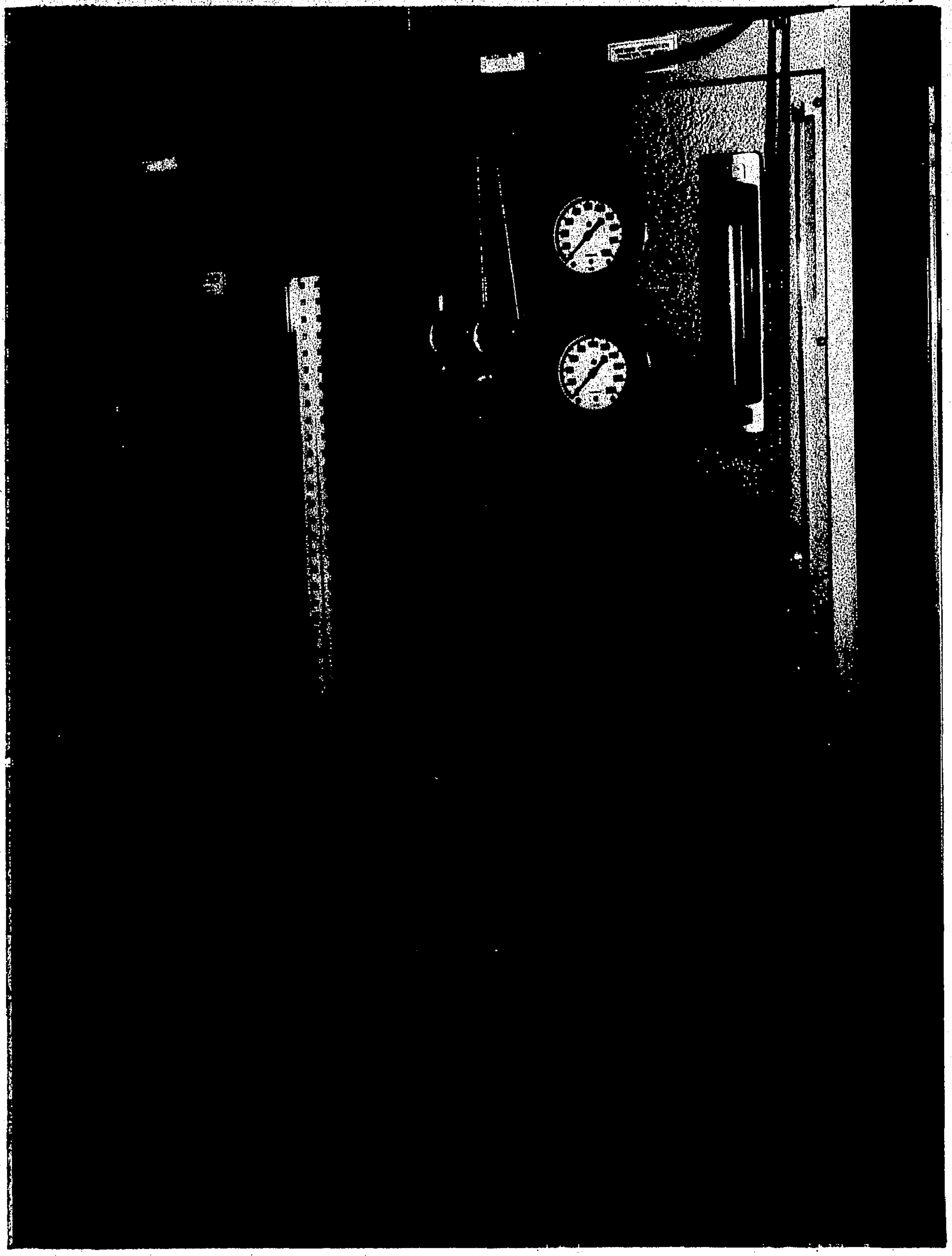

FIGURE 24 CALORIMETRIC PROBE GAS SAMPLE FLOW RATE SYSTEM AND COOLANT SUPPLY

indication of velocity. For measuring temperature fluctuations, one usually resorts to an aspirating type probe which (by using a sonic flow orifice arrangement) essentially eliminates the velocity effects through proper calibration. Another technique might be to include dual sensors, each maintained at a different temperature. Various other sophisticated techniques similar to those used in hot-wire anemometry may also be applicable. It is only possible to accurately obtain quantitative measurements of one of the variables if the remaining ones are known. Therefore, the results obtained from the sensor used in the present investigation will only be useful as a qualitative measurement of the heat transfer rate. The heat flux probe assembly and mounting is shown in Figure 25 together with an enlarged schematic of the sensor portion. The probe was used in conjunction with a specially designed electrical bridge which measured the instantaneous rate of heat transfer from the arc wake region to the small cylindrical sensor (0.006 inches o.d.). The platinum film, cooled by the internal water flow, acted as a resistor which the associated electronic circuit maintained at a constant resistance (subsequently a constant temperature). The sensor was coated with a thin layer of quartz to electrically insulate it from the arc region. When a fluctuation occurred in the environmental conditions, the circuit varied the electrical power into the sensor to maintain a constant surface temperature. The amount of heat being transferred

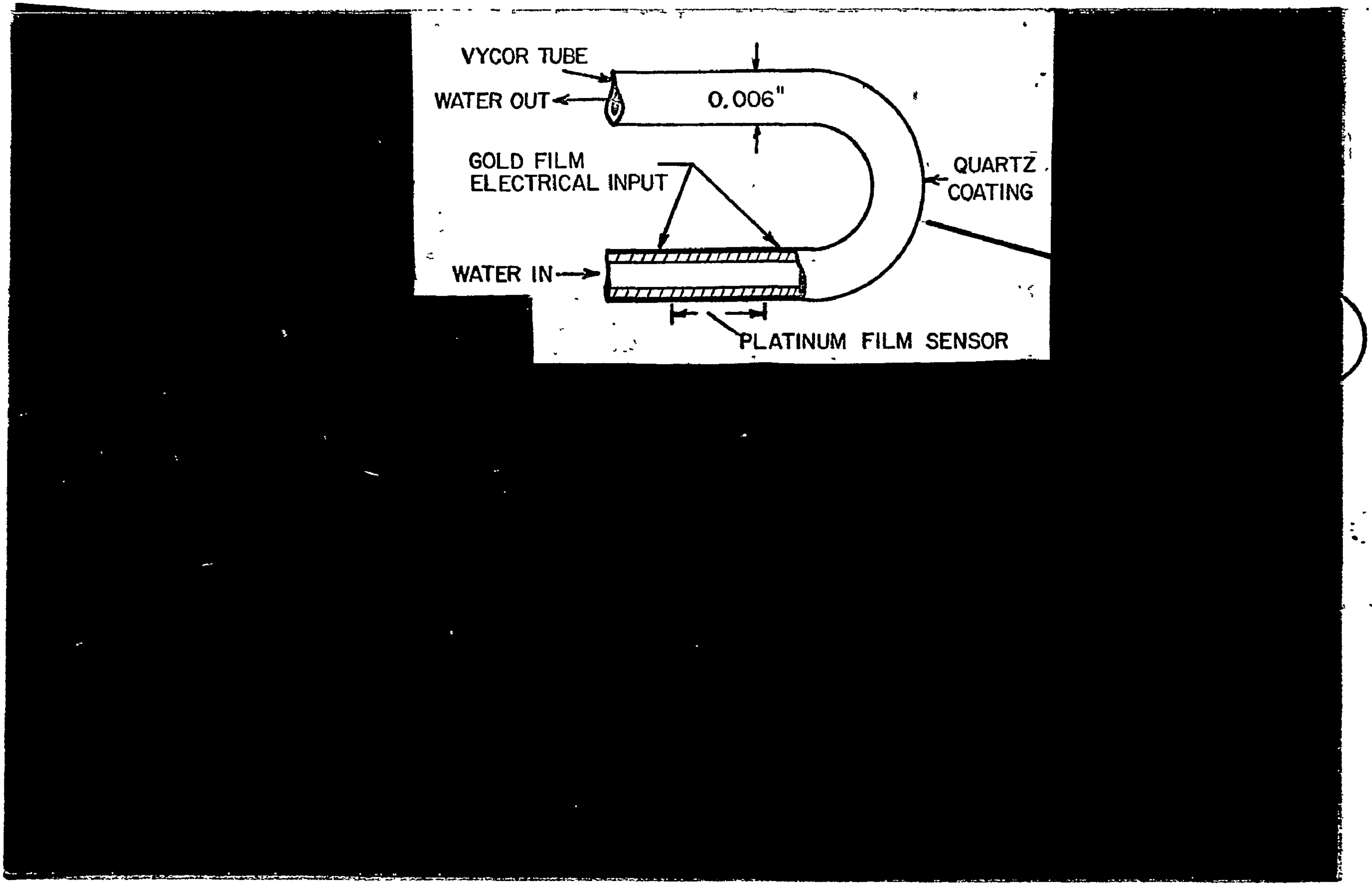

FIGURE 25 HEAT FLUX PROBE ASSEMBLY AND MOUNTING

to the internal cooling water was constant due to the constant sensor temperature and was determined from previous calibration tests. Thus, the instantaneous heat transfer rate from the environment to the sensor was given by the difference between the heat transfer to the water and the instantaneous probe power. An rms meter was used to monitor a voltage which was proportional to the instantaneous probe power to give a relative indication of the turbulence in the wake.

D. Test Procedure

Prior to each test run the cross-flow arc apparatus was readied for operation according to the check list outlined below:

1. All electronic recording equipment was turned on one hour in advance of testing to allow sufficient time for complete warm-up. After warm-up each recording channel zero reference was checked.

2. All gas supply systems were checked for proper valving and pressure.

3. The building cooling water was turned on and the electrodes and cooling sections checked for leaks at building supply pressure.

4. The vacuum exhaust ventilation system was turned on.

5. The cooling water to the magnet was turned on, the magnet power supply energized, and a zero reference calibration check was made on the current read-out.

6. The magnet and nozzle assembly were indexed to the full-out starting position.

7. The starter was placed into position.

8. The desired sonic nozzle combination was opened and the upstream stagnation pressure read-out channel was zeroed on the recorder.

9. The high pressure water pump was turned on, and the flowmeters set at the desired operating range. A spot-check was made for component water leaks under the high pressure.

10. All shielding was installed and the front protection hood closed.

11. The cathode gas injection system was turned on and adjusted to the proper flow rate.

12. The d.c. rectifier cooling fans were started, and the moving coils were set to the starting power range.

13. The d.c. power supplies were simultaneously energized followed by the solenoid starter activation and arc ignition.

14. Temperature read-outs of all components were made after proper stabilization had taken place. All electronic recording equipment was checked for proper signal.

15. A visual check was made of the anode spot striking pattern through an overhead mirror.

16. The magnet and nozzle assembly were indexed into the full-in test position.

17. The blowing rate and magnetic field strength were simultaneously increased in small increments so as to keep the arc balanced in the vertical position at all times. A continuous visual check was made of centerline alignment through the magnet view hole.

18. After test conditions were reached, continual checks were made of all temperature and recording equipment read-out.

V. DISCUSSION OF EXPERIMENTAL RESULTS

A. Arc Size and Shape

The instrumentation used for the simultaneous lateral and upstream viewing of the arc was discussed previously in Section IV, (Figure 19). A Linhof press camera with a shutter speed of 1/500 sec was used. A calibration procedure was used to account for the magnification factor and losses of light over the path through the different lenses and mirrors used for projecting the arc column image onto the photographic film. A standard source was employed for this calibration of each path.

The determination of a representative arc diameter is somewhat arbitrary due to the fact that by using different filter densities, combined with under- or over-exposing the photographic film, one can arrive at a variety of different apparent diameters. The typical temperature profiles shown in Figure 4 clearly indicate the difficulty in defining a representative arc diameter corresponding to a given boundary temperature. One method to obtain a representative arc diameter would be to take a photograph of the arc column and then use the relative density of the photograph negative as measured with a densitometer (maintaining constant film exposure). An alternate method would be to vary the exposure time over a range and plot the measured radius as a function of exposure time. The resulting curve should have a plateau which would correspond to the radius of the current conducting core. Based on prior experience gained with an electric arc in a similar configuration (including an argon injection cathode system), whose temperature profile was determined from continuum intensity measurements (in addition to having photographs taken), a comparison was made to select a suitable camera shutter speed, neutral density filter, and film exposure time to be used in the present experiment. The diameter arbitrarily selected in this way should represent reasonably well an argon arc column with a boundary temperature of 6000 $\pm$ 1000 °K. Below this range the electrical conductivity drops to a negligibly small value (Figure 5). The important factor, however, is that once an arbitrary column diameter has been selected and defined through a chosen photographic technique, all other measurements with varying parameters were referred to this reference diameter. In this way, the various diameter changes of the arc column under the influence of the external fields were systematically compared.

Figure 26 graphically represents the results obtained for the variation of the representative arc column diameter as a function of the transverse blowing velocity with arc current as the parameter. The increasing curve (approximately linear) for each current level was obtained from measurements in the upstream view and the

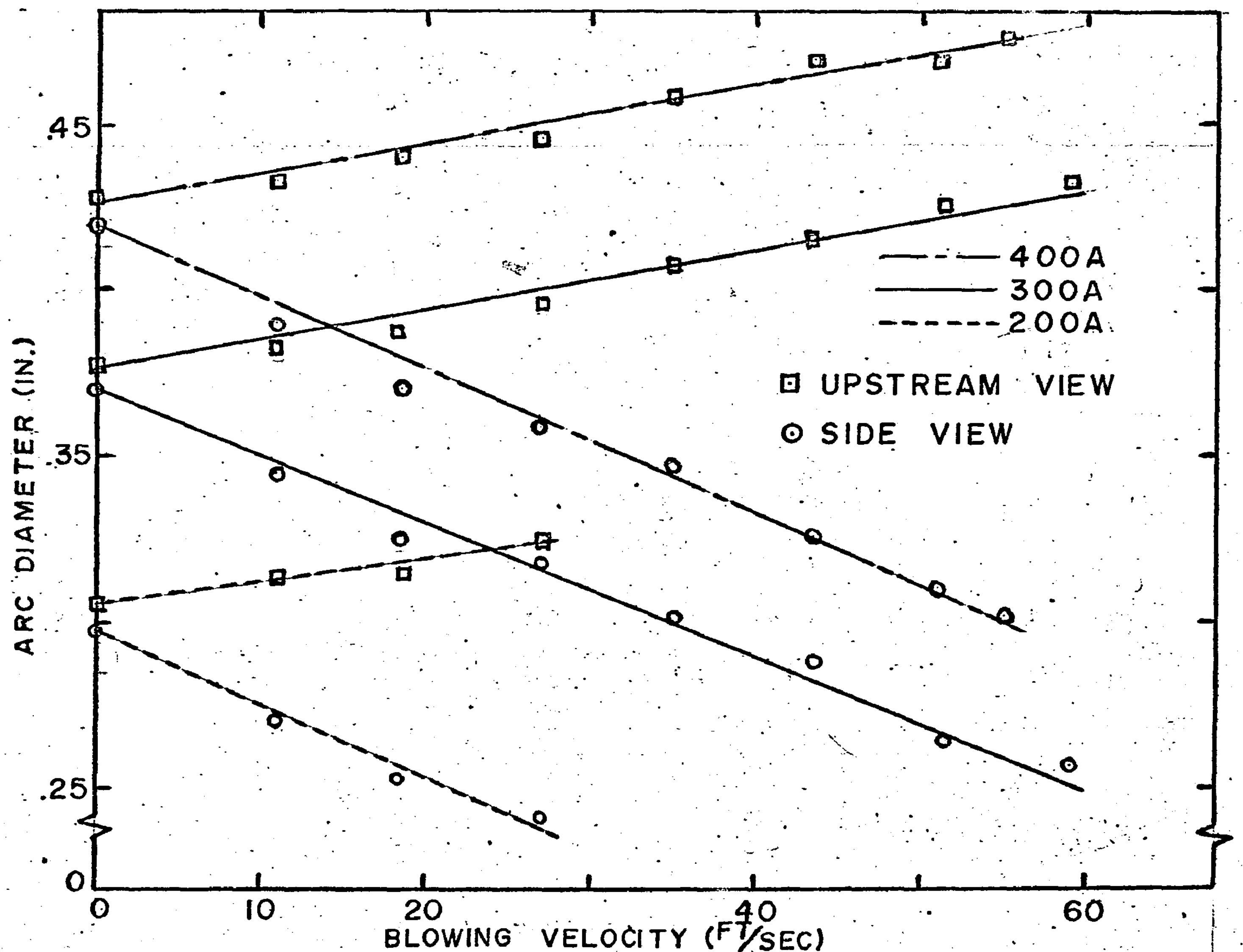

ARC DIAMETER AS A FUNCTION OF BLOWING VELOCITY

FIGURE 26

corresponding decreasing curve (also approximately linear) resulted from measurements in the lateral view through the magnet hole. It indicates that the initial circular cross-sectional shape of the column changes with increasing flow velocity and magnetic field into a shape which may resemble an ellipse, with the major axis transverse to the flow direction. Because this variation of the cross-sectional shape (in particular, the increase of the arc width transverse to the flow direction) was quite unexpected, a series of additional tests were made which reconfirmed the initial observations. The question is then opened: "What is the true cross-sectional shape of the arc column when bounded by these two orthogonal dimensions?" If one assumes that the arc columns' boundary may be convex and symmetrical with respect to the major and minor axes, then an ellipse may be a reasonable conclusion. The possibility of the arc cross-sectional shape being similar to a flat plate configuration with approximately blunt edges appears remote. If the constraint of the arc boundary convexity is removed and symmetry is required only in the direction transverse to the external flow, then a shape similar to an ellipse dented inward toward the column centerline on either the upstream or downstream portion is also a possibility. For simplicity and until more experimental work can be put forth in this area, an elliptic cross-sectional shape was assumed.

Arc column oscillations and pulsations at high frequency either in the streamwise or transverse to flow direction were checked by taking simultaneous orthogonal-view pictures with a high-speed camera (7000 frames/sec). It would be reasonable to expect that a very rapidly oscillating column could give the visual appearance of having a larger representative diameter than in the non-oscillating case. The results showed negligible movement in the direction transverse to the blowing and a very small amplitude (less than 0.04 in.) oscillation (frequency approximately 720 c.p.s.) in the streamwise direction. This may indicate that the arc's true minor axis was slightly less than that measured. In addition, the column executed a small radial pulsation (a so-called "breathing mode" of approximately 120 c.p.s. frequency), which may have been caused by the power ripple of the rectifier power supplies.

The arc cross-sectional area was calculated using the two-view dimension measurements of the major and minor axes of an ellipse. Calculations of the arc cross-sectional area before transverse blowing (assumed cylindrical), compared with those after the external fields were applied (assumed elliptical) indicated a slight reduction. This would indicate, since the current remained constant, a proportional increase in the average current density (e.g., 300 ampere arc, before blowing: J_{ave} approximately 2750 amps/in^2; after 42 ft/sec blowing: J_{ave} approximately 3200 amps/in^2). However, in view of the assumptions used for the geometrical shapes, these data will be within the experimental accuracy. Thus, for practical purposes the cross-sectional area and average current density may be assumed to be unaffected by the transverse blowing and magnetic field; however, it appears likely that it may considerably alter the distribution of the current density.

The difference between the two-view dimensions measured at the no external blowing condition (Figure 26) was attributed to the absorption due to the additional mirror in the side view optical path. It is within the experimental accuracy.

Previous experimental and theoretical work of other authors (35, 47, 50, 52), indicated that the diameter of a free-burning arc increased almost linearly with increasing arc current for constant atmospheric pressure conditions. Figure 27 shows the results of the present investigation. The arc's major axis is shown as a function of arc current with blowing velocity as the parameter. The approximate linear increase was confirmed over the range investigated. The major axis of the arc transverse to the flow was used as the representative arc dimension, D, in this and all subsequent plots and in all calculations involving the significant arc dimension from the aerodynamic point of view.

To estimate the influence of the cathode gas injection rate on the representative diameters, the gas injection mass flow rate to the cathode was both increased and decreased by a factor of two, while simultaneously photographing the major and minor axes. A

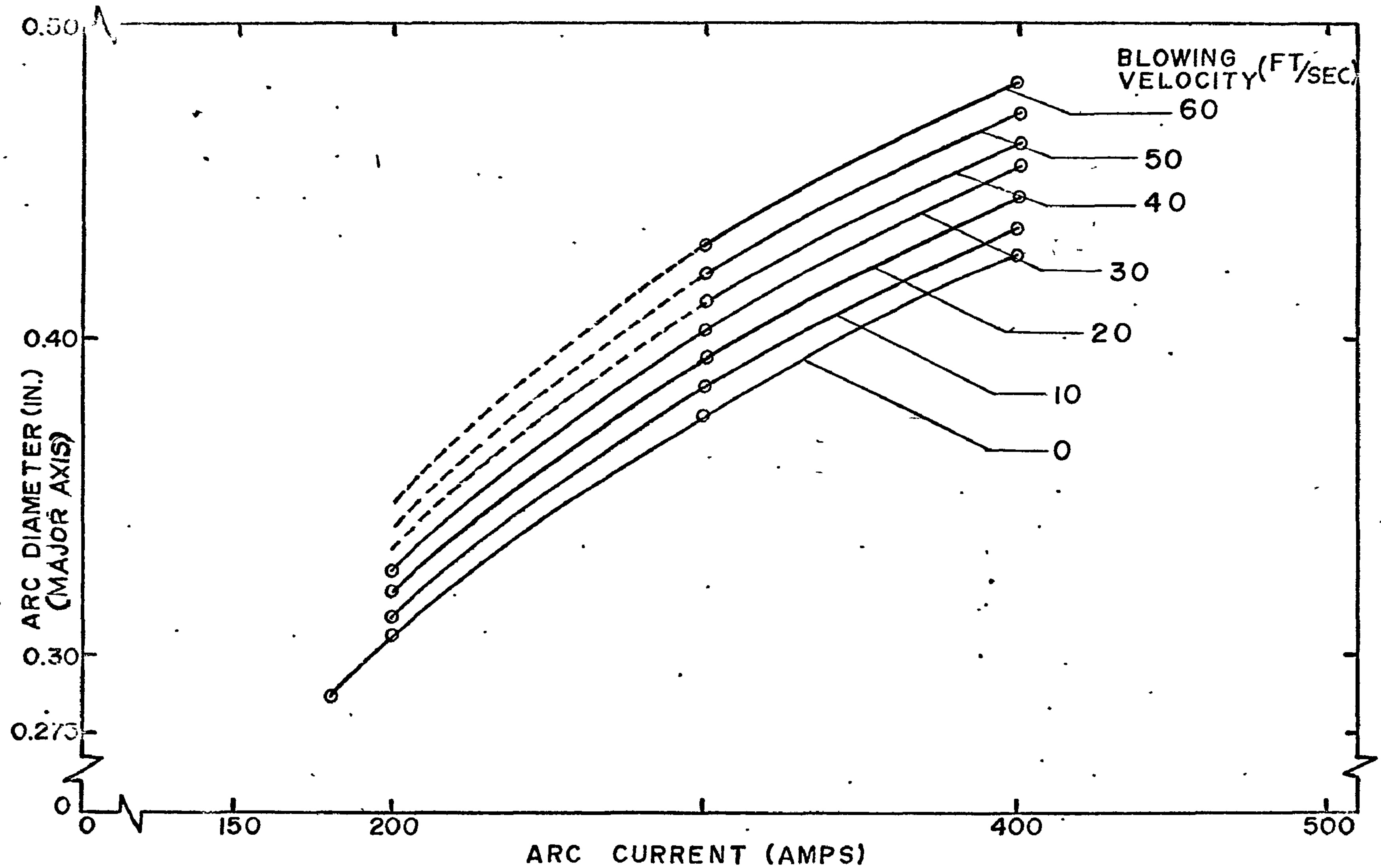

ARC DIAMETER AS A FUNCTION OF ARC CURRENT
FIGURE 27

negligible effect was found and no noticeable trend (either an increase or decrease) of the major or minor axes with increase or decrease of gas injection rate was obtained.

Correlation of the arc's diameter measured in this investigation with those of other investigators is not possible since, in practically all cases, different operating ranges and configurations were used. Almost all of the previous investigators had to resort to estimating the arc column diameter because of the lack of optical accessibility and/or the extremely short test times, in addition to associated arc instabilities and rapid arc motion. No indication was found in the literature that the column was viewed from different directions.

Qualitatively, the cross-sectional shape change of the arc positive column may be explained through the existence of a dual-vortex flow system within the arc column; such a system may be generated by a magnetically induced pumping process. Further experiments will be necessary to determine the flow pattern within the column of the arc proper.

B. Drag Aspects

The next phase of the investigation was to determine the relation between the external magnetic field strength and the transverse blowing velocity. If it were found that the magnetic field strength was proportional to the velocity squared, arc current held constant, then a drag coefficient could be defined in the customary manner, and the equation $BI = (1/2)\,\rho\, C_D V_\infty^2 D$ could be used to determine an effective drag coefficient (where D is the significant arc dimension transverse to the free-stream direction). Figure 28 shows the external magnetic field strength as a function of transverse blowing velocity with arc current as a parameter. For comparison, the line representing the slope of the quadratic function is also shown. The magnetic field strength which was approximately proportional to V_∞^2, as measured by several previous investigators (31, 52)[in different operating ranges], was verified within the investigated experimental test range. Since the density is essentially constant, the B proportional to V_∞^2 relationship would indicate that the arc current should be approximately proportional to $C_D D$.

The value of C_D has been estimated (based on an assumed arc significant dimension) by numerous authors, particularly those concerned with rail accelerators and with arcs rotating around circular annular gaps. The values reported range from a low of 0.334 to a high of 10.1. Because of its importance in the question often raised, "Does an arc column actually behave analogously to a heated solid body?", a brief tabulation of these previous experimental investigations, the configurations used, parameter ranges, C_D values and method of determination, is shown in Table I. (All experiments, with the exception of Thiene's, were done with arcs in atmospheric air.)

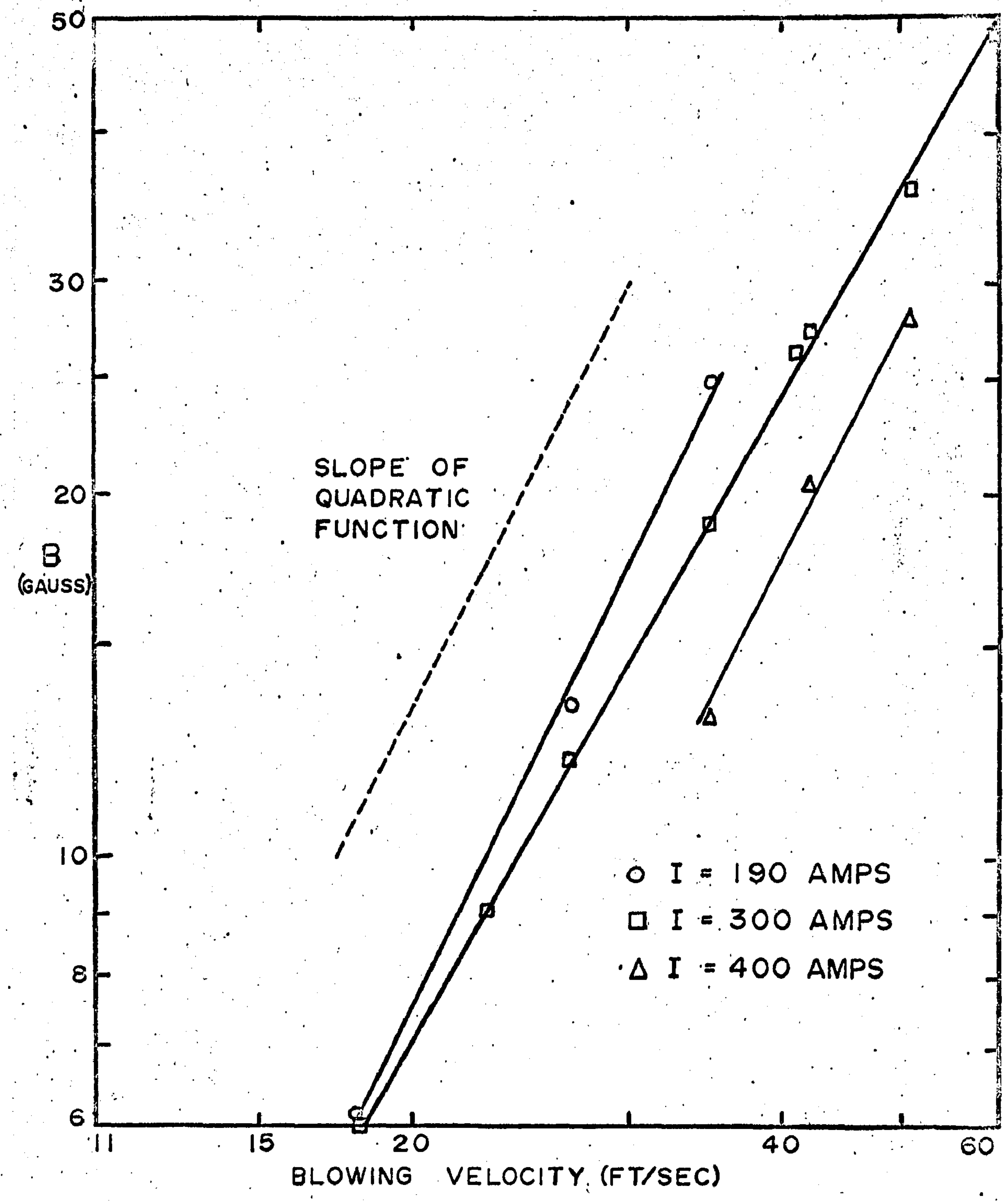

LOG-LOG PLOT OF EXTERNAL MAGNETIC FIELD INTENSITY AS A FUNCTION OF BLOWING VELOCITY

FIGURE 28

INVESTIGATOR	CONFIGURATION	I_{arc} (amps)	B_{ext} (gauss)	V (m/sec)	C_D	DETERMINATION
Steenbeck and Von Engel (21)	Parallel rail electrodes	2	10	1	0.4-0.9	From measured arc diameter
Angelopolos (22)	Parallel rail electrodes	85-980	0-800	≤ 250	6.7-10.1	Arc diameter was estimated as being the same as the side wall spacing
Blix and Guile (25)	Ring electrodes in two planes	80-400	340-1060	≤ 200	0.63	Not measured - postulated from solid cylinder analogy
Féchant (27)	Vertical parallel rail electrodes (with side walls)	300-5000	20-5000	≤ 500	1.6-3.5	From wall width measurement
Adams (68)	Annular ring electrodes	100-760	60-940	≤ 187	1-5	From photographic pictures of arc column diameter
Jedlicka (64)	Concentric cylindrical electrodes	Purely theoretical investigation			0.63	Postulated from solid rod analogy in turbulent flow regime
Hesse (9)	Parallel rail electrodes	95-800	none - driven by self-magnetic field	≤ 130	0.344	From photographic pictures of arc column
*Thiene (31) $P \approx 1$ atm. - argon	Horizontal opposing pin electrodes within vertical wind tunnel	4	≤ 1.4	≤ 1.55	6.3	From photographically measured arc column diameter
Lord and Broadbent (7)	Concentric cylindrical electrodes	150-700	60-940	28-270	0.7-1.5	From photographic pictures of arc column

TABLE I C_D ESTIMATION BY VARIOUS INVESTIGATORS

Comparison of the values of the drag coefficient obtained by the numerous investigators is extremely difficult when the many different configurations, gaps, electrode materials, wide range of test conditions and measurement techniques are taken into consideration. It should be pointed out that the validity of the C_D determination from $BI = (1/2)\rho C_D V_\infty^2 D$ for the case of a moving arc is questionable from two aspects. First, the magnetic driving force equation is derived for a solid body, which is completely impervious to flow, where any force exerted on the charged particles inside the body acts on the entire body. This is not true for the balanced arc. Secondly, the equation is strictly applicable to bodies which have reached uniform velocity. There is no guarantee in many of the parallel rail electrode experiments, in particular those where intermittent electrode spot sticking occurred (Figure 1), that this criteria was satisfied. In contrast to this, because of the stable arc column behavior obtained in the present experiment,and the indication of a relatively impervious arc column to the transverse flow, a reasonable representative value of C_D was expected.

To better aid in comparing the C_D value calculated in the present investigation with C_D values of solid bodies of different characteristic shapes, Figure 29 graphically shows the measured drag coefficient as a function of Reynolds number. The density was calculated on the basis of the free-stream temperature, and the

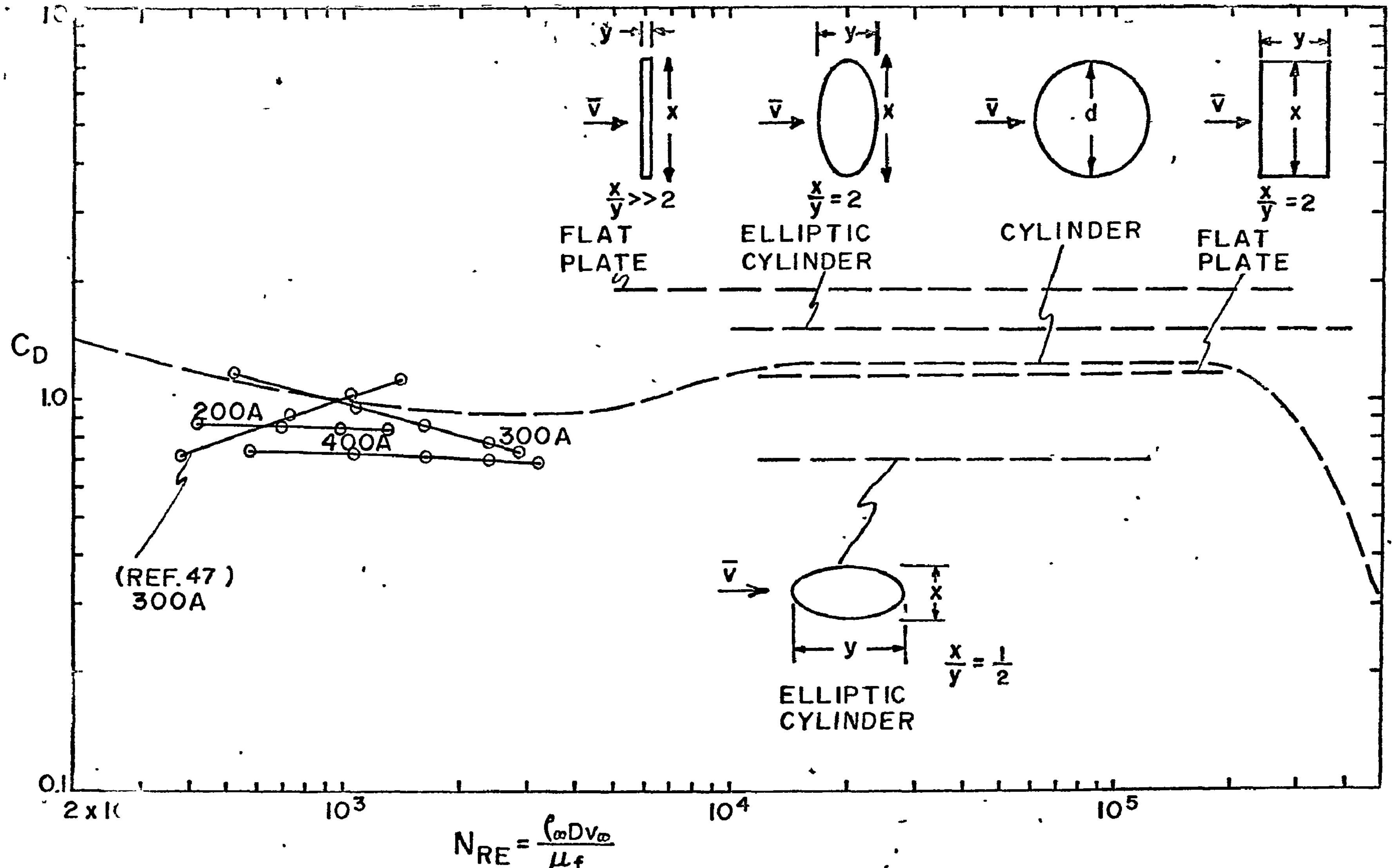

VARIATION OF DRAG COEFFICIENT WITH REYNOLDS NUMBER

FIGURE 29

viscosity was calculated on the basis of the mean film temperature (average between the arc boundary temperature and the free-stream temperature). The dashed lines indicate the C_D values of solid bluff bodies of the characteristic shapes shown in the right-hand portion of the graph. The C_D values obtained by Lord and Broadbent (47), for an arc traveling in a circular annular gap, [data from Adams (48)] are also presented for comparison. (Note that the C_D values of Lord and Broadbent were calculated for the Reynolds number based on the film temperature for evaluating the density and the viscosity and are plotted accordingly.) The agreement with the C_D values for solid bodies was good considering that the values previously reported differed by greater than one order of magnitude. The trend was for the C_D value to decrease slightly (from 1.2 to 0.7) as the Reynolds number was increased from 4×10^2 to 4×10^3. (An increase in the Reynolds number was accompanied by a slight increase in D.) This is because B was proportional to V_∞^2 and ρ was essentially constant; therefore, this verifies the prior assertion that for a constant current, the $C_D D$ product should have remained approximately constant. The curve of Lord and Broadbent, on the other hand, shows an increase in C_D with Reynolds number, since their calculation was based on the assumption that the arc diameter decreases with increasing cross-flow blowing velocity. Unfortunately, the limitation in the blowing velocity range excluded verification in the higher Reynolds number range where many of today's rotating arc heater devices operate.

The optimum way of calculating total drag would be to measure the complete velocity distribution in the wake of the arc column, and then equate the momentum deficit to the drag of the body (58). In principle, this method can be used only for two-dimensional flow. In the present experimental apparatus, this technique could not be applied because of the free-jet open configuration and the inability to account for all the flux losses through the lateral control surface. (The two-dimensional flow requirement is also not rigorously satisfied.) If the experiment had been conducted in a closed geometry wind tunnel whereby the streamlines would have closed behind the body, this technique may have been feasible.

The results which had been obtained up to this point gave strong indication that the arc column does behave analogously to a solid drag body. In an attempt to verify this finding more fully, flow visualization experiments by particle injection were conducted.

C. Flow Visualization by Particle Injection

It was anticipated that the injection of particles both upstream of the arc column and downstream of the arc column just behind the cathode region might give some visual indications of the degree of perviousness of the arc column to the transverse flow. Spherical aluminum particles 2 to 20 microns in diameter were used. It can be shown that if the value of the quantity

$$\frac{9}{2}\left(\frac{\rho_{gas}\, D_{arc}}{\rho_{particle}\, r^2_{particle}\, V_{gas}}\right)$$

is much greater than one, the particle streamlines represent true flow streamlines (59). If the value is less than or equal to one, the particles will possess too much momentum to be capable of accurately tracing an actual streamline path. This criteria is applied to solid particles, whereas, in the region surrounding the very hot arc column, vaporization of the individual particles may take place. However, it was hoped that some qualitative information of value would be obtained.

Figure 30 is a typical photograph (looking upstream) of a 300 ampere arc in the balanced mode. (Figure 31 shows a similar view without the arc present to better illustrate the configuration.) The blowing velocity was 35 ft/sec. At the central elevation and on the right boundary of the arc column in Figure 30 the particle injection tube can be seen. It appears as a horizontal line in the nozzle exit with its discharging attachment just to the right of the arc column. For this particular test the tube was located 3/8 in. to the right of the centerline. The shutter speed of the camera was 1/200 sec., the aperture setting was f/64, and a 1.0 neutral density filter was

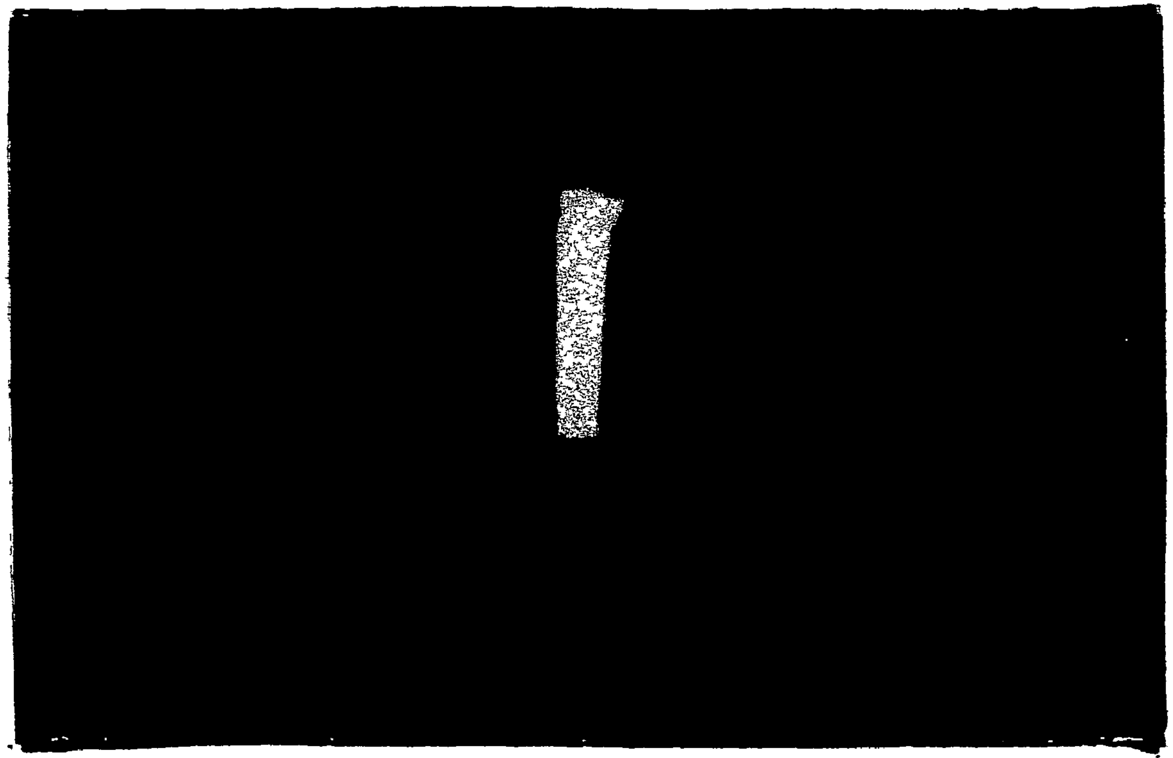

UPSTREAM VIEW OF 300 AMPERE ARC AND BLOWING NOZZLE ($\overline{V}_{\infty}$ = 35 FT/SEC) WITH 10 μ ALUMINUM PARTICLES INJECTED 3/8 " TO THE RIGHT OF ARC CENTER LINE

FIGURE 30

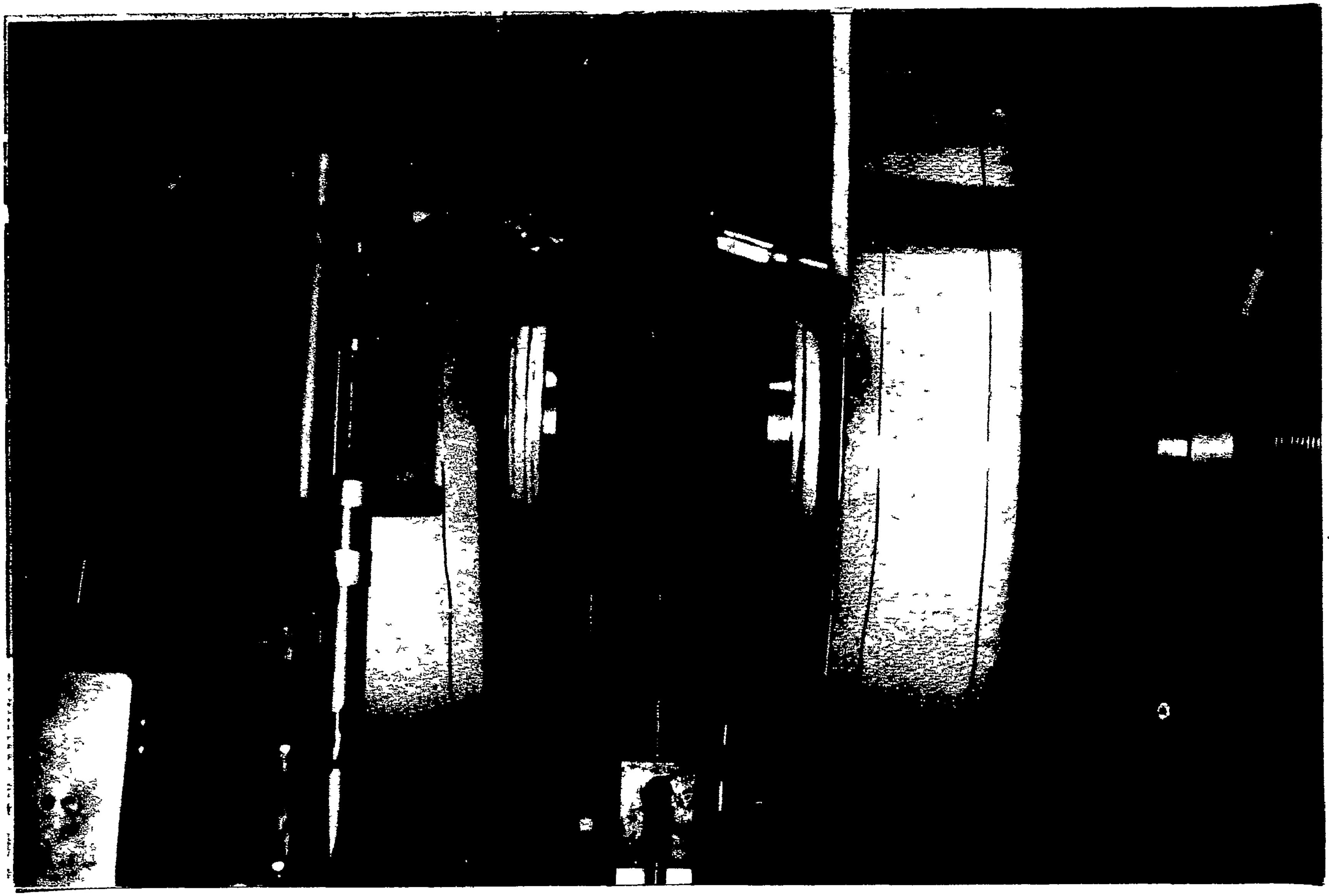

FIGURE 31 UPSTREAM VIEW OF TEST SECTION

used. The film was Anscochrome. Numerous attempts were made to photograph the particles in the wake of the arc with a range of different filters (including narrow band pass), camera settings, and film types (including infra-red sensitive). The conditions given above were the best obtainable.

In order to provide some qualitative indication of the flow behavior immediately behind the arc column, an injector was developed which would inject the aluminum particles vertically (at a low injection rate) from the elevation of the bottom locator's top surface directly behind the arc column. This injector tube is visible in Figure 30. High speed photographs (7000 frames/sec) from both the downstream direction and through a bottom mirror (Figure 20) were obtained which indicated the presence of a reasonably stagnant region directly behind the column. As shown in Figure 20, a portion of the bottom locator was removed so that the camera viewed the wake in a nearly vertical direction looking upward toward the top locator. The flow of vaporized particles, when viewed on the high-speed motion pictures, indicated a rising flow similar to the free convection at the boundary of a strongly heated body. There was at no time an indication of particles being sucked into the rearward portion of the arc's boundary or being rapidly driven downstream from the rear boundary as would be the case if some of the transverse flow penetrated the arc periphery.

Figures 32 and 33 are a few typical sequences of flow visualization pictures obtained through the bottom mirror looking upward along the rear surface of the column. The 7000 frames/sec high-speed camera was used with Ansco type 231 color film. In Figure 32 the injector was positioned in the center of the blowing nozzle exit. In Figure 33 the injector was positioned 3/8 in. toward the front magnet face. (Similar to Figure 30.) In all tests the injector was traversed from one side of the arc column (3/4 inches from centerline), through the centerline, and on to the equivalent distance on the other side. With the injector centered, a verification of wake boundary symmetry was obtained. Evaluation of single frame sequences resulted in clear evidence that vortices were shedding from the inner side of the arc wake boundary. No indication was observed of a flow in the wake on the centerline slightly downstream of the column. This region, being relatively cool (partially due to secondary flow entrainment from below), did not permit photographic detection of the vaporized particles.

D. Downstream Velocity Profiles

The next experimental phase was directed toward measuring the velocity profiles in the downstream region of the arc. Unless otherwise specified, the velocity profiles were taken at an elevation midway between the top and bottom locators. To establish the influence of the magnet walls on the open-jet flow, a series of cold

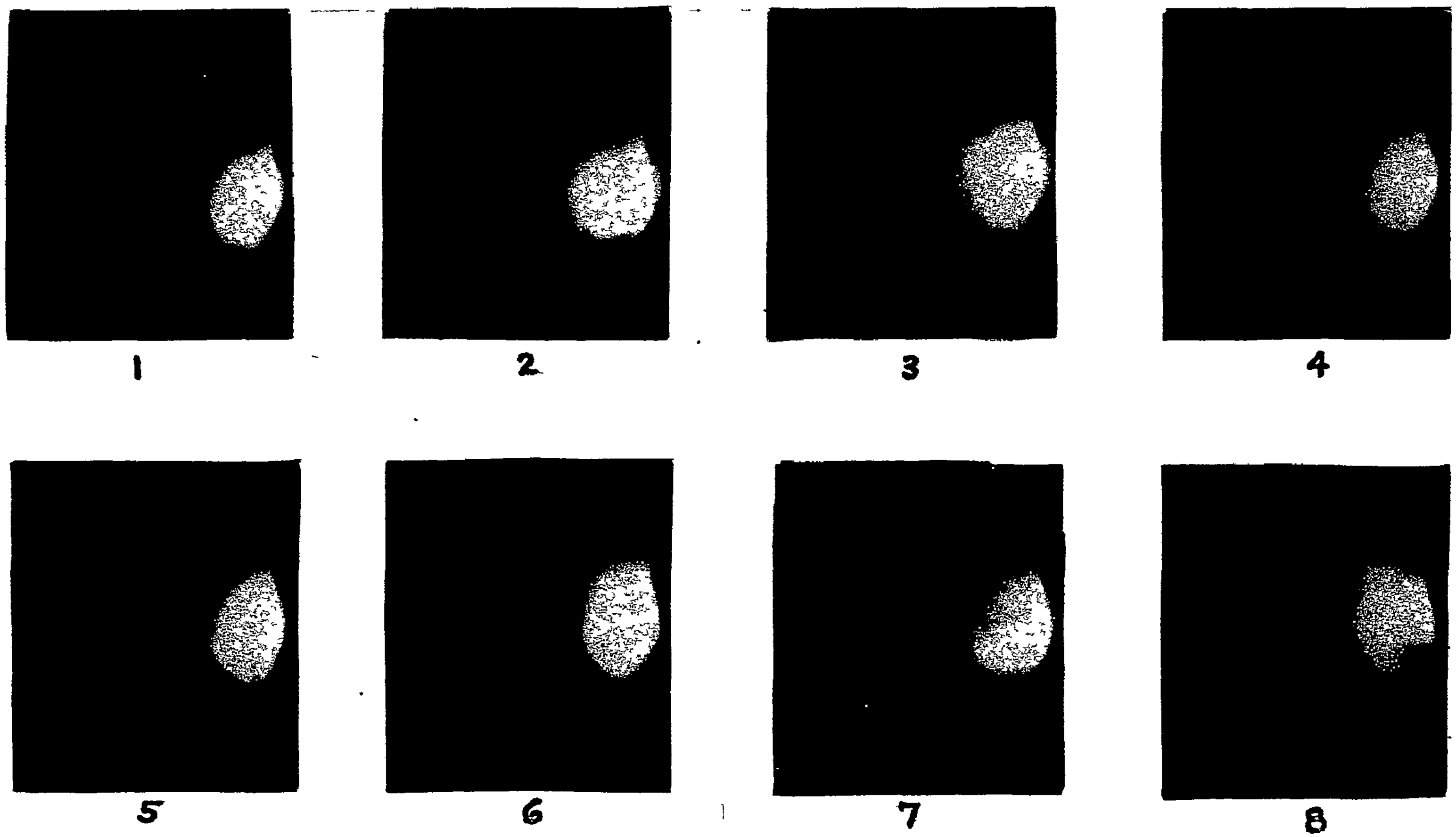

FIGURE 32 WAKE FLOW VISUALIZATION, PARTICLE INJECTOR ON ARC CENTER LINE
I = 300 AMPERES, V_{∞} = 35 FT/SEC RIGHT TO LEFT, 7000 FRAMES/SEC.

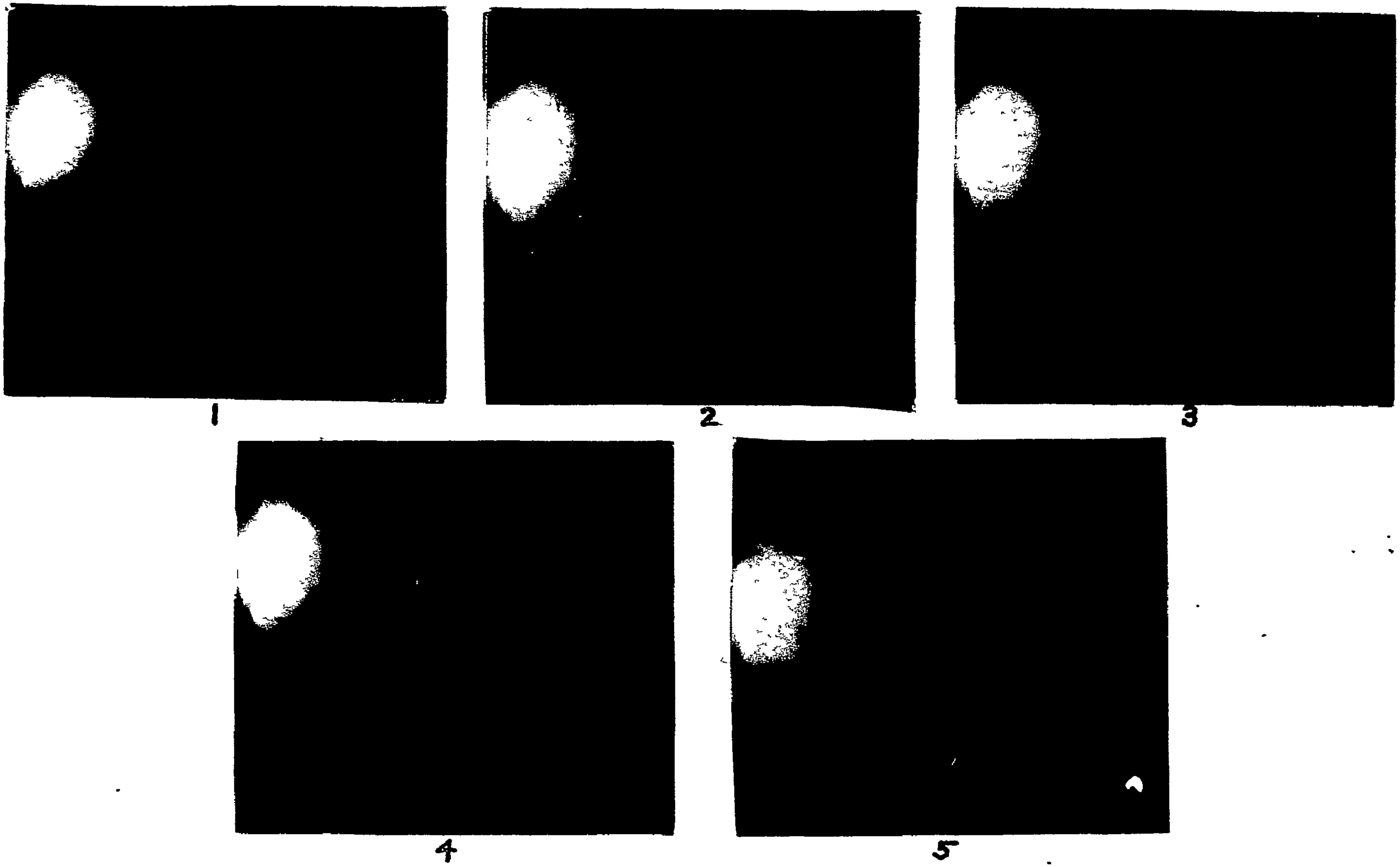

FIGURE 33 WAKE FLOW VISUALIZATION, PARTICLE INJECTOR 3/8 " OFF ARC CENTER LINE, I = 300 AMPERES, V_∞ = 35 FT/SEC LEFT TO RIGHT, 7000 FRAMES/SEC.

flow tests were conducted. In these tests, the arc was replaced by solid bodies of different shapes. The 1/16 inch o.d. enthalpy probe was used to measure the stagnation pressure from which the velocity was calculated with the assumption of atmospheric static pressure. The probe was mounted on a traversing mechanism with the output of the pressure transducer electrically read out on the Brown recorder. Table II gives a key to the stations used for the downstream profile measurements. The velocity profiles in the graphs were staggered according to the downstream location of the stations at which they were measured (i.e., the ordinate represents both distance and velocity). The method of determining a representative wake boundary, particularly when no distinct change in the slope of the velocity profiles occurs, requires an arbitrary definition. Therefore, for comparing the results of the velocity profiles, the location of the wake boundary at a specific downstream location was arbitrarily defined as that position transverse to the flow where the local velocity was half of the maximum velocity occurring at that downstream location. The line through these points (designated the wake boundary) was represented in the graphs by a rippled line. The line connecting the end of the measured wake boundary to the arc boundary is shown as a dashed rippled line. This line extrapolates the wake boundary line to the arc boundary, since probe measurements were restricted to a minimum distance of 1/4 inch from the arc axis.

TABLE II

KEY TO FIGURES 34 THROUGH 46 AND 51 THROUGH 54

STATION	(1)**	IS	0"	DOWNSTREAM	OF ARC	SYMBOL	⊗
STATION	(1*)	IS	$\frac{3}{8}$"	DOWNSTREAM	OF ARC	SYMBOL	•
STATION	(1)	IS	$\frac{1}{4}$"	DOWNSTREAM	OF ARC	SYMBOL	○
STATION	(2)	IS	$\frac{1}{2}$"	DOWNSTREAM	OF ARC	SYMBOL	x
STATION	(3)	IS	$\frac{3}{4}$"	DOWNSTREAM	OF ARC	SYMBOL	▽
STATION	(4)	IS	1"	DOWNSTREAM	OF ARC	SYMBOL	△
STATION	(5)	IS	$1\frac{1}{4}$"	DOWNSTREAM	OF ARC	SYMBOL	◊
STATION	(6)	IS	$1\frac{1}{2}$"	DOWNSTREAM	OF ARC	SYMBOL	□

Figures 34 and 35 show by the solid and dashed lines, respectively, the velocity profiles obtained both with and without the magnet walls present. The two solid drag bodies with diameters as shown in the figures were two inches long in the axial direction. These shapes were selected as being representative of the extremes of possible arc column cross-sections. Other bodies with various shapes were also tested. The measured wake boundaries fell between the two extremes of Figures 34 and 35.

First, the symmetry of the flow distribution was verified in a series of traverses across the entire wake. A typical example is shown in the far right of Figure 36. For this particular example the lower electrode assembly and bottom locator were modified (permissible in cold flow only) to facilitate measurements in the plane of the body centerline. Use of the longer, straight 1/8 inch o. d. probe also permitted checks to be made at these points.

Figure 37 shows velocity profiles downstream of three bluff bodies of varying significant dimension. It was found that with increasing bluntness the wake boundaries became slightly wider and more rapidly diverging. Also included in Figure 36 are the profile plots for cylindrical rods of various diameters. In planned future work these profiles will be compared with similar profiles of highly heated cylinders under identical flow and configuration conditions. As an intermediate step, these cold-flow velocity profiles were compared with the profiles obtained with the arc.

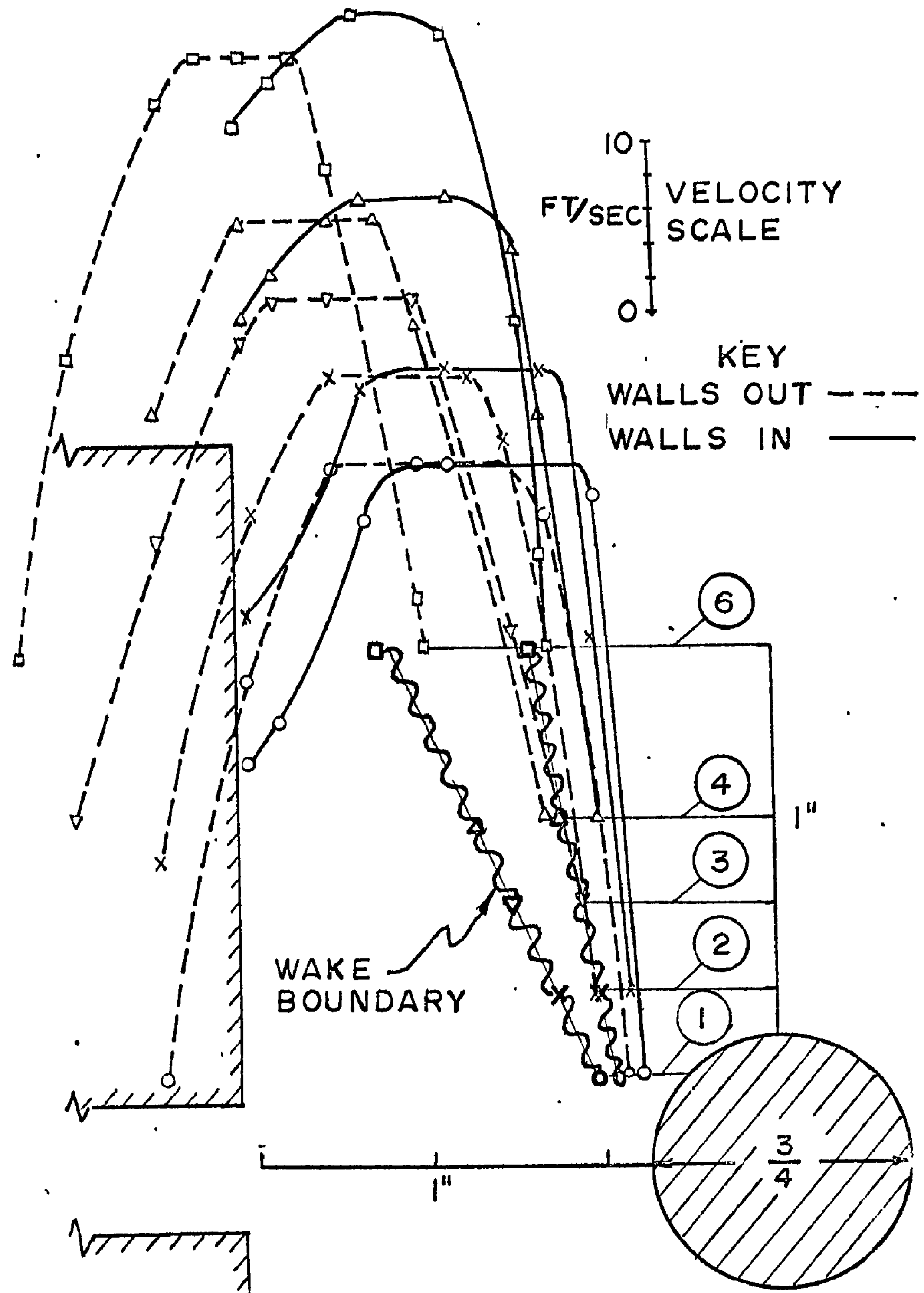

VELOCITY PROFILES DOWNSTREAM OF SOLID CYLINDER
(BLOWING VELOCITY = 42 FT/SEC)
FIGURE 34

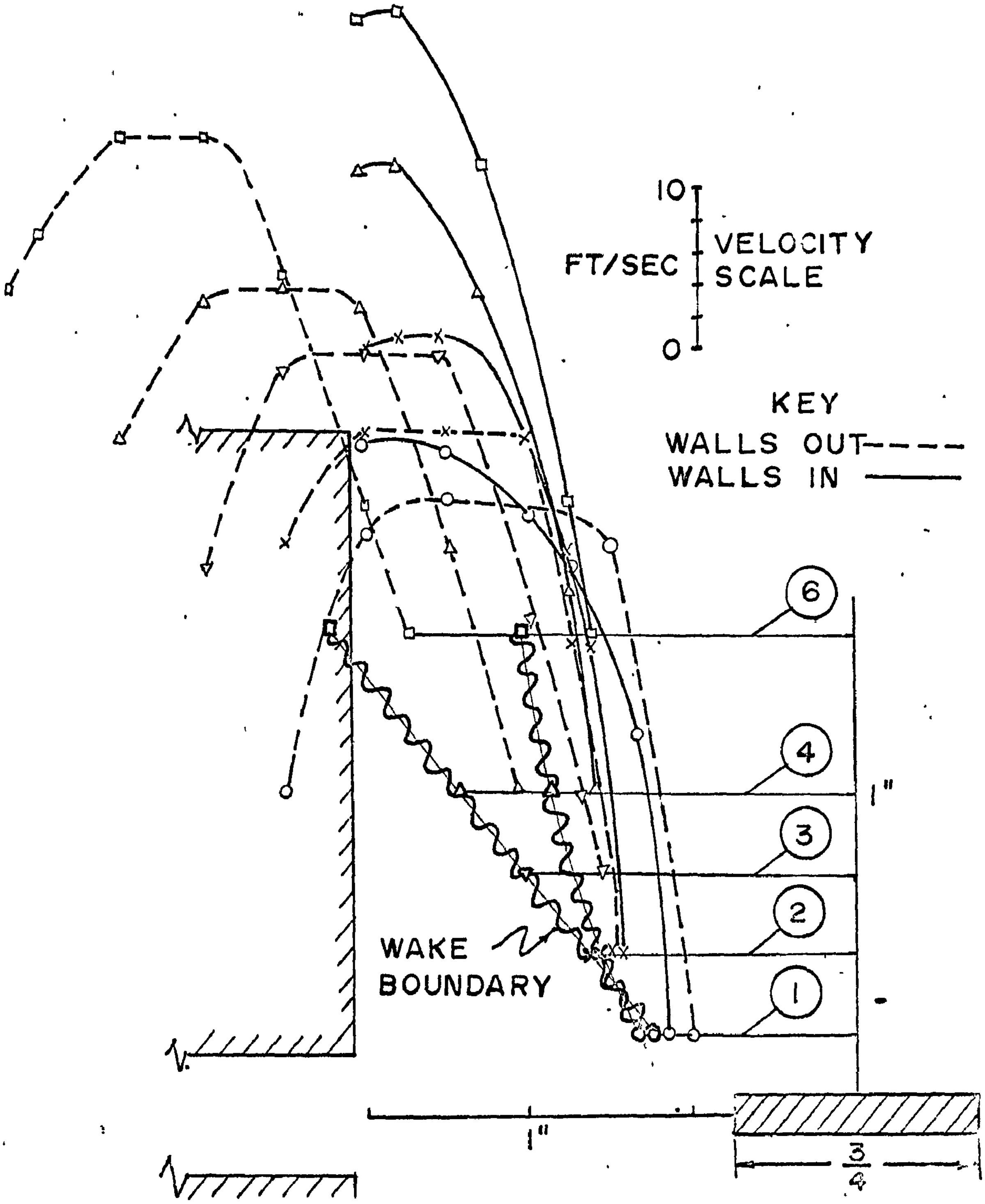

VELOCITY PROFILES DOWNSTREAM OF FLAT PLATE
(BLOWING VELOCITY = 42 FT/SEC)
FIGURE 35

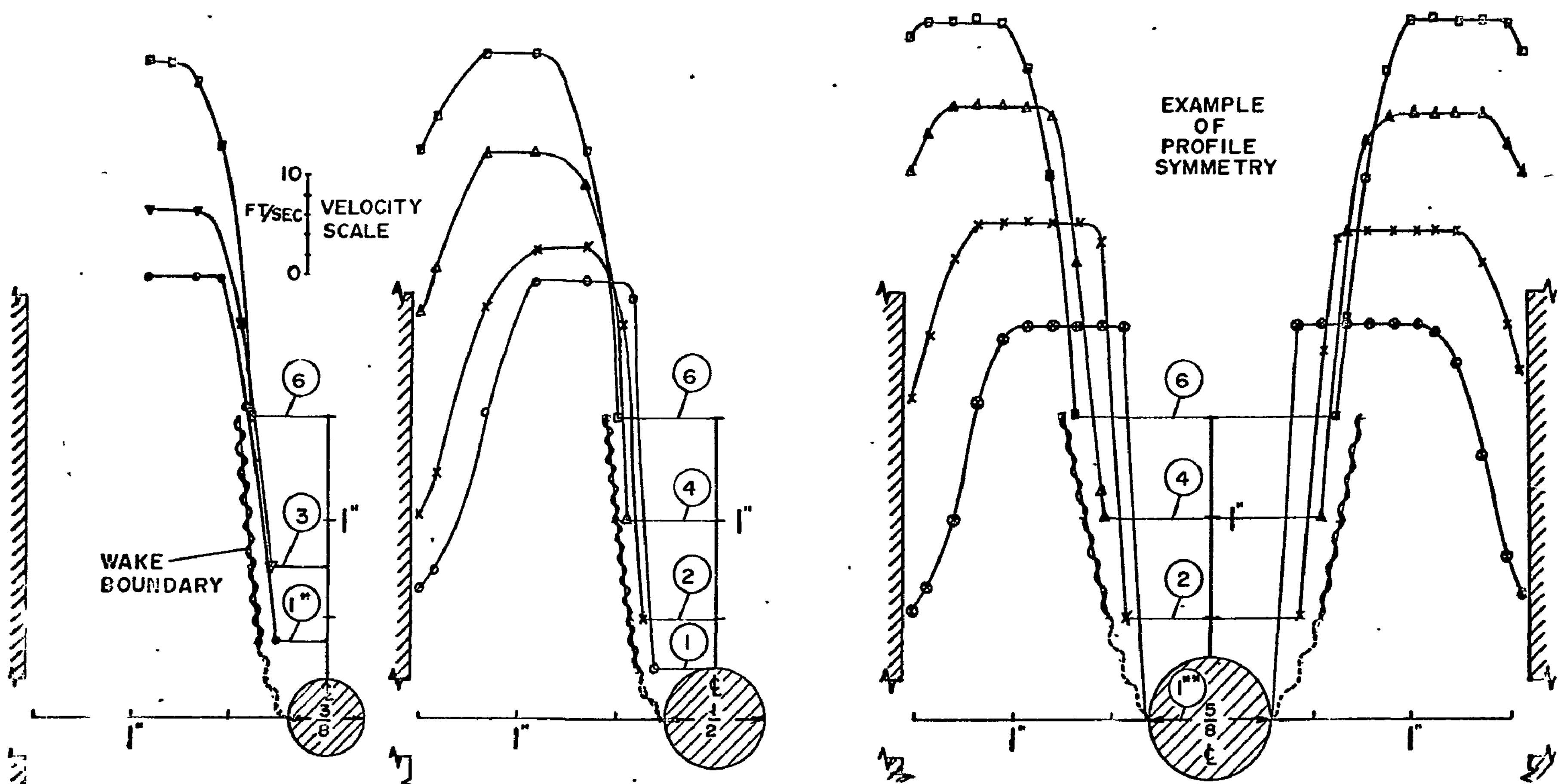

VELOCITY PROFILES DOWNSTREAM OF SOLID CYLINDERS
(BLOWING VELOCITY = 42 FT/SEC)

FIGURE 36

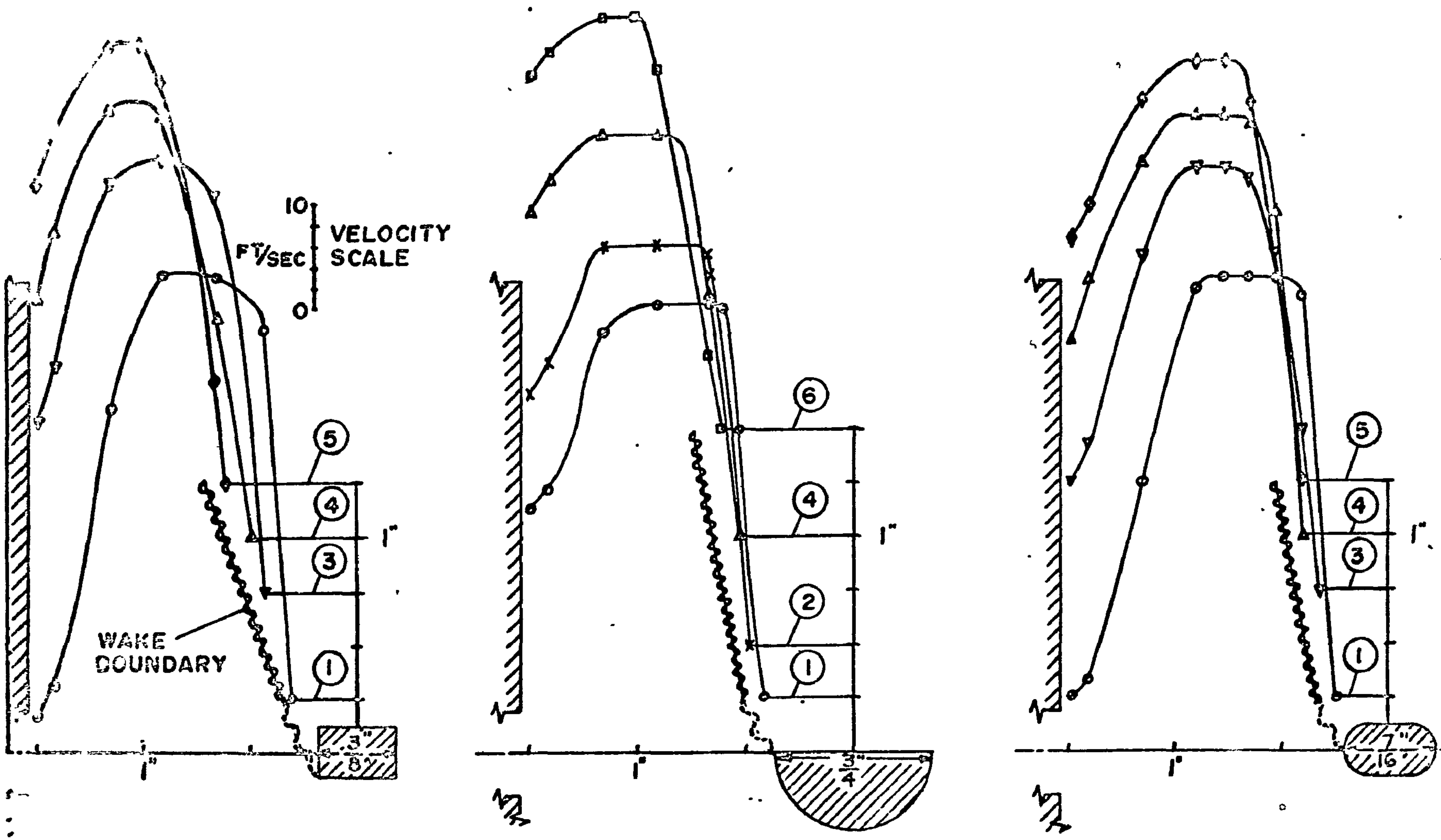

VELOCITY PROFILES DOWNSTREAM OF SOLID BLUFF BODIES
(BLOWING VELOCITY = 42 FT/SEC)
FIGURE 37

As a next step, similar measurements with the arc in the balanced mode were conducted, with the arc current and the blowing velocity being varied. Again, first the existence of profile symmetry behind the arc column was verified. Figure 38 shows that reasonably symmetric wake boundaries were obtained. The arc column cross-sectional contour was represented by the dashed line, using the data from Figure 26 as the major and minor axes of the assumed ellipse. Since the wake was symmetric with respect to the plane through the arc centerline and flow axis, data for most of the tests were obtained for only one-half of the arc wake.

Figures 39 through 42 illustrate the effect of increasing current on the flow distribution for constant blowing velocity. In general, with increasing current, the wake boundary was displaced outward. This effect was more pronounced at high blowing velocities (see e.g., Figure 42). It can only be partially explained by the increase of the arc diameter. It may be possible that some fluid from the interior of the arc was being expelled laterally, causing flow separation to occur sooner.

Figures 43 through 45 show the effect of increasing blowing velocity for constant arc currents. This effect was far less pronounced than the effect of increasing current at constant velocities. In fact, in some cases the wake boundary was unaffected. This

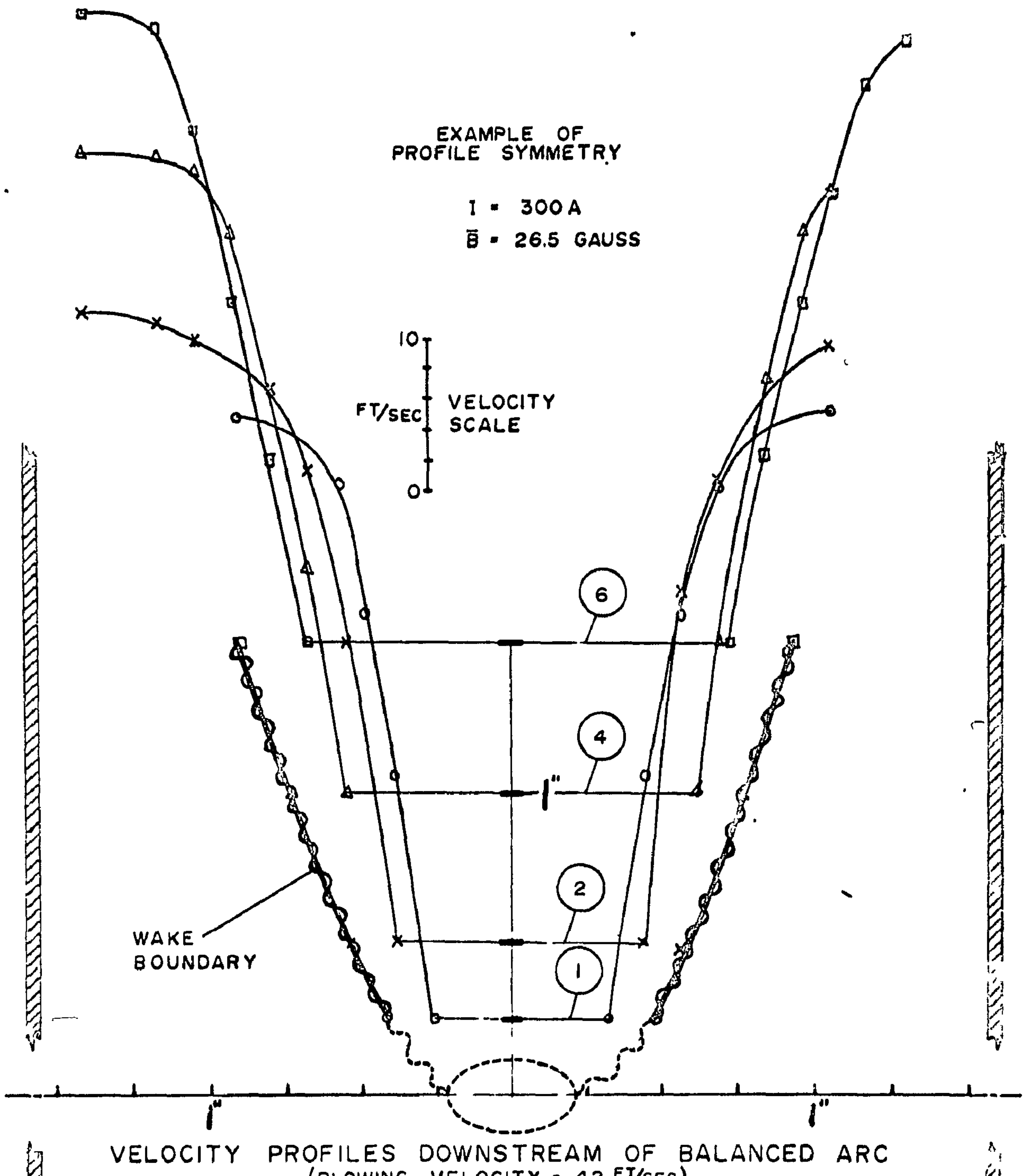

VELOCITY PROFILES DOWNSTREAM OF BALANCED ARC
(BLOWING VELOCITY = 42 FT/SEC)

FIGURE 38

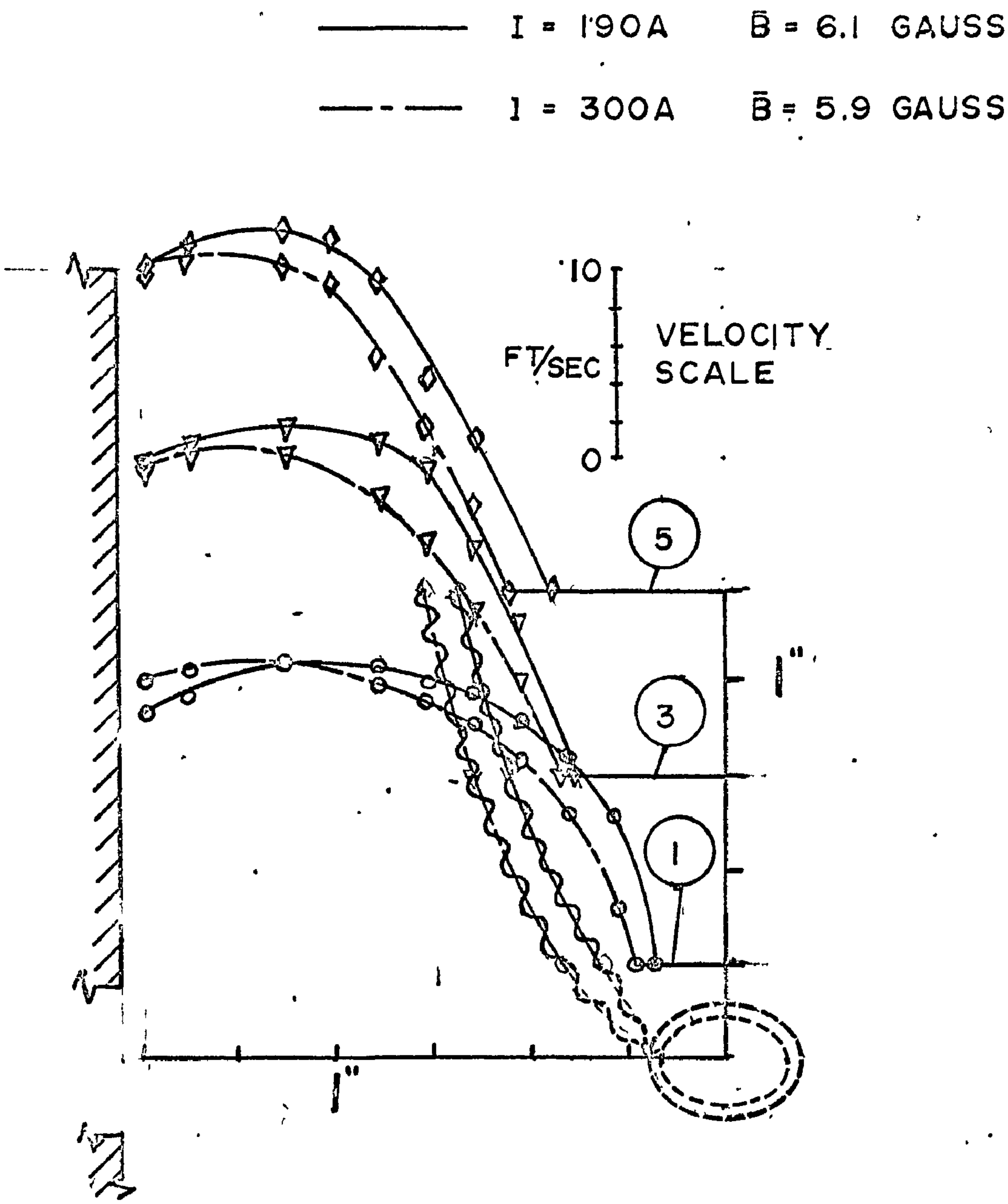

VELOCITY PROFILES DOWNSTREAM OF BALANCED ARC
(BLOWING VELOCITY = 18 FT/SEC)
FIGURE 39

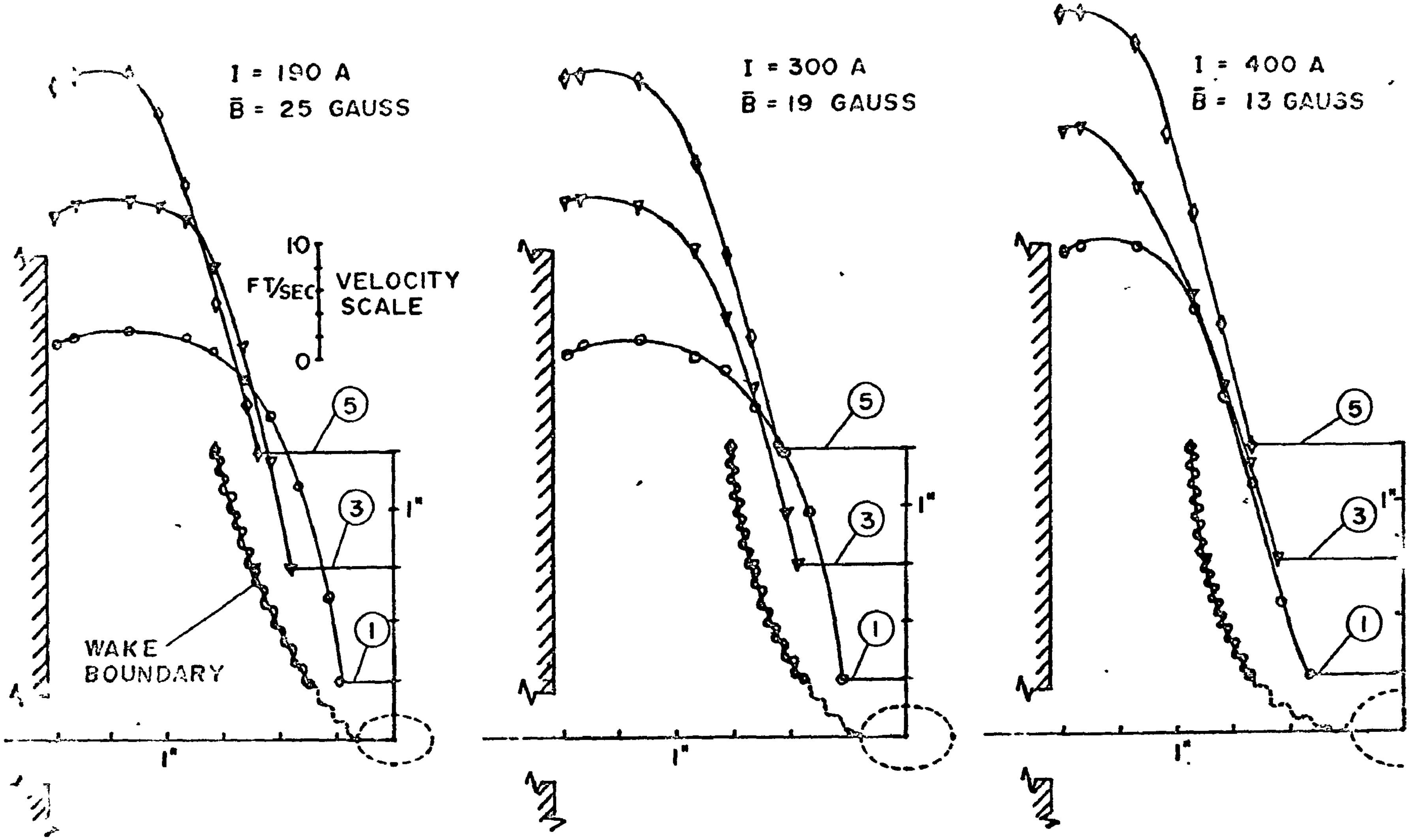

VELOCITY PROFILES DOWNSTREAM OF BALANCED ARC
(BLOWING VELOCITY = 35 FT/SEC)

FIGURE 40

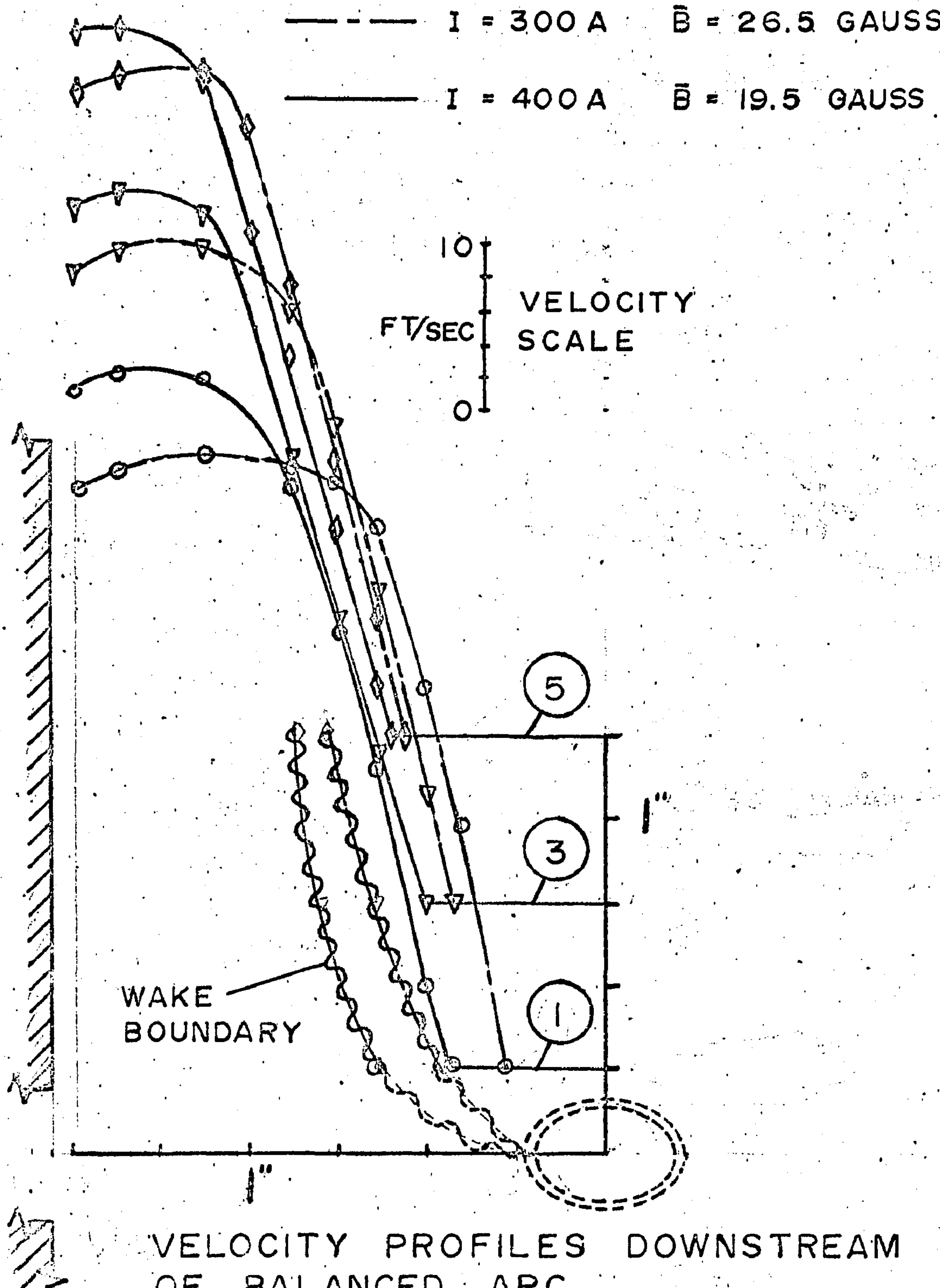

VELOCITY PROFILES DOWNSTREAM OF BALANCED ARC
(BLOWING VELOCITY = 42 FT/SEC)

FIGURE 41

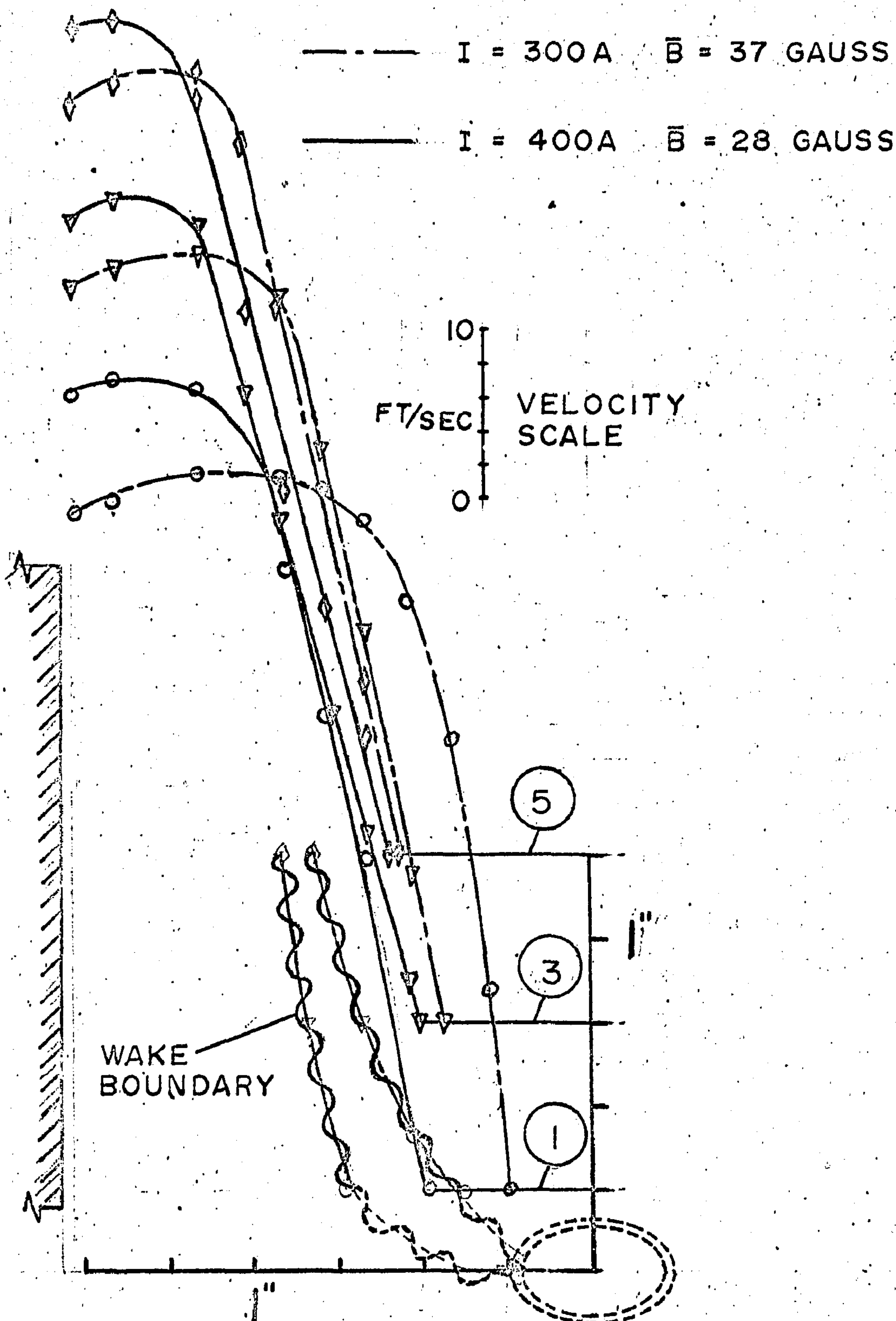

VELOCITY PROFILES DOWNSTREAM OF BALANCED ARC
(BLOWING VELOCITY = 51 FT/SEC)

FIGURE 42

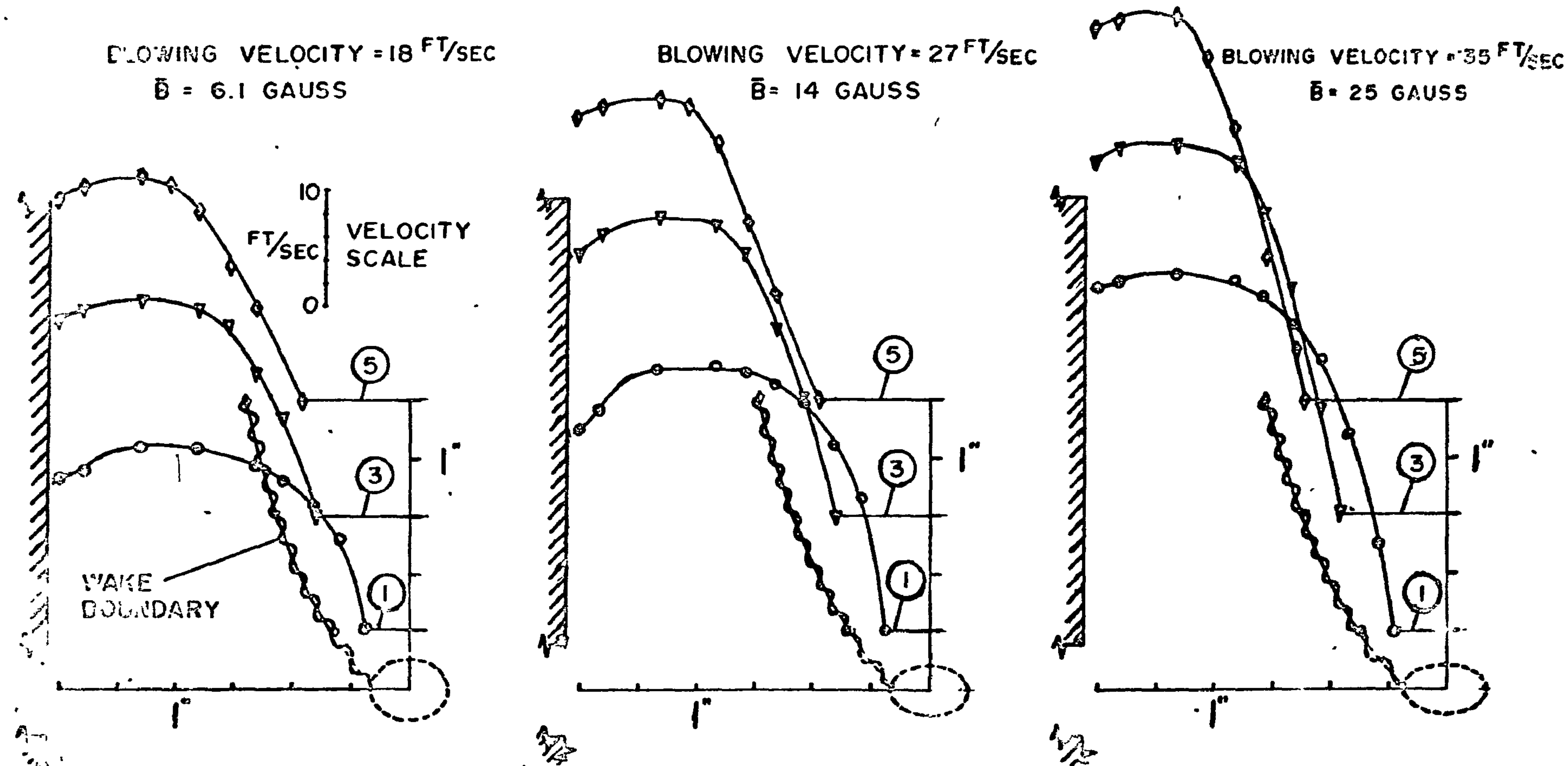

VELOCITY PROFILES DOWNSTREAM OF BALANCED ARC
(I = 190 A)

FIGURE 43

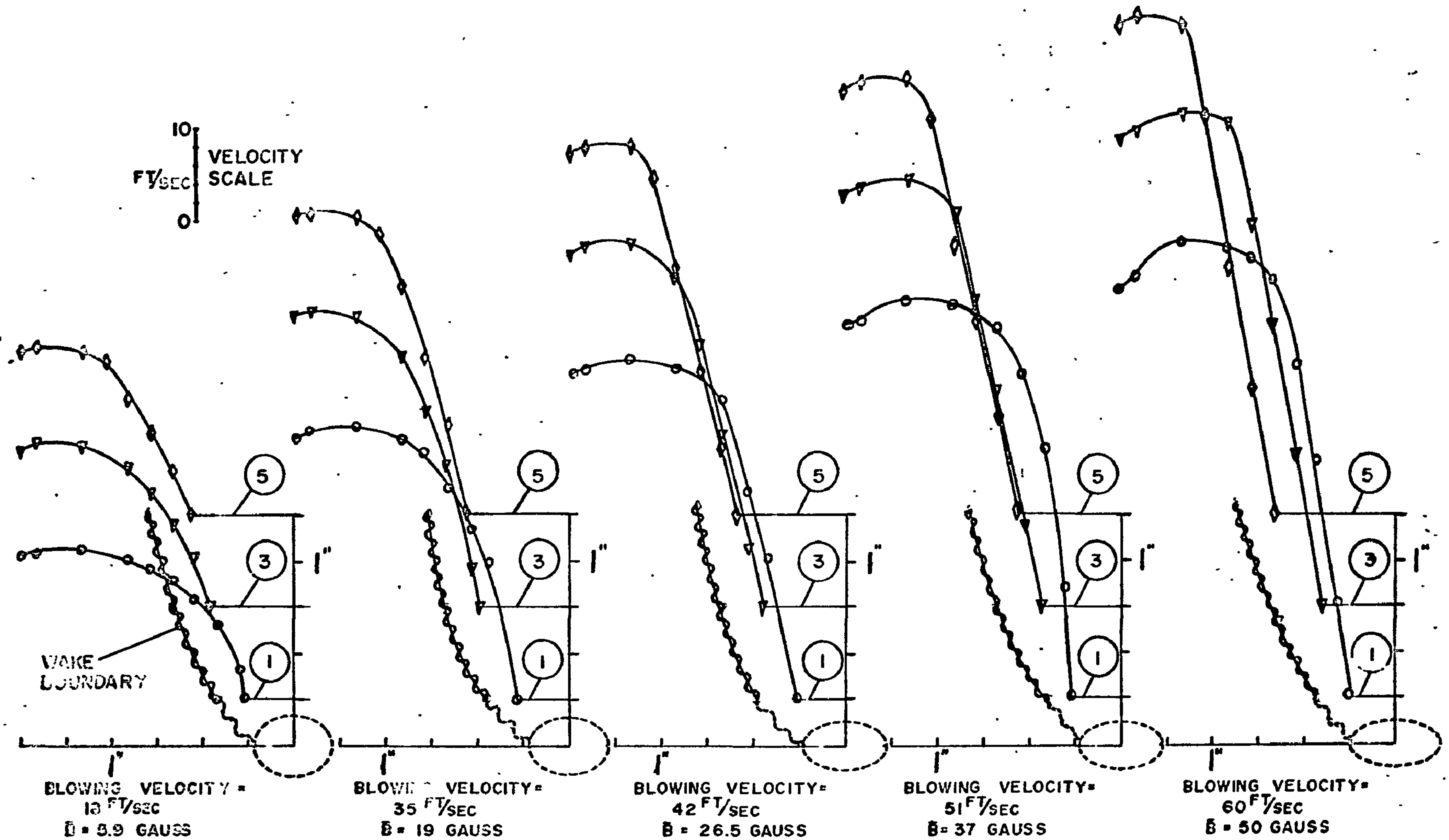

VELOCITY PROFILES DOWNSTREAM OF BALANCED ARC (I= 300 A) (MAGNET WALLS OMITTED FOR CLARITY)

FIGURE 44

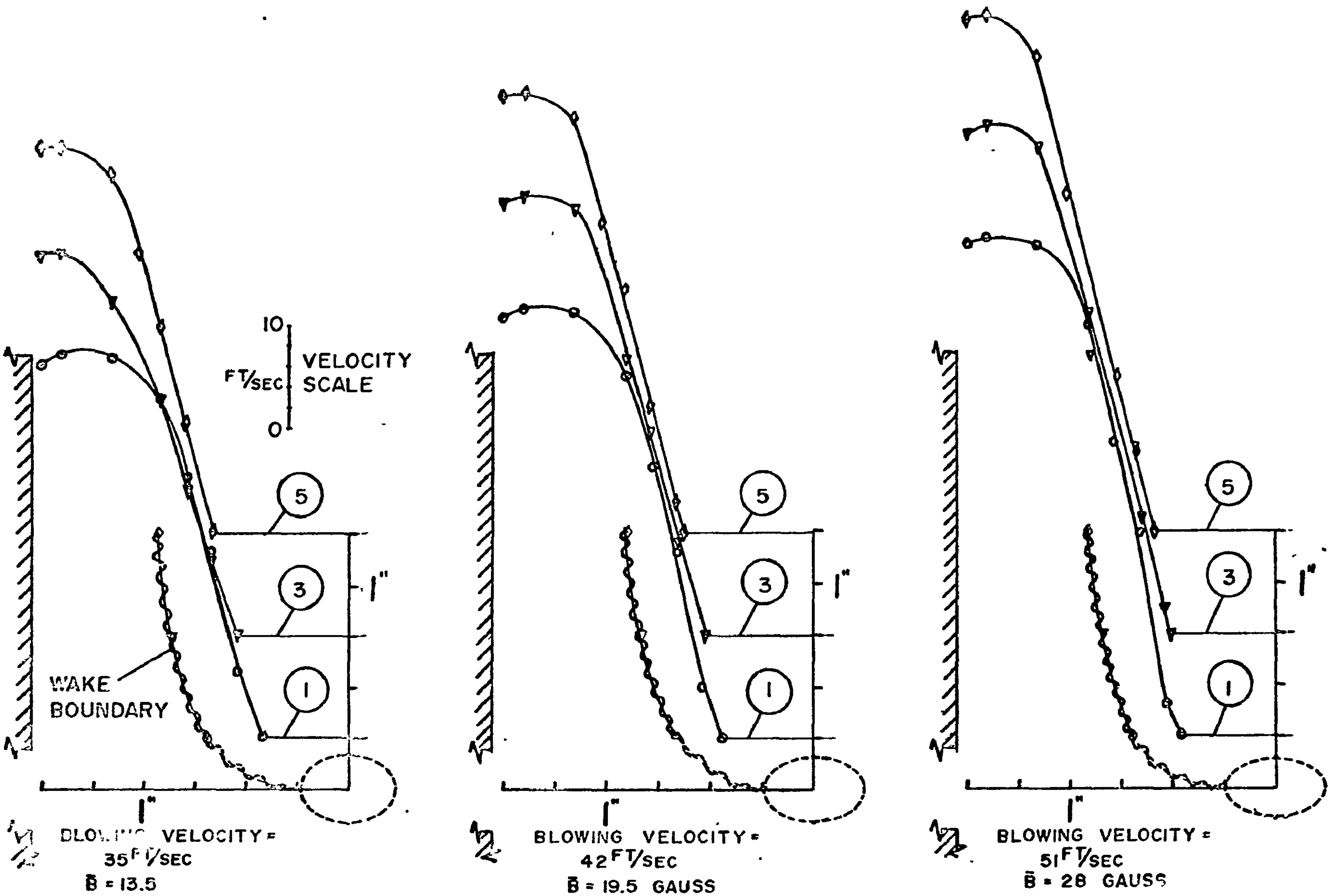

FIGURE 45 VELOCITY PROFILES DOWNSTREAM OF BALANCED ARC
(I = 400 A)

result was surprising, in so far as an increase of the blowing velocity invariably resulted in a flattening of the arc (Figure 26), which would be expected to broaden the wake.

In the solid body experiments the flow may be considered two-dimensional; however, with the arc experiments the flow must be considered three-dimensional due to the vertical flow components within the arc (cathode jet) and the vertical free-convection boundary layer flow. Therefore, traverses were made with a probe at three different vertical elevations. The results are shown in Figure 46. The trend shown by the wake boundary was to widen slightly at higher elevations. This was anticipated both on the basis of the observed slight growth of the arc column in the vertical direction (see Figure 30), and also of free convection effects. The vertical velocity component near the arc was determined to be negligible with a properly placed enthalpy probe (90°-bend model). Figure 22 shows the test set-up. Several traverses were made in the region directly behind the arc column at three different elevations. Only very insignificant velocities, being lower than 1 ft/sec, were measured.

The solid bluff body comparison profiles in Figures 36 and 37 showed that the wake was considerably narrower for any solid body having a transverse dimension D approximately the same as that of the arc. However, an analogy of an arc to an unheated cylinder would not be expected to be as valid as one with a heated cylinder.

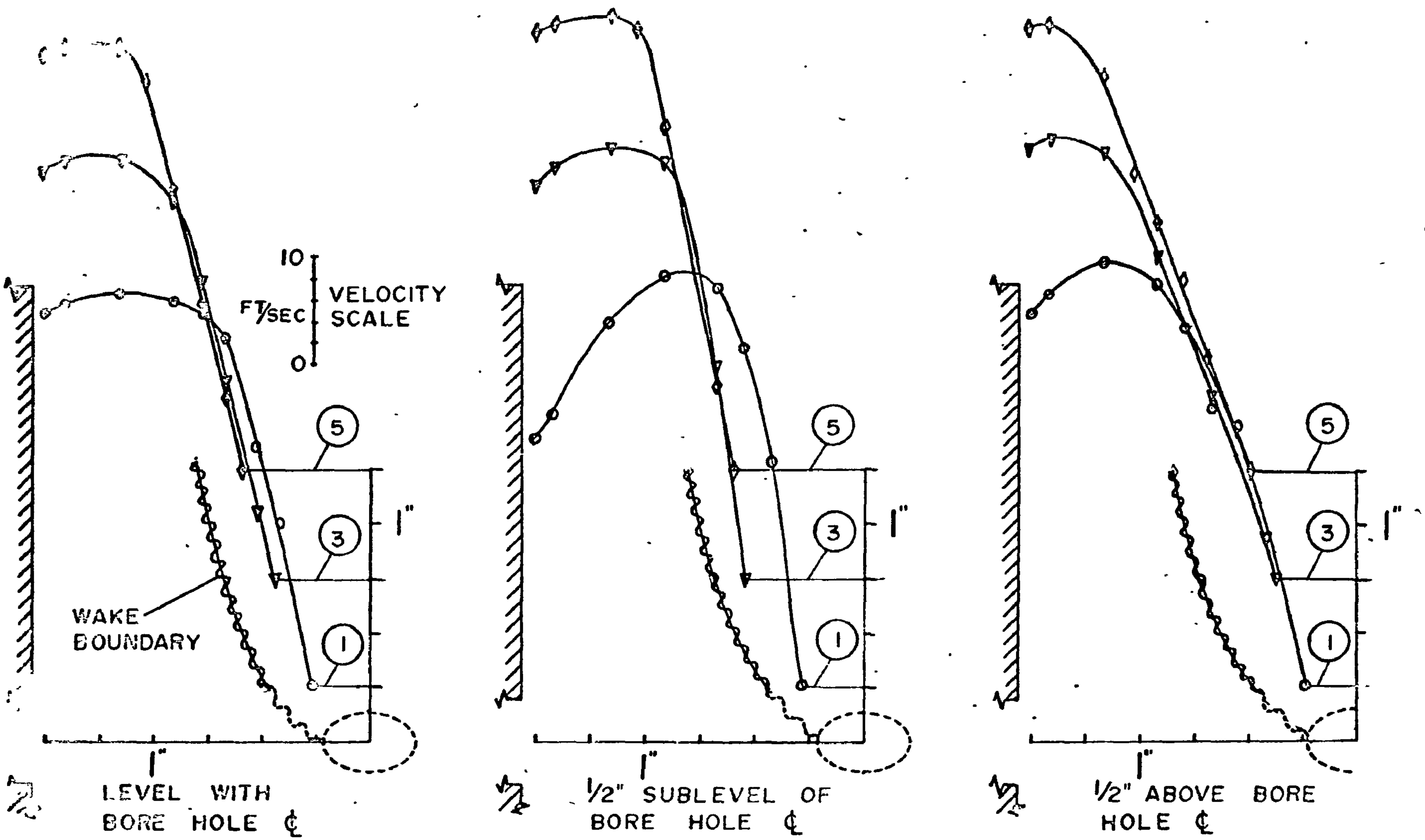

VELOCITY PROFILES DOWNSTREAM OF BALANCED ARC AT 3 ELEVATIONS
I = 300A BLOWING VELOCITY = 42 FT/SEC $\bar{B}$ = 29 GAUSS

FIGURE 46

Because no drag nor wake data were found in the literature for highly heated cylinders, some preliminary tests were performed with a heated cylinder positioned similarly to the arc column between the locators. Surface temperatures of up to 1600 °C, considerably below those of the arc, were obtained in these preliminary tests. The heated cylinder wake boundary width increased up to 100 per cent over the unheated cylinder wake width and more nearly approximated that of the arc wake. However, the arc wake was still wider than any of the heated cylinder data with a D comparable to the D of the arc.

E. Enthalpy Distributions Downstream of the Arc

The next phase of experimentation was concerned with the measurement of the enthalpy distribution downstream of the arc. This provided definite information on the mechanism of energy dissipation of an arc in cross-flow and on the local distribution of this energy. Figure 47 represents the results of the enthalpy determinations in the wake of a cross-flow arc for the 300 ampere case. Since the majority of the previous test data (including many recalibration and reproducibility check runs) were taken for the 300 ampere arc, these measurements were also conducted at a current of 300 amperes. Because all previous checks on wake symmetry demonstrated good agreement, only one side of the arc's wake was scanned for determining the specific stagnation enthalpy distributions. The 1/16 inch o.d. calorimetric probe was operated, as

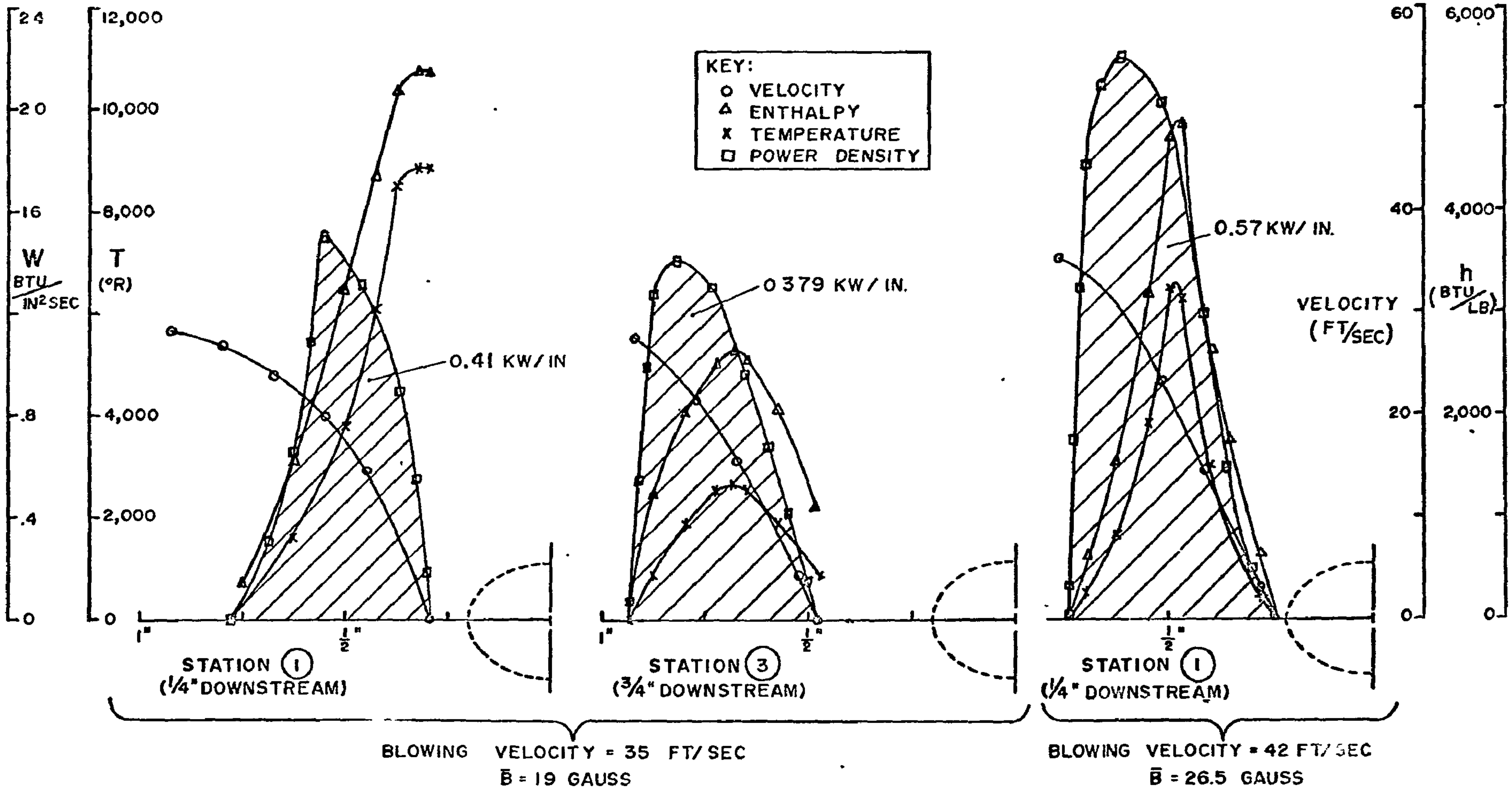

POWER DENSITY, ENTHALPY, TEMPERATURE, AND VELOCITY DISTRIBUTIONS DOWNSTREAM OF BALANCED ARC (I = 300 AMPS)

FIGURE 47

discussed previously in the experimental equipment section, utilizing the "tare" measurement technique. Sufficient time was spent at each traverse test position to allow the probe to reach equilibrium. The temperature profiles shown were calculated from the measured stagnation enthalpy values on the basis of the known temperature dependence of the specific heat of air. Assuming atmospheric static pressure, the density was obtained from tables of air data. Using the wake velocity obtained earlier, the energy flux W (KW/unit area) was calculated at each point in the wake according to the formula $W = \frac{hV_\infty P}{RT}$, where P is the ambient pressure and R is the gas constant. The curve shown in Figure 47 by the solid line with square marker points represents the local energy flux, which was calculated. By integrating the W values across the wake, the total energy per unit arc length in the wake was obtained. The KW/in values indicated in Figure 47 are for one-half of the wake. These values should be nearly the same for the two plots on the left. The difference between the two values is less than the experimental uncertainty. By comparing the cases for the two blowing velocities treated in Figure 47, an increase in power per unit arc length is noted with increasing blowing velocity. Further, a slight decrease from station (1) to station (3) in the power carried in the wake can be observed. The shape and position of the calculated energy flux profiles show that the maximum heat flux occurs approximately at the wake boundary.

The values obtained for the power added to the flow were considerably smaller than had been anticipated. Lord and Broadbent (47) state: "As much as 25 times more heat goes into the wake of an arc magnetically held in a cross-flow than from an equivalently heated cylinder". However, if this were true, certainly a large amount of flow ought to penetrate the hot arc boundary or else the heat transfer process from the arc's boundary to the surrounding flow would have to be extremely high e.g., due to an unusually intense turbulent mixing. However, the applicability of the data used from Adams to the model proposed by Lord is open to criticism. Under these circumstances, it seemed of importance to have a check of the measured power dissipation obtained by another method. A way to do so consisted in evaluating the overall power balance of the arc.

F. Overall Power Distribution

In order to determine how the power consumed by the arc was distributed among the different types of heat losses, an effort was concentrated on each particular heat loss mode. Before proceeding with a discussion of this phase, a brief explanation is required on the method of determining the power input to the portion of the arc column under test.

The technique most frequently employed and used in all the previous investigations reported in the literature was the conventional one in which the voltage gradient was determined through measurements of the total arc voltage for constant current but different arc lengths. The slope of the curve of the voltage between the electrodes as a function of the arc length provided the voltage gradient. The gradient obtained by this technique, however, depends on the gap length and the magnitude of the end effects. For most experiments where the arc column was observed to oscillate rapidly, the gap distance measured between the electrodes was used in computing the voltage gradient. This electrode gap may be significantly different from the actual length of the arc column. Photographic techniques would be a better method to measure the true length of the arc column. In addition, there is no guarantee that the changing of electrode gap does not have an effect on the electrode drop region, particularly when under the influence of external magnetic fields.

Suits (67) determined the voltage gradient by employing a unique vibrating electrode technique. The electrode was vibrated in the axial direction at a frequency of approximately 30 cycles per second throughout an amplitude of a few millimeters. Measurements of the corresponding periodic change in arc voltage were used to give the voltage gradient. This technique is valid only for low current arcs between relatively large gaps which are reasonably free from the electrode jet effects.

The technique in the present investigation used the locators themselves to measure the potential. There is some error introduced by the cathode jet effect in the region of the bottom locator, but since the constriction "pinch" effect of the locator was minimized this should be a local effect and the main portion of the column may be relatively unaffected. This technique, therefore, appears to be a more reliable indication of true voltage drop for that portion of the positive column investigated.

The results of the voltage gradient measurements as a function of blowing velocity, with current as a parameter, are shown in Figure 48. The voltage gradient appears to increase almost linearly for each particular current level until a threshold region of blowing velocity is reached. Here, a more rapid increase begins, as the blowing velocity is increased still further. Voltage gradient data were also obtained by using a 1/16-inch o.d. water-cooled copper probe which contacted both the upstream and downstream arc boundary. These data show considerably more scatter and indicated a somewhat greater slope than Figure 48. Therefore, the voltage gradient values from Figure 48 were used for the power distribution comparisons. The voltage gradient measured in the free-burning case (i.e., without external transverse fields) compared favorably with the values reported by King (60) for free-burning arcs with relatively large gaps in the same current range. The

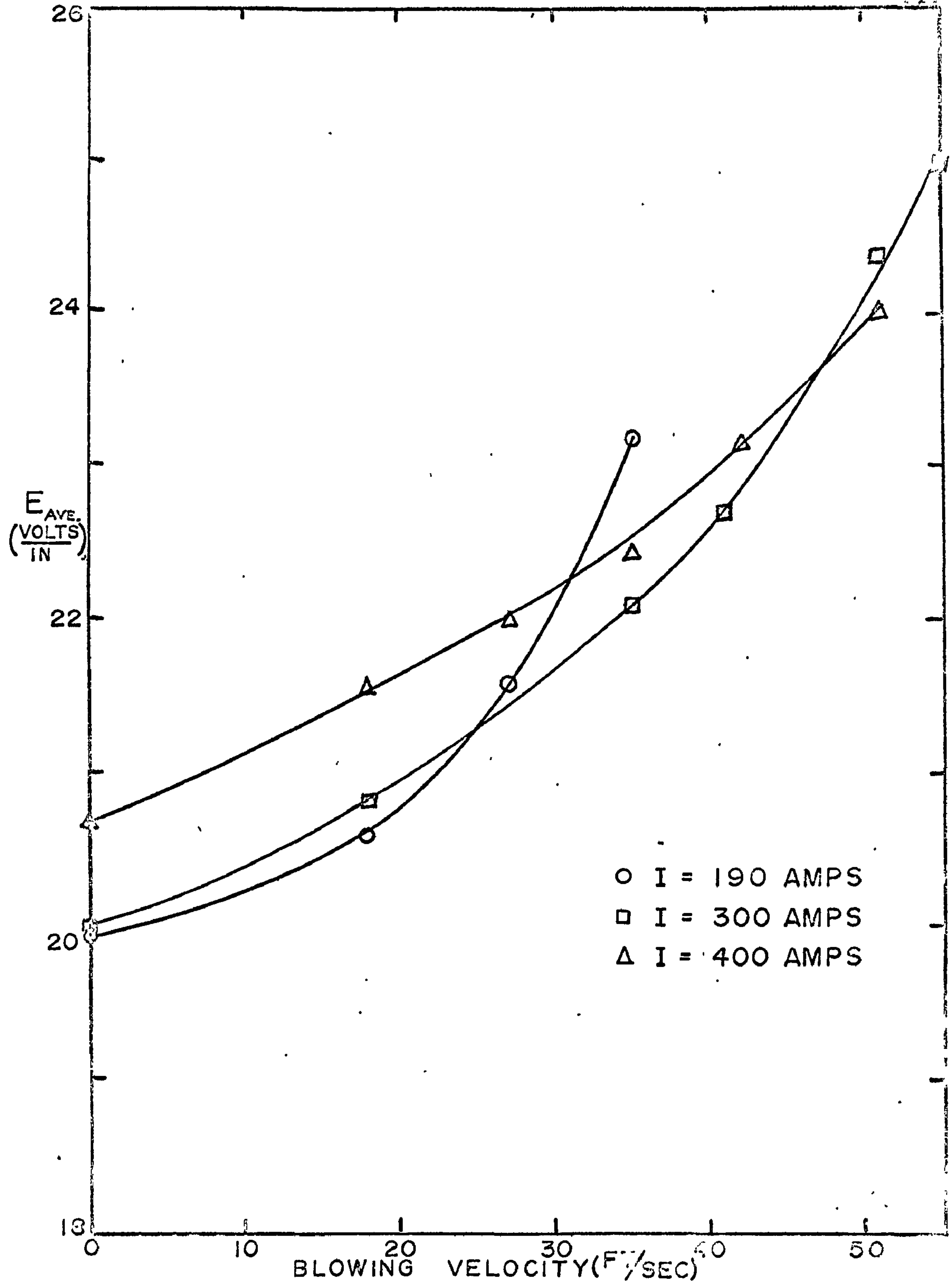

POSITIVE COLUMN VOLTAGE GRADIENT AS A FUNCTION OF TRANSVERSE BLOWING VELOCITY

FIGURE 48

range of values reported for the voltage gradient by previous investigators of magnetically-balanced cross-flow arcs when in the balanced mode are shown below:

Thiene (31)	E:	17.8 to 20.3 volts/in.
Bond (39)	E:	35.5 volts/in.
Myers (52)	E:	55.8 to 132.0 volts/in.

The large differences in these values of voltage gradient may be attributed to the fact that each of these investigations was conducted in operating ranges which did not coincide. In the present investigation the positive column average voltage gradient, as seen in Figure 48 at current levels between 200 to 400 amperes, increased from the no-blowing value of approximately 20.5 volts/in. to a maximum of 25 volts/in. corresponding to a blowing velocity of 55 ft/sec.

In the overall power distribution analysis, the different types of losses were accounted for by making the measurements indicated below.

1. Conduction — the kilowatts of power dissipated to the solid elements surrounding the arc were calculated, knowing the mass flow rate of cooling water through each individual element and the temperature difference between the inlet and outlet sections. The temperatures were read out automatically on the Brown stepping recorder while the water flow rates in gallons per minute were read

on the flowmeters. A water-cooled calorimeter and copper shield were fabricated to measure the power loss up the stack of the anode region. The copper shield was identical to the mu metal shield shown in Figure 10, and was located directly above it. The calorimeter was mounted directly above the copper shield. The calorimeter was made by winding 1/4-inch o. d. copper tubing into a convergent nozzle configuration. The top of the calorimeter (apex of the cone) was sealed off. Each of the individual calorimeter elements were electrically floating.

2. Forced convection — the kilowatts of input power to the arc column which were dissipated to the wake of the arc in the cross-flow mode were measured with the calorimetric probe discussed in the experimental equipment section.

3. Radiation — the kilowatts of input power to the arc column which were dissipated to the surroundings by radiation were measured with a thermopile (Figure 49). The thermopile was calibrated against two standards of total radiation (integrated over wavelength). The standards were carbon filament lamps obtained from the Bureau of Standards. The following assumptions were made in the test measurements: the plasma was optically thin, the radiation was isotropic, and the lateral distance from the thermopile to any volume element within the column was approximately the same. Knowing the constant of the thermopile (linear

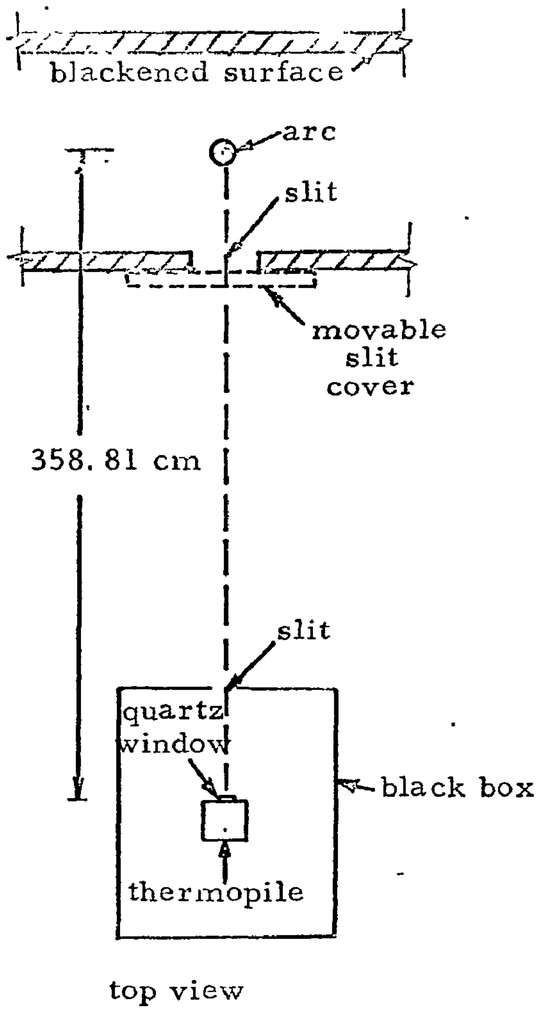

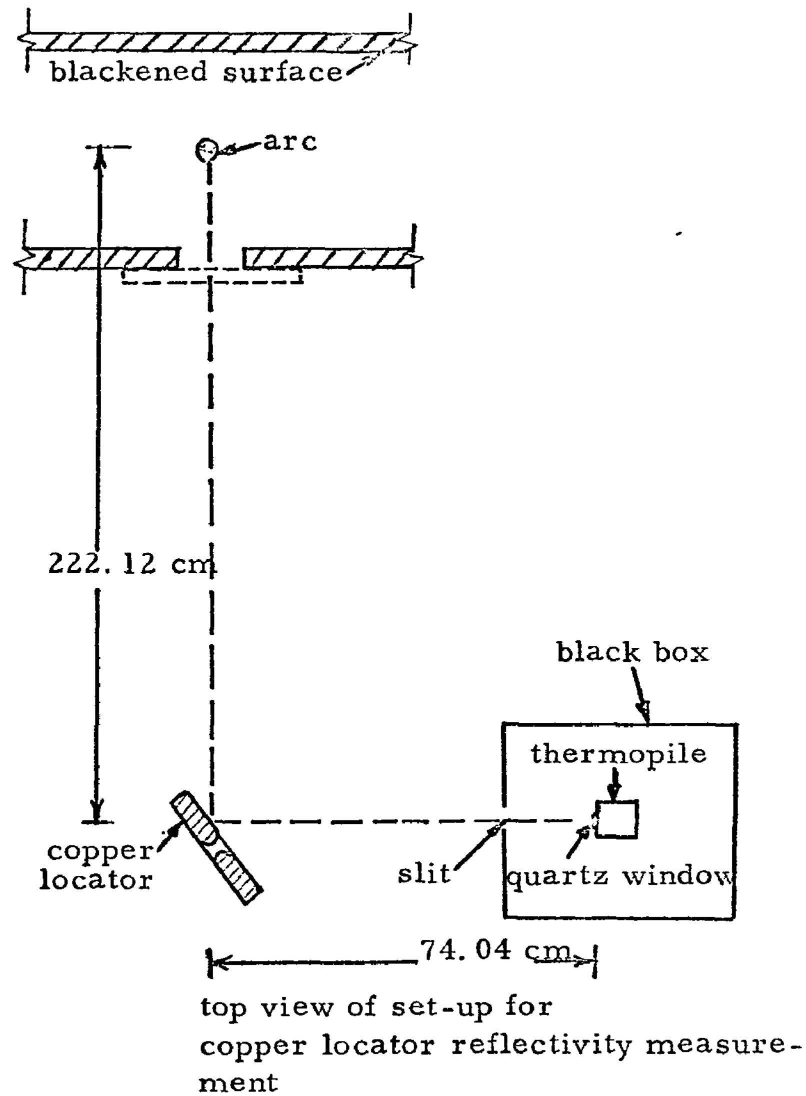

FIGURE 9 SCHEMATIC OF APPARATUS FOR RADIATION MEASUREMENTS

response) and the output voltage read out on a nanovoltmeter allowed the total power collected by the thermopile to be calculated. By correcting for the approximate solid angle through which the radiated power escaped from the column without hitting anything, the total power radiated in kilowatts was determined. This correction included taking into account the absorptivity of the top and bottom locators (Figure 49).

4. Free convection —— the losses due to free convection were not measured, but represented only a small percentage of the overall power input.

Table III shows the resulting power distribution for the free-burning arc (i.e., no external fields applied). The total input powers indicated were calculated from the total arc voltage and current. It is important to note that closing off the anode region with the copper shield and the coiled copper calorimeter had a very definite influence on the anode behavior. It caused the voltage measured from the top locator to the anode to decrease. However, no influence on the column between the locators was detectable. As can be seen from Table III, for the 300 ampere case the upper locator, anode, top calorimeter and shielding absorbed almost 75 per cent of the total power input. Radiation accounted for 3.7 per cent of the total power input. Therefore, the results for the free-burning tests indicated that only a very small fraction of the

TABLE III
POWER DISTRIBUTION
FREE-BURNING, NO CROSS-FLOW

	POWER MEASURED (K.W.)			
Cathode	0.212	0.265	0.370	
Bottom Calorimeter	1.070	2.500	3.050	
Top Calorimeter	0.657	1.410	2.150	
Bottom Locator	2.240	4.930	6.050	
Top Locator	5.620	8.500	12.330	
Anode	7.600	13.700	22.300	
Metal Shield	1.313	3.410	5.520	
Copper Shield	2.940	4.270	4.680	stack losses
Calorimeter Coil	5.220	5.300	5.960	
Radiation	1.01	1.74	2.57	
TOTAL	27.882	46.025	64.980	
Power Input	29.80	47.70	67.20	
Unaccounted For	1.918	1.675	2.22	
	(I = 200A)	(I = 300A)	(I = 400A)	

total power input goes into the gas surrounding the arc. Less than 3.5 per cent was left unaccounted for in the 300 ampere case. Part of this may be due to the free-convection heat transfer to the surrounding air.

In Table IV are shown results obtained for the power distribution with the arc in the balanced mode after the external fields were applied. The copper shield and coiled calorimeter above the anode were removed for these tests because of the undesirable anode behavior obtained in their presence. As also manifested in the change of the total input power, the voltage between the anode and the top locator changed when the calorimeter shields were removed. A slight portion of this input power change was due to the voltage increase between the locators when the external fields were applied due to a change in the arc's resistance. The same percentage power losses were assumed for the stack as measured in the free-burning case. The top locator and anode region dissipated almost 70 per cent of the total power input in the 300 ampere case. Four per cent of the total power input was measured in the wake of the arc. Approximately three per cent was left unaccounted for. The results appear to confirm the power dissipation measurements of the enthalpy probe made in the wake of the arc.

The positive column between the two locators was the principal area under investigation; consequently, a power distribution

TABLE IV
POWER DISTRIBUTION
CROSS-FLOW CONDITION
(V_∞ = 42 ft/sec)

	POWER MEASURED (K.W.)		
Cathode	0.289	0.340	0.423
Bottom Calorimeter	1.150	2.610	3.790
Top Calorimeter	0.715	1.610	2.340
Bottom Locator	2.680	5.580	7.740
Top Locator	6.200	9.100	13.300
Anode	10.150	16.100	21.010
Magnet Plates	0.941	1.555	2.194
Pole-Cap Shields	0.512	0.740	1.024
Metal Shield	1.527	3.680	5.670
Tunnel Shroud	0.205	0.280	0.512
Stack Losses (minus magnet plates)	7.219	8.010	8.44
Radiation	1.01	1.74	2.57
Wake	1.90 (est.)	2.26	2.6 (est.)
TOTAL	34.498	53.605	71.610
Power Input	35.4	55.50	76.6
Unaccounted For	0.902	1.895	4.99
	(I = 200A)	(I = 300A)	(I = 400A)

analysis was also made of this section alone before and after external fields were applied. The results are shown in Table V. For this case the distribution of power losses from the positive column contribution to each of the locator's upper and lower portion was measured. This was necessary because the measurement of the voltage was taken to be at each individual locator's horizontal centerline. Two individually cooled locators mounted back-to-back with insulation between them were used to determine this distribution. As a typical example, measurements showed that 71 per cent of the total power dissipated to the top locator was due to the portion of the column below the locator's horizontal centerline. This increase of heat measured was attributed to the slight radial growth of the arc column and free convection flow below the top locator. Similarly, measurements showed that 40 per cent of the total power dissipated to the bottom locator was due to the portion of the column above the locator centerline. It was also assumed that the axial gas flow energy flux entering and leaving the column region along the locator's centerline was approximately the same (i.e., fully-developed case). Radiation and the heat in the wake accounted for 11.5 per cent and 15.7 per cent, respectively, of the total power input between the locators after the external fields were applied. A most remarkable result shown by Table V was that the wake carried an amount of heat which was only as much as

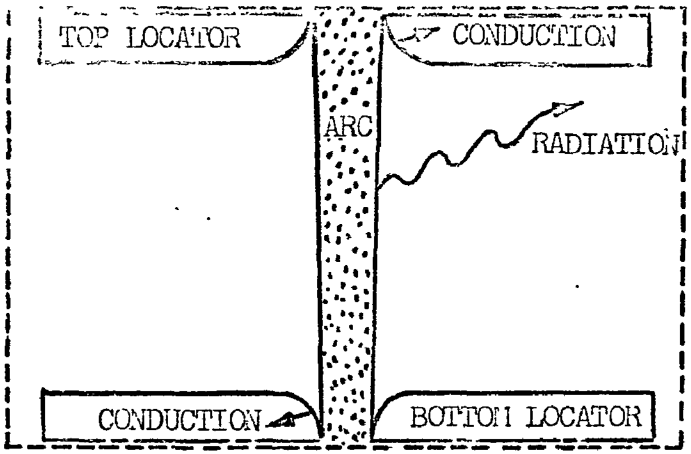

FREE BURNING CASE

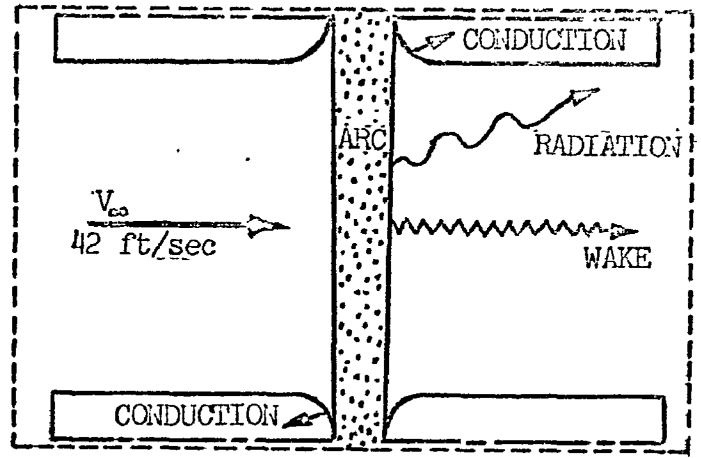

TRANSVERSE BLOWING CASE

	POWER MEASURED (K.W.)	
Bottom Half Top Locator	5.95	
Top Half Bottom Locator	3.01	
Radiation	1.38	
TOTAL	10.59	
Power Input	11.80	
Unaccounted For	1.21	10%

Additional Electrical Power Input Required by Transverse Blowing

2.40 K.W.

	POWER MEASURED (K.W.)	
Bottom Half Top Locator	6.64	
Top Half Bottom Locator	3.41	
Radiation	1.65	
Wake	2.26	
TOTAL	13.96	
Power Input	14.40	
Unaccounted For	0.44	3.1%

TABLE V TEST SECTION POWER DISTRIBUTION WITH AND WITHOUT EXTERNAL FIELDS (I = 300A) the additional power added to the positive column between both locators after the external fields were applied.

G. Heat Transfer Aspects

Figure 50 shows the results of the heat transfer calculations for the arc and comparison with a heated solid cylinder. The Nusselt number is shown as a function of Reynolds number with the arc current as a parameter. The differences in results obtained by using the upper bound arc boundary temperature of 7000 °K or the lower bound temperature of 5000 °K in the arc heat transfer calculations were negligible. Therefore, a mean value of 6000 °K was used for the arc boundary temperature in calculating the density and viscosity based on the mean film temperature for the arc. The surface area of the elliptic cylinder, the temperature difference between the arc boundary and the free stream, and the increased power input as a result of the cross blowing were used to evaluate an average heat transfer coefficient corresponding to a given blowing velocity. These heat transfer coefficients were then used for calculating Nusselt numbers using the arc's significant dimension; the coefficient of thermal conductivity was evaluated at the mean film temperature.

The curve empirically determined by numerous independent experimental investigations on heated cylinders in transverse flow and commonly referred to as Hilpert's curve (69) (Hilpert measured the heat transfer over the largest range of Reynolds numbers), is also shown. It is generally accepted that the Nusselt number for any two-dimensional laminar boundary layer is proportional to the square root of the Reynolds number (assuming the boundary layer thickness small compared to the significant body dimension).

Figure 50 shows that there is a reasonably good agreement between the Nusselt number of an arc and of a solid cylinder particularly in the higher current range. The calculations of Lord and Broadbent (47) based on Adams' experimental data (48) are also plotted in Figure 50. Their curve for a 300 ampere arc is shown by the dotted line. (Radiation effects were considered.) The difference between the data reported by Lord and Broadbent for arcs and those obtained by Hilpert for solid cylinders was found to be greater than one order of magnitude. It is believed that this difference was due to the questionable applicability of the experimental data used by Lord and Broadbent.

From a review of the literature, it is immediately evident that experimental data on the heat transfer from highly heated cylinders in a cross-flow is lacking. However, local distribution of heat transfer on cylinders with a temperature difference between the cylinder surface and the free-stream temperature of the flow of less than or equal to 200 °F is known and leads to some interesting comparisons with the arc. The work of previous investigators on the nature of fluid flow and on the local distribution of heat transfer

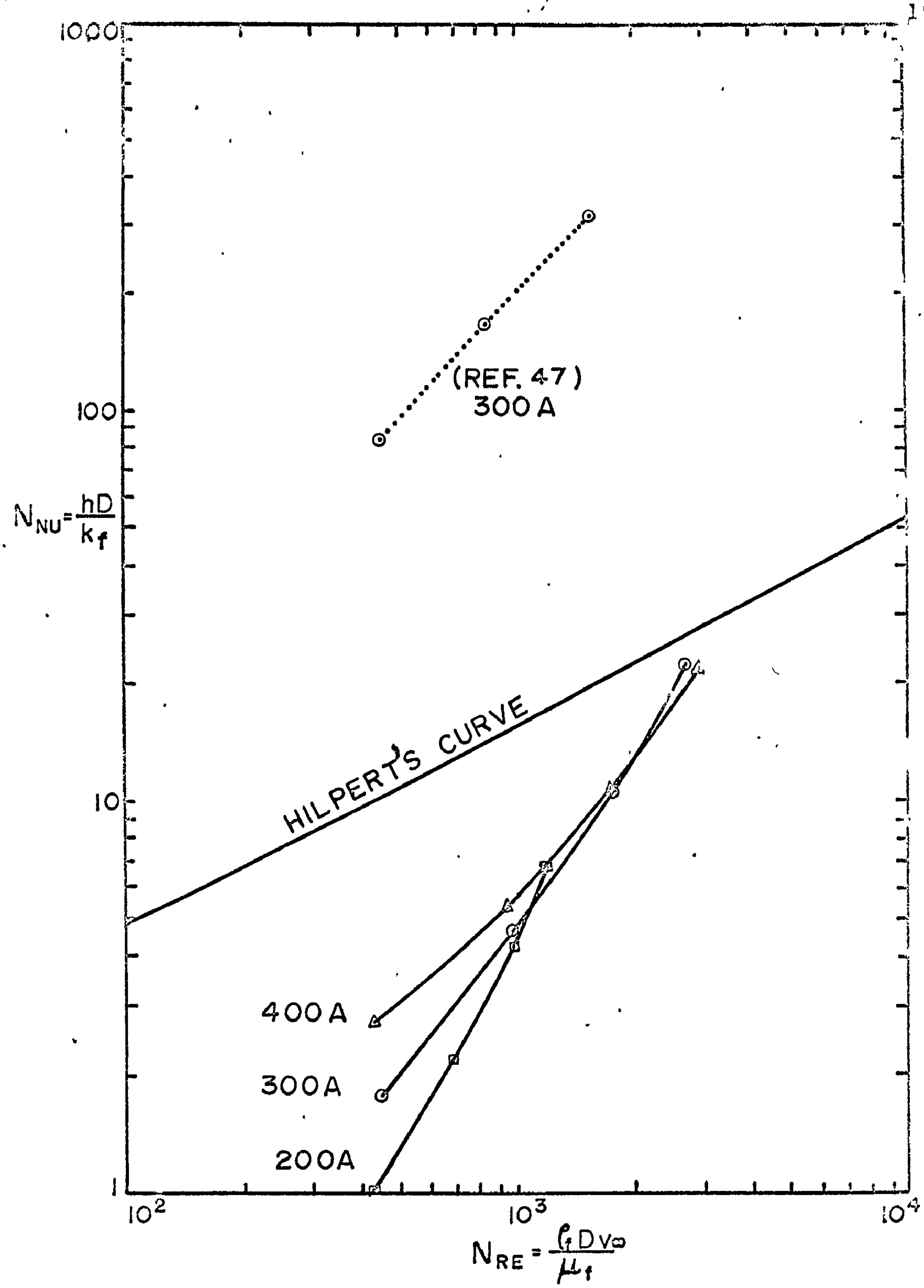

LOG-LOG PLOT OF NUSSELT NO. VS REYNOLDS NO.
FIGURE 50

on bodies in transverse flow indicated considerable variation of the local heat transfer coefficient with azimuthal position. Thus the local coefficient of heat transfer will be a function of the angular position, and of the Reynolds number (assuming the Prandtl number remains essentially constant). The experimental results of Eckert and Soehngen (62) on local heat transfer coefficients measured on heated cylinders in cross-flow spanned the very low Reynolds number range from 20 to 500. Similar experiments by Schmidt and Wenner (63) covered the Reynolds number range from 5000 to 426,000. The intermediate range of Reynolds numbers between these two experiments have been experimentally measured by several authors. All the results fall within $\pm$ 10 per cent of Hilpert's curve. However, the temperature difference between the cylinder and the free-stream was two orders of magnitude lower than that for a cylinder with a boundary temperature equivalent to that of an electric arc column.

When the measurements from the various investigations on the local coefficient of heat transfer are plotted versus ϕ (circumferential angle measured from forward stagnation point) for Reynolds numbers between 400 and 5000, the results indicate the following trends: At the low Reynolds numbers the thermal boundary layers are quite thick and separation occurs farther downstream than at the high Reynolds numbers (approximately 120° from the forward stagnation point). The heat transfer into the upstream side of the cylinder is much larger than into the downstream side. (The stagnant region in the rear only contributes approximately 15 per cent.) At the higher range of Reynolds numbers, the thermal boundary layers become thin and the separation point moves upstream (approximately 90° from the forward stagnation point). The heat transfer into the upstream side of the cylinder remains significantly larger than into the downstream side. (The stagnant region in the rear contributes approximately 25 per cent.)

The experimental results of Eckert and Soehngen showed, at Reynolds numbers of greater than or equal to 20, vortices separating alternately on both sides of the heated cylinder. These were carried downstream and formed von Karman vortex streets. This vortex shedding was also evident in the wake of the arc (Figure 33).

It is well known that the wakes of different bluff bodies are similar. The flow separates on the two sides of the body. This is followed by a transition region which extends a short distance downstream from the body, and then vorticity formation and shedding occur. For flow past a bluff cylinder, the width of the wake is related to the "bluffness" of the cylinder (compared with the cylinder diameter). The bluffer body tends to diverge the flow more, create a wider wake, and to have a larger drag. Similarly, the width of the wake is also related to the shedding frequency. The shedding frequency, represented by the Strouhal number, therefore, is one parameter which may be used to compare the wakes of the different bodies. The Strouhal number is defined as $\frac{fD}{V_\infty}$, where f is shedding frequency, D is the significant dimension, and V_∞ is the free stream velocity. The Strouhal number decreases with increasing bluntness. An additional check of the similarity of an arc with an impervious solid body may therefore be made by considering the vortex shedding rate. The periodic shedding frequencies were measured from the high-speed color motion pictures (7,000 frames/sec). The Strouhal number for both solid circular and elliptic cylinders remains essentially constant at a value of 0.2 (61). Data were only available for a Reynolds number range above 10^4. The Strouhal number calculated for the arc ranged between 0.3 to 0.4. Perhaps a more accurate analysis may be obtained by introducing a wake Reynolds number and a wake Strouhal number; however, comparison between the cold flow results and the hot flow results using the arc should not be carried too far, since there are significant differences between the shear flow around a solid body and the shear-free flow around an arc.

The next phase of testing utilized the water-cooled miniaturized heat flux sensor. The same traversing mechanism, with slight modifications, was used. The probe shaft and tip sensor were inclined 10° from the vertical toward the arc axis. The extent of traversing possible with this probe was more limited than with the calorimetric probe due to the shape of the probe (Figure 25). Since no reference material was available on the use of this probe near the vicinity of a high-current electric arc discharge, extreme caution had to be maintained at all times to prevent damage (electrical or thermal), to the very delicate sensor element.

Figures 51 through 54 show the results obtained by using the heat flux sensor probe. Three arc currents were investigated. For the blowing velocities the same values as in the previous investigations were chosen. The stations are labeled by the same key numbers as used in the velocity profile tests (Table II). Unfortunately, due to the restricted travel range of the probe transverse to the flow direction, the profile for station 3 extends only to approximately the wake boundary. At station 5, it was possible to traverse beyond the wake boundary. Therefore, the results pertaining to station 5 give a meaningful indication of the relative changes of the heat flux to the sensor across the wake boundary. The results (Figures 51 through 54), indicate the following trends. In each case the heat flux rapidly increased as the wake boundary was approached. A region of peak heat flux was measured at station 5. When the wake boundary obtained from previous measurements (Figure 47) was extrapolated to station 5, it appeared that the peak of the heat flux lies approximately at the wake boundary (indicating a high temperature). A reduction in heat flux

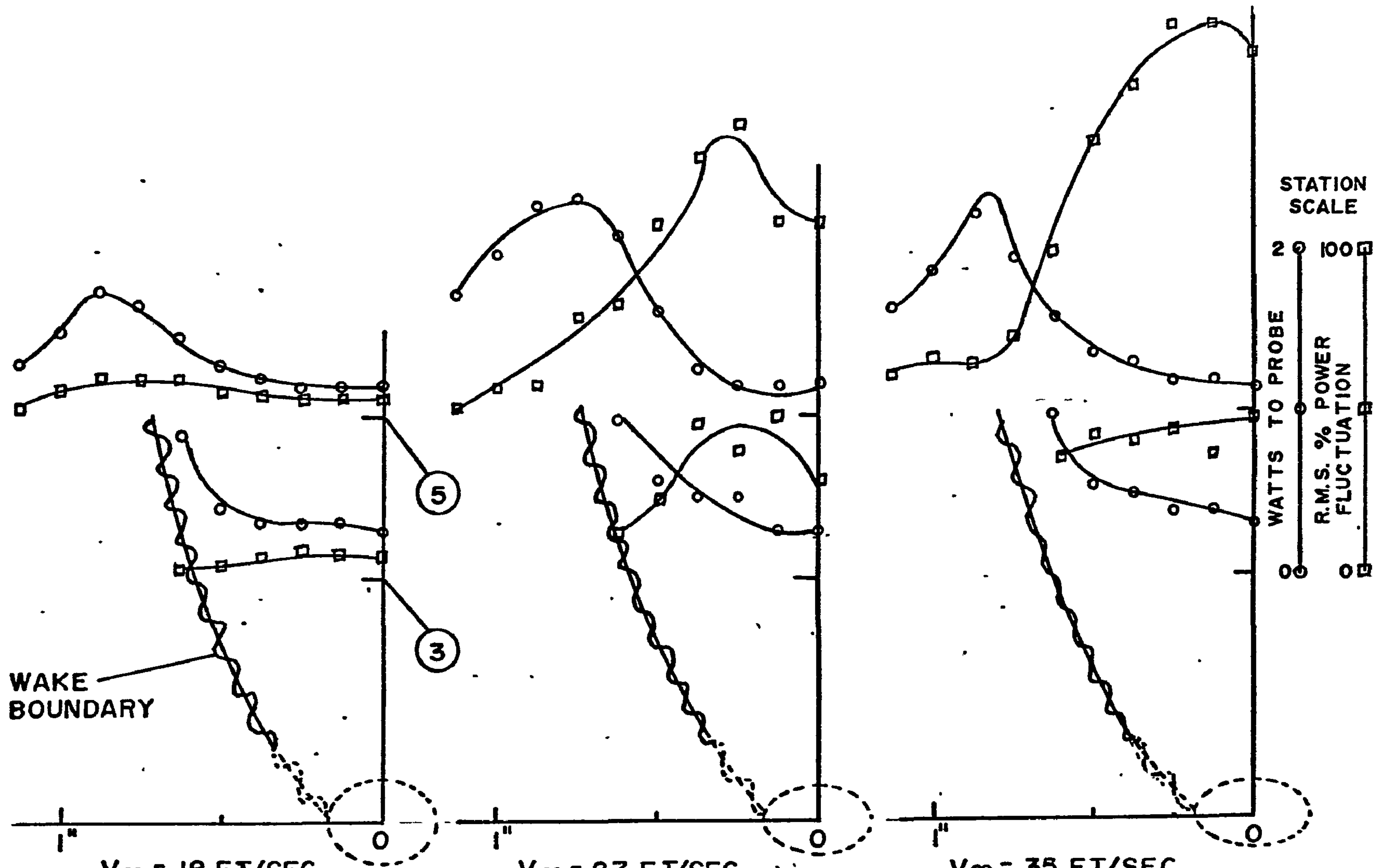

HEAT FLUX SENSOR MEASUREMENTS IN WAKE OF 200 AMPERE ARC

FIGURE 51

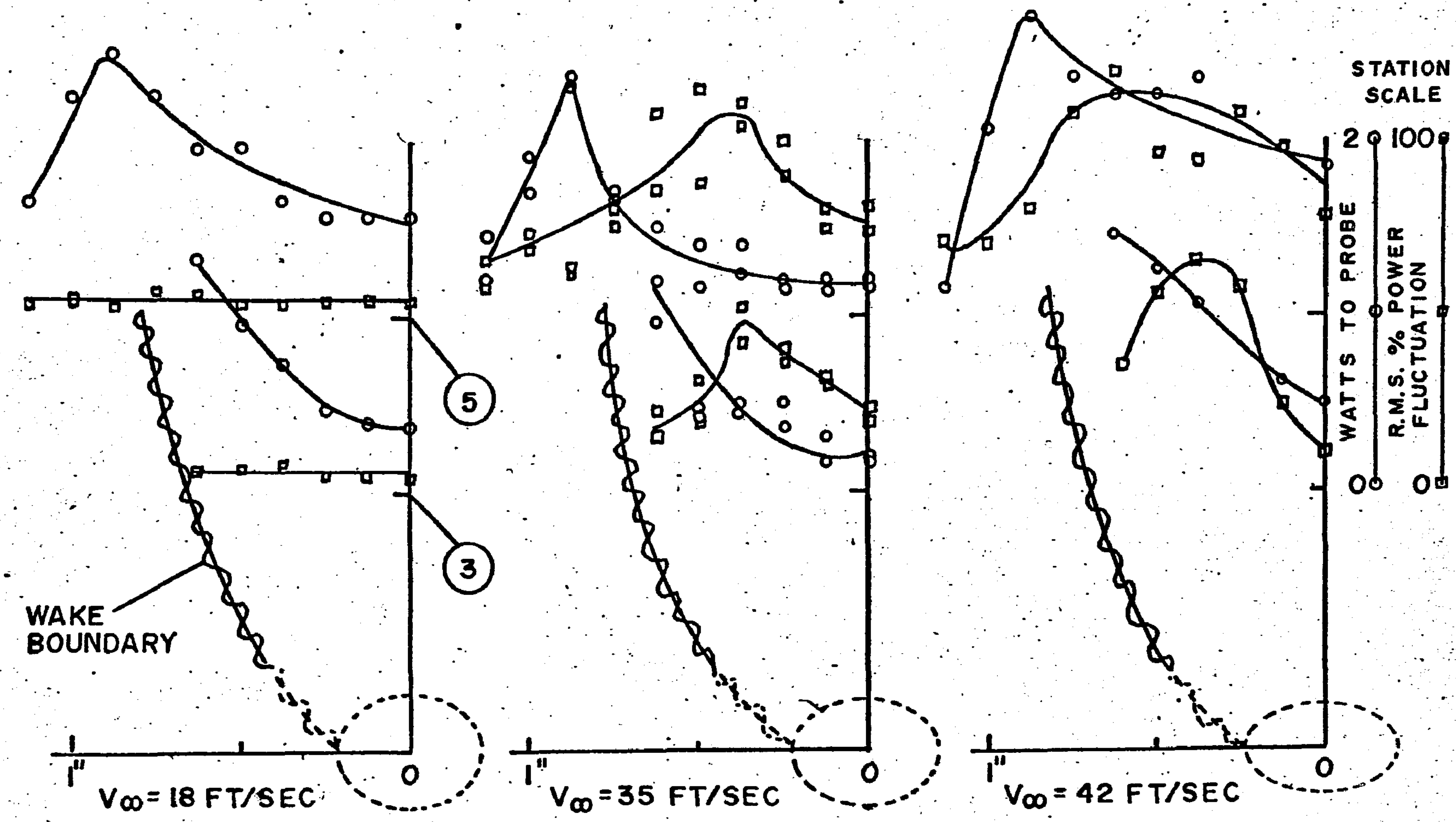

HEAT FLUX SENSOR MEASUREMENTS IN WAKE OF 300 AMPERE ARC

FIGURE 52

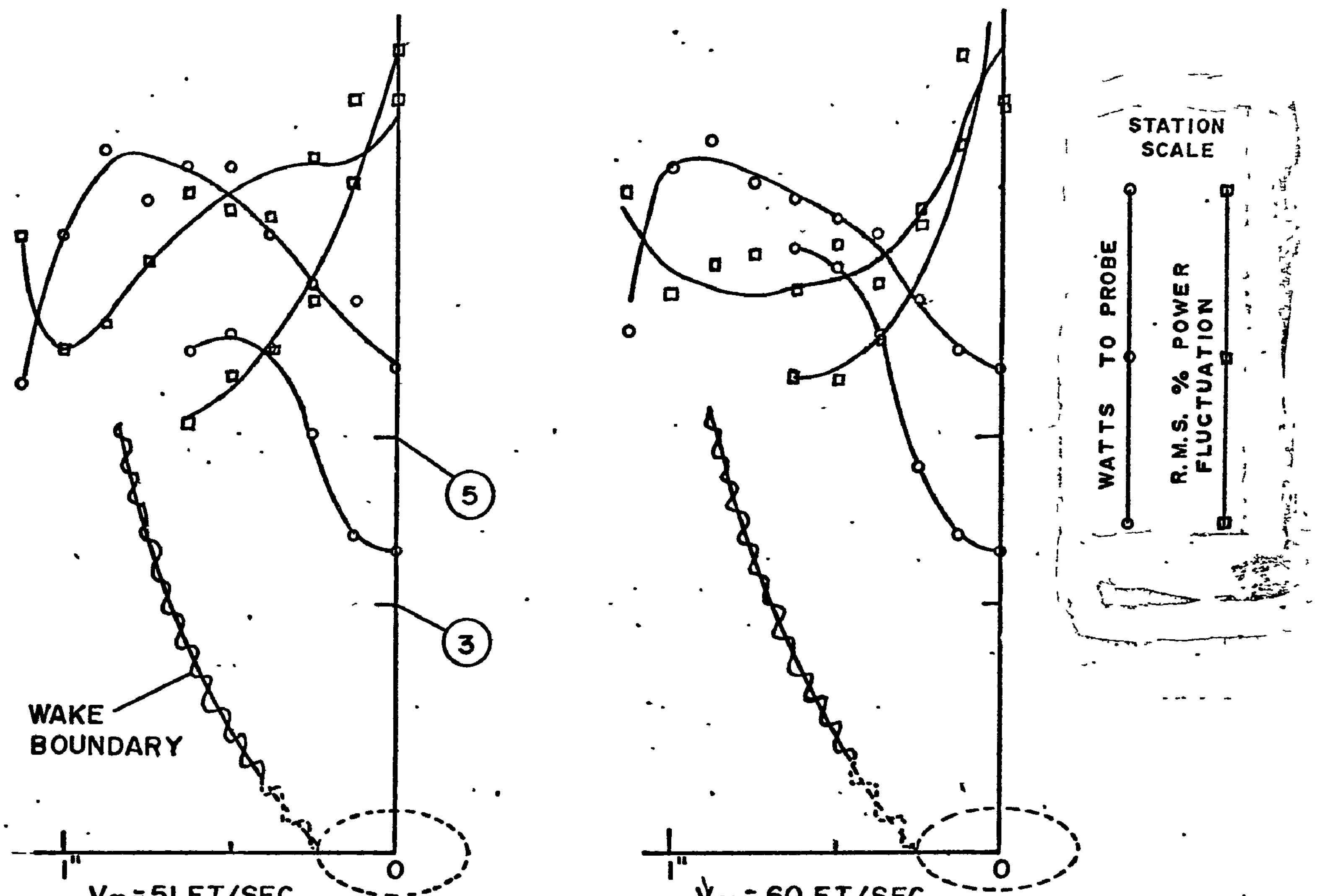

HEAT FLUX SENSOR MEASUREMENTS IN WAKE OF 300 AMPERE ARC

FIGURE 53

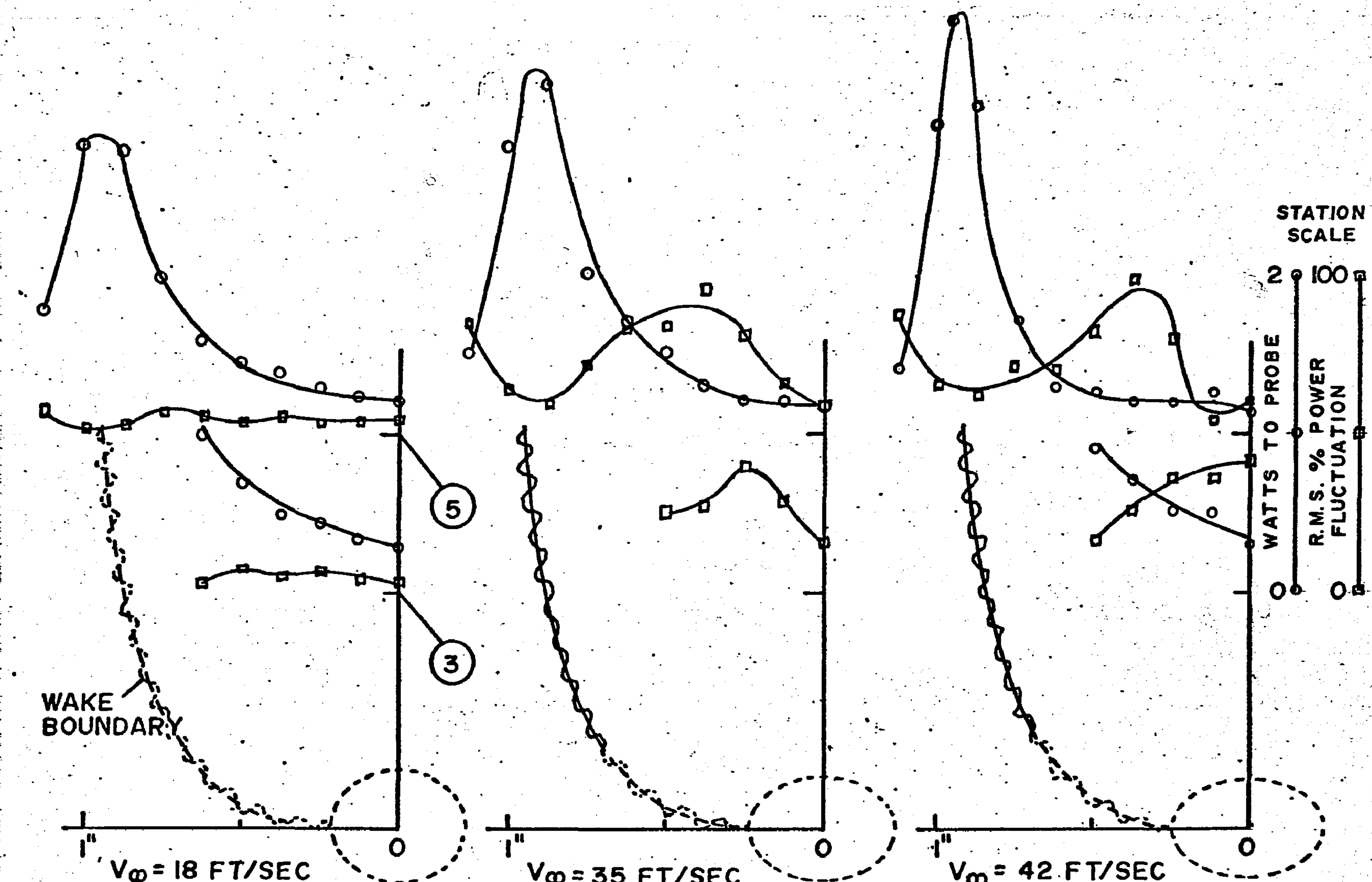

HEAT FLUX SENSOR MEASUREMENTS IN WAKE OF 400 AMPERE ARC

FIGURE 54

magnitude when proceeding from station 3 to station 5 is also evident from the graphs. The results of the rms per cent power fluctuation measurements (which are an indication of turbulence level) are also shown in the figures. The upper limit of the frequency range covered by the sensor and instrumentation was 100 kilocycles. The trend of the profiles was to shift toward the centerline as higher blowing velocities are applied. The level of fluctuation decreased considerably as the wake boundary was approached because of the high viscosity associated with the high temperature present there, and then increased again as the traverse was continued outward. The distinct vortex shedding observed on the high-speed films of the flow visualization tend to confirm the finding of high turbulence just inside the wake boundary. The frequency of the turbulence obtained from the heat flux probe measurements for a 300 ampere arc with blowing velocities of 18.5, 35, and 51 ft/sec resulted in Strouhal numbers of 0.24, 0.29, and 0.30, respectively. These Strouhal numbers compare favorably with the photographic results.

VI. SUMMARY AND CONCLUSIONS

Stabilization of the electric arc column was possible for currents in the range 200 to 400 amperes, transverse atmospheric pressure air velocities up to 60 ft/sec, and external transverse magnetic fields up to 50 gauss for run times on the order of an hour. An argon injection system satisfactorily shielded the cathode from the oxidizing environment. The balanced arc column was simultaneously viewed from the side and rear, and the influence of arc current and transverse blowing velocity on the arc's shape was observed. By means of the balancing magnetic force, the aerodynamic drag of the arc was determined. A flow visualization study using aluminum particles and high-speed photography was conducted. The velocity profiles downstream and to within 1/4 inch of the arc centerline were measured with a water-cooled stagnation pressure probe. A miniaturized, water-cooled heat flux sensor was used to measure the heat flux distribution, relative turbulence level and turbulence frequency in the arc wake. The enthalpy distribution in the arc wake was measured with a miniaturized water-cooled suction-type calorimetric probe. Thereby studies of the arc wake behavior were completed. The voltage gradient in the arc's positive column was determined independently of the cathode and anode potential. As a check on the power distribution, an overall energy balance was performed on the arc. Approximately 95 per cent of the power input was accounted for.

From these tests, the following conclusions can be drawn:

1. The arc's major and minor axes varied linearly with the transverse blowing velocity and the arc current.

2. The arc cross-section widened in the direction transverse to the external flow with increasing arc current and transverse blowing velocity. Assuming an elliptical shape, the cross-sectional area remained practically constant.

3. The cross-sectional area shape change was not due to oscillations; these were observed but were negligible. Neither was it due to the cathode gas injection.

4. The magnetic field strength required to balance the arc was proportional to the blowing velocity squared. Therefore a drag coefficient was defined analogous to that of a cylinder.

5. The calculated drag coefficient agreed closely with that of a solid cylindrical rod.

6. The flow visualization studies showed a distinct wake, symmetric on both sides. No signs of the passing of gas through the arc as a result of the transverse blowing were detectable. The arc therefore appeared impervious to the flow. However, free-convection type movement was observed.

7. The velocity profiles downstream of the arc showed similarity between the wake growth of the arc and solid bodies. In addition, a slight widening of the wake occurred in the vertical direction.

8. Increasing the arc current distinctly broadened the wake. Increasing the transverse blowing velocity had very little effect on the width of the wake.

9. The arc wake was wider than that of a similarly sized circular or elliptical cylinder. This was probably due to the gas stream being heated by the arc.

10. The wakes of similarly sized highly heated cylinders more nearly approximated the arc wake than those of unheated cylinders.

11. Distinct vortex shedding was observed with frequencies comparable to those of bluff bodies in a similar flow field.

12. High turbulence was present in the vortex shedding region just inside the wake boundary; the greatest energy flux in the wake occurred approximately at the position of the wake boundary.

13. The power convectively transferred to the transverse gas stream per unit arc length when in the balanced mode was approximately equal to the additional power input per unit arc length above what was required in the free-burning case. This convective energy

transfer was about 19 per cent of the no-blowing energy input per unit length for a transverse blowing velocity of 42 ft/sec.

14. The convective power transfer from the arc column was comparable to that from a solid cylinder having the same surface temperature.

VII. RECOMMENDATIONS

Considerable room remains for both experimental, as well as theoretical research on the cross-flow arc phenomena both with and without external magnetic fields. From the experimental standpoint, the following steps should be taken to extend the scope of the present study.

1. Develop an improved anode which will permit extending the range of the cross-flow velocity and external transverse magnetic field strength.

2. Attempt to reduce the cathode-jet effect and thereby reduce the strength of the axial gradients.

3. Perform experiments with one or two adjacent highly heated cylinders (boundary temperatures of greater than or equal to 1000 °K) to determine how closely their flow, heat transfer and drag characteristics approach those of the arc. Pressure measurements on the boundary should also be included. Various degrees of internal gas injection and cylinder rotation might be required to simulate the arc behavior.

4. Perform the experiment entirely in a single gas instead of using different gases for cathode protection and transverse blowing.

5. Extend pressure levels to those of interest in current arc-heater technology.

6. Use transient probe techniques (e.g., Hall probe) to make measurements inside the arc region.

7. Use appropriate spectroscopic techniques to determine internal arc temperature and property distributions.

8. Perform an experiment using a vertical free-falling mercury column to simulate the arc. A direct current could be passed through the column and then the external fields applied. (The possibility of using a magnetic fluid also exists.) With the column in the balanced mode, platinum particles could be placed on the forward surface and their paths traced with microscopic observations. This may determine the possible existence of the postulated double-vortex internal circulation. In addition, simultaneous two-view photos could be made of the column to determine whether a cross-sectional area distortion takes place.

VIII. REFERENCES CITED

1. Schoenherr, O., "________________," ETZ-A 22, 138 (1909).

2. Kirschstein, G. and Koppelmann, F., "The Electric Arc in High Velocity Gas," ASTIA NCL 1344/1+ 2 (August, 1937).

3. Headquarters, Arnold Engineering Development Center, Tenn., Air Force Contract 40(600)-1034 (1966).

4. Personal Communications with Mr. Erich E. Soehngen, Director, Thermo-Mechanics Research Laboratory, Aerospace Research Laboratories, Wright-Patterson AFB, Ohio.

5. Stine, H. and Watson, V., "The Theoretical Enthalpy Distribution of Air in Steady Flow Along the Axis of a Direct Current Electric Arc," NASA TN-D-1331 (1962).

6. Westinghouse Electric Corporation, Arc Heater Project, Trafford, Pennsylvania, Air Force Contract AF 33(615)-2975 (1966).

7. Lord, W. and Broadbent, E., "An Electric Arc Across an Air Stream," RAE Tech Report No. 65055 (1965).

8. Buechner, G., "Verlangern von Lichtbogen Mit Hilfe Magnetischer Felder Zum Unterbreuchen von Wechselstromen," ETZ-A, 80-3 (1959).

9. Hesse, D., "Uber den Einfluss des Laufschienenfeldes auf die Ausbildung und Bewegung von Lichtbogefusspunkten," Archiv. fur Electrotechnik XLV-3 (1960).

10. Maecker, H., "On the Motion of Arcs," Proceedings of VIIth International Symposium on Ionization Phenomena in Gases, Belgrade (1965).

11. Guile, A. and Blix, E., "Column Control in the Magnetic Deflection of a Short Arc," Brit. Journal of Appl. Phys. 16, (1965).

12. Guile, A. and Spink, H., "The Movement of High Current Arcs in Transverse External and Self-Magnetic Fields in Air at Atmospheric Pressure," A.R.C. Rpt. 25930 (May, 1964).

13. Saha, M. N., "______________," Phil. Mag. 40, (1920).

14. Refer to Retrograde List in Appendix F.

15. Sommerville, J., "The Electric Arc," Methuen and Co., Ltd., John Wiley and Sons Inc. (1959).

16. Finkelnburg, W. and Maecker, H., "Elektrische Bogen und Thermisches Plasma," Handbuch der Physik, XXII, Springer-Verlag, Berlin (1956).

17. Cobine, J., "Gaseous Conductors," Dover Publications, Inc., N. Y. (1950).

18. Personal Communications with Mr. Paul W. Schreiber, Research Scientist, Aerospace Research Laboratories, Wright-Patterson AFB, Ohio.

19. Thiene, P. G., "Flexure of a Two-Dimensional Arc Under Forced Convection," AFOSR TN 59-947 (August, 1959).

20. Kuhnert, E., "Uber die Lichtbogenwanderung in Engen Isolierstoffspalt bei Stromen Bis 200 KA," ETZ-A 81, (May, 1960).

21. von Engel, A. and Steenbeck, M., "Elektrische Gasentladungen," Vol. 2, Springer-Verlag, Berlin, pg. 151 (1934).

22. Angelopoulos, M., "Uber magnetisch Schnell fortbewegte Gleichstrom-Lichtbogen," ETZ-A 79-16, 572 (1958).

23. King, L. A., "Theoretical Calculation of Arc Temperatures in Different Gases," Colloquium Spectroscopicum International VI, Amsterdam Pergamon Press Ltd., London (1956).

24. Cambel, A., "Plasma Physics and Magnetofluidmechanics," McGraw-Hill Book Company, Inc., New York (1963).

25. Blix, E. and Guile, A., "Column Control in the Magnetic Deflection of a Short Arc," Brit. J.A.P. 16, 857 (1965).

26. Maecker, H., "Plasmastromungen in Lichtbogen Infolge Eigenmagnetischer Kompression," Zeitschrift fur Physik 141 (1955).

27. Féchant, M., "Vitesses de deplacement d'arcs electriques dans l'air," Revue General de L'Electricite, 68-9, 519 (1959).

28. Weizel, W. and Rompe, R., "Theorie Elektrischer Lichtbogen and Funken," (Text) Leipzig (1949).

29. Smith, H. and Early, H., "Investigation of Heating an Air Stream in a Wind Tunnel by Means of an Electrical Discharge," Army Ordnance Contract DA-20-018, University of Michigan (1954).

30. Rother, H., "Uber den Einfluss der Konvektion auf Einen Lichtbogen," Ann. der Phys., (Leipzig), 20, 230 (1957).

31. Thiene, P., et al., "An Experimental Investigation of the Behavior of an Arc Positive Column in Presence of Forced Convection," Plasmadyne Corporation Report 682 (1961).

32. Serdyuk, G., "Calculating a Welding Arc in a Transverse Magnetic Field," Avtomaticheskaya Svarka 11-92, 31 (1960).

33. Chen, M., "Theory for a Positive Column Subjected to a Transverse Gas Flow," AVCO-RAD Memo G-305 (1961).

34. Sherman, C. and Yos, J., "Scaling Laws for Electric Arcs Subject to Forced Convection," J. of Appl. Physics 32-4, 744 (1961).

35. Lord, W., "Some Magnetofluiddynamic Problems Involving Electric Arcs," R.A.E. Tech. Note 2909 (1963).

36. Alferov, V. and Bushmin, A., "Electrical Discharge in a Supersonic Air Flow," Soviet Phys. J.E.T.P. 17-6, 1190 (1963).

37. Kalachev, B., "Investigation of a Pulsed Discharge in a High-Velocity Air Stream," Soviet Physics, J.E.T.P. 18-1, 59 (1964).

38. Fay, J., "Comments on Convective Flexure of a Plasma Conductor," Phys. of Fluids 7-4, 621 (1964).

39. Bond, C., "The Magnetic Stabilization of an Electric Arc in Supersonic Flow," Ph.D. Dissertation, University of Michigan (1964).

40. Hogan, W., "Experimental and Analytical Study of the Fundamental Interaction and Energy Exchange Process Between Electric Arc Discharges and Cross-Flow of Pre-Ionized Gases With and Without the Presence of Transverse Magnetic Fields," AF Contract 33(657)-11310, AVCO-RAD Corporation (1964).

41. Malliaris, A., "Gas Acceleration Through Interaction of Electrical Discharges With Pre-Ionized Gases and Magnetic Fields," AF Contract 33(657)-11310, AVCO-RAD Corporation (1965).

42. Baranov, V. and Vasiléva, I., "An Electric Arc in a Flow of Argon," Teplofizika Vysokikh Temperatur 2, 609 (1964).

43. Lord, W., "Effects of a Radiative Heat Sink on Arc Voltage-Current Characteristics," Agardograph 84, Pt. 2, 673 (1964).

44. Anderson, J., "Hall Effect and Electron Drift Velocities in the Plasma of the Positive Column," Physics of Fluids 7-9, 1517 (1964).

45. Ecker, G. and Kanne, H., "Cylindrical Plasma Column in a Transverse Magnetic Field," Phys. of Fluids, 7-11, 1834 (1964).

46. Broadbent, E., "A Theoretical Exploration of the Flow About an Electric Arc Transverse to an Airstream Using Potential Flow Methods," R.A.E. Tech. Report No. 65056 (March (March, 1965).

47. Lord, W. and Broadbent, E., "An Electric Arc Across an Airstream," R.A.E. Tech. Report 65055 (1965).

48. Adams, V. W., "The Influence of Gas Streams and Magnetic Fields on Electric Discharges," Aeronautical Research Council Current Paper 743 (1964).

49. Olsen, H., "Investigation of the Interaction of a Pre-Ionized Gas With an Electric Arc," AF Contract 33(615)-1105, Northrop Space Labs. (1965).

50. Broadbent, E., "Electric Arcs in Cross-Flow," R.A.E. Tech. Memo Aero. 897 (July, 1965).

51. Noeske, H., "Interaction of an Electrical Discharge With a Cross-Flow," AF Contract 33(657)-11310, AVCO-RAD Corporation (1965).

52. Myers, T., et al., "Experimental Investigation of a Magnetically Balanced Arc in a Transverse Argon Flow," J. of Eng. for Power 88-1, 27 (1966).

53. Kookekov, G., "Mechanism of Heat Transfer in Transverse Blown Arcs," Engr. and Physics Journal 9 (1965) (in Russian).

54. Schrade, H., "On Arc Pumping and the Motion of Electric Arcs in a Transverse Magnetic Field," ARL Tech. Report 65-178 (1965).

55. Benenson, D., "Investigation of the Effects of Forced Convection Upon the Steady-State Characteristics of Electric Arcs," AF Contract 33(615)-1797, The New York State University at Buffalo (1965).

56. Fischer, E., "DC Arcs in Transverse Force Fields," AF Contract 61(052)-805, Technical University of Aachen (1965).

57. Han, L., "Study of the Convective Heat Transfer and Arc Curvature in Cross-Flow," AF Contract 33(615)-3205, The Ohio State University (1965).

58. Schlichting, H., "Boundary Layer Theory," McGraw-Hill Book Co., Inc., New York (1960).

59. Mason, B., "The Physics of Clouds," Clarendon Press, Oxford (1957).

60. King, L., "The Voltage Gradient of the Free Burning Arc in Air or Nitrogen," Electrical Research Association Report G/XT 172 (1959).

61. Delany, N. and Sorensen, N., "Low-Speed Drag of Cylinders of Various Shapes," NACA TN 3038 (November, 1953).

62. Eckert, E. and Soehngen, E., "Heated Cylinder in Crossed Convective Flow," Trans. of ASME (1952).

63. Schmidt, E. and Wenner, K., "Warmeabgabe Uber den Umfang Eines Angeblasenen Geheizten Zylinder," Forschung auf dem Gebiete des Ingenienrwesens 12-2 (1941).

64. Jedlicka, J., "The Shape of a Magnetically Rotated Electric Arc Column in an Annular Gap," NASA TN D-2155 (1964).

65. Wienecke, R., "Uber das Geschwindigkeitsfeld der Hochstromkohlebogensaule," Zeitschrift fur Physik 143 (1955).

66. Rohloff, E., Zeitschrift fur Physik 126 (1949).

67. Suits, C., "High Pressure Arcs in Common Gases in Free Convection," Physical Review 55 (March, 1939).

68. Adams, V., "The Influence of Gas Streams and Magnetic Fields on Electric Discharges, Part I: Arcs at Atmospheric Pressure in Annular Gaps," R.A.E. Tech. Note Aero 2896 (June, 1963).

69. McAdams, W., "Heat Transmission," McGraw-Hill Book Company, Inc., New York (1954).

APPENDIX A

SURVEY OF PUBLISHED LITERATURE

THEORETICAL ANALYSES OF THE STATIONARY ARC

Transverse Blowing Only

Weizel and Rompe (28) primarily concerned themselves with the problem of why an arc discharge channel straightens itself if it had accidentally assumed a curved form. This straightening occurs as soon as the arc channel is no longer subject to any disturbing influence such as free or forced convection or external magnetic fields. The straightening tendency has occasionally been interpreted as tensile stress in the longitudinal direction. In contrast to this, however, is the experimentally verified fact that the electrodes are being repelled, instead of being attracted, by the discharge. If one blows continuously on an arc with a cross-flow, the arc is displaced by this blowing. If this cross-flow velocity is below the magnitude required to extinguish the arc, an equilibrium state may be established whereby the arc remains in a curved configuration. The tendency of the arc to straighten out is balanced by the flow forces. For a horizontal arc, this cross-flow is induced by the buoyancy effect of the highly heated gas of the arc. Because of gravitational forces the hot gas rises and is replaced by cold gas flowing in from below. The highest flow velocity should therefore exist in the center of the column. Thus, a continuous stream of gas flows through the arc column vertically.

Since the electric current prefers to pass through the highest conducting area, the column distorts upward until a stable condition is reached. Thus, assuming the arc does not extinguish, an equilibrium may be established between restoring forces (which increase with arc curvature) and the upward displacement of the arc. In this manner the free convection, horizontal arc acts like a pump. Cold gas being sucked in from below and hot gas being ejected above. A certain similarity exists between the deflected arc due to cross-flow and a deflected arc due to a transverse external magnetic field. In both cases an equilibrium state results in which the tendency of the arc to straighten itself and the influence of the external field balance each other.

The calculations of Weizel and Rompe were based on the differential energy equation relating ohmic heating, radiation, heat convection, diffusion, and conduction losses:

$$E \cdot j - S = \frac{\partial}{\partial t}\left(\rho C_V T + \frac{\rho V^2}{2}\right) + \nabla \cdot \left[V\left(\rho C_V T + \frac{\rho V^2}{2}\right)\right] + \nabla P \cdot V + \nabla \cdot (k \nabla T). \tag{9}$$

The terms on the left side of the equation are the ohmic heating and radiation; the terms on the right side are the total energy density of the gas, change of energy density of the flow, energy deformation and heat conduction, respectively. The results indicated that the velocity with which a curved element of arc moves toward its curvature center increases with the power per unit length and with the cross-sectional area of the channel and decreases with radius of curvature and internal energy per unit length. Thus, $V = \frac{2LR^2}{u\rho}$ where L = power per unit length, R = arc channel radius, u = energy per unit length, ρ = arc radius of curvature. This is in partial agreement with some experimental observations, especially with regard to cross-sectional area of the arc channel. Discharges with small cross-sectional areas are much more susceptible to bending through convective flexure than those with a large cross-sectional area. The velocity which the horizontal arc channel achieves due to its own buoyancy was equated to the velocity calculated for the curved arc channel moving toward its curvature center at the equilibrium condition to yield a parameter which indicated the range of stability of the arc. Exceeding this calculated parameter value indicated that the arc would blow out and would not be capable of straightening itself. This parameter A was found to be equal to

$$K \frac{ST_o u d^3}{4FU^2R^2 \eta},$$

where K = a constant based on geometrical shape

S = gas density

T_o = maximum arc temperature

u = energy/unit length

d = electrode gap

F = electrical conductivity

U = discharge voltage

R = arc channel radius, and

η = viscosity.

Weizel and Rompe gave no consideration to the arc's self-magnetic field influence, the possibility that the arc may not actually assume a sector of a circle for its shape, electrode region effects and the $P\nabla \cdot V$ term in the energy equation.

Rother's analysis (30), like that of Weizel and Rompe, primarily considered the curvature and range of stability of a horizontal arc perpendicular to a gas flow. The arc was found to bend to the point where the unsymmetrical cooling of the column due to convection was exactly compensated by the unsymmetrical heating on the concave side due to the curvature and increased electric field. The Heller-Elenbaas differential energy equation was used together with an assumed radial temperature distribution in the arc of the form $T = T_o - (a)(x^2 + y^2)$, where T_o is the centerline arc temperature and a is a constant. By initially assuming a uniform velocity field which was not affected by the arc, the resultant decoupled approximate energy equation was solved assuming constant conductivities by finding the appropriate Green's function. Whereas Weizel and Rompe assumed that the constant a in the radial temperature distribution could be determined from the radius at 1/2 of the maximum temperature, which led to the result that the radius of curvature was proportional to the power input, Rother claimed this to be erroneous and that there is no connection between a and radius. The relation obtained by Rother was of the form $\frac{1}{\rho} = \frac{V}{4} \frac{C_P}{K_o} (1 - \frac{S_o}{L_o})$,

where ρ = radius of curvature

V = convection velocity

S_o = radiation in middle of arc

C_P = specific heat

K_o = heat conduction coefficient

L_o = power density in middle of arc.

That is, the radius of curvature is practically independent of the power. The theory of Rother predicts the dependence of arc curvature on the arc pressure and arc power and was said to agree quite well with his experimental results for carbon arcs in air and argon arcs. However, no description of the experimental conditions, measurement techniques, or range of parameters was given. Again, like Weizel and Rompe, no consideration was given to the effects of the self-magnetic field or electrode region effects.

The main difficulty which occurs in any simple theory for predicting the flexure of an electric arc column under forced convection is how to account for the flow field around and through the column. Thiene (31) investigated this using the same configuration as Weizel, Rompe, and Rother. By assuming that the flow through the column was essentially two-dimensional, a qualitative analogy was made between the convection-loaded arc and the flexure of a structural beam under a distributed load. The simple assumption was made that the curvature at any point, x (y), where the y axis is the original undeflected column and the x-axis is perpendicular to the y-axis in the plane of flexure, was proportional to the mass flux. The constant of proportionality was defined as the "flexural rigidity" of the arc column. Thiene's analysis included the energy balance, equation of motion, continuity equation, Maxwell's equations, and entropy changes. It was assumed that the isotherms within the arc were parallel to the electric field lines. Thiene justified this assumption by stating that under steady state conditions, conservation of charge and Ohm's law require that

$$\nabla \cdot j = E \cdot \nabla\sigma + \sigma\nabla \cdot E = 0, \text{ where } \sigma = \text{ electrical conductivity.} \tag{10}$$

In addition, Poisson's equation and charge neutrality require that

$$\nabla \cdot E = 4\pi e(n_i - n_e) = 0. \tag{11}$$

Therefore, $E \cdot \nabla\sigma = 0$ or the isotherms (lines of constant conductivity) are parallel to the electric field and current lines. This assumption has been shown to be not necessarily valid (38).

The temperature distribution in the zone of ohmic heating was derived by assuming the following linear conductivity variation $\sigma = a(T - T_o)$ with $T > T_o$, where T_o is the maximum arc temperature. All other properties were assumed independent of T. Because of Thiene's low blowing velocities, the stagnation enthalpy was assumed equal to the free-stream enthalpy. In addition, radiation and viscous losses were neglected.

Thiene's results indicated that the flexural rigidity of the column should decrease with the specific heat of the gas and increase with the thermal conductivity, radiation, and ambipolar diffusion. Thiene's analysis omitted boundary conditions at the electrodes, electrode effects, and no consideration was given to the possibility that the mass flux through the column may differ from the free-stream mass flux upstream of the column. (Account was taken for the change in mass flux within the column due to its change in curvature.)

Fay (38) offered a comment on Thiene's assumption that the electric field is divergence-free because the plasma is exactly neutral. Fay pointed out that although $\nabla \times \bar{j}$ is perpendicular to both ∇T and $\bar{j}$, it cannot be concluded that the latter two vectors are necessarily mutually perpendicular. Therefore, the current does not necessarily flow in the isothermal surfaces, as Thiene had assumed, but since the current always has a tendency to flow through regions of the highest electrical conductivity, it may approximately follow such a path.

Since the many different processes occurring in the arc positive column are each affected differently by changes in arc dimensions, pressures, velocities, etc., a study of arc scaling laws may furnish a powerful tool for establishing which of the processes are most important in determining arc operating characteristics. Sherman and Yos (34) dealt with a dimensional analysis of scaling laws for electric arcs subject to forced convection. The important processes considered for viscous, compressible flow were heat conduction and convection, ohmic heating, and radiative heat transfer. The effects of natural convection, non-equilibrium, electrodes, and external and self-magnetic fields were excluded. The resultant scaling expression was

$$\phi = \frac{I}{L\sigma} F \left[\left(\frac{\mu C_P}{k}\right)\left(\frac{P}{\rho V^2}\right)\left(\frac{\rho V L}{\mu}\right)\left(\frac{I^2}{L^2 \mu\sigma h}\right)\left(\frac{q\rho^2 L^2}{\mu h}\right)\right]$$

This equation includes the effect of the electrical conductivity, σ; pressure, P; density, ρ; velocity, V; viscosity, μ; specific heat, C_P; thermal conductivity, k; enthalpy, h; power radiated per unit volume, $q\rho^2$; and a typical length, L; on the arc column voltage, θ. Even though some effects which apply to many of the most important processes in the arc column-flow interaction are excluded, scaling laws do include a number of effects which may be important in the interaction mechanism of the arc column with external flow. It should be noted, however, that if natural convection, non-equilibrium, electrode, external and self-magnetic fields, or induced current effects are important, or if other effects not considered in the analysis are important, then the scaling law will not hold.

Chen (33) applied the steady state energy equation to a positive column subjected to a transverse gas flow to show that the arc may be stable or unstable. The following assumptions were made:

1) MHD effects were neglected.

2) Pressure was uniform everywhere.

3) Chemical and thermal equilibrium exists everywhere in the arc column. (The important consequence of this assumption is that for a given pressure, the physical properties and composition are functions of temperature only.)

4) Radiation was neglected. (This assumption may not be valid, especially at higher pressures.)

5) The gas is incompressible.

A temperature perturbation was introduced and a stability criterion derived. This estimated the arc diameter to be $D = \pi / E \sqrt{\frac{k}{\frac{d\sigma}{dT}}}$. The conductive heat loss equation for a hot cylindrical rod was applied to determine that 97% of the energy transfer from the arc column is by means of conduction through the arc boundary layer. (Therefore little flow, if any, goes through the arc.) The numerical results indicated the column temperature is not greatly increased with pressure. Since radiation was neglected, the pressure effect may be exaggerated since the significantly increased radiation losses at higher pressure may result in lower temperatures than those predicted.

Broadbent (46) applied the energy, continuity, and momentum equations together with the assumption that pressure variations are small to explore the flow about an electric arc. Outside the arc the flow was assumed inviscid and incompressible. A circular cross-section was assumed for the arc, which acted as the heat source in the potential flow. An iteration procedure was required to obtain the complete solution of the equations. This led to the result that the stream tubes which pass through the arc column change density, whereas those that pass around the arc column remain incompressible. This method involved guessing a velocity and density distribution within the arc. The model is somewhat unrealistic, since it results in a negative arc drag, as long as the flow field is deduced solely by potential methods. In the actual case of viscous flow, a wake originates that induces vortices and leads to a positive drag. Mathematically, Broadbent obtained a positive drag by introducing a velocity discontinuity and a heat sink in the downstream flow. The heat source and the heat sink were made of equal magnitude. The models used were somewhat questionable, since they gave unrealistic temperature distributions. A more reasonable temperature distribution could be realized by introducing an inner region defined by an impenetrable boundary which would act as a line heat source for the external convection.

Benenson (55) is currently developing an analytical method for determining the local intensity distribution from experimental measurements of integrated intensity. In this method, the local intensity is expressed in terms of a polynomial expansion in x and y. A set of equations are obtained describing the integrated intensity in terms of the unknown coefficients of the polynomial expansion. For the case of the circularly symmetric arc, the analytical method has been found so far to be in good agreement with the exact Olsen method (49). The next step will be to apply the method to the asymmetrical arc case. It is also contemplated to determine the temperature based on absolute intensity measurements of the continuum radiation.

Noeske (51) analytically derived the amount of mass flux which actually crosses the arc boundary by using a current-sheet model and making the following assumptions:

1) Electrode regions are excluded,

2) no conduction or radiation in the direction perpendicular to the current and the flow,

3) the current lines are concentric circles (with the model only valid for bending up to a half-circle),

4) incompressible and inviscid flow,

5) the electrical conductivity was defined as: $\sigma = 0 \quad T < T_o$
$\sigma = \theta \ (T - T_o) \quad T \geq T_o$,

6) estimated average value of C_p and k.

The perviousness was given by $\frac{\dot{m}_x}{\dot{m}_\infty} = \frac{-1 + \sqrt{1 + 2(T_i/T_o - 1)}}{(T_i/T_o) - 1}$,

where $\dot{m}_\infty$ = initial flow mass flux

$\dot{m}_x$ = mass flux actually crossing arc column

T_o = temperature outside arc

T_i = maximum arc temperature.

The derived equations represented relations between the voltage, current, curvature and thickness of the current-sheet, the thermodynamic properties, the mass flux of the fluid which penetrates the boundaries, and the temperature distribution within the discharge. The temperature field in the vicinity of an arc in cross-flow was compared with the temperature field of a heated solid cylinder, and a horizontal free-burning arc subject to natural convection. The plots of arc characteristics and the effect of current and cross-flow blowing on arc diameter indicate: the arc voltage increases with mass flow rate and decreases with increasing initial gas temperature; the arc diameter increases with increasing current, decreasing flow rate, and increasing initial gas temperature. A stability criteria was developed on the basis of two assumptions:

1) The maximum temperature in the column must be upstream of the arc center.

2) $dq/di_o = 0$,

where q = heat flux and i_o = arc column current.

Compared to previous investigations, this was the first to consider the difference between the mass flux through the column compared to the mass flux upstream of the column.

Han (57) is analytically studying the convective heat transfer and arc curvature in cross-flow. The first phase of the investigation deals with establishing the model for the growth of the arc column radius in a vertical orientation. The analysis is not valid at the electrode because of a strong singularity existing there. Three basic models of the arc column are being considered for numerical solution:

1) A solid cylinder with internal heat generation. (Conduction is the primary mode of heat transfer within cylinder, radiation is being neglected.)

2) A solid cylinder surrounded by an annulus of ionized gas. (Conduction and radiation are the primary modes of heat transfer.)

3) A completely fluid cylinder with internal heat generation. (Conduction, convection, and radiation are the primary modes of heat transfer. It is planned to determine the convection-originated flexure by analyzing the "fringe-shift" of the isotherms due to the asymmetrical cooling of the arc column.)

<u>Transverse Magnetic Field Only</u>

The investigations of Anderson (44) and Ecker and Kanne (45) concerning transverse magnetic field effects on the plasma column deal with the very low pressure, low current regime (electron temperature >> neutral gas temperature). The discussions are limited to very low magnetic fields, which allow introduction of linear perturbation theory. Therefore, the results are not directly applicable to this investigation and will not be discussed further.

Fischer(56) analytically determined the influence of a transverse force field for two types of arcs: (1) A wall-stabilized arc where the force is caused by a uniform weak external transverse magnetic field and, (2) a free-burning arc where the force is caused by an external transverse gas flow. The energy, momentum, and continuity equations were applied. For case (1) a double-vortex type flow appears with the arc core displaced in the $\overline{J} \times \overline{B}$ direction. The calculations yielded the temperature distribution, electrical conductivity, and the flow field. For case (2) the arc column shifted into the direction of the flow. It was assumed that the electric field and isotherms were parallel and heat conduction along the arc axis was negligible. A perfect gas relation, a radially symmetric arc profile with temperature distribution of the form $T = T_o + \dfrac{T_A - T_o}{(1 + r^2/r_o^2)^{\alpha}}$ (necessary to determine the flow field), and a small dynamic pressure, compared to the static pressure were the additional assumptions made. In this equation T_A is the arc centerline temperature, T_o is the gas temperature, r_o is the radius of the arc boundary, and α is a constant. The flow field was calculated from the momentum equation, continuity equation, and equation of state. The results were only valid in the upstream half of the column and not in the wake region, because here the temperature profile is no longer radially symmetric and the inertial forces become important. The results indicated the per cent of flow going through the arc increases with increasing gas temperature and decreasing arc temperature, in agreement with Noeske (51).

Schrade (54) conducted an analytical investigation of the transverse forces which act on an arbitrarily curved current-carrying plasma channel in a transverse magnetic field. This study was primarily motivated by the arc retrograde motion problem and deals with low current arcs at low pressure (< 1 atm.). The transverse forces consist of the Lorentz force in the Amperian direction and an electro-magnetically induced gas-dynamic thrust in the retrograde direction. This gas-dynamic thrust is due to the gas being expelled from the low pressure side of the arc, and being replaced by gas drawn in from the side where the magnetically-induced pressure is greatest. The balance of the forces and, therefore, the motion of the arc was found to depend on the relations between the outer magnetic field, the self-magnetic field and the curvature of the discharge axis. When the discharge channel moves relative to the outer cold gas, an additional transverse force corresponding to the drag of a heat source in a flow field must also be considered. The balance of these forces lead to an equation which, in general, permitted the calculation of the curvature behavior of the discharge channel.

Transverse Blowing and Transverse Magnetic Field

Thiene's (31) analytical investigation was predicated on the assumption that an external transverse magnetic field applied to the arc column so as to oppose the convective force would give rise to an internal double-vortex flow pattern due to the $\overline{J} \times \overline{B}$ body force acting on the arc plasma. A stagnation point was assumed to exist within the column in order for the arc to be stationary in the transverse gas flow. The steady-state momentum equation was applied, neglecting the viscous forces. Thiene assumed that along the external flow axis within the column, some fraction of the $\overline{J} \times \overline{B}$ force was balanced by the pressure gradient. It was also assumed that outside the column, the pressure gradient was balanced primarily by the inertia effect. Integrating the equations along a streamline to the stagnation point gave the same result that would be obtained by equating the magnetic force to the aerodynamic force on a conducting cylinder (i.e., $BI = (1/2)\,\rho C_D V^2 D$).

Lord (35) analytically treated the convected arc held at rest by an applied transverse magnetic field. The following assumptions were made:

1) No effects on the arc from the external circuit.

2) The electrodes were in the same plane as the jet sides.

3) Uniform flow existed upstream of the arc.

4) The external magnetic field is applied such that a perfect balance is achieved at each arc segment.

5) The arc center is a straight line perpendicular to the electrodes.

6) Outside the arc column $\sigma = 0$, and k, ρ, V, and C_P are constant and equal to the value of the free stream condition.

7) Inside the arc column σ, k, ρ, C_P, V are constant and equal to the value at the temperature and pressure of the arc center. Only the uniform column portion of the arc was considered; therefore, the following additional assumptions were made:

8) The arc periphery is circular in cross-section.

9) The column radius varies with the velocity of imposed flow.

10) The arc periphery is non-porous.

11) Partial matching of the various properties at the arc periphery is permissible.

12) No convection occurs within the arc.

13) The arc periphery can withstand tangential stress.

14) The total magnetic field is the sum of the induced plus internal magnetic field.

15) The pressure distribution inside the arc is the sum of the static pressure plus magnetic pressure.

16) The heat flux and temperature distribution are the same as for the corresponding static arc.

The momentum and energy equations, Ampere's and Ohm's law and $BI = (1/2)\rho C_D V^2 D$ were applied to the arc with the following quantities continuous at the arc periphery: The pressure at the forward stagnation point, the total force, the temperature, and the total heat transfer. Thus, P, T, B_r, B_θ and j_z were obtained inside and P and T on the periphery. The arc characteristics were also obtained in non-dimensional form. The following general conclusions were reached. The major effects of increasing the current at constant magnetic field are to decrease the voltage gradient and to increase the size of the arc. The relative velocity of the arc and the flow, and the temperature of the arc, are only slightly affected by increasing the current. The major effect of increasing the magnetic field at constant current is to increase the relative velocity of the arc and the flow; the voltage gradient, the size of the arc, and the temperature of the arc, are affected to a lesser extent.

Lord (43) analytically derived equations for the arc characteristics and the fraction of input power lost by radiation using a radiative heat sink model. The following assumptions were made:

1) Radial symmetry (circular arc boundary),
2) thermal equilibrium,
3) no convection inside arc, and
4) constant conductivity inside arc.

The effects of the applied external magnetic field, particularly on the conductivity, were not considered although the magnetic field was used to stabilize the arc. The theoretical results were derived by means of an analogy with a wall-stabilized static arc combined with the Nusselt-Reynolds relationship for convective heat transfer. The results indicated that the fraction of the input power lost due to radiation decreases as flow velocity is increased or as pressure is increased. This latter conclusion is reached because the arc decreases in size as the pressure increases. Therefore, even though radiation loss per unit volume does increase with pressure, the decrease in cross-sectional area with increase of pressure is such that the radiation loss per unit length of column also decreases with increasing pressure.

Lord and Broadbent (47) semi-empirically analyzed an electric arc in a transverse subsonic air stream held stationary by an external magnetic field. A simple model was put forth by making an analogy with an equivalent arc of circular cross-section which carried the same current, but was free from convection within the column. The following assumptions were made:

1) Charge neutrality exists in the plasma column.

2) The gas inside the arc is in thermal equilibrium.

3) A definite boundary exists outside of which the electric current is zero.

4) No variation of properties along the column axis.

5) Steady two-dimensional flow exists.

6) The arc boundary is of circular cross-section.

7) The electrical conductivity inside the arc is constant corresponding to the centerline temperature.

8) No convection is present inside the arc.

9) The radiated power density is constant.

The energy equation, Ohm's law, momentum equation and Maxwell's equations were applied to obtain expressions for the heat flux and arc radius as a function of the E, I, and arc properties. The results were compared with the annular gap, traveling arc experimental data of Adams (48). Lord and Broadbent concluded that a model based on a heated solid cylinder analogy is not valid. One may indicate possible sources of discrepancy:

1) The boundary layer difference with regard to laminar and turbulent flow between solid cylinders and arcs.

2) The extrapolations necessary due to lack of experimental data for cross-flow on very highly heated cylinders.

3) The application of the rotating arc results to a stationary balanced arc condition (the effects of small electrode gaps, effect of induced swirl in the wake of the arc due to vortices, departures of the arc shape from uniform cylinder, stream velocity and power supply fluctuations, electrode jet effects, and contamination of arc by electrode vaporization are neglected).

Broadbent (50) semi-empirically analyzed the behavior of a magnetically driven electric arc in cross-flow. The assumptions were that --

1) A uniform column exists where electrode effects are not important.

2) The drag law $BI = \rho C_D V^2 r_o$ is valid. Broadbent compared his data with the experimental annular gap traveling arc experiment of Adams. The heat transfer was compared with that for a heated solid cylinder. The results indicated that at comparable Reynolds numbers, the arc Nusselt number was greater than ten times that for the heated solid cylinder. The Nusselt number was calculated from experimentally measured arc properties. To verify the observed heat transfer, future spectroscopic temperature measurements throughout the arc were planned. Broadbent also derived similarity laws which indicated that the parameters EI, BI/V, and V^2I/E (E = voltage gradient, I = current and V = velocity) are quite important in describing the stationary arc behavior.

EXPERIMENTAL ANALYSES OF THE STATIONARY ARC

Transverse blowing only

Thiene (31) reported experimental measurements of the deflection of a small horizontal electric arc between co-linear tungsten electrodes in the presence of subsonic, laminar forced convection. Studies were conducted for arc currents from 2 to 6 amps, arc voltages between 30 to 50 volts, electrode gaps from 4 to 8 mm and blowing velocities up to 200 cm/sec. Argon gas was used at atmospheric pressure and the tunnel test section was 1-3/4" square. Photographs of the deflected column as functions of various parameters were taken and analyzed. The effect of the cathode jet was noticed, and numerous attempts were made to eliminate or reduce it. Although the occurrence of such a jet was not unexpected, it was presumed that at sufficiently low arc currents, the cathode jet effect would be negligible. The compromise design finally adopted was a pointed thoriated tungsten rod surrounded by an electrically floating tungsten sleeve. The sleeve provided the necessary boundary condition and appeared to significantly reduce the jet effect. An interesting observation made by Thiene was that as the flow velocity was increased beyond the maximum value used for recording data, the column became increasingly "horseshoe" shaped and pulsated upstream and downstream at several cycles per second. If the blowing velocity was further increased, arc blowout resulted. This pulsation may have been due to the interaction of the electrode-tip vortices. The stiffening effect on the column exerted by the electrode sleeves was observed from the photographs. Thiene postulated that the increased electric field on the concave side of the column when in the convection-bowed shape contributed to the flexural rigidity. Numerous effects were neglected by Thiene in the experimental evaluation which may have had a significant influence:

1) The difference between a horizontally burning arc exposed to natural convection and an arc in a forced cross-flow.

2) The difference of mass flux through the arc column compared to free-stream mass flux of the undisturbed flow.

3) The "horseshoe" shape effect compared with small arc deflection. (This severely deflected arc case actually consists of two separate problems with regard to flow pattern. One dealing with axial flow and the other dealing primarily with true cross-flow.)

Alferov and Bushmin (36) studied arc discharges drawn across the exit of a closed wind tunnel convergent-divergent nozzle. The air flow Mach numbers investigated were 0, 0.5, 1.5, 3.0 and 4.5, which were obtained by using interchangeable nozzles. The stagnation temperature was maintained constant at T_o = 283 °K, and the static pressure was varied (in the range of 15 to 330 mm Hg.) in order to have the same gas density at the various Mach numbers. The electrodes were solid molybdenum, 5 mm in diameter, which extended into the tunnel. They were surrounded by a teflon sheath, and were variable to gaps of 10, 15, 20, and 25 mm. The discharge was investigated using two electric circuit variants:

1) A stabilizing ballast resistor and,

2) a shunted ballast resistor.

Photographs were taken of the form and behavior of the discharge. In the first variant, the discharge was in the form of a series of flashes in the absence of gas flow, but in the presence of gas flow the discharge exhibited high stability which increased with increase of flow velocity. The discharge had a falling current-voltage characteristic, indicative of a stable arc discharge. Voltages of approximately 8 KV and currents of 0.5 to 3 amperes were typical. Comparison of the current both with and without air flow showed that the gas flow considerably reduced the duration of the current pulses. In the second variant, the discharge was similar to the breakdown of a discharge gap and was characterized by a pre-breakdown glow and an increase of the breakdown voltage with increase of the Mach number of the gas flow, other conditions being equal. Paschen curves were obtained for the various Mach numbers.

Baranov and Vasiléva (42) experimentally investigated a low current arc drawn across a high velocity flow of argon. The arc currents varied from 0.4 to 20 amperes, gas pressure ranged from 0.1 to 60 mm Hg. and flow speeds from 10^2 to 10^4 cm/sec. A closed circuit system was used in which a $\overline{J} \times \overline{B}$ arc accelerator upstream of the 4 cm. diameter glass tube test section provided the flow. Steel or covar anodes were used together with oxide cathodes (indirectly heated). The electrodes were approximately 2.5 cm in diameter and mounted flush with the tube walls. High-speed photography was used for the diagnostics. The velocity was measured by the transverse displacement of a spark. The gas pressure, flow speed and arc current all affected the shape and displacement of the arc. A critical flow speed (approximately 3×10^3 cm/sec) was determined, which increased with current. When the flow speeds were below this critical value, the luminous region followed the curved contour of the laminar Poiseuille flow in the tube, thereby causing the arc to tend to follow the walls of the tube. When the flow speeds were greater than or equal to the critical value, luminous streaks extended across chords between the electrodes of the curved contour. This indicated that an ionized path had been formed in the flow near the front of the arc where the electric field strength was highest. It was noted that low frequency voltage fluctuations accompanied the breakdown. At higher speeds, the entire arc region became diffuse. It appeared to be made up of a series of breakdowns whose frequency increased with flow speed.

Kalachev (37) experimentally studied a pulsed discharge in a high velocity air stream. The apparatus was identical to that used by Alferov and Bushmin. The same air flow Mach numbers were used, but the static pressures were limited to the range of 15 to 252 mm Hg. The discharge, produced by a capacitor bank discharge, was investigated using high-speed photography, oscillograms of the discharge current and voltage, and conventional photography. The results indicated that luminescence precedes the breakdown followed by an initially straight discharge which drifts downstream. A comparison of the photographs of the luminescence with the flow pattern of the electrodes obtained by Alferov and Bushmin showed shock waves on the background of the luminescence. It was concluded that the high-velocity air flow has a significant effect on pre-breakdown phenomena in the discharge gap; in particular, it modifies the shape of the discharge channel. However, the electrical characteristics such as the time dependence of the current and voltages are not significantly affected by the air stream.

Benenson (55) is presently investigating the effects of low velocity forced convection upon the steady-state characteristics of electric arcs. The objective is to determine the arc characteristic shape, temperature distribution within the arc (asymmetrical) and the voltage gradient as a function of the arc current, gas velocity, and electrode gap. The experimental apparatus consists of a 15 to

100 ampere electric arc established across a 1-3/4" square test section of a small wind tunnel. Argon gas blowing velocities in the 0 to 5 ft/sec range are used, and the pressure is approximately atmospheric. The electrode gap can be varied between 1/16" and 1-1/4". A 0.040" diameter tantalum cathode electrode and a 0.187" diameter copper anode electrode are used. The electrodes (both unshielded) are co-linear with the gravitational field, with the convective blowing oriented in the horizontal plane. The test facility may be rotated so that the influence of gravity (which may have a significant effect at the low blowing velocity, low arc current, and large gap regime) may be determined. A vertical, relatively stable arc has been achieved. Gross instabilities (both visually and in the arc current and voltage output) were found to exist in the initial experimentation, but these were significantly reduced by using a cylindrical, tantalum cathode together with a cylindrical copper anode. Two stable modes have resulted with accompanying voltage ripple $\leq 2\%$. For $I \leq 20$ amps a bow-shaped arc results. For $I > 20$ amps a cusp-shaped arc results. Both shapes are convex in the downstream direction, and both occur in the presence of forced convection. Both modes were found with the same electrode arrangement, and therefore are associated with the cathode electrode material, its properties, its shape, and the jet effect. At the low current range, local melting of the cathode tip occurs forming a spherically shaped tip. A diffuse spot attachment appears to occur; therefore, a reduced current

density and correspondingly a reduced electrode jet effect. At the higher current operating range, a transition occurs wherein the cathode attachment spot region appears to be more highly localized at a point, thus promoting the jet effect. The jet effect then results in the cusp-shaped formation. The experimental technique being devised to determine the arc's characteristic dimensions and local integrated intensity of arc radiation will consist of small mirrors located along one side of the wind tunnel test section at different azimuthal locations. The images of the arc will be reflected from these primary mirrors to a secondary set of mirrors which then reflect the light to two cameras. Each camera is simultaneously triggered and contains a different narrow band interference filter. From the data obtained, the arc characteristic dimensions may be determined together with details on the arc radiation intensity using a 2-line or absolute intensity method.

Transverse External Magnetic Field Only

Serdyuk (32) investigated a welding arc under the influence of an external transverse uniform magnetic field. Two cases were considered: An arc with magnetic deflection (i. e., shifting of anode and cathode spots together with the column), and an arc with magnetic deformation (i. e., stationary cathode spot, movement of anode spot and deformation of the column). The latter was much more difficult to obtain experimentally. The first case was empirically described by $B = 4C\rho\sqrt{\frac{V^3}{I}}$ (where C = dimensionless coefficient for arc currents of 100 to 1000 amperes). The influences of electrode material, electrode jets, self-magnetic field and configuration effects were not included. The second case was investigated using a 310 ampere carbon arc of 15 mm length in a uniform external transverse magnetic field with the aid of a high-speed camera. The high-speed pictures showed that the cathode remained fixed while the arc column and anode spot were free to move. An increased deflection at increasing distance from the cathode was observed. The nature of the deformation was explained by the effect of the forced gas flow of the arc column, directed under normal conditions from the cathode to the anode. Consequently, deformation began at the cathode and increased on its way toward the anode depending upon the rate of motion of the arc column plasma. Such a phenomenon was also observed during the application of a variable external transverse magnetic field. In this case, the arc column was continuously deformed by the time changing magnetic field. A delay was noted, and attributed to the resistance of the medium to the movement of the arc column. An interesting phenomenon was observed in the case of employing a copper anode. As the arc column was being deformed by the transverse magnetic field, the gas stream (i.e., cathode jet) from the cathode to the anode changed its direction relative to the surface of the anode accompanied by a decrease in its component rate in the direction of the anode. This facilitated the conditions for the origination of a visible stream of gases from the anode spot (an anode jet), suppressed under ordinary conditions by the slower initial rate of its formation and the cathode stream. The observations showed that the maximum role was played by the vapors coming from the copper anode as compared to other tests using aluminum or iron anodes. These data are in agreement with the evaporation energy values of the particular metallic materials. An equation of dynamic equilibrium was applied to the deflected arc column. This included the inertia force, resistive force of the medium, elastic (i.e., restoring) force, and the magnetic driving force. A non-linear differential equation was formed from the force balance and analyzed by creating approximate expressions for the individual members. The equation could not be solved in general form through elementary functions, however, a solution was obtained for the simplest case of an arc in a constant uniform external transverse magnetic field. The obtained formulae could be used for calculating the stability limit of the arc in a transverse external magnetic field in addition to the magnitude of the deformation due to the magnetic field.

Olsen (49) is presently investigating the interaction of an external transverse magnetic field with an electric arc. (He is also investigating the interaction of a transverse pre-ionized gas flow with an electric arc.) The apparatus consists of a free-burning, 1.1

atmosphere, 400 ampere argon arc drawn between a 1/8" diameter thoriated tungsten rod cathode and a copper plate anode. The electrode separation is varied from 5 to 15 mm, with the cathode always the top electrode. Enclosing the arc is an octagonal aluminum housing with eight ports for viewing or probe insertion. During the portion of the investigation concerned with the transverse pre-ionized gas interaction with the vertical free-burning arc, an F-40 Thermal Dynamics plasma arc torch is mounted in one of the ports. Contamination level, which is extremely important for maintaining free-burning arc stability and minimum electrode erosion, is carefully monitored and held to an extreme minimum. This investigation is part of a long-range research effort directed at a fundamental understanding of interacting plasmas in an external magnetic field. Two stumbling blocks for such a basic research effort have been the unavailability of plasmas with independently well-known properties, and the lack of a method for making detailed local measurements of internal properties of the asymmetrical plasma produced by the interaction. During 1965 Olsen succeeded in developing a series representation method for precisely inverting externally measured asymmetrical spectral intensity distributions to true radial distributions of the emission coefficients for optically thin sources. The method has been successfully applied to experimental and analytical data under the condition of an assumed mirror plane of symmetry. The inversion method has been tested on numerous assumed models (formed of both symmetric and displaced distributions) with greater than 0.1% accuracy. Olsen's free-burning argon arc has been operated in an external magnetic field of up to 100 gauss. Photographs were taken of the distorted arc at angular positions of 0°, 45°, and 90° with respect to the mirror plane of symmetry in the plasma. From these photographs the asymmetrical plane of symmetry was confirmed. A cross-flow induced by the field interaction was also noted. With a maximum external magnetic field for which stable operation can be maintained (approximately 100 gauss) the plasma was deflected from the cathode with a radius of curvature such that the gas stream developed a component in the reverse direction to that of the cathode jet. This observation was also made by Serdyuk (32). Work is presently proceeding in the direction of verifying the inversion method for a magnetically distorted plasma.

Transverse Blowing and Transverse External Magnetic Field (Pre-ionized Flow)

As part of a long-range Air Force sponsored research program, Hogan (40) initiated an experimental investigation of the fundamental interaction and energy exchange process between electric arc discharges and cross-flow fields of pre-ionized gases with and without the presence of transverse magnetic fields. The objective was to examine the phenomena taking place in the $\overline{J} \times \overline{B}$ region and obtain information on the appearance and behavior of the discharge. The diagnostics included high-speed photography of the discharge, measurement of the electrical characteristics, and measurement of the heat transfer to the electrodes. The experimental apparatus consisted of a rectangular 2" x 4" test section. The source of the pre-ionized flow of nitrogen was a 3/4" diameter unconfined plasma jet with an enthalpy of approximately 5000 BTU/lb_m. The pressure range was 3 to 760 mm Hg, currents used were 500 and 1000 amperes, the external magnetic field was 1000 gauss and the electrode gap was 1/2". Five different electrode configurations were tried, varying from flat to semi-cylindrical to conical. The results indicated that a stable discharge was not obtained over the above range of test conditions. A filament type discharge repetitively moved downstream over the electrodes. Malliaris (41) is presently doing a continuation study of the phenomena taking place within the $\overline{J} \times \overline{B}$ region. This new effort includes studies of the radiation emitted by the discharge, current distribution within the $\overline{J} \times \overline{B}$ region, principal mode of energy transport from the discharge to the gas, effect of the applied external magnetic field on the discharge and effect of varying the incident flow parameters. The experimental conditions are approximately the same with the exception that the external magnetic field is varied from 0 to $\pm$ 5000 gauss. An approximate theory is being developed which when correlated with the data is only partially satisfactory. So far the main conclusions reached were these --

1) The electrical discharge had arc-like characteristics,

2) the column occupied a small fraction of the cross-sectional area in the flow,

3) the fraction of the input power used for acceleration was small,

4) the predominant mode of energy transport from the discharge was by convection,

5) conduction and radiation were negligible, and

6) the input power increased in the presence of the magnetic field, but the electrical conductivity was independent of the magnetic field up to 5000 gauss.

The increase of power is thought to be a result of the increased convection through the arc by electromagnetic pumping rather than a result of plasma acceleration or decrease of the electrical conductivity in the presence of the applied magnetic field.

Transverse Blowing and Transverse External Magnetic Field (Cold Flow)

Smith and Early (29) conducted an experimental feasibility study of heating an air stream in a wind tunnel by an electrical discharge. The experimental apparatus consisted of a small, 1" x 1" cross-section, approximately four second run-time, blow-down wind tunnel. Both dry nitrogen and air in the Mach number range of 3 to 5 were used. The static pressure was approximately 5 mm Hg, the arc current was less than or equal to 15 amperes, and the externally applied transverse magnetic field varied from 0 to 6000 gauss. The anode and cathode electrodes formed the divergent portion of a wedge nozzle. Various other geometries were used including horn-shaped and pin-type electrodes. Up to 5 kw of electrical power were dissipated. One of the more important observations was that the arc showed a strong tendency to concentrate in the tunnel boundary layer region near the walls i.e., away from the higher velocity free stream, and thereby filled only approximately 1/2 of the tunnel cross-section. Two possible reasons for the arc's strong preference for the boundary layer are the reduced density in the boundary layer and the reduced cooling there (due to the lower velocity). In addition, the arc assumed a skewed orientation (a slant angle of 20 to 70°), with the cathode spot always downstream of the anode spot. The arc was also observed to be 3 to 4 times as great in the dimension parallel to the flow as in the transverse direction. Numerous unsuccessful attempts were performed in trying to eliminate the arc slanting. It was also noted that slight changes in the thickness of the top or bottom boundary layer or in the orientation of the magnetic field made the discharge jump all the way from one dielectric tunnel wall to the other. These rapid fluctuations in the arc location were observed with high-speed motion pictures (7000 frames/sec). Pulsed discharge experiments of up to 1500 amps were also conducted, but the arc still concentrated near the boundary layer. The arc was also observed to become more diffuse as the external magnetic field increased. Smith and Early concluded that the arc slanting did not necessarily depend upon phenomena occurring at the electrode sites; but was more a result of the momentum transfer mechanism in the arc column itself. It is extremely interesting to note that when the flow went subsonic, the arc immediately localized on the tips of the horn electrodes and located itself in the center of the tunnel away from the boundaries. However, it still maintained the characteristic "S" shape with the anode attachment again upstream. Possible areas of uncertainty were the following --

1) Non-uniform flow condition in the boundary layer,

2) flow separation,

3) strength and fringe effect of the magnetic field for the various geometries used,

4) amount of non-uniform heating into the tunnel walls and electrodes,

5) distinguishment between electrode spot and column interaction phenomena,

6) true equilibrium being reached in the approximate 4-second run time,

7) turbulence level in the flow, and

8) after-glow radiation persisting in the flow downstream.

Thiene (31) conducted some exploratory investigations with a weak external magnetic field applied to the blowing apparatus previously discussed under the transverse blowing only section. A magnetic field of up to 1.4 gauss was applied transverse to the column so as to oppose the forced convection effect. Thiene postulated that this magnetic field would give rise to a circulatory convection due to the $\overline{J} \times \overline{B}$ body force acting on the arc plasma. A stagnation point was assumed to exist within the arc boundary. The arc current used was 4 amperes and the blowing velocities reached a maximum of 5 ft/sec. The momentum equation (neglecting viscous forces) was applied in an analysis of the phenomena. Thiene assumed that within the column, some fraction of the $\overline{J} \times \overline{B}$ force was balanced by the pressure gradient. The equation was integrated along a streamline from a free-stream position to the stagnation point. Outside the column, it was assumed that some fraction of the pressure gradient was balanced principally by the inertial reaction. Because of the low blowing velocities used, it was assumed that P_∞ was approximately equal to P_{static}. The resulting equation was the same relationship that would have been obtained by equating the aerodynamic drag force to the magnetic restoring force (i.e., $BI = (1/2) \rho\, C_D V^2 D$.

The following conclusions were reached by Thiene:

1) The magnetic field required to balance the arc was directly proportional to V^2.

2) The deflection force due to the self-field was of the same order of magnitude as the externally applied force.

3) The contribution of the magnetic field to the enthalpy flux due to ambipolar diffusion was negligible.

4) The effect of the magnetic field on the current density was negligible.

5) The contribution of the magnetic field to the rate of energy production term $[(\overline{E} + \overline{V} \times \overline{B}) \cdot \overline{j}]$ was negligible.

6) The use of scalar transport coefficients was justified, since the cyclotron frequency was small compared with collision rates.

Some possible sources for error were --

1) Effect of earth's magnetic field,

2) effect of stray fields from electrode leads,

3) effect of ferromagnetic materials in the vicinity of the test section,

4) determination of the voltage gradient and power in the positive column,

5) neglect of radiation,

6) tunnel wall effect at the low blowing velocities (superimposed effect of free convection), and

7) effect of electrodes protruding into tunnel test section.

Bond's (39) dissertation, paralleling the research effort of Smith and Early (29), dealt with the experimental investigation of magnetically stabilizing an electric arc in a supersonic flow. The experimental setup consisted of two parallel cylindrical uncooled rail electrodes mounted in a supersonic blow-down wind tunnel and oriented with the electrode axes parallel to the tunnel flow direction. The electrode gaps used varied from 0.6 to 1.1 inches. The arc was initiated by exploding a wire at the upstream end of the electrodes. Electrode materials of carbon, brass, steel, copper and oxygen-free high-conductivity copper were used. The average tunnel run time was 0.8 seconds during which time the data were obtained. Throughout the majority of the tests the Mach number was 2.5, (corresponding to V = 1800 ft/sec), P_{stag} = 20.2 in. Hg., and arc currents of 300 to 1000 amperes. External field coils provided a non-uniform transverse magnetic field in the range of approximately 1000 to 4000 gauss. The magnetic field was oriented such that the magnetic field increased in the flow direction. This helped to stabilize the arc from streamwise displacements. Typical values of magnetic field were 1300 gauss at the anode root and 4300 gauss at the cathode root. The following observations were obtained:

1) The cathode root was always located downstream of the anode root (also noted by Smith and Early (29)).

2) The positive column assumed a slanted orientation with respect to the electrode axis (angle of approximately 60 to 70° measured from the vertical). No change was observed in the slant angle with different electrode materials or shapes. Therefore it is doubtful that slant was primarily due to an electrode phenomena. (Also noted by Smith and Early (29).)

3) The angle of slant did not vary with current (within the range 130 to 1000 amperes) or P_{stag} (within the range 10 to 24 in. Hg.), but changed sign with electrode polarity reversal.

4) The slant angle was in the correct direction for the Hall angle, but it did not show dependence on B or I which would be expected if slant was primarily due to the Hall effect.

5) The slant angle was approximately equal to the Mach angle (lines along which infinitesimal pressure disturbances must propagate) at Mach numbers of 2 and 2.5.

6) The slanting took place at approximately the angle where $E_{11}/P_{stag}{}^{*}$ was a maximum. ($P_{stag}{}^{*}$ = stagnation point pressure of a solid slanted cylinder, and E_{11} is the component of the electric field parallel to the column.)

7) The aerodynamic force increased with increasing arc current. Bond therefore assumed the arc diameter increased with current. (High-speed photographs, 7000 frames/sec, indicated this to be approximately true.)

8) The arc had a characteristic curve with a negative slope.

9) The average transverse magnetic field required to balance the arc was independent of I_{arc} (over the range 150 to 700 amperes), but increased from approximately 2000 gauss at P_{stag} = 10 in. Hg. to approximately 3500 gauss at P_{stag} = 25 in. Hg.

It was found that the arc could be held stationary in two modes. In the first the arc was confined to the downstream portion of the electrodes. It had considerable curvature and occurred at weak external magnetic fields. This mode was postulated to be due to the arc curvature and fringing electric field. In the second mode the arc was confined to the cylindrical portion of the electrodes. The arc was skewed but relatively stable. This mode was postulated to be due to column fluid-mechanical interaction mechanisms.

Using the length of the slanted column, the voltage gradient E was estimated to be 14 volts/cm at M = 2.5 and P_{stag} = 20 in. Hg. It was independent of arc current from 200 to 700 amperes. The electrical conductivity σ was also estimated to be 10 mho/cm. For the arc in the balanced mode at M = 2.5 and I_{arc} = 300 amperes, Bond obtained the empirical relationship

$$B_{ext} = 0.829\,(P_{stag})^{1/2}.$$

For supersonic flow $P_{stag} \propto \rho$ (assuming T_{stag} = constant), therefore $B \propto (\rho)^{1/2}$. Comparing this to $BI = (1/2)\,\rho_\infty\,C_D V^2 D$ for subsonic flow one would expect $B \propto \rho$. This difference may be explained due to differences between subsonic and supersonic flow regimes. Questionable aspects of the experiment were --

1) The short run times (question of true equilibrium being reached),

2) flow separation effects,

3) effects of non-uniform heating into electrodes and tunnel walls,

4) electrode region and column coupling interaction phenomena,

5) after-glow radiation persisting in the downstream direction,

6) data taken at one Mach number, thereby not explicitly relating external magnetic field and velocity, and

7) large external magnetic field gradient along column.

Myers (52) investigated a magnetically balanced electric arc in a transverse subsonic gas flow of argon. The objective was to extend the range investigated by Thiene from the very low velocity and magnetic field range to higher velocities and extremely high magnetic fields. The possibility of significantly increasing the electrical conductivity by heating the electrons to a significantly higher temperature than that of the positive ions and atoms was also investigated. The experimental apparatus consisted of a small blow-down type wind tunnel of a one and one-fourth inch by three-fourths inch rectangular test section. Argon gas was used at static pressures of approximately 1.3 atmospheres and velocities of 0 to 300 ft/sec. The arc current ranged from 20 to 100 amperes and the external magnetic field from 2000 to 28,500 gauss. Myers used unshielded electrodes similar to Benenson (55); (Thiene (31) on the other hand, used shielded electrodes) composed of 3/32" diameter 2% thoriated tungsten rods. (Ground flat at the tip as compared to Benenson's conical shaped tips.) The electrode gap was varied from 5/32" to 7/8". The average run time was approximately 5 seconds. The convective force on the arc was found to be quite similar to the aerodynamic force of a subsonic gas flow on a solid cylinder. The assumption that the arc could be replaced by a solid cylinder with a diameter varying directly as the current satisfactorily explained the relation between the gas flow velocity and the external magnetic field required for balancing. The balancing was found to be proportional to the velocity squared and independent of the arc current. The arc characteristic curves were found to be typically negative with the arc voltage increasing as the magnetic field was increased. An analysis was made to predict the dependence of the column voltage gradient on the magnetic field. This compared favorably with the experimental data points. The results indicated that the column voltage gradient increased nearly linearly with increasing external magnetic field (constant arc current). An analysis similar to that of Thiene's was applied to give an estimation of the electric arc cross-sectional area. (Thiene's C_D value was used to obtain the arc diameter.) Because of the positionment of the electromagnet and tunnel configuration used, no high-speed pictures were possible; however, the discharge was visually observed to pulsate intermittently in the stream direction (similar to Smith and Early (29)). From the assumed arc cross-sectional area, the theories of non-equilibrium conductivity were applied to estimate the dependence of the arc's average electrical conductivity on the magnetic field in addition to an estimate of the electron temperature.

The data obtained experimentally best fit the equation $\sigma_{\beta_\perp} = \frac{1}{1 + \beta^2} \sigma_o$,

where $\beta = \omega\tau$,

ω = electron cyclotron frequency,

τ = electron collision time,

$\sigma_{\beta_\perp}$ = electrical conductivity perpendicular to the magnetic field,

σ_o = electrical conductivity before the external B field is applied.

Therefore, the conductivity decreased by a factor of $1 + \beta^2$ upon applying the external transverse magnetic field. Questionable aspects of the experiment were --

1) Applicability of conductivity equations,

2) electrode effects combined with magnetic field effects in the electrode region,

3) temperatures assumed for heat transfer and energy calculations,

4) neglect of heat loss to electrodes (especially for such short test times),

5) estimation of positive column voltage gradient and electrode drops, and

6) arc shape, stability, and behavior during test data measurement.

Kookekov (53) studied the motion of an electric arc with transverse blowing under the influence of an external, transverse magnetic field. The objective was to obtain experimental data on the arc current, voltage gradient, and velocity relationships. No description of the experimental setup, measurement techniques, or range of parameters was reported. A semi-empirical analysis was made based on the conservation of energy, Ohm's law, and the minimum principle to obtain the relation $E = A\sqrt[3]{V^2/I}$, where A was found from the experimental data. By assuming that the energy input to the arc was equal to the convective heat transfer losses, along with independence of ρ, h, σ, and r on I and V, the relation $EI/V = A\,(I^2/V)$ was obtained. This, combined with empirical data, led to the final result $V = 0.595\sqrt{B/M}\sqrt[3]{I/\rho^2}$. (M was undefined.) From the experimental results and the fact that the ionized particle density was found to be 4 to 5 orders of magnitude lower than the values for an isolated arc led Kookekov to the conclusion that there is turbulence in the transverse blown arc. Questionable aspects of the investigation were these --

1) Neglect of radiation and conduction heat transfer, and

2) independence of ρ, h, σ, and r on I and V.

APPENDIX B

CALIBRATION CURVES

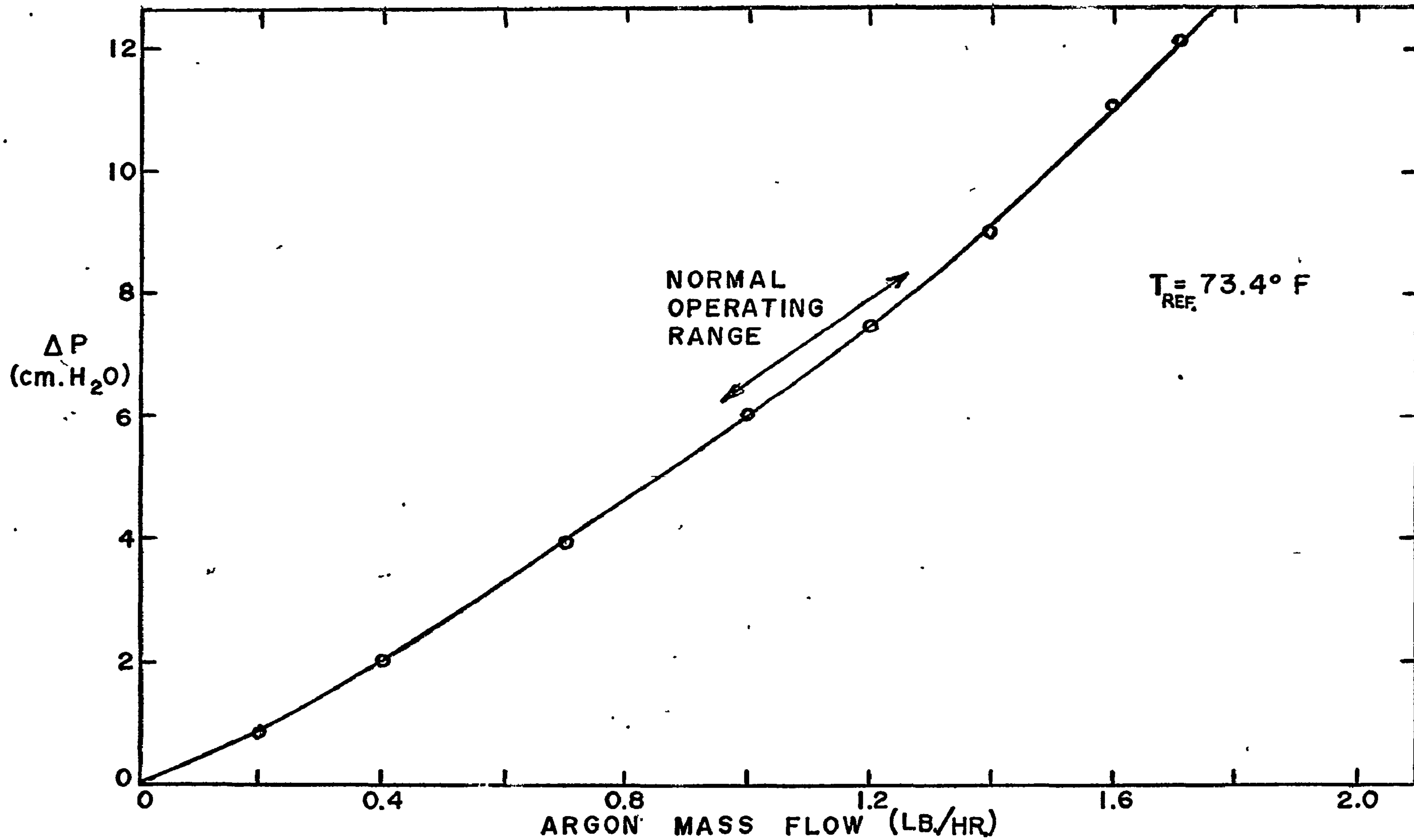

FIGURE 55 CALIBRATION CURVE FOR CATHODE CAPILLARY FLOWMETER

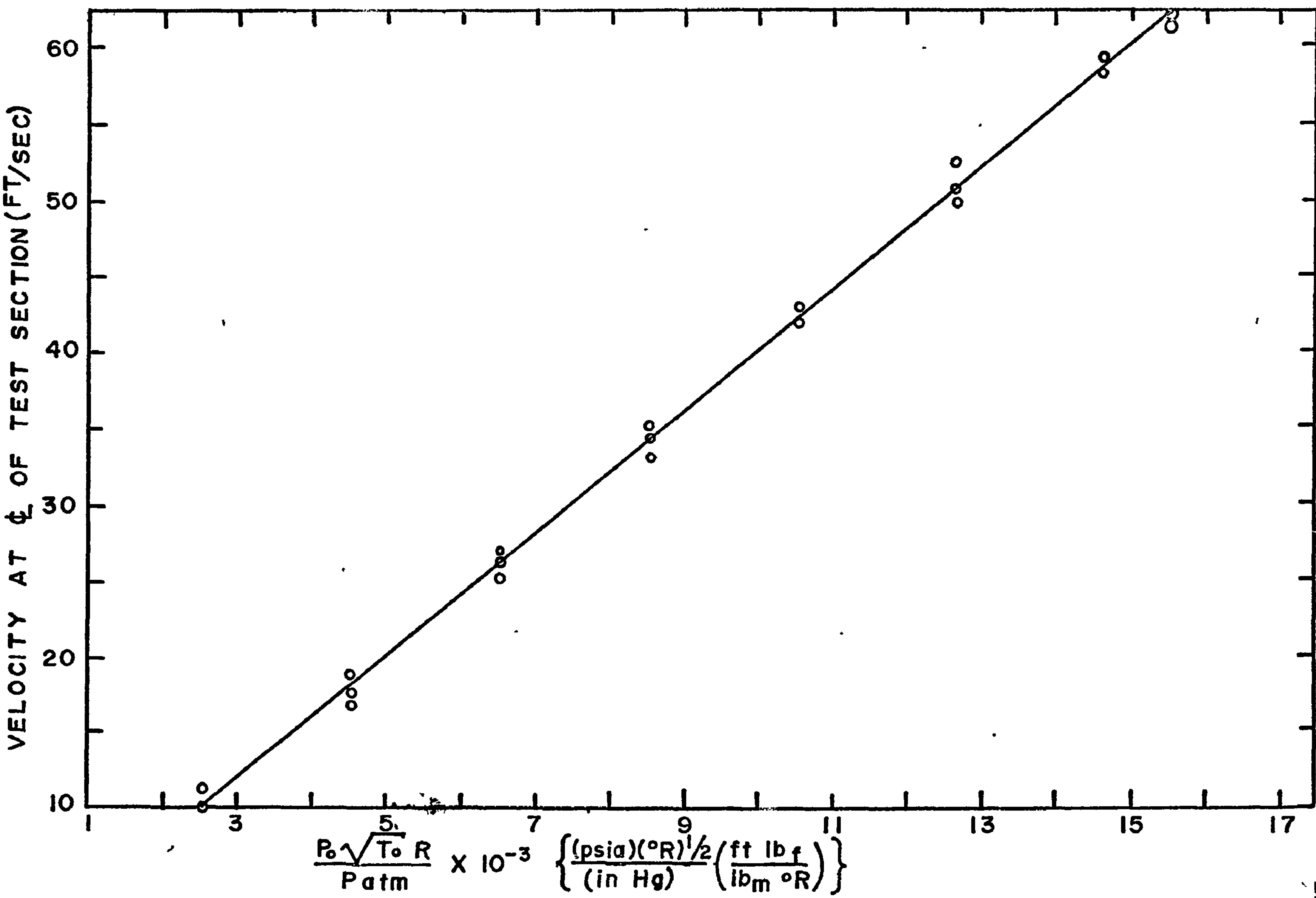

FIGURE 56. CALIBRATION CURVE FOR GREY-RAD VELOCITIES (COLD FLOW)

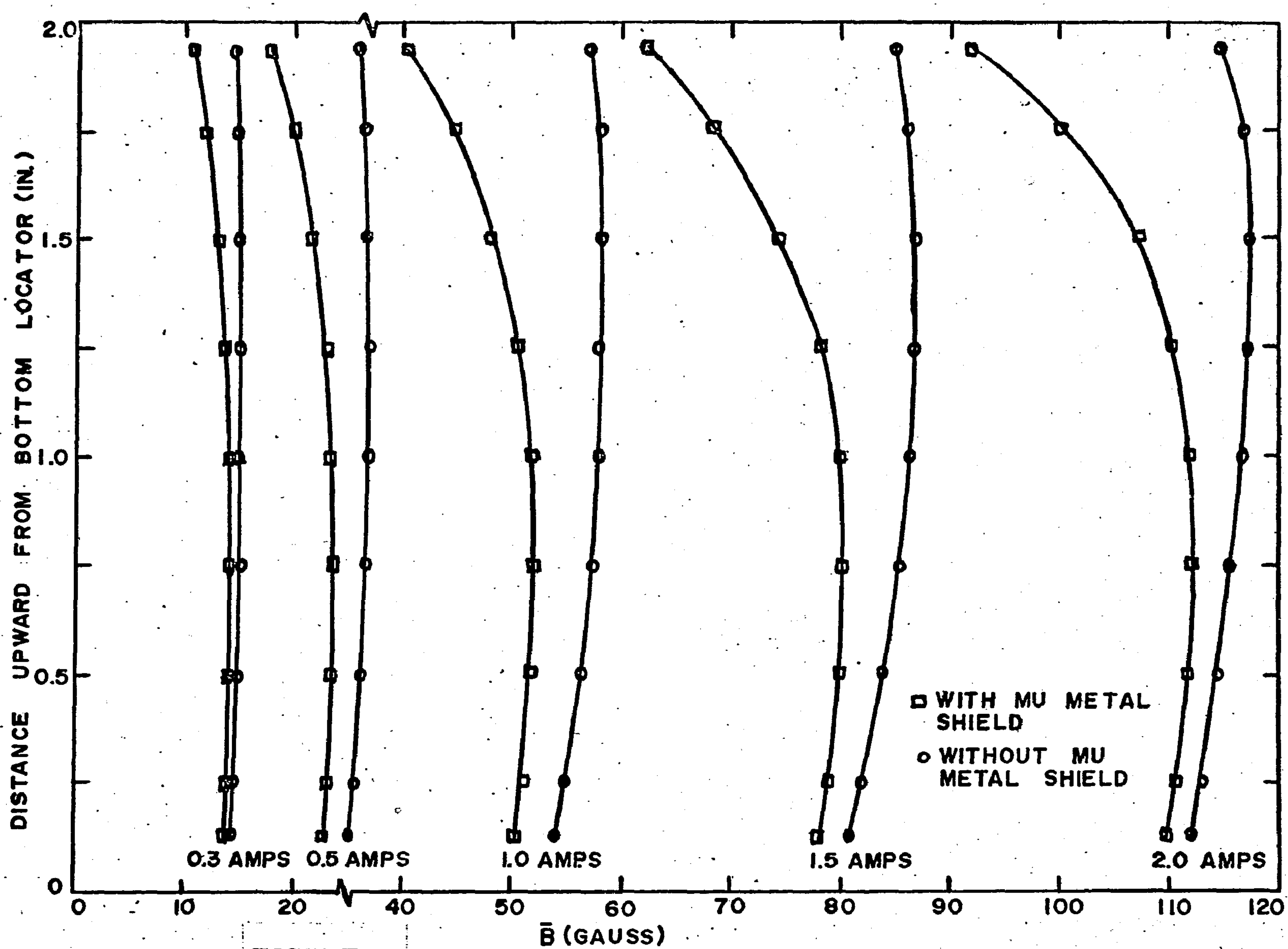

FIGURE 57 MAGNETIC FIELD PLOT

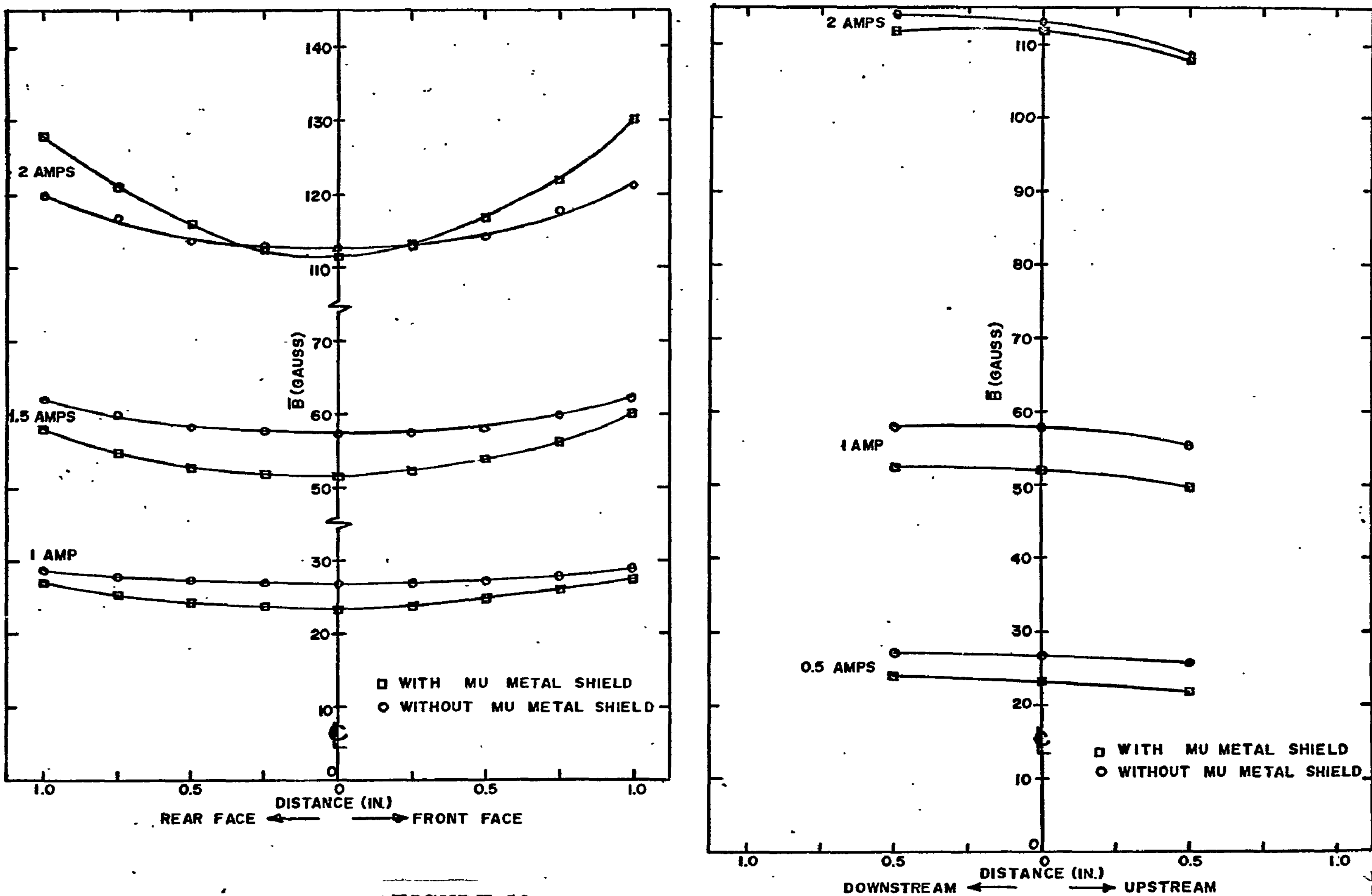

FIGURE 58 MAGNETIC FIELD PLOTS

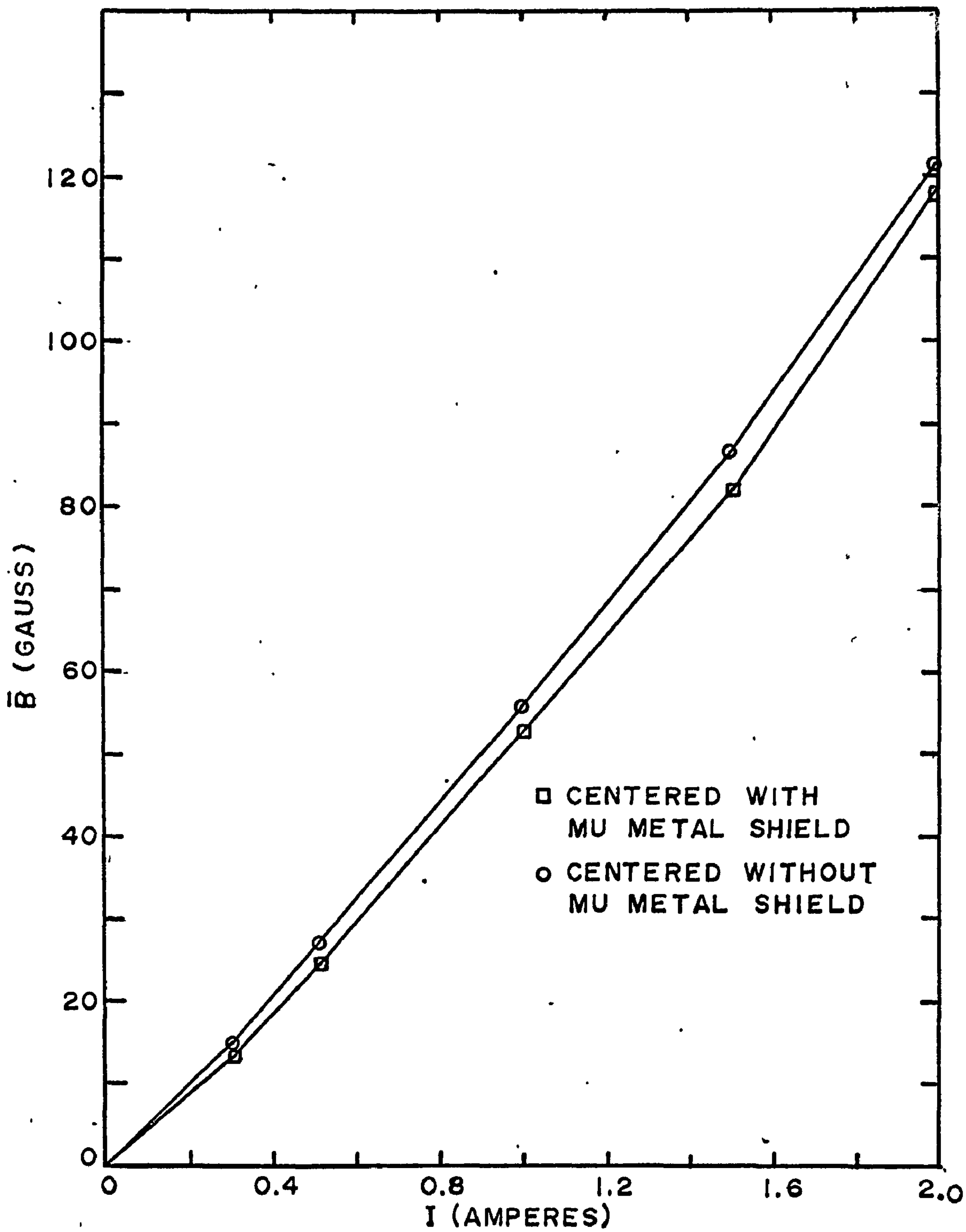

MAGNET CALIBRATION MADE WITH BELL "110" TRANSVERSE PROBE.

FIGURE 59

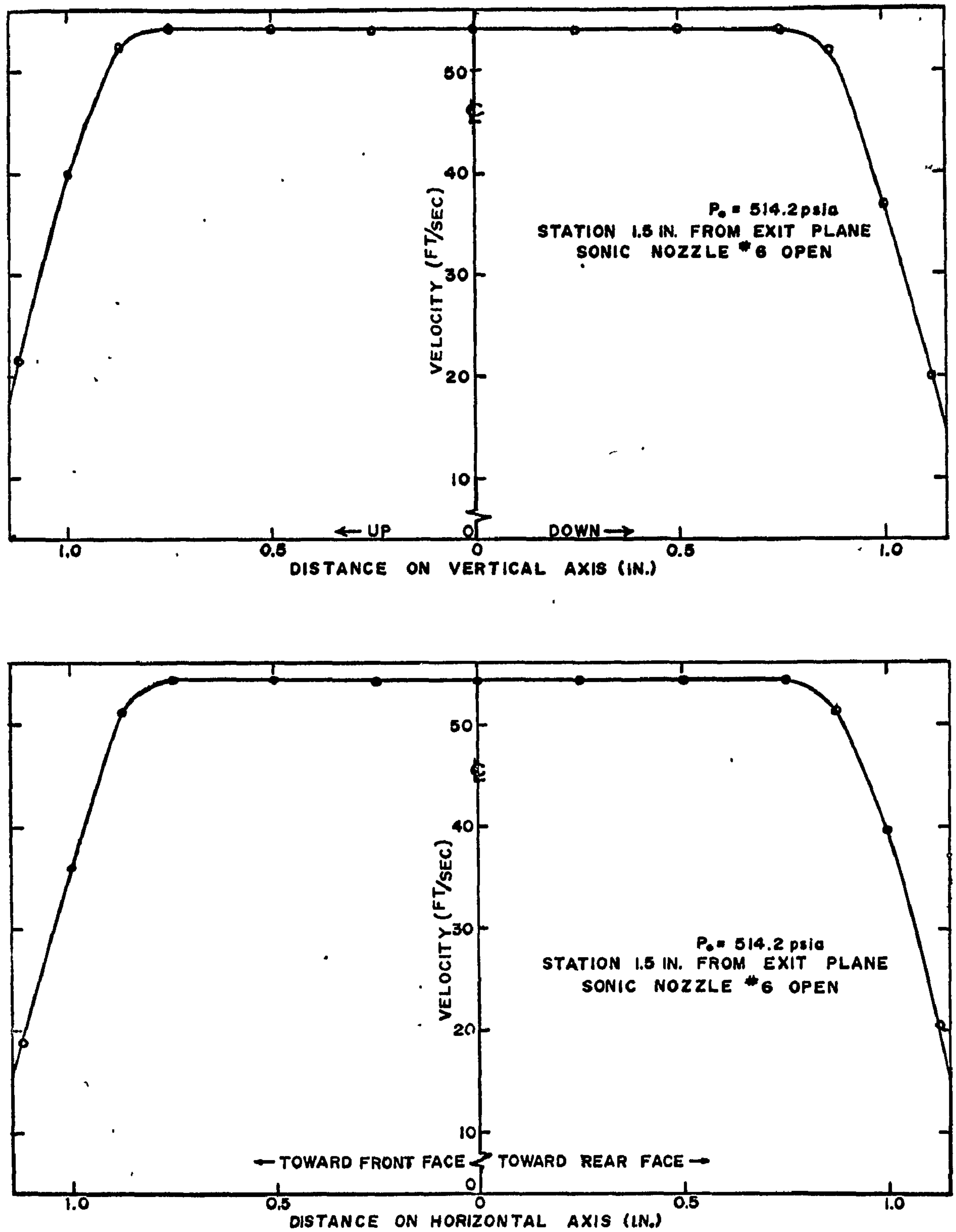

VELOCITY PROFILES FOR BLOWING NOZZLE

FIGURE 60

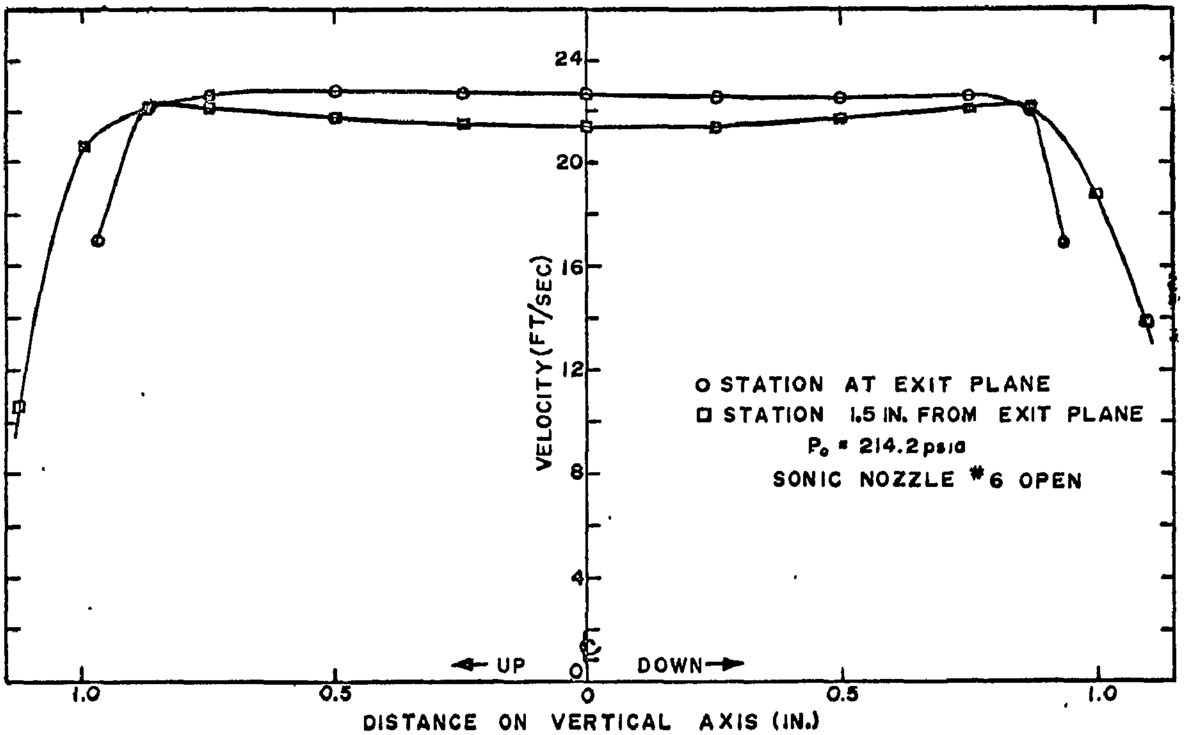

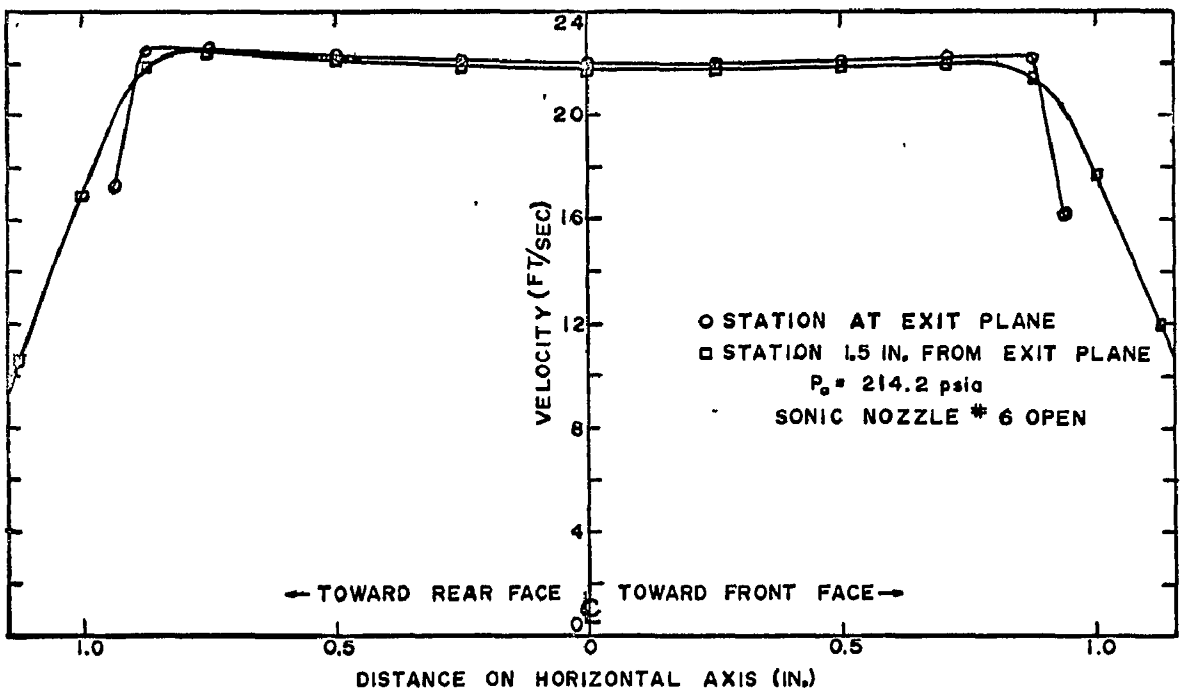

VELOCITY PROFILES FOR BLOWING NOZZLE

FIGURE 61

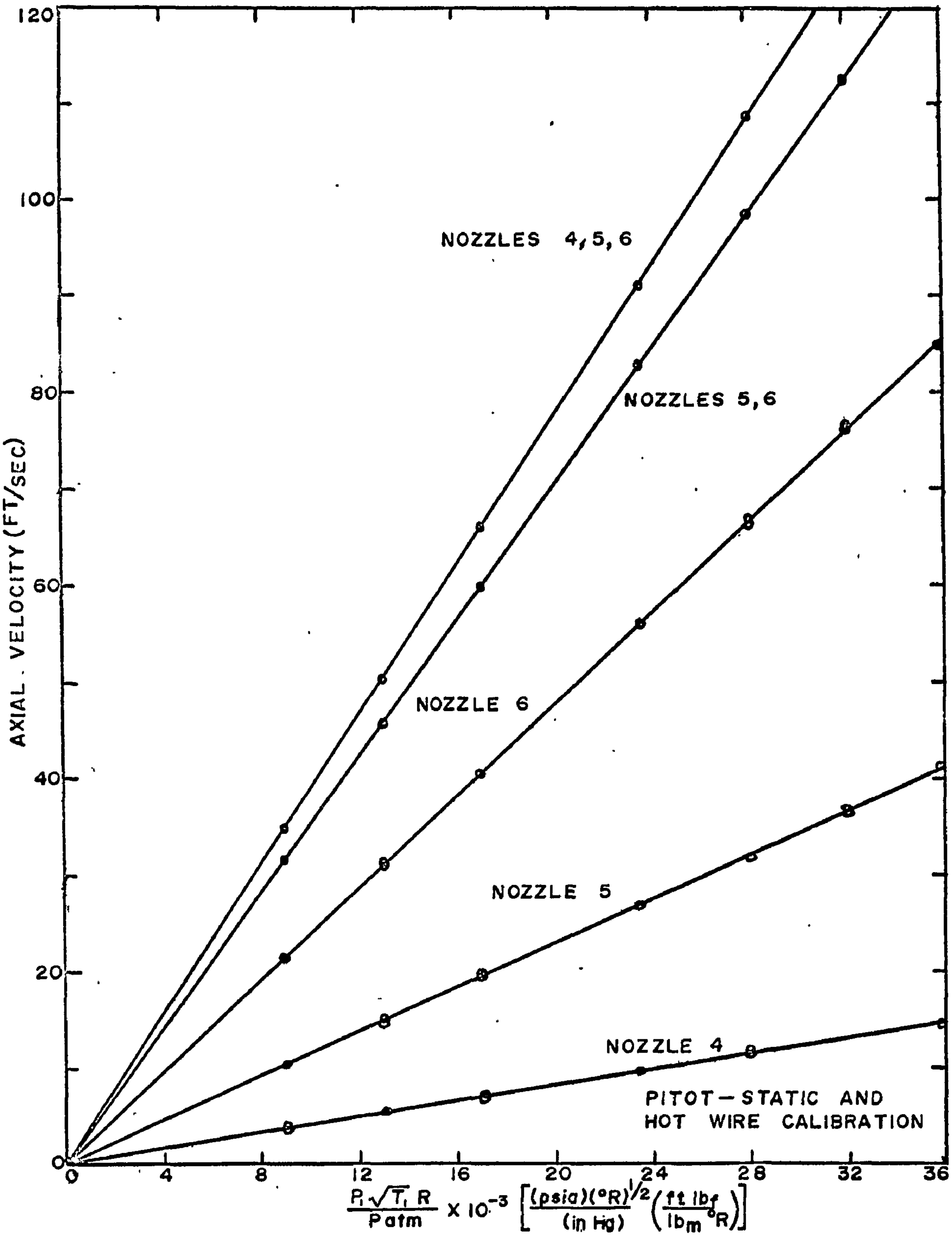

SONIC NOZZLE VELOCITY CALIBRATION
FOR CROSS FLOW BLOWING NOZZLE
FIGURE 62

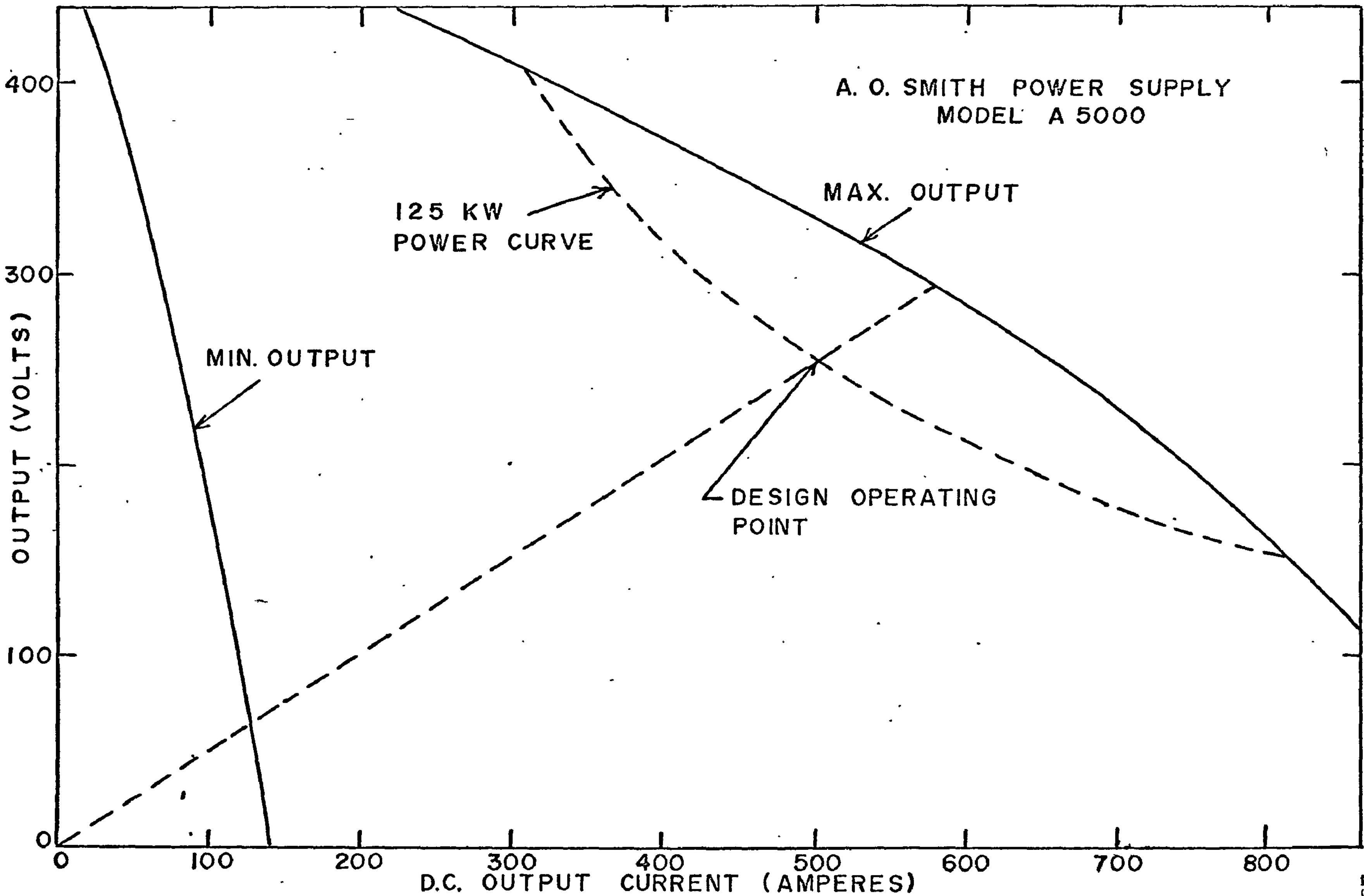

FIGURE 63 - VOLT-AMPERE CHARACTERISTIC CURVE

APPENDIX C

LIST OF EXPERIMENTAL EQUIPMENT USED

1.	Item:	electromagnetic
	Type:	iron core - low impedance - open yoke design
	Rating:	4" diameter pole caps, 4" air gap, 0-3800 gauss, 3/8" view hole through pole caps, uniformity of field over test section $\pm$ 3%, wt. 500 lbs.
	Make:	Varian Associates, Inc., Palo Alto, California
	Model:	V-4005S
2.	Item:	electromagnet power supply
	Type:	D. C. Varicell
	Rating:	0-15 amperes, 0-30 volts
	Make:	Superior Electric Company, Bristol, Connecticut
	Model:	13015
3.	Item:	gaussmeter
	Type:	Hall element
	Rating:	0-30,000 gauss range
	Make:	Bell Laboratories, Inc., Columbus, Ohio
	Model:	110
4.	Item:	electric arc power supply
	Type:	3-phase transformer type rectifier
	Rating:	500 volts open circuit, 125 k. w.
	Make:	A. O. Smith Corporation, Elkhorn, Wisconsin
	Model:	A-5000
5.	Item:	ammeter
	Type:	D. C.
	Rating:	0-500 amperes
	Make:	Weston Company
	Model:	FS 50M
6.	Item:	voltmeter
	Type:	D. C.
	Rating:	0-500 volts
	Make:	Assembly Products Inc.
	Model:	4
7.	Item:	barometer
	Type:	direct read-out barometric pressure with altitude compensation
	Rating:	28-31 inches of mercury
	Make:	Air Force Supply
	Model:	MS 24134-1

8. Item: water pump
Type: positive displacement
Rating: 68 gpm - 530 psig
Make: Worthington Corporation, Harrison, New Jersey
Model: No. 2P747

9. Item: electric motor power supply for water pump
Type: 3-phase
Rating: 25 hp
Make: Fairbanks-Moorse Inc., Chicago, Illinois
Model: F-145305

10. Item: water flowmeters
Type: float
Rating: 0-6 gpm of water
Make: Fischer and Porter, Hatboro, Pennsylvania
Model: B521-10/27

11. Item: high pressure water valves
Type: positive shut-off
Rating: 0-1000 psig
Make: Jamesbury Corporation
Model: A-SS

12. Item: water filter
Type: cartridge
Rating: 0-125 psi
Make: Cuno - Aquapure, Meriden, Connecticut
Model: P-10

13. Item: water pressure gauge
Type: high pressure
Rating: 0-600 psig
Make: Ashcraft
Model: 1JA41565

14. Item: cathode injection gas heater bath and coiled capillary flowmeter
Type: coil heater
Rating: constant temperature 78°F, 0-2 lb_m/hr Argon
Make: Air Force Inventory
Model: No. 5016

15. Item: pressure gauge for sonic nozzle system
Type: Bourdon
Rating: 0-1000 psi
Make: Heise, Newton, Connecticut
Model: H29589

16. Item: pressure gauge for cathode chamber and pitot-static tube
    Type: micromanometer
    Rating: 0-2 inches water
    Make: RGI
    Model: G 1500

17. Item: pressure transducer for sonic nozzle system
    Type: strain gauge
    Rating: 0-1000 psig
    Make: Computran, Division of International Resistance
    Model: 70-2201-CN

18. Item: regulator valve for sonic nozzle system
    Type: reducing and relief regulator
    Rating: 0-1000 psi
    Make: Grove Company
    Model: 15-LH6

19. Item: control valves for sonic nozzle system
    Type: needle valve
    Rating: 0-2000 psi
    Make: Hoke Company
    Model: RB-273

20. Item: temperature gauge for sonic nozzle system
    Type: pyrometer
    Rating: 75-225°F
    Make: Simplytrol, Chesterland, Ohio
    Model: 351

21. Item: pitot-static probe
    Type: United Sensor
    Rating: 0.059 O.D. standard L shape
    Make: Air Force Inventory
    Model: 66605 30112

22. Item: hot wire anemometer
    Type: dual element direct read-out
    Rating: 0-150 ft/sec
    Make: Flow Corporation, Massachusetts
    Model: B

23. Item: particle injector gas supply flowmeter
    Type: dual range float
    Rating: 5-25 SCFH Argon
    Make: Air Reduction Corporation, New York
    Model: 805-1601

24. Item: anode electrode and locator actuator
Type: linear
Rating: 0-6 inch stroke
Make: Lear Inc., Piqua, Ohio
Model: 400A

25. Item: electromagnetic positioning actuator
Type: linear
Rating: 0-6 inch stroke
Make: Lear Inc., Piqua, Ohio
Model: 4230

26. Item: power supply for linear actuators
Type: D. C.
Rating: 0-10 amps D. C.
Make: Labpack, Model Rectifier Corporation, Brooklyn, New York
Model: S-28-10-F

27. Item: unislide traversing mechanism
Type: screw drive - 3-dimensional scan
Rating: 0.025" traverse per 1 revolution of dial
Make: Tropel Inc., Fairport, New York
Model: 6-1/40

28. Item: oscilloscope
Type: dual beam
Rating: D. C. - . 10 megacycles
Make: Tektronix
Model: 555

29. Item: dynograph
Type: 8-channel recorder - individual strip read-out
Rating: 0-100 cps sensitivity to 5 μ volts
Make: Offner Electronics Inc.
Model: R

30. Item: electronic potentiometer recorder
Type: 12-channel stepping recorder
Rating: 0-2 mv
Make: Minneapolis-Honeywell Corporation - Brown Electronic
Model: Y-153X62

31. Item: electronic potentiometer recorder
Type: 2-channel continuous read-out recorder
Rating: 0-8 mv and 0-2 mv
Make: Minneapolis-Honeywell Corporation

32. Item: calorimetric probe
Type: single-jacketed probe using "tare" measurement
Rating: 1 atm - 10,000°K - 10,000 BTU/lb_m
Make: Greyrad Corporation, Princeton, New Jersey
Model: G-1-7 1/16" O. D. 30° angle probe
Model: G-1-8 1/8" O.D. straight and 90° angle probe

33. Item: auxiliary equipment for Greyrad probes
Type: a) closed cycle high pressure coolant system
b) sonic orifice pressure and temperature recording system
Rating: a) coolant system: 0-1000 psi
b) P: 0-30 in. Hg; T: 32-120°F
Make: Greyrad Corporation, Princeton, New Jersey
Model: a) G4 coolant system
b) G5A recording system

34. Item: hot wire heat flux sensor
Type: cooled, miniaturized 0.006" O. D. by 0.08" long
Rating: 5000°F environment, atmospheric pressure, velocities to 200 ft/sec.
Make: Thermo-Systems Inc., Minneapolis, Minnesota
Model: HF-21

35. Item: heat flux system
Type: a) high pressure coolant system
b) power and bridge circuitry system
Rating: a) coolant: 1000 psi - 0.019 gallons/min sensor
b) power: 15 watts to sensor; frequency response 20 kilocycles
Make: Thermo-Systems Inc., Minneapolis, Minnesota
Model: a) sensor water supply 1120
b) power and bridge circuitry 1000A unit 6

36. Item: high speed camera
Type: Fastax - film Ansco color type 231
Rating: 16 mm - 7000 frames/sec
Make: Wollensak
Model: W-163269

37. Item: high speed camera
Type: Dynafax
Rating: 16 mm - 5000-26,000 frames/sec
Make: Beckman-Whitley

38.	Item:	press camera
	Type:	Linhof 4" x 5"
	Rating:	1: 8/90 Super-Angulon lens
	Make:	Linhof, West Germany
	Model:	77370
39.	Item:	polaroid camera
	Type:	Graphic 4" x 5" positive plate or 8 exposure roll
	Rating:	3000 speed film, type 47
	Make:	Polaroid Land Corporation, Cambridge, Mass.
	Model:	B 49093
40.	Item:	spectrograph
	Type:	grating
	Rating:	16 A/mm resolution
	Make:	Cenco
	Model:	Cat. No. 87102 Serial No. 462
41.	Item:	thermopile
	Type:	2 mm diameter sensor
	Rating:	17.2 μ volts/μ watt
	Make:	Scwartz
	Model:	FT17
42.	Item:	nanovoltmeter
	Type:	Z
	Rating:	full-scale center-zero ranges of $\pm$ 0.1 volt to $\pm$ 100.0 millivolts D.C; accuracy $\pm$ 3% at full scale on all ranges
	Make:	Astrodata
	Model:	TDA-121

APPENDIX D

DESIGN DRAWINGS

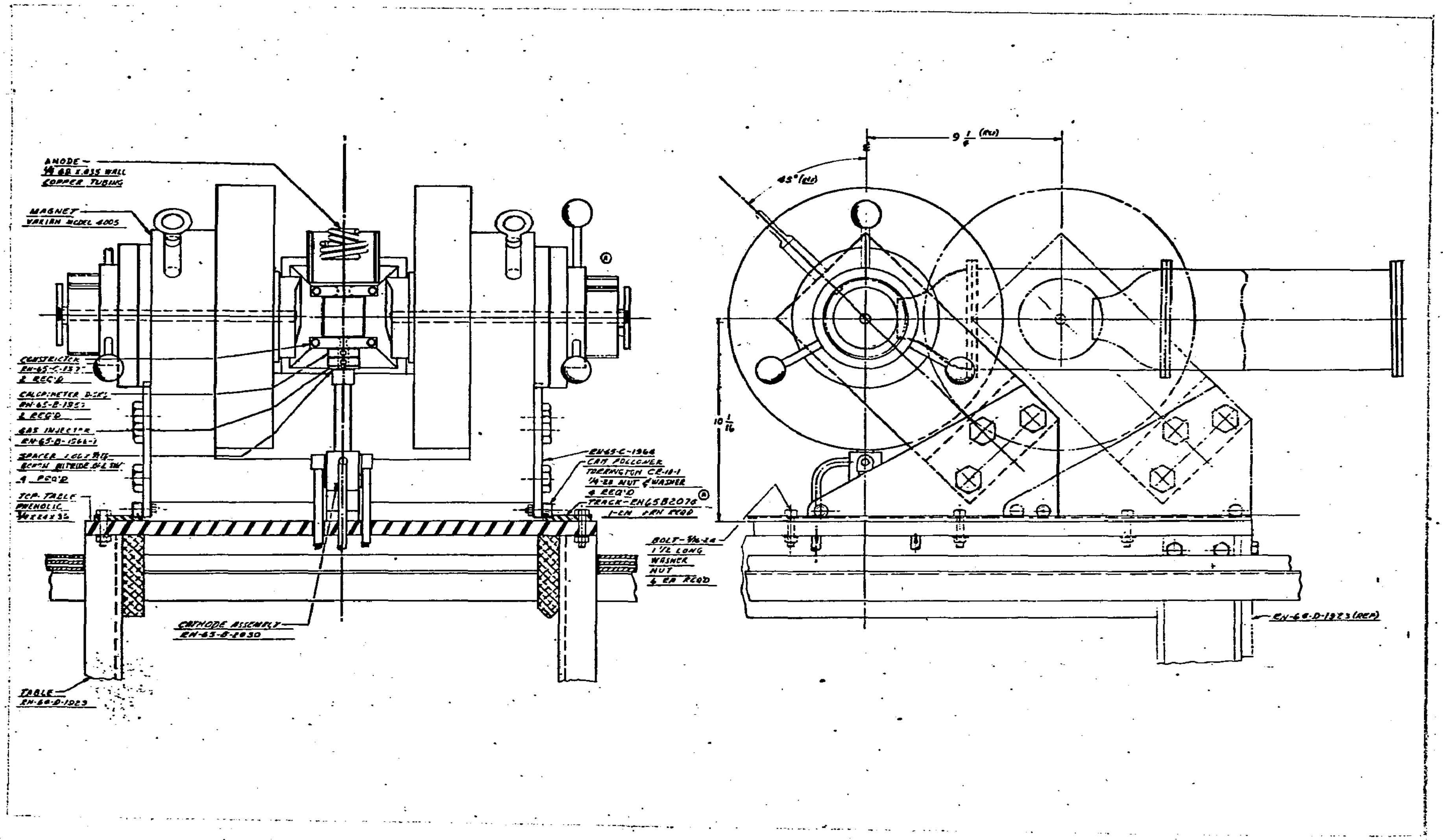

FIGURE 64 SCALE DRAWING OF TEST CONFIGURATION

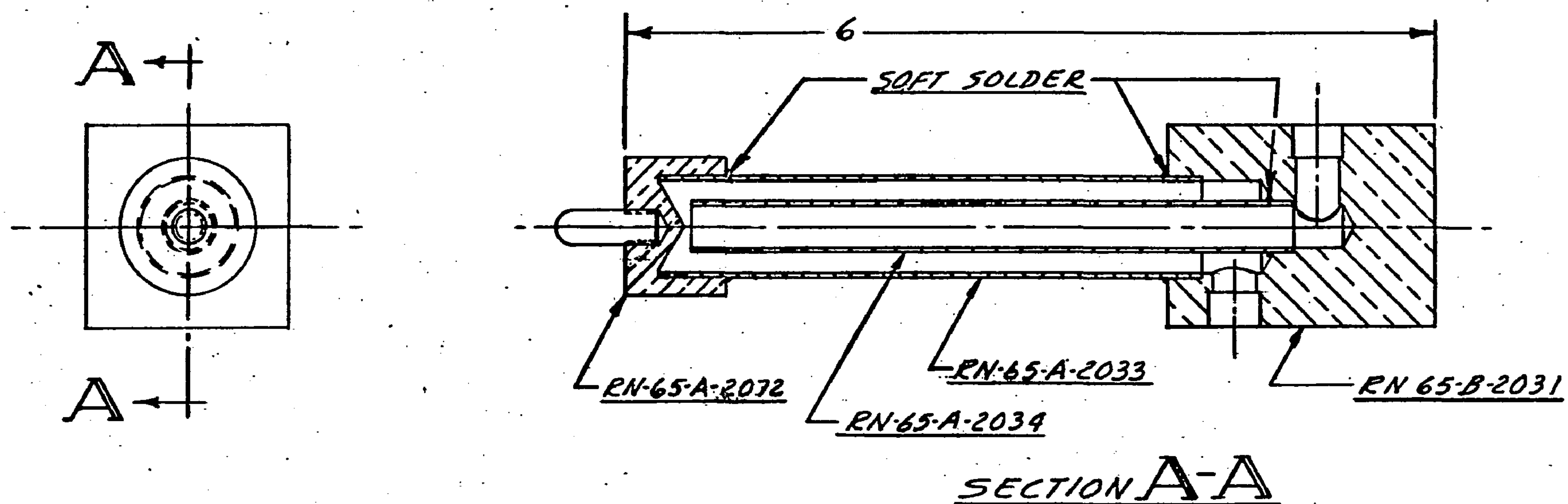

FIGURE 65 SCALE DRAWING OF CATHODE

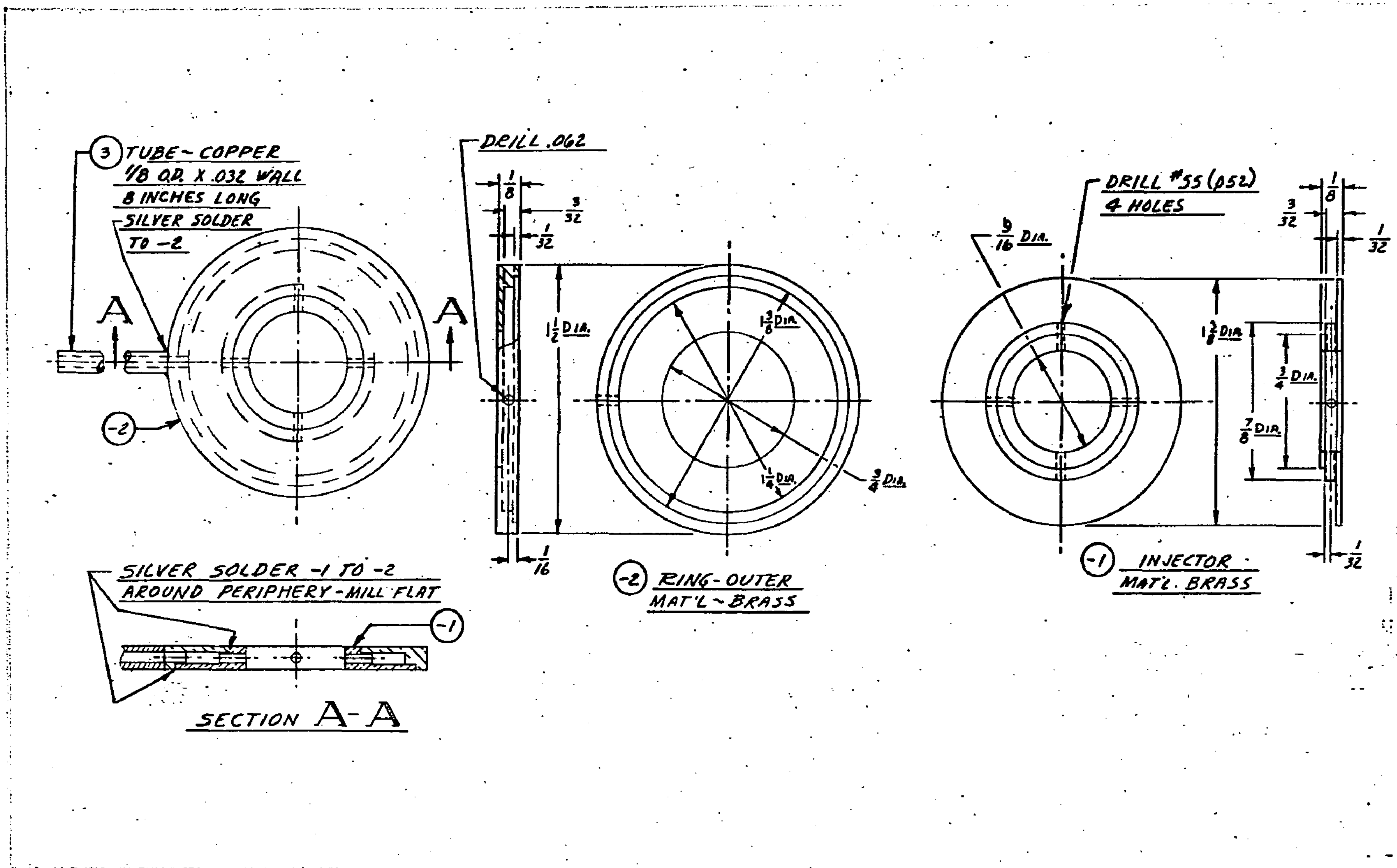

FIGURE 66 SCALE DRAWING OF CATHODE GAS INJECTOR (RADIAL FLOW)

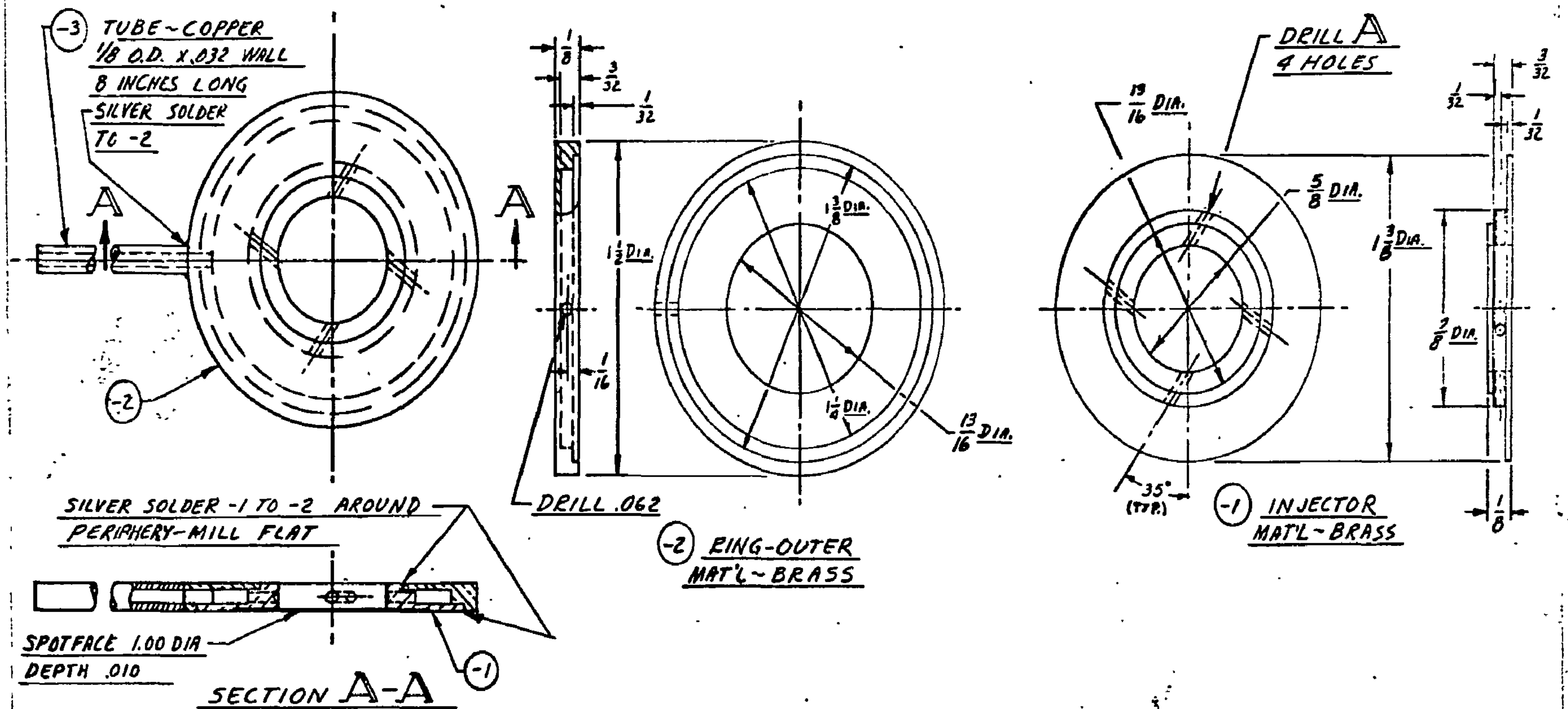

FIGURE 67 SCALE DRAWING OF CATHODE GAS INJECTOR (VORTEX FLOW)

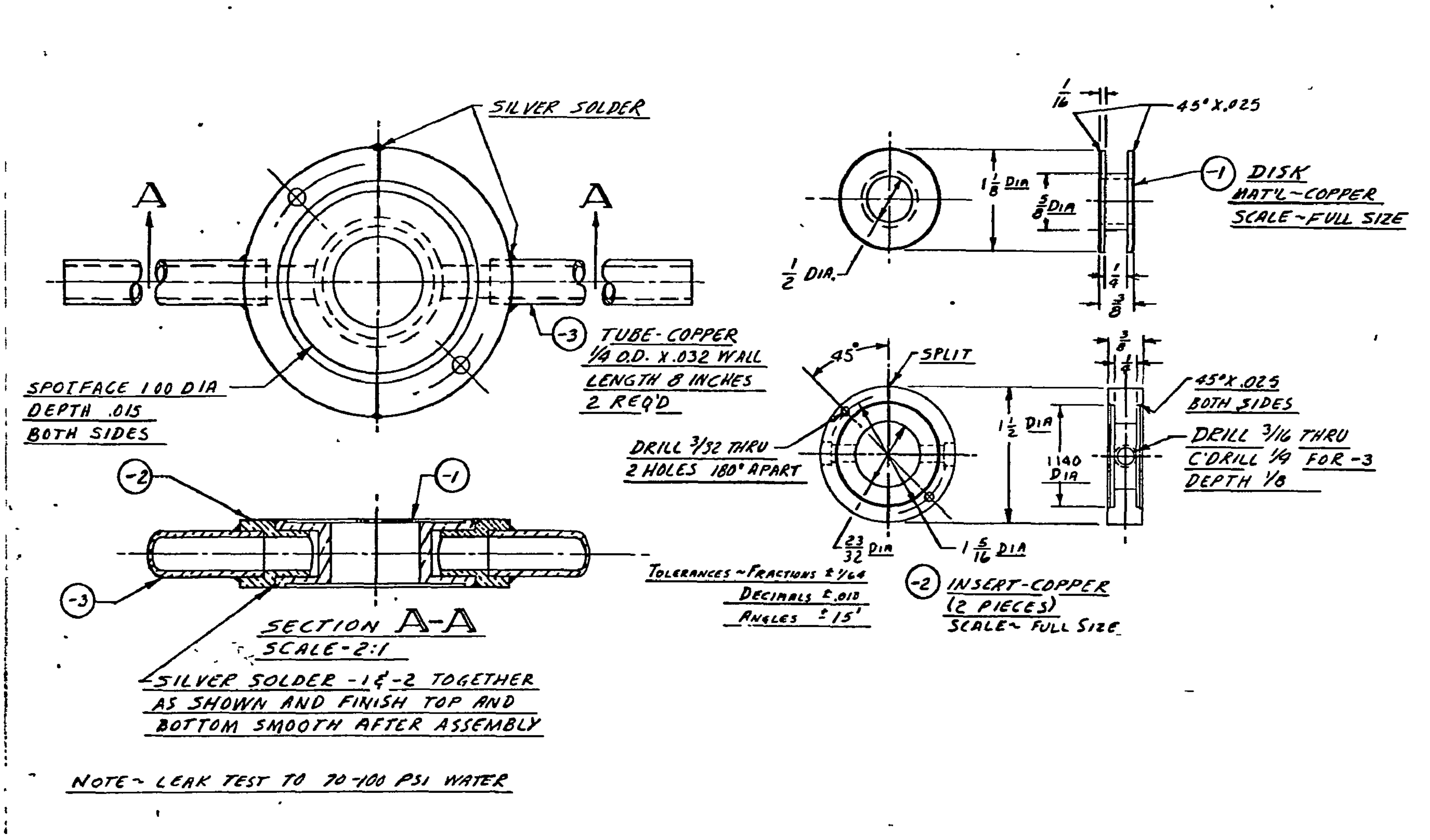

FIGURE 68. SCALE DRAWING OF WATER-COOLED CALORIMETER

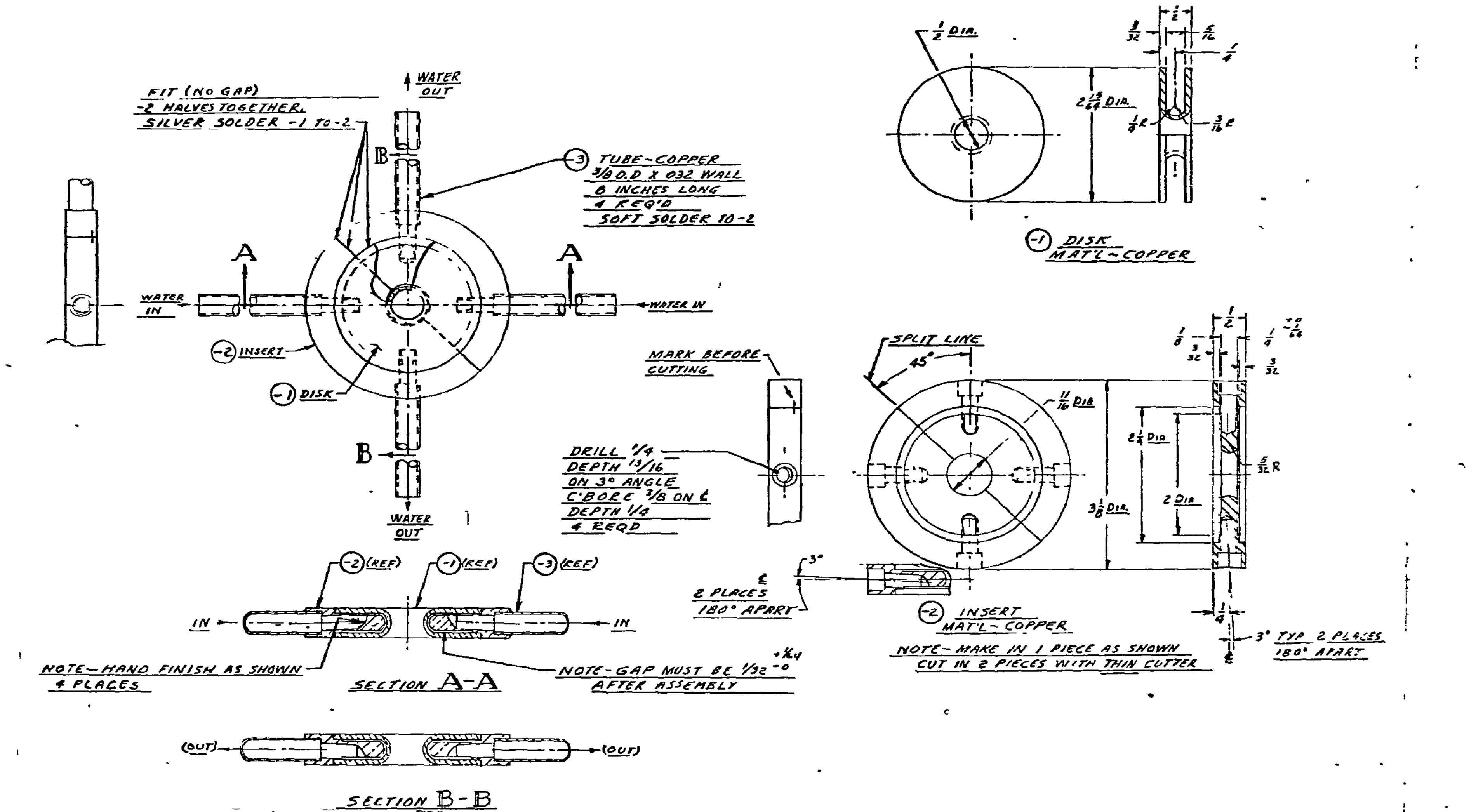

FIGURE 69 SCALE DRAWING OF WATER-COOLED LOCATOR

APPENDIX E

FEASIBILITY AND OPTIMIZATION STUDIES

An important step in any exploratory type of experimental research program is to determine the range of satisfactory experimental conditions in which reproducible data may be obtained. Previous experimental investigations with electric arc devices have demonstrated that within different operating ranges of parameters such as current, pressure, magnetic field strength, electrode material, configuration and gap, severe limitations and both upper and lower operating bounds exist. In an effort to determine the permissible and safe operating range of the experimental apparatus conceived for this investigation, some preliminary feasibility and optimization studies were conducted. Since this appears to be the first experimental investigation utilizing the unconfined cross-flow configuration the importance of the optimization studies for future parallel research efforts merits their inclusion. Of paramount concern was the behavior of the anode and cathode regions under the influence of a transverse external magnetic field. All previous experimenters located the cathode and anode electrodes within the test section and consequently were unable to eliminate the obscuring electrode effects from the main positive arc column. The subject of the anode will be briefly discussed first.

The problem was to design an anode capable of long time operation under high heat loads and external transverse magnetic field effects. The first approach taken was to try and locate the anode electrode as far from the column test section region as possible. With this configuration the fringing external magnetic field would have decayed to a minimum level and hopefully would not have adversely affected the anode behavior. It was experimentally determined that instability aspects rapidly became a significant contributor to anode operation in this configuration. In addition, the portion of the arc which connected the anode spot region to the main column was acted upon by a non-uniform external, transverse magnetic field and consequently was deflected into several water-cooled collimating ring sections which were used to channel the arc column upward to the distant anode electrode. Severe erosion occurred at the edges of the ring sections and subsequently contaminated the anode region. Instabilities, both in the column and in the anode spot region were detected.

An unfortunate aspect incurred when conducting a cross-flow arc experiment with an electromagnet is that a fringing transverse magnetic field will always be present. The cross-flow blowing nozzle and associated baffling, on the other hand, may restrict the aerodynamic flow field to only the positive column test section. This immediately opens up the alternate possibility of using some type of secondary flow scheme within the fringing magnetic field region in an effort to balance the column. This approach requires much trial and error and imposes the additional requirement of a secondary blowing system, ducting, and elaborate cooling requirements. The difficulties involved did not warrant a continued effort in this direction.

A simple plug type anode electrode was tried, but a strong jet effect was noted together with the characteristic cusped-shaped arc. These factors along with the rapid anode material erosion (since the anode spot remained essentially fixed) eliminated this approach.

Some preliminary work was done with hollow, water-cooled, copper anodes employing a variety of gas injection schemes in hopes of inducing the required anode spot motion. The over-all results were not completely satisfactory. It appeared that the magnitudes of flow fields required to insure proper anode spot motion were far in excess of those capable of being supplied with the existing equipment.

The two remaining alternatives were to design an anode which would use the fringing magnetic field to its advantage (i. e., to help move the anode spots rapidly over the electrode surface) or try to shield the anode spot and connecting column region from the influence of the external magnetic field. In the former case, numerous unsuccessful attempts were made with various anode designs in an effort to promote rapid anode spot movement. The majority of these designs did not provide sufficient anode spot movement. This induced local melting followed by rapid electrode failure.

Effort was therefore concentrated on designing an anode electrode which would provide the necessary cooling for the anode spot by rapidly moving the attachment spots over the surface and at the same time provide a reasonably stable operation which would not be detrimentally affected by the transverse fringing external magnetic field. The anode used in the present study was the result of these many optimization studies. The basic idea was to use an anode composed of coiled copper tubing such that the interaction of the arc column with the self-generated magnetic field would provide the necessary high-speed motion of the anode spots. Simultaneous existence of multiple spots was shown to exist from analysis of high-speed motion pictures. (Figure 70.) The anode spot rotation speeds obtained from 26,000 frames/sec high-speed photography indicated maximum values of 3000 rev/sec. By surrounding the anode region with a cylindrical water-cooled mu metal shield, the external magnetic field influence was reduced to a tolerable level.

Originally, currents from 200 to 1000 amperes were to be investigated. In an attempt to achieve operation in the upper current regime, a technique was developed whereby the anode current was split into three separate paths. Three identical coiled anodes were positioned one above the other and separated by an air gap. (Both convergent and divergent shaped anodes were alternately tested.) By connecting each of these anodes to a separate variable resistor,

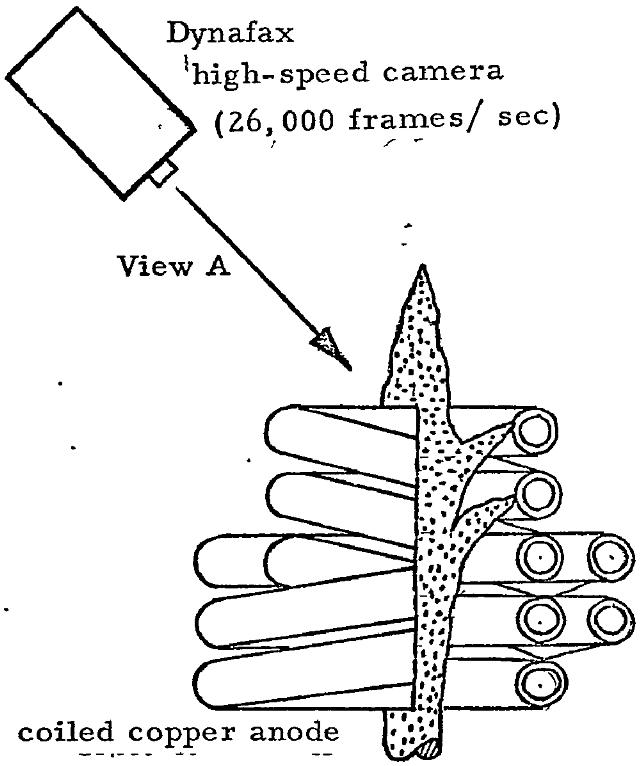

View A

FIGURE 70 HIGH-SPEED PHOTOGRAPH OF MULTIPLE ANODE SPOT PHENOMENA it was possible to split the anode current up into any desired ratio while still maintaining adequate movement of the attachment spots. However, erratic behavior and some unpredictable column stability effects in the anode region were noted which reduced the reliability aspects of this technique.

A single coiled anode without the influence of the fringing external transverse magnetic field allowed current levels of up to 600 amperes to be achieved. This was reduced to approximately 450 amperes when the fringing external magnetic field effects, combined with aerodynamic and stability aspects, were present. At current levels slightly above this value, unusual anode behavior resulted e.g., the anode spot region had a strong tendency to be driven downward out of the coiled anode and would randomly oscillate in the vertical plane. Severe oscillations in noise level accompanied this peculiar behavior. A stable, reproducible, safe upper limit of 400 amperes was, therefore, selected for the cross-flow external magnetic field experiment based on the anode criteria.

The cathode had to be designed so as to meet the following requirements:

1) a minimum of electrode material erosion and subsequent contamination of the column,

2) sustained operation throughout the 100-500 ampere range,

3) stable cathode spot attachment (particularly under the influence of an external transverse magnetic field),

4) minimum cathode jet effect.

Based on the previous electric arc investigations conducted at the Aerospace Research Laboratories, a hollow, well-type cathode design was selected. The incorporation of a two per cent thoriated tungsten cathode dictated the exclusion of oxidizing gases from the cathode region. Both argon or nitrogen gas were used but experience showed that bathing the tungsten cathode in argon gas resulted in less erosion and somewhat more stable arc spot behavior. In addition, the thermodynamic property data available for the monatomic gas is somewhat simpler to interpret. The final design reached was a compromise between one which provided a minimum cathode jet, significant erosion, and some instabilities, and another of a relatively strong cathode jet, negligible erosion, and relatively stable operation. Reducing the cooling water flow rate to the tungsten cathode element allowed the cathode tip temperature to rise, thereby somewhat reducing the current density while correspondingly reducing the strength of the jet. The jet, however, was not significantly reduced because of the hazard of local melting of the cathode tip and contamination of the column.

One questionable aspect worthy of investigation was the static pressure within the cathode chamber. This links closely to the problem of gas entrainment or ingestion into a chamber as a result of a possible pressure differential. A small static pressure tap was installed within the cathode chamber flush with the walls and connected to a micromanometer. A cursory investigation was made to determine the effect of arc current level, non-oxidizing gas injection rate, cathode electrode and chamber shape, and locator hole size on the static pressure within the chamber. The results indicated that the static pressure within the chamber remained within $\pm$ 0.02 in. water of atmospheric pressure for the 200 to 400 ampere range, gas injection rates over the available range and a 1/4 in. i.d. locator hole size. Therefore, the possibility of ambient air being ingested into the chamber was remote.

The sizing of the hole in the bottom locator was based on the requirement that minimum pinching of the arc column should exist. From past experience, an arc column which is accompanied by a rapid flare-out above and below a circular hollow disc through which it is drawn indicates magnetic compression and pumping of some of the surrounding ambient air into the column. This effect was checked with high-speed cameras as a function of arc current and gas injection rate. No flare-out was detected.

Some optimization experimentation was directed toward establishing the ideal cathode tip shape and method of protective gas injection. The choice was a cylindrical plug cathode with a hemispherical tip. (See Appendix D, Figure 65.) For gas injection, straight radial inflow, slight vortex flow injection, and tangential injection schemes were tried in order to promote a cathode spot which was well established and stable at the cathode tip and relatively unaffected by the fringing transverse external magnetic field. A vortex injection technique appeared to behave the best. The requirement for keeping the cathode spot at the electrode tip and the arc vertically aligned was quite important since as soon as the cathode jet becomes misaligned, some back-flow and flare-out may occur.

The final diameter of the top locator hole was a result of conducting tests with the arc under the influence of both the aerodynamic and external magnetic fields. Using a hole in the top locator the same diameter as used in the bottom locator introduced a slight flare-out under the top locator. This was attributed to the free convection growth of the column along the 2 in. gap from the bottom locator to the top locator. The boundary layer effect of the transverse flow along the underside of the upper locator was also an influencing factor, but difficult to eliminate. When high transverse blowing velocities and balancing magnetic fields were applied, small "tongues" randomly appeared below the top locator and slight instabilities were noted in the anode region. This undesirable effect was eliminated to a degree by increasing the hole diameter of the top locator and exercising extreme care in balancing the arc exactly in the vertical plane. This effect was the primary reason for the limitation in the velocity and magnetic field range used.

A final aspect of the optimization studies dealt with a spectrographic survey examination of the positive column region. The objective was to confirm the presence of argon in the column and minimum contamination due to other elements (confirmation that air ingestion was minimized). A grating spectrograph which had been previously calibrated with a mercury vapor lamp was used to obtain photographs of the arc spectrum at three equally spaced elevations between the locators. The entire extent of the spectrum from approximately 2500 to 8000 angstroms was photographed with a single exposure. A linear comparator (readings to 1 micron) was used to measure the distance between the spectral lines on the film. The principal lines were identified using M. I. T. wavelength tables. The assumption that the column was predominantly argon (4000 to 5000 angstrom range) with minute impurities due to slight erosion of the tungsten cathode, copper locators, and boron nitride inserts was confirmed. A few strong lines of Helium were also detected and attributed to impurities within the Argon bottle source.

The most predominant secondary effect was the cathode jet. In order to better estimate this effect, a quartz window was installed in the cathode assembly, (Figure 71). This permitted high-speed color photographs (7000 frames/sec) to be taken of the cathode spot and the relative column growth in the near vicinity of the cathode electrode. The hemispherical tip of the cathode electrode is visible in the top photograph of Figure 71. The bottom photograph is a

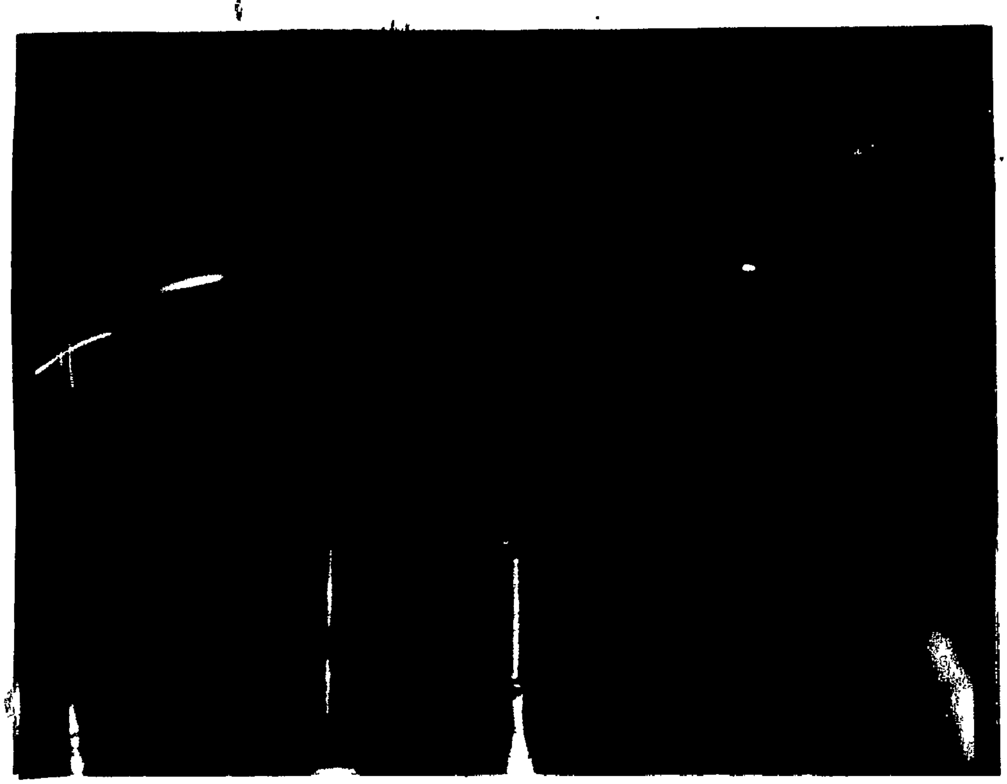

VIEW INTO CATHODE CHAMBER THROUGH
QUARTZ WINDOW USED FOR PHOTOGRAPHING
CATHODE SPOT SIZE

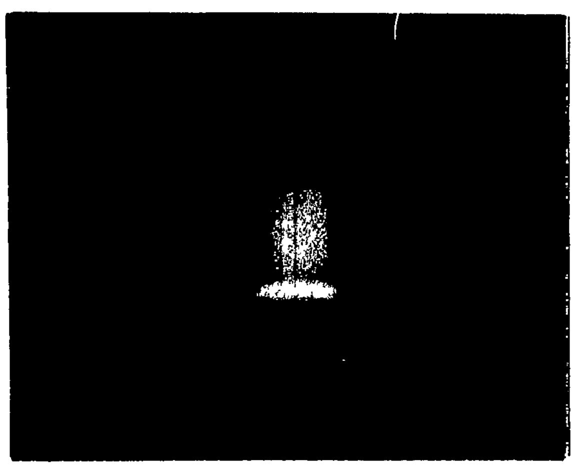

FASTAX PICTURE OF ARC CATHODE
SPOT SIZE AND COLUMN GROWTH
(I = 300 AMPS)

FIGURE 71

representative frame taken from the film. By measuring the effective cathode spot diameter (approximately 0.381 cm); a calculation was made to determine the maximum axial velocity expected in the cathode region. A typical value of current density reported in the literature (17) for a one atmosphere argon arc in the range of 300 amperes and burning on a thoriated tungsten cathode is approximately 10^4 amps/cm^2. The current density in the present investigation was calculated to be 2.632×10^3 amps/cm^2. Using this value together with the derived Maecker equations (Figure 7) yielded a maximum axial velocity of 247 m/sec in the cathode region. Maecker calculated a maximum axial velocity of 350 m/sec for a 200 ampere arc burning on a carbon cathode in atmospheric air. One would expect this velocity to decrease quite rapidly in the axial direction because of frictional dissipation to the neighboring volume elements. Wienecke (65) experimentally measured the axial velocity along the arc's centerline and along the arc's boundary. A pulsed technique was used to determine the inner core velocity, whereas small carbon particles were injected into the outer boundary region near the cathode to indicate the velocities in that region. In order to correlate his data with that of Maecker, Wienecke also used a 200 ampere carbon arc burning in atmospheric air. The electrode gap was approximately five cm. Through the use of a Thyratron the arc was interrupted and upon re-ignition, a high-speed camera was synchronized to photograph the propagation of the luminous core. The "snow-plow" effect which occurs during re-ignition when the hot plasma travels into the relatively cold gas may have caused some error in the jet velocity measurements. Therefore, the results photographed may show too great an axial drop in velocity. If Wienecke's data are extrapolated, a maximum axial velocity of 340 m/sec is obtained. The velocity determination from the ground carbon particles injected into the outer boundary are also subject to some error. A mean velocity of approximately 20 m/sec was measured using the carbon particle traces. This velocity was only applicable outside the arc core. For similar conditions, Rohloff (66) computed a mean velocity of approximately 40 m/sec from the force exerted on the anode.

An extrapolation to the present experiment is questionable due to the different electrode configuration, injection system, and gas. However, one would anticipate the axial velocity of the argon arc to be somewhat less than the air arc due to the wider core. As a result of high-speed photographs taken of the 300 ampere argon arc in a pulsed mode, the average axial velocity was approximately 30 m/sec at the elevation mid-way between the locators (i. e., approximately two in. from the cathode tip). As an alternate check, the arc was operated with widely varying argon gas injection rates simultaneously with varying only the external transverse magnetic field, (no transverse blowing). By first operating the arc with reduced argon mass flow and then applying the external transverse magnetic field, a pronounced arc curvature resulted. The argon injection rate was then increased until the arc was brought back to the vertical position. Using the experimental data obtained together with the equation of motion allowed a rough estimate to be made of the mean axial velocity. The value calculated was 160 m/sec. Unfortunately, no information could be obtained on the axial velocity gradient. For the particular test range investigated, the outer boundary axial velocity was estimated to be approximately 10 m/sec.

A further experimental indication that a strong axial velocity gradient existed within the core was the existence of a relatively bright luminous cone with its apex approximately 1/2 in. below the mid-elevation between the locators.

Other secondary effects present were:

1) The third dimensional flow due to secondary cool air entrainment from below and downstream of the bottom locator.

2) The superpositionment of the self- and external magnetic fields (both of the same order of magnitude).

APPENDIX F

RETROGRADE AND RAIL-ACCELERATOR REFERENCE LISTS

(CHRONOLOGICALLY ARRANGED)

Retrograde

Many closely related areas exist, however, these cited references deal mainly with the problem of retrograde motion. Such related areas as cathode theories, electrode natural vapor jets, etc., can be found in the cited reference lists of the individual papers.

De la Rive, A. M., "Recherches l'action qu exerce le magnetism sur les jets electriques qui se propagent dans les milieux gareux tres-rarefies," Arch. d. Sc. Phy. et Nat. 27, 289 (1866).

De la Rive, A. M. and Sarasin, E., "De l'action du magnetism sur les gas traverses par des decharges electrique," Arch. d. Sc. Phy. et Natural 41, (1871).

De la Rive, A. M. and Sarasin, E., "Sur la rotation sous l'indluence magnetique de la decharge electrique dans les gas rarefies et sur l'action mecanique que peut exerger cette decharge dans son mouvement de rotation," Ann. de Chim. et de Phys. 29, 207 (June, 1873).

Lehmann, O., "Electric and Magnetic Wind," Annal. Phys. Chem. 63, 285 (1897).

Kobel, E., "Pressure and High-Velocity Vapour Jets at the Cathode of a Mercury Vacuum Arc," Physical Review 36, 1636 (1897).

Stark, J., "Induktionerscheinungen am Quecksilberlicht-bogen im Magnetfeld," Physikalische Zeitschrift 4, 400 (1903).

Weintraub, E., "Investigation of the Arc in Metallic Vapours in an Exhausted Space," Philosophical Magazine 7, 95 (Feb., 1904).

Minorsky, M. N., "La rotation de l'arc electrique dans un champ magnetique radial," J. de Phys. et Rad. 4, 127 (1928).

Tanberg, R., "Motion of an Electric Arc in a Magnetic Field Under Low Gas Pressure," Nature 124, 371 (1929).

Tanberg, R., "On the Cathode of an Arc Drawn in Vacuum," Phys. Rev. 35, 1080 (May, 1930).

Tiberio, U., "L'Azione del campo magnetico sull arco elettrico nel vapore di mercurio," L'Elettrotecnica 17, 485 (1930).

Compton, K. T., "Theory of the Mercury Arc," Physical Review 37, 1077 (May, 1931).

Tanberg, R. and Berkey, W., "On the Temperature of Cathode in Vacuum Arc," Phys. 38, 296 (July, 1931).

Tonks, L., "Rate of Vaporization of Mercury From an Anchored Cathode Spot," Phys. 54, 634 (October, 1938).

Tonks, L., "Theory of Magnetic Effects in the Plasma of an Arc," Phys. Rev. 56, 360 (August, 1939).

Smith, C. G., "The Mercury Arc Cathode," Phys. Rev. 62, 48 (July, 1942).

Smith, C. G., "Motion of the Copper Arc in Transverse Magnetic Field," Phys. Rev. 63, 217 (1943).

Quill, J. S. and Rader, L. T., "D-C Arc Interruption for Aircraft," Elect. Eng. Trans. 63, 883 (1944).

Smith, C. G., "Cathode Dark Space and Negative Glow of a Mercury Arc," Phys. Rev. 69, 96 (1946).

Gallagher, C. J. and Cobine, J. D., "Retrograde Motion of an Arc Cathode Spot in a Magnetic Field," Phys. Rev. 71, 481 (1947).

Longini, R. L., "Motion of Low Pressure Arc Spots in Magnetic Fields," Phys. Rev. 72, 184 (1947).

Longini, R. L., "A Note Concerning the Motion of Arc Cathode Spots in Magnetic Fields," Phys. Rev. 71, 642 (1947).

Cobine, J. D. and Gallagher, C. J., "Current Density of the Arc Cathode Spot," Phys. Rev. 74, 1524 (November 1948).

Himler, H. and Cohn, G. J., "The Reverse Blowout Effect," Electrical Engineering 67, 1138 (December, 1948).

Smith, C. G., "Arc Motion Reversal in Transverse Magnetic Field by Heating Cathode," Phys. Rev. 73, 543 (1948).

Bohm, D., "The Characteristics of Electrical Discharges in Magnetic Fields," edited by A. Guthrie and R. K. Wakerling, Chapter 2, Section 5. (New York: McGraw-Hill, 1949).

Gallagher, C. J. and Cobine, J. D., "Reverse Blowout Effects," Electrical Engineering 68, 469 (1949).

Hochrainer, A., "Uber die Umkehrung der Magnetischen Blaswirkung," Elin. Zeitschrift 1, 61 (1949).

Holm, R., "The Vaporization of the Cathode in the Electric Arc," J. of Appl. Phy. 20, 715 (July, 1949).

Gallagher, C. J., "The Retrograde Motion of the Arc Cathode Spot," J. of Appl. Phy. 21, 768 (1950).

Early, H. C. and Dow, W. G., "Supersonic Wind at Low Pressures Produced by Arc in Magnetic Field," Phys. Rev. 79, 186 (July, 1950).

Rothstein, J., "Holes and Retrograde Arc Spot Motion in a Magnetic Field," Phys. Rev. 78, 331 (1950).

Yamamura, S., "Immobility Phenomena and Reverse Driving Phenomena of the Electric Arc," J. of App. Phy. 21, 193 (1950).

Smith, C. G., "Motion of an Anchored Arc Impelled by a Magnetic Field," Phys. Rev. 82, 570 (1951).

Smith, C. G., "Retrograde Arc Motion of Supersonic Speed," Phys. Rev. 84, 1075 (1951).

Dallas, J. P., "Arc Interruption Phenomena in a Magnetic Field at Altitude," Trans. AIEE 71, 319 (1952).

McBee, W. and Dow, W., "Influence of a Transverse Magnetic Field on an Unconfined Glow Discharge," AIEE (July, 1953).

Robson, A. E. and von Engel, A., "Origin of Retrograde Motion of Arc Cathode Spots," Phys. Rev. 93, 1121 (March, 1954).

Miller, C. and Saunders, N., "Motion of the Arc Cathode Spot in a Magnetic Field," Phys. Rev. 93A, (1954).

St. John, R. M. and Winans, J. G., "Motion of Arc Cathode Spot in a Magnetic Field," Phys. Rev. 94, 1097 (June, 1955).

Cobine, J. D. and Burger, E. E., "Analysis of Electrode Phenomena in the High-Current Arc," J. of Appl. Phy. 26, 895 (July, 1955).

Guile, A. E. and Secker, P. E., "Arc Cathode Movement in a Magnetic Field," J. of Appl. Phy. 29, 1662 (December, 1955).

Hernquist, K. G. and Johnson, E. O., "Retrograde Motion in Gas Discharge Plasmas," Phys. Rev. 89, 1576 (June, 1955).

St. John, R. M. and Winans, J. G., "Motion and Spectrum of Arc Cathode Spot in a Magnetic Field," Phys. Rev. 98, 1664 (June, 1955).

Germer, L. H. and Boyle, W. S., "Two Distinct Types of Short Arcs," J. of Appl. Phy. 27, 32 (January, 1956).

Robson, A. E. and von Engel, A., "Motion of a Short Arc in a Magnetic Field," Phys. Rev. 104, 15 (October, 1956).

Eidinger, A. and Rieder, W., "Das Verhalten des Leichtbogens im Transversalen Magnetfeld," Archiv fur Elektrotechnik 43, 94 (1957).

von Engel, A. and Robson, A. E., "The Exitation Theory of Arcs with Evaporating Cathodes," Proceedings of the Royal Society A242, 217 (1957).

Guile, A. and Mehta, S., "Arc Movement Due to the Magnetic Field of Current Flowing into the Electrodes," Proc. Inst. Elec. Engr. A-104, 533 (1957).

Kesaev, I. G., "On the Causes of Retrograde Arc Cathode Spot Motion in a Magnetic Field," Dokl.(2) Aked. Nauk. 113, 71 (1957).

Robson, A. E. and von Engel, A., "An Explanation of the Tanberg Effect," Nature 179, 625 (1957).

Smith, C. G., "Motion of an Arc in a Magnetic Field," J. of Appl. Phy. 28, 1328 (November, 1957).

Ecker, G. and Muller, K. G., "Theory of Retrograde Motion," J. of Appl. Phy. 29, 1606 (November, 1958).

Ecker, G. and Muller, K. G., "Theorie der Retrograde Motion," Zeitschrift fur Physik 151, 577 (1958).

Wroe, H., "Vacuum Arcs on Tungsten Cathodes," Nature 182, 338 (August, 1958).

Ecker, G., "Electrode Components of the Arc Discharge," Inst. fur Theor. Physik der Univ. Bonn, (1959) (personal communication).

Kesaev, I. G. and Pashkova, V. V., "The Electromagnetic Anchoring of the Cathode Spot," Soviet Physics 4, 254 (December, 1959).

Robson, A. E., "The Motion of an Arc in a Magnetic Field," IVth Int. Conf. on Ioniz. Phenom. in Gases, Upsala, p IIB, 346 (1959).

Zei, D. Winans, J. G., "Motion of High Speed Arc Spots in Magnetic Fields," J. of Appl Phy. 30, 4, 1913 (November, 1959).

Lewis, T. J. and Secker, P. E., "Effect of Cathode Surface Roughness and Oxidation on Arc Movements," Nature, 186, 30 (April, 1960).

Secker, P. E., "The Dependence of Arc Root Mobility on Electrode Conditions," Ph.D. Thesis, University of London (1960).

Guile, A. E., Lewis, T. J., and Secker, P. E., "The Motion of Cold-Cathode Arcs in Magnetic Fields," Inst. Elec. Eng. Proc. 108, C-14, 463 (May, 1961).

Lewis, T. and Secker, P. E., "Influence of the Cathode Surface on Arc Velocity," J. of Appl. Phys. 32, 54 (1961).

Hull, A. W., "Cathode Spot," Phys. Rev. 126, 1603 (June, 1962).

James, D. R., "An Experimental Examination of Retrograde Motion of an Electric Arc," Wright-Patterson AFB, Ohio, Air Force Institute of Technology, Master's Thesis (1962).

Guile, A., Lewis, T., and Secker, P., "The Emission Mechanism and Retrograde and Forward Motion of Cold-Cathode Arcs," Proc. of the VIth Int. Conf. on Ioniz. Phen. in Gases, 2, 283 (1963).

Rauchschindel, Gunter, "Experimental Dissertation on Retrograde Motion," Darmstadt, W. Germany (1963).

Roman, W. C., "Some Observations on the Motion of Electric Arcs in Transverse Magnetic Fields," 4th Symposium on the Engineering Aspects of MHD, Univ. of Calif., Berkeley (1963).

Roman, W. C., "The Mysterious Phenomena of Retrograde Motion," OAR Review, II-18 (1963).

Roman, W. C., "Some Observations on the Forward and Retrograde Motion of Electric Arcs in Transverse Magnetic Fields," VIth Int. Conf. on Ionization Phenomena in Gases, Paris (1963).

Blix, E. D. and Guile, A. E., "The Magnetic Deflection of Short Arcs Rotating Between Annular Electrodes Above and Below Atmospheric Pressure," A.R.C. 26, 268 (1964).

Kesaev, I. G., Cathode Processes in the Mercury Arc. (Authorized Translation from the Russian. New York, Consultants Bureau, 1964).

Hull, A. W., "A Basic Theory of the Mercury Cathode Spot," J. of Appl. Phy. 35, 490 (March, 1964).

Schrade, H., "On Arc Pumping and the Motion of Electric Arcs in a Transverse Magnetic Field," VIIth Int. Conf. on Ioniz. Phen. in Gases, Belgrade, ARL 65-178 (1965).

Weichel, H., "On the Retrograde Motion of a Low Pressure Arc Discharge in a Transverse Magnetic Field," VIIth Int. Conf. on Ioniz. Phen. of Gases, Belgrade (1965).

Giannotta, S., "Retrograde Arc and Cathode Spot Motion in Crossed Electric and Magnetic Fields," AFIT Master's Thesis, Wright-Patterson AFB, Ohio (1966).

Rail-Accelerator

Nichol, J., "The Rotation of the Electric Arc in a Radial Magnetic Field," Proc. Roy. Soc. A82, 29 (October, 1909).

Stolt, H., "Rotation of the Electric Arc," Annalen Der Physik, 74-1, 80 (April, 1924).

Slepian, J., "Theory of the Deion Circuit Breaker," AIEE Transactions, 4, 523 (1929).

Burghoff, H., "Uber die Magnetische Ablenkung von Gleishstromlichtbogen," Dissertation, Braunschweig (1933).

Burghoff, H., "Uber die Magnetische Ablenkung von Lichtbogen," Elektrotechn und Masch., 52, 49 (February, 1934).

Bron, O. B., "Soufflage de L'arc par un Champ Magnetique," Cigre-Bericht, NR 128 (1937).

Freiberger, H., "Lichtbogenwanderung in Schaltanlagen," ETZ, 61-38, 865 (September, 1940).

Bron, O. B., "Motion of an Electric Arc in a Magnetic Field," Russian Translation, Moscow-Leningrad (1944), ASTIA, AD No. 258489 (1961).

Babakov, N. A., "Speed of Motion of a Short Electric Arc," Elektrichestov 7, 74 (1948).

Hochrainer, A., "Uber die Unkehung der Magnetischen Blaswirkung," ETZ-A 1, 61(1949).

Kouwenhoven, W. B., and Jones, T. B., "Arcs Between Moving Electrodes," E. E. 68, 834 (October, 1949).

Allen, N. L., "Heavy-Current Arcs in a Transverse Magnetic Field," Univ. of Birmingham (January, 1951).

Hurtle, R. L., "Controlling D. C. Arcs," AIEE Trans. II 225 (1953).

Edinger, A. and Rieder, W., "Uber das Verhalten des Gleichstromlichtbogens in Transversalem Magnetfeld," Phys. Verk. 5, 227 (1954).

Lee, T. H., "Properties of a D. C. Arc in a Magnetic Field," (Ph.D. Dissertation, Dept. of Electrical Eng., Rensselaer Polytechnic Institute) (1954).

Dunkerley, H. S. and Schaefer, D. L., "Observations of Cathode Arc Tracks," J. Appl. Phys. 26, 11 (November, 1955).

Rieder, W. and Edinger, A., "Magnetic Blast in Circuit Breakers," C.I.G.R.E., Paris, Paper No. 107 (1955).

Walker, R.C. and Early, H. C., "Velocities of Magnetically Driven Arcs in Air and Helium up to 30 Atmospheres," AIEE Conf. Paper (1955).

Winsor, L. P. and Lee, T. H., Phys. Rev. 98, 562 (A) (1955).

Hochrainer, A., "Die Bewegung des Kurzschluss-Lichtbogens in Hochspannungs-Schaltanlagen," ETZ-A, 77, 302 (1956).

Lee, T. H., "Properties of a D.C. Arc in a Magnetic Field," Communications and Electronics (1956).

Winsor, L. P. and Lee, R. H., "Properties of a D.C. Arc in a Magnetic Field," Trans. AIEE, 75, 143 (May, 1956).

Eidinger, A. and Rieder, W., "Das Verhalten des Lichtbogens im Transversalem Magnetfeld," Arch. Elektrotech 43, 94 (1957).

Guile, A. E., "The Movement of an Arc between Parallel Horizontal Rods fed from one end in Still Air and in a Wind," E.R.A. Report, Ref. O/T 19 (1957).

Guile, A. E. and Mehta, S. F., "Arc Movement Due to the Magnetic Field of Current Flowing in the Electrodes," Inst. of Elec. Eng. Proc., 104-18, 533 (December, 1957).

Guile, A. E., Lewis, T. J. and Mehta, S. F., "Arc Motion with Magnetized Electrodes," Brit. J. Appl. Phys., 8, 444 (November, 1957).

Guile, A. E., Lewis, T. J., and Mehta, S. F., "Arc Movement and Electrode Magnetism," Nature (London), 179, 1023 (May, 1957).

Angelopoulos, von M., "A Direct Current Arc with Rapid Translational Motion caused Magnetically," ETZ-A 79-16, 572 (1958).

Guile, A. E. and Secker, R. E., "Arc Cathode Movement in a Magnetic Field," J. Appl. Phys., 29, 1662 (December, 1958).

Mosch, W., "Die Bewegung Langer Wechselstrom-Lichtbogen im Modeleversuch," Wissenshaftliche Zeitshrift der Technischen Hochschule Dresden, 8, 859 (1958/9).

Muller, L., "Movement of Short Arcs of High Current in Self-Field," Elektrizitatswirtschaft, 541, 196 (1958).

Secker, P. E. and Guile, A. E., "Magnetic Deflexion of Arcs," Nature (London), 181, 1615 (June, 1958).

Buechner, Gerhard, "Verlangern von Lichtbogen mit Hilfe Magnetischer Felder Zum Unterbreachen von Wechselstromen," ETZ-A, 80, 71 (1959).

Buechner, Gerhard, "Extinction of Arcs by Lengthening in a Magnetic Field," Eng. Digest 20, 209 (1959).

Fechant, "Vitesse de Deplacement D'Arcs Electriques dans L'Air," Revue Generale de L'Electricite 68, 519 (1959).

Koppin, H. and Schmidt, E., "Beitrag zum Dynamischen Verhalten d. Lichtbogens in oelarmen Hochspannungs-Leistungsschaltern," ETZ-A 80, 805 (1959).

Menke, H., "The Movement of Electric Arcs by the Arc's Own Field Reinforced by Ferromagnetics," ETZ-A, 80, 112 Era Translation Trans/1B 1739 (1959).

Secker, P. E. and Guile, A. E., "Arc Movement in a Transverse Magnetic Field at Atmospheric Pressure," Instn. of Elec. Eng. Proc. 106, 311 (August, 1959).

Secker, R. E., "The Influence of Cathode Surface Conditions on Arc Movement," Proc. IVth Conference on Ionization Phenomena, Upsala, 1, 350 (August, 1959).

Gonenc, I., "Lichtbogenwanderung an Runden Staben," ETZ-A 81, 132 (1960).

Hesse, D., "Zur Bestimmung des Laufschienenfeldes am Wandernden Lichtbogen," Archiv fur Elektrotechnik 45, 466 (1960).

Hesse, D., "Uber den Einfluss des Laufschienenfeldes auf die Ausbildung und Bewegung von Lichtbogenfusspunkten," Archiv. fur Electrotechnik XLV-3, 188 (1960).

Kuhnert, E., "Uber die Lichtbogenwanderung im engen Isolierstoffspalt bei Stromen bis 200 KA," ETZ-A 81-11, 401 (1960).

Lewis, R. J. and Secker, P. E., "Effect of Cathode Surface Roughness and Oxidation on Arc Movement," Nature (London) 186, 30 (April, 1960).

Mosch, W., "Die Bewegung Langer Lichtbogen auf Grossflachigen Elektroden," Monatsberichte der Deutschen Akademie der Wissenschaften zu Berlin, 2-1, 16 (1960).

Reid, J. W. and Ghai, M. L., "A Study of Arc Rotational Speed," Johns Hopkins Univ. Contr. 77774, G.E. ARO-Evendale, Ohio (1960).

Secker, P. E., "Explanation of the Enhanced Arc Velocity on Magnetic Electrodes," Brit. J. Appl. Phys. 11, 385 (August, 1960).

Secker, P. E., "The Dependence of Arc Root Mobility on Electrode Conditions," Ph.D. Thesis, University of London (1960).

Clingman, D. L., and Rosebrock, T. L., "Generalized Electromagnetic Field of the Rail Type Accelerator," Allison Div. RPT, GMC, Indianapolis, Indiana, AF OSR-1279 (1961).

Guile, A. E., Lewis, T. J., and Secker, P. E., "The Motion of Cold-Cathode Arcs in Magnetic Fields," Instn. Elec. Eng. Proc. 108, 463 (May, 1961).

Hesse, D., "Uber den Einfluss des Laufschienen-materials auf die Wanderungsgeschwindigkeit von Lichtbogen," Arch. fur Elek. 46-3, 149 (1961).

Lewis, T. J. and Secker, P. E., "Influence of the Cathode Surface on Arc Velocity," J. of Appl. Phys. 32, 54 (1961).

Newmann, J., "Loschung von Lichtbogen in engen Spalten Zwischen Isolierstoffwanden," ETZ-A 82, 336 (May, 1961).

Palmer, G. M., "Analysis of Energy Efficiency of Rail Accelerators," Allison Div. GMC. Engr. Dept. RPT. 225 (July, 1961).

Pardo, W. B., "Arc Studies in a Magnetic Field," Miami Univ. Coral Gables, Florida, Plasma Phys. Bul. 1, 25 (1961).

Secker, P. E. and Guile, A. E., "A Theory of Cold-Cathode Arc Movement in a Magnetic Field," Nature (London) 190 (April, 1961).

Boldman, D. R., Shepard, C. E., and Falsan, J. C., "Electrode Configurations for a Wind-Tunnel Heater Incorporating the Magnetically Spun Electric Arc," NASA TN D-1222 (1962).

Guile, A. E. and Spink, H. C., "Magnetic Deflection of High Current Arcs," Proceedings of IVth MHD Symp., Berkeley, Calif. (1962).

Hochrainer, A., "Kurzschlusslichtbogen in Hochspannungsschaltanlagen," ETZ-A, 83-7, 202 (1962)

Kadomtsev, B. B., "Convection of the Plasma of a positive column in a Magnetic Field," Sov. Phys. Tech. Phys. 6-11, 927 (1962).

Mayo, R. F. and Davis, D. D., "Magnetically Diffused Radial Electric Arc Heater Employing Water-Cooled Copper Electrodes," ARS Preprint 2453-62 (March, 1962).

Ozawa, M., "Study of Electrode Phenomena of a High Current Arc," Bulletin of the Electrotechnical Lab., Tanashi-Machi, Kitama-Gun, Tokyo, 26-5, 329 (1962).

Roman, W. C., "Investigation of the Behavior of Magnetically Driven Electric Arcs," Thesis, The Ohio State Univ. (1962).

Roman, W. C., "Some Observations on the Motion of Electric Arcs in Transverse Magnetic Fields," Proceeding of First Plasma Arc Seminar, ARL 63-151, 495 (1962).

Roman, W. C., "The Behavior of Magnetically Driven Electric Arcs," OAR Review, 1, 17 (1962).

Schutte, H. G., "Uber den Einfluss von Stromungsvorgangen auf die Lichtbogenwanderung in Engen Spalten," ETZ-A 83-1, 16 (1962).

Secker, P. E., Guile, A. E., and Caton, P. S., "Skin Effect as a Factor in the Movement of Cold-Cathode Arcs," Brit. J. Appl. Phys. 13, 282 (June, 1962).

Zharinov, A. V., "A Rotating Plasma Arc in a Discharge in a Magnetic Field;" Sov. J. Atom. Energy 10, 368 (1961). J. Nucl. Energy 4, 63 (1962).

Adams, V. W., "The Influence of Gas Streams and Magnetic Fields on Electric Discharges - Part I - Arcs at Atmospheric Pressure in Annular Gaps," A.R.C. C.P. 743 (June, 1963).

Adams, V. W., "The Influence of Gas Streams and Magnetic Fields on Electric Discharges - Part II - The Shape of an Arc Rotating Round an Annular Gap," R.A.E. Tech. Note - AERO 2896 (June, 1963).

Benenson, D. M., "A Study of the Effects of Convection Upon an Electric Arc," AIEE, 956 (February, 1963).

Boldman, D. R., "Performance Evaluation of a Magnetically Spun DC Arc Operating in Nitrogen," AIAA 1, 802 (1963).

Broufman, A. I., "Arc Travel in the Annular Clearances of Sparkgaps in Magnetic Rotating Arc Arrestors," Elektrichestvo 8, 56 (1963).

Fehling, "The Behavior of the Roots in Heavy Current Switching Arcs," ETZ-A 84, 499 (1963).

Pratt, J. and Rieder, W., "A. C. Arc Movement in a Transverse Magnetic Field," Proceedings VIth International Conf. on Ionization Phenomena in Gases, 2 (1963).

Roman, W. C., "Some Observations on the Motion of Electric Arcs in Transverse Magnetic Fields," IVth Symposium on Engr. Aspects of MHD, Univ. of California at Berkeley (1963).

Schaper, J., "Kurgschlusstrom-Begrenzung durch hohe, Lichtbogen-spannung in Flussigkeiten," ETZ-A 84, 140 (1963).

Knabe, W., "A Review of Magnetically Induced Motion," Proceedings of First Plasma Arc Seminar, ARL 63-151 (1963).

Guile, A. E., Lewis, T. J., and Secker, P. E., "The Emission Mechanism and Retrograde and Forward Motion of Cold-Cathode Arcs," Proceedings VIth International Conf. on Ionization Phenomena in Gases, 2, 283 (1963).

Blix, E. D., and Guile, A. E., "The Magnetic Deflection of Short Arcs Rotating Between Annular Electrodes Above and Below Atmospheric Pressure," A.R.C. 26, 268 (1964).

Fabri, J., "Analyse des Resultats Experimentaux Obtenus sur un Arc a l'Argon," AGARDograph 84, Pt. 2, 709 (1964).

Jedlicka, J. R., "The Shape of a Magnetically Rotated Electric Arc Column in an Annular Gap," NASA TN D 2155 (1964).

Kouwenhoven, W. B. and Jones, T. B., "Arcs Between Moving Electrodes," E. E. 68, 834 (1964).

Salge, J., "The Movement of Heavy Current Arcs in Narrow Gaps at Low Pressure," ETZ-A 85, 11 (1964).

Shaw, J. M., "The Calculation of the Shape of an Electric Arc Discharge Rotating in an Annular Gap under the Influence of a Non-uniform Longitudinal Applied Magnetic Field," R.A.E. Tech Note 2965 (June, 1964).

Roman, W. C., "On the Motion of Arcs over Rail Electrodes," Report on Research, ARL 64-1 (1964).

Blix, E. D. and Guile, A. E., "Column Control in the Magnetic Deflection of a Short Arc," Brit. J. Appl. Phys. 16 (1965).

Spink, H. C. and Guile, A. E., "The Movement of High-Current Arcs in Transverse External and Self-Magnetic Fields in Air at Atmospheric Pressure," A.R.C. C.P. No. 777 (1965).

Broadbent, E. G., "Electric Arcs in Cross-Flow," R.A.E. Tech. Memo Aero 897 (1965).